Characterization of the Structure, Regulation, and Function of CsgD-mediated *Escherichia coli* Biofilms

By

William Henry DePas

A dissertation submitted in partial fulfillment
of the requirements for the degree of
Doctor of Philosophy
(Microbiology and Immunology)
in the University of Michigan
2014

Doctoral Committee

Associate Professor Matthew Chapman, Chair
Assistant Professor Eric Martens
Assistant Professor Lyle Simmons
Professor Michele Swanson

To my parents, Dennis and Mary, and my brother Wade

Acknowledgements

First of all, I would like to thank Matt Chapman for his guidance and support throughout my graduate career. Matt loves life, loves science, and is great at both of them. His curiosity and enthusiasm are infectious, and I knew from the first time I interviewed with him that he would be a fantastic boss to work for. Matt sets the tone of the lab as a fun, open, and productive place to do work. I cannot imagine a better environment to have performed my thesis work in or a better PI to have worked for.

My fellow Chapman lab members have not only been fantastic co-workers, they have been some of my best friends while at the University of Michigan. Specifically Yizhou, Maggie, and Dave have made my time here extraordinarily enjoyable. Yizhou is an amazing scientist who offered patient help no matter how busy she was. She was a constant smiling presence in the lab. Maggie joined the lab at the same time I did, and has been a fantastic friend and colleague for the past five years. Maggie's ideas and opinions have been invaluable, and she has developed her project into one of the coolest stories I have heard of. The trip to Sweden I took with Matt, Maggie, and Yizhou has been one of the highlights of my life. As soon as Dave started rotating, it was obvious that he fit into the lab well, and he has since become a great friend. Dave shares my passion for wrinkled colonies, and seeing him develop into an insightful, independent scientist has been a great experience. I could not imagine a better trio to share five years with. I am confident that Neha will carry on the proud Chapman lab traditions, she is already fitting in very well.

The Chapman lab old guard also deserves a large share of thanks. Neal Hammer trained me well in lab and starcraft techniques, both of which proved useful. Dan Smith's encyclopedic knowledge of all things curli was a valuable resource for me in my early graduate career. Former post-docs Luz Blanco and Matt Badtke were great

friends and taught me a lot of useful techniques. The knowledge base created by all the other former lab members has been a fantastic tool.

I have been fortunate to share lab space with Bob Bender, Blaise Boles, and their respective labs. I cannot think of anything about *E. coli* metabolism that Bob does not know. He is a fun and knowledgeable mentor. Bob's last graduate student, Ryan Frisch, was also a great colleague. Even though I was a young roton in a different lab, Ryan went out of his way to teach me techniques and science that I still use to this day. Seeing Blaise start a faculty job and succeed immediately has been fun and inspirational. He has been a great resource. The Boles lab has offered up an energetic, intelligent group of people to do science with. Kelly, Adnan, Dave, Matt, Matt, and Rachel have been nothing but supportive and helpful during my time here. They have also been very good friends. I've had the opportunity to work most with Adnan due to his love of making agar plates out of various substances and his appreciation for all things ecological. Collaborating with him on chapter 4 was a great experience.

My undergraduate and masters research assistants, David Warshaw, John Lee, and Vinay Saggar, have been very helpful, and working with them has been a lot of fun. Without their hard work and willingness to take on new projects, I would have a much narrower and less exciting dissertation.

My committee has been amazingly supportive throughout my graduate career. They were constantly offering suggestions, reagents, and time, all of which helped me along.

Being in the Microbiology and Immunology department while residing in an MCDB lab has often presented logistical problems, but both department staffs have been amazing and infinitely patient while dealing with me. Heidi Thompson and Mary Carr specifically have been awesome. Gregg Sobocinski has been a huge help with the imaging aspects of my project.

I would also like to thank the Rackham graduate school and the Genetics Training Grant for providing me with funding.

Most importantly, I would like to thank my family for their constant support and encouragement.

Table of Contents

List of Figures

List of Tables

Chapter 1
General Introduction

Escherichia coli

Basic Phylogeny and Biology

Escherichia coli is a fascinatingly diverse organism. While the typical *E. coli* genome contains roughly 4800 genes, only 2000 or so are shared by every *E. coli* strain (1). In total, the full complement of *E. coli* genes numbers to roughly 16,000 (1, 2). Such genomic plasticity permits *E. coli* strains to colonize numerous ecological niches and participate in various commensal and pathogenic interactions with its mammalian and reptilian hosts (3, 4). *E. coli* is one of the first bacteria to colonize the intestinal tract of human infants, where it establishes a stable population of roughly 10^8 CFUs/g of feces by adulthood (4-6). As a facultative anaerobe, *E. coli* is well-adapted to the oxygen limiting intestinal tract, as it can reduce several alternate electron acceptors such as nitrate, fumarate, DMSO, and TMAO (7). Mice colonization studies have revealed that in the intestine fumarate reductase, nitrate reductase, and *bd* oxidase (high affinity oxygen cytochrome) are particularly important for *E. coli* fitness (8, 9).

Pathogenesis

By acquiring specific virulence factors, *E. coli* strains can colonize and cause disease at different sites in the human body (3). Intestinal pathogenic *E. coli* (IPEC) cause gastroenteritis by interacting with and adversely affecting intestinal epithelial cells (3, 10). There are a variety of IPEC subtypes, most of which can be characterized and identified by the presence of specific virulence genes (3). For instance, enteropathogenic *E. coli* (EPEC) harbor a pathogenicity island called the locus of enterocyte effacement (LEE). Included in the LEE are genes that encode a type III secretion system as well as various effector molecules (11, 12). EPEC is a common cause of infant diarrhea in developing countries as well as travelers' diarrhea (3).

Enterohemorrhagic *E. coli* (EHEC) is a pathogenic subtype that encodes the LEE pathogenicity island and also produces shiga toxin (13). Shiga toxin inactivates the host 60S ribosomal subunit, halting protein synthesis and leading to apoptosis (14). EHEC can cause serious gastrointestinal disease such as hemolytic uremic syndrome (HUS), and is a source of food poisoning outbreaks worldwide (13). There is currently no effective treatment for EHEC infections, and antibiotics can induce expression of shiga toxin, leading to exacerbation of disease symptoms (15, 16).

Some *E. coli* strains have adapted to cause disease at sites in the human body other than the intestinal tract. Collectively, these bacteria are termed extraintestinal *E. coli* (ExPEC). ExPEC infection can lead to neonatal meningitis, sepsis, and urinary tract infections (UTIs), with UTIs being the most common ExPEC infection (17). Indeed, uropathogenic *E. coli* (UPEC) account for roughly 80% of the uncomplicated UTIs in the US (18). In contrast to IPEC, there doesn't seem to be a unique set of virulence factors that are specific to UPEC. However, UPEC strains are well-adapted to the bladder environment (19). Specifically, urine is iron-limiting, and UPEC expresses at least 10 iron acquisition systems (20, 21). Vaccines raised against outer-membrane iron-receptors are effective at protecting mice against UTIs (22, 23). Zinc receptors also contribute to UPEC fitness in the bladder (24).

The first step in UPEC infection is ascension up the urethra, a process that requires flagella (25, 26). Once in the bladder, fimbriae aid in the attachment of UPEC to epithelial cells. Type 1 pili are particularly important for bladder colonization. The FimH subunit of type 1 pili binds to mannosylated glycoprotein receptors, mediating UPEC attachment to uroepithelial cells (27-29). Multiple receptors for FimH have been reported, including uroplakins and β1 and α3 integrins (30, 31). UPEC is also able to invade uroepithelial cells (32). Cell invasion is first initiated by type 1 pili-mediated attachment (27). Entry also involves fusiform vesicles. Apical exocytosis of fusiform vesicles helps regulate bladder volume, and drugs that increase exocytosis can decrease the number of intracellular *E. coli* in a mouse UTI model (33). Once in the cytosol, UPEC can rapidly divide and form polysaccharide encased cellular aggregates termed intracellular bacterial communities (IBCs) (34, 35). IBC formation helps UPEC

evade the immune response, and can likely serve as a reservoir for recurrent infections (25, 36).

Transmission

E. coli is transmitted from host to host by the fecal-oral route. A large body of work exists investigating how EHEC strains, particularly EHEC O157:H7, make their way from environmental reservoirs to humans (37). The intestinal tract of domesticated cattle serves as the primary reservoir for EHEC in the United States (38, 39). Intestinal EHEC can contaminate meat during the slaughter process. Additionally, EHEC is shed in feces of contaminated animals and can survive in manure for months (38, 40-42). Contact with animal feces is a risk factor for spontaneous EHEC infections, and the use of untreated manure can result in contaminated produce (37, 43-45). While contaminated manure or water can directly inoculate the surface of plants, there is also evidence that EHEC can also invade plant tissue (44-46).

ExPEC transmission is not as well characterized as that of IPEC, but evidence suggests that ExPEC can also spread via the fecal-oral route (47). ExPEC can be found on food products, and outbreaks of UTIs caused by UPEC have been reported (48, 49). The primary source of UPEC that colonizes the urethra is a patient's own intestinal tract (50). UPEC seems to be able to live in the intestine without causing any disease, and recent work has shown that UPEC has no fitness defects in the gut environment when compared with commensal *E. coli* strains (51).

Once *E. coli* is excreted in stool there is generally a net-negative fitness cost compared to growth in most host environments (6, 52). However, as *E. coli* is constantly being excreted, it has been estimated that half of the *E. coli* cells on Earth exist outside the host (6). The factors influencing survival outside the host have been described most extensively for IPEC, namely for common EHEC strains. One major factor affecting persistence in the non-host environment is the production of matrix encased bacterial communities called biofilms.

Biofilms

A biofilm is a group of surface-associated bacteria encased in a self-produced extracellular matrix. Biofilm formation correlates with resistance to a variety of environmental stresses, including antibiotics, the immune system, and predation (53).

Biofilms confer protection through at least two distinct mechanisms. First, the extracellular matrix forms a physical barrier that can resist shear stress and recognition and phagocytosis by immune cells (53). Secondly, bacteria within biofilms often assemble into subpopulations that have distinct physiological characteristics. Subpopulation development can be triggered by mutations, stochastic gene expression, or chemical gradients that develop during biofilm formation (54-57). For instance, bacteria at the biofilm surface are exposed to more oxygen, causing them to undergo a higher rate of aerobic respiration (54, 58, 59). Metabolic changes often coincide with resistance to different stresses (56, 60). A biofilm community with multiple subpopulations, each resistant to differing stresses, therefore confers a broader range of stress resistance to the biofilm community as a whole (54, 56, 60).

Bacteria use varying extracellular polymers to produce the biofilm extracellular matrix. In general, bacteria secrete proteins, polysaccharides, and DNA as biofilm components. In laboratory conditions a number of components can contribute to *E. coli* aggregation. These include type 1 pili, flagella, antigen 43, β-1,6-N-acetylglucosamine (β-1,6-GlcNAc), capsule sugars, colonic acid, curli fibers, and cellulose (61). Curli and cellulose are generally co-expressed due to their mutual dependence on the transcriptional regulator CsgD (62-64) (Fig. 1.1).

CsgD-mediated Biofilms

CsgD is a FixJ/LuxR/UhpA type response regulator (62). The C-terminus of CsgD, like most response regulators, contains a typical helix-turn-helix DNA-binding domain (62). The N-terminus of response regulators gets phosphorylated by a partner histidine kinase, leading to altered DNA-binding capabilities (65-67). Alternately, the N-terminus of response regulators can respond to small molecule signals (67, 68). CsgD, like other atypical response regulators, lacks conserved aspartic acid residues in the N-terminal region that are necessary for phosphorylation (69, 70). However, acetyl phosphate can phosphorylate CsgD *in vitro*, and the presence of acetyl phosphate reduces CsgD's ability to bind particular promoters (69).

The expression of *csgD* is controlled by a large, and still-expanding, list of transcriptional regulators and small RNAs (71, 72). In general, low salt, low temperature, and the absence of glucose trigger *csgD* expression (62, 71, 73-75).

Additionally, *csgD* expression requires the stationary phase sigma factor RpoS (63, 76), and is controlled by the small molecule cyclic-di-GMP. (77). Multiple diguanylate cyclases or phosphodiesterases, enzymes that produce or degrade cyclic-di-GMP respectively, affect the levels of CsgD in the cell (78, 79). However, the mechanism by which cyclic-di-GMP controls CsgD is unknown.

CsgD controls a modest regulon of roughly 13 genes/operons (62, 80-82). Notably, CsgD induces expression of the RpoS stabilizing protein IraP, leading to a relay system in which CsgD requires RpoS for expression and causes increased RpoS stability (81). CsgD also directly represses the flagella biosynthesis genes *fliE* and *fliF* (82). Finally, CsgD induces expression of two biofilm matrix components, curli and cellulose (Fig. 1.1).

The Basics of Curli

Curli were identified in both *E. coli* and *S. enterica* ser. Enteritidis as fibronectin-binding fibers (73, 83). Curli production has since been reported in various *Salmonella* spp., *Citrobacter* spp. and *E. coli* strains (63, 84-87). It is now recognized that curli regulation, assembly, and operon structure is well conserved among members of the *Enterobacteriaceae* (63, 64, 88, 89). Curli biogenesis initiates with expression of *csgD*. CsgD directly activates the *csgBAC* operon (62, 82) (Fig. 1.1). CsgA is the major curli fiber subunit that polymerizes into an amyloid fiber on the cell surface (90). The minor fiber subunit CsgB templates fiber polymerization and, along with the accessory protein CsgF, helps attach curli fibers to the cell surface (91-94). Both CsgA and CsgB are secreted through the inner membrane via the SecYEG complex and then through the outer membrane via the lipoprotein CsgG (Fig. 1.2A) (95, 96). CsgG is encoded in the *csgDEFG* operon, so its expression, along with the expression of the curli accessory proteins CsgE and CsgF, coincides with expression of the curli subunit genes. During curli expression, CsgG forms discrete puncta on the cell surface that are aggregated around curli fibers (97).

Curli fibers were the first described extracellular fibers to polymerize by the nucleation-precipitation mechanism (91, 92, 98). CsgB provides a template on the cell surface that allows secreted CsgA to adopt an amyloid fold and form cell-associated fibers (93). A *csgB* mutant secretes unfolded CsgA that can polymerize on the surface

of a *csgA* mutant (which presents a surface-associated CsgB), in a process called 'interbacterial complementation' (91, 98) (Fig. 1.2B). Zhou *et. al.* demonstrated that curli subunits from three different species could cross-seed *in vitro*. Furthermore, interbacterial complementation between *E. coli* and *S. enterica* ser. Typhimurium was observed *in vivo*. Interspecies curli production restored agar adherence to mixed species bacterial communities (88).

Amyloid Properties of Curli

A fascinating aspect of curli fibers is that they are biochemically defined as amyloid (98). β-sheet amyloid fibers have long been the hallmark of human neurodegenerative diseases, but amyloids are increasingly appreciated as a functionally diverse protein fold. Amyloids are remarkably stable protein polymers that form β-sheet rich fibers with a diameter of 5-10 nm. The amyloid fold is unique in that it is adopted by a variety of proteins with varying primary sequences.

The first step in amyloid fiber formation is aggregation of monomers into intermediate oligomers, or seeds. Once seeds form, they nucleate rapid fiber elongation, with the final amyloid structure being essentially a stack of β-sheet rich monomers, aligned so that each β-strand is perpendicular to the fiber axis (Fig. 1.3). Dense hydrogen bonding between adjacent β-sheets then provides fiber stability (99-105). Amyloidogenic proteins can polymerize in the absence of an energy source, so it is not surprising that amyloid fibers such as CsgA are a common component of the microbial extracellular matrix, where energy sources can be scarce and environmental conditions can wreak havoc on lesser protein folds (98, 106-110).

The necessary structural features of an amyloid fiber, β-sheet formation and hydrogen bonding between β-sheets, are partly conferred by the polypeptide backbone and do not require complex amino acids (111-115). These properties are proposed to lend themselves to the universality of the amyloid fold, and, indeed, there is a hypothesis that the amyloid fold, with its tendency towards elementary amino acid composition and resistance to harsh environmental conditions, was a fundamental structure in the early history of life (116). Most proteins can adopt the amyloid fold, although the majority of 'non-native' amyloids require exposure to harsh denaturing conditions to destabilize their native structure before they can re-organize into an

amyloid (117-119). Conversely, some proteins readily form amyloids. These polypeptides often contain specific regions that promote the amyloid fold (120-122). Transfer of amyloidogenic stretches of amino acids to normally non-amyloidogenic proteins can force amyloid formation (123, 124).

Similarly, the amyloid fold confers common biophysical characteristics to proteins that might be dissimilar at the primary sequence level. For instance, a defining characteristic of an amyloid, regardless of primary amino acid sequence, is the ability to bind certain dyes such as Congo red and thioflavin T (125). Additionally, antibodies have been designed that recognize general epitopes of amyloid fibers or amyloid oligomers (108, 126-129), and small molecules have been identified that affect fiber formation of multiple amyloids (130).

Amyloids have been thoroughly studied because of their historical association with neurodegenerative conditions such as Alzheimer's disease. The Alzheimer's amyloid β (Aβ) peptide was one of the first described disease-associated amyloids and is among the most thoroughly studied (131). Amyloid formation is also the hallmark of Parkinson's disease (132), Huntington's disease (133), and type II diabetes (134). Because amyloid fibers were identified in connection with various diseases, it was assumed that amyloid fibrils themselves were toxic (135). Although new data suggest that mature amyloid fibers are relatively inert, non-cytotoxic, and maybe even protective (135). Instead, amyloid-related toxicity is likely caused by small oligomers formed as an intermediate step in fiber polymerization (127, 135-138). Indeed, the oligomeric species of various disease causing amyloids have been shown to be toxic (139-141).

How *E. coli* Safely Manipulates Curli Biogenesis

Because of the toxicity inherent to amyloid proteins, a good deal of research has been dedicated to describing how *E. coli* safely wields amyloid proteins such as CsgA. Since small oligomers are widely considered to be the toxic species in amyloid formation, one mechanism for avoiding toxicity has been hypothesized to be rapid passage through the oligomeric stage (142). In agreement with this hypothesis, *E. coli* uses a nucleator protein, CsgB, to seed rapid polymerization of the major curli component, CsgA, on the cell surface (Fig. 1.1A). CsgB itself can form amyloid fibers *in vitro* and the addition of CsgB seeds allows CsgA to bypass the characteristic lag phase

associated with amyloid fiber formation (93, 143). Specific amino acids in CsgA mediate interaction between these two fiber subunits, and mutation of these residues results in a CsgA protein that is secreted from the cell in a soluble state (90, 144). The main functions of CsgB *in vivo* then seem to be templating extracellular CsgA amyloid formation and, along with the surface-exposed CsgF protein, anchoring CsgA fibers to the cell (93, 94), outlining a model where CsgA monomers are kept unfolded and soluble until they are transported across the outer-membrane where they encounter CsgB seeds. CsgA then rapidly folds into an amyloid fiber, potentially bypassing the toxic oligomeric stage.

Perhaps the most direct mechanism for avoiding amyloid toxicity is through manipulation of the amyloid protein's primary amino acid sequence. The chief component of curli fibers, CsgA, is able to polymerize into amyloid fibers in a wide variety of environmental conditions (145). These results contrast with non-native amyloids that need to be exposed to specific, destabilizing conditions to aggregate (117, 146, 147). Investigations into the primary sequence of CsgA have revealed that particular residues play crucial roles in the polymerization of this amyloid-by-design. The amyloidogenic domain of CsgA is composed of 5 imperfect repeats (R1-R5) that share 30% amino acid identity to each other (148, 149). The two terminal repeating subunits, R1 and R5, readily form amyloid fibers *in vitro*, while R2 and R4 do not form fibers and R3 forms short, fibrous aggregates (150). Wang *et. al*. demonstrated that R2, R3, and R4 contain 'gatekeeper' residues that inhibit the aggregative propensity of these peptides and therefore the entire CsgA protein (151). A CsgA mutant in which the gatekeeper residues were substituted with amino acids that bolster amyloid formation, CsgA*, polymerized more rapidly than WT CsgA *in vitro* and formed mislocalized fibers without the need for CsgB *in vivo*. Overexpression of CsgA* was significantly more toxic to the cell than overexpression of WT CsgA (151). These data indicate that the CsgA protein sequence has evolved specific traits to allow for manageable amyloid formation by the cell. Additionally, both curli fiber components, CsgA and CsgB, indeed the majority of secreted proteins, are composed of a disproportionate amount of inexpensive amino acids (152), indicating that the CsgA protein is designed for both safe amyloid formation and for cost-effectiveness.

A third mechanism to control amyloid formation is the use of cellular chaperones. In curli biogenesis, the role of CsgB as an outer-membrane nucleator implies that CsgA must be maintained in a soluble, unfolded state as it is trafficked through the cytoplasm and periplasm. Consistent with this hypothesis, various *E. coli* chaperones, including cytoplasmic DnaK and Hsp33 and periplasmic Spy, were demonstrated to inhibit CsgA aggregation (153). Once in the periplasm, CsgA encounters a specificity factor for curli secretion, CsgE. In addition to trafficking unfolded CsgA to the outer-membrane pore CsgG during secretion, CsgE has been demonstrated to inhibit CsgA polymerization *in vitro* (154, 155). These data are consistent with a model of CsgA maintaining an unfolded, unstructured state on its voyage through the cytoplasm and periplasm, and it appears that various cellular chaperones are able to inhibit inappropriate CsgA aggregation before secretion.

The Basics of Cellulose

Bacterial cellulose production was first described in 1887, and *Gluconacetobacter xylinus* has been a model organism for the study of cellulose biosynthesis for decades (156-158). It was not until 2001, however, that cellulose production by the *Enterobacteriaceae* family was described (64). Cellulose is a polysaccharide composed of linear chains of (1,4)-β-linked glucose monomers. Most non-K12 *E. coli* strains can produce cellulose as a component of the biofilm matrix (64, 84-86, 159). However, K12 *E. coli* strains do not produce cellulose (64, 159). In the case of *E. coli* W3110, the cellulose defect is due to a mutation in *bcsQ*, and repairing *bcsQ* on the chromosome restores cellulose synthesis (160). CsgD modulates cellulose synthesis by activating transcription of *adrA*, and deletion of *adrA* ablates cellulose production in most *E. coli* and *S. enterica* ser. Typhimurium strains (64, 85, 159, 161) (Fig. 1.1). AdrA contains a GGDEF domain typical of diguanylate cyclases (161, 162). *E. coli* and *S. enterica* encode a number of diguanylate cyclases and phosphodiesterases to regulate cytoplasmic levels of cyclic-di-GMP (78, 79, 162). AdrA presumably activates the cellulose synthase BcsA via cyclic-di-GMP production, as BcsA contains a cyclic-di-GMP binding PilZ domain (163, 164) (Fig. 1.1). Some *E. coli* strains have been reported to produce cellulose independently of CsgD. At least one of these strains, *E. coli* 1094, utilizes the diguanylate cyclase YedQ in place of AdrA (159).

Curli and Cellulose *in vivo*

Various interactions between curli and host systems have been reported. Curli mediate binding to and internalization by host cells (165-167), with these attributes being at least partly imbued by curli's fibronectin-binding capacity (73, 168). Curli have also been shown to interact with major histocompatibility complex I (MHC-I), but whether or not the amyloid properties of curli fibers affect these interactions is unclear (169).

In contrast, the amyloid properties of curli might impact human amyloidosis. Amyloidosis is a condition in which aberrantly folded amyloids deposit on tissues or organs, disrupting proper function and causing inflammation (170). AA amyloidosis results from the abnormal deposition of a protein fragment from the typically soluble serum amyloid A (SAA) protein. These aggregates can be seeded by small SAA fragments, and indeed by other amyloid-like fibrils, thus exacerbating the symptoms of amyloidosis (171-174). Lundmark *et. al.* showed that exogenously added amyloid-proteins including Sup35 from *Saccharomyces cerevisiae*, silk from *Bombyx mori*, and either purified curli or curliated *E. coli* increased the occurrence of SAA aggregates in mice (175). Further work exploring whether there are direct interactions between SAA and microbial amyloids will help to clarify the role of cross-seeding in amyloidosis.

There is strong evidence that the cross-β structure of curli fibers interferes with host blood clotting mechanisms (176). Fibrin, a major component of blood clots, displays a cross β-sheet structure and other amyloid-like characteristics (177). Fibrin activates the mammalian tissue-type plasminogen activator (tPA) by promoting contact between tPA and its substrate, plasminogen. tPA can then cleave plasminogen into the active serine protease plasmin, which degrades fibrin and results in blood clot dissolution. (178). Kranenburg *et. al*. showed that the cross-β structure specifically allows for tPA activation (177). Indeed, various other amyloid-like proteins, such as Aβ and IAPP (the amyloid associated with β-cell toxicity in type II diabetes) have been shown to effectively activate tPA and trigger the degradation either of themselves or of fibrin (177, 179). Curli, either purified or on the surface of *E. coli* or *S. enterica*, is both able to sequester tPA and plasminogen from plasma, and both of these proteins are functional when bound to curliated bacteria (180).

Curliated *E. coli* and *Salmonella spp*. are also able to interfere with the host contact system, which is an enzymatic cascade triggered when blood contacts surface material (176). As part of the contact cascade, the activated form of plasma zymogen Factor XII (FXII) can cleave another plasma protein, high-molecular weight kininogen (HK). Cleavage of HK results in the release of the peptide hormone bradykinin (BK), which leads to an inflammatory response. Curliated *E. coli* or *S. typhimurium* can bind and sequester various contact phase proteins such as FXII, HK, and fibrinogen, resulting in release of the pro-inflammatory signals BK and fibrinopeptides (181-184). Intriguingly, although the *in vivo* activators of FXII are not completely understood, Maas *et al.* demonstrated that various unfolded proteins, including pre-fibrillar Aβ, induce FXII autoactivation (185), leading to the question of the folding state of CsgA upon binding to FXII. Concurrent with an increase in inflammation, curliated bacteria reduced clotting in isolated plasma as well as in an *in vivo* mouse model, likely due to curli-mediated sequestration of blood clotting elements such as fibrinogen (182-184). Bian *et. al*. demonstrated that serum from patients diagnosed with *E. coli* bacteremia contained anti-CsgA antibodies, while no such antibodies were present in sera from healthy patients (186). Finally, *E. coli* isolated from sepsis patients is more likely to produce curli at high temperatures than *E. coli* isolated from patients without sepsis (187). Collectively, these results allude to the interesting hypothesis that bacteria could use curli, and potentially other amyloids, as a mimetic of host amyloids to trigger specific pathways.

The importance of amyloid fibers in microbial pathogenesis is further cemented by reports of interactions between curli and the immune system. Human macrophages produce increased levels of pro-inflammatory cytokines, including interleukin-8 (IL-8), when exposed to curliated *E. coli* compared to non-curliated *E. coli* (186). Likewise, mice injected with *E. coli* showed curli-dependent increases in expression of nitric oxide synthase, increases in nitric oxide levels, and decreased blood pressure (188). In studies with *S. typhimurium*, curli-mediated induction of nitric oxide and IL-8 in HEK293 cells depends on the host toll-like receptor 2 (TLR2) (189, 190). Different bacterial structures are recognized by varying TLRs, either alone or in combination. For example, TLR2 can also bind lipoprotein, lipoteichoic acid, and peptidoglycan (191, 192). TLR4

recognizes LPS (193), and TLR5 recognizes flagellin (194). Once bound, a signaling cascade is triggered that results in an immune reponse. TLR5 is specific for flagellin, and cannot be activated by fibrous flagella (195). In contrast, only CsgA curli polymers fully stimulate TLR2 induction of HEK293 cells, while monomeric CsgA has little activity (190). Interestingly, another amyloid, Aβ fibers, induces IL-8 production in human macrophage-like (THP-1) cells in a TLR2-dependent-manner (190). The same pattern was observed with Nos2 mRNA production in microglia cells (190). TLR2 has independently been shown to recognize Aβ fibers as well as SAA, indicating that it may function partly as a general amyloid receptor (196-200). However, curli fiber recognition additionally involves TLR1 and CD14 signaling, while Aβ recognition also involves TLR4 and TLR6, indicating that the interactions between amyloids and the immune system are likely complex (200-203).

Amyloids also interact with host-derived antimicrobial peptides (AMPs). LL-37 is a human AMP important for resistance to bacterial infection of the urinary tract (204), and curli was expressed on 59% of *E. coli* urinary tract infection (UTI) isolates (205). Expression of curli increased *E. coli* survival after LL-37 exposure in broth culture. Additionally, LL-37 was shown to bind to curli fibers and monomers by surface plasmon resonance and inhibit *in vitro* polymerization of CsgA (206), implying a dynamic interplay between LL-37 and CsgA within the host. In the same study, cellulose dampened the immune response against *E. coli* in a UTI mouse model (206).

Curli and Cellulose *in vitro*

In the Non-Host Environment

In *S. enterica*, curli and cellulose expression provide resistance to desiccation, bleach, and chlorine stress (207-209). EHEC curli expression increases attachment to produce and abiotic surfaces (210, 211). The environmental conditions that favor *csgD* expression -- low temperatures, low salts, low sugars -- suggest that CsgD-mediated biofilms are important outside the host. Indeed, an expression study in *S. enterica* demonstrated that the curli promoter was not induced during passage through a mouse host, but was activated once the bacteria were excreted in feces (208).

Laboratory Models of Biofilm Formation

In laboratory conditions, *E. coli* produces at least two distinct biofilm types that are dependent on various extracellular polymers (61, 64, 212-214). The first type relies on type-1-pili, Poly-β-1,6-GlcNAc, antigen 43, and flagella (212, 213, 215) (216). (Fig. 1.4A). This type of biofilm only manifests as rings of biomass around the air-exposed edges of polyvinyl chloride wells.

The second major biofilm type relies on expression of the CsgD-regulated matrix components curli and cellulose. Glucose, temperatures >30°C, and high salt content inhibit CsgD-mediated biofilms (75, 76, 212, 217). In contrast to the first type of biofilm, curli/cellulose-dependent biofilms can manifest in a variety of ways (Fig. 1.4). In liquid low-salt media at room temperature, *E. coli* can form ring biofilms around the edge of 96-well polyvinyl chloride plates (212) (Fig. 1.4B). Additionally, *E. coli* can form pellicle biofilms in wells of 24-well polyvinyl chloride plates (212) (Fig. 1.4C). Pellicles are thick sheets of curli/cellulose-encased cells that span the entire air-liquid interface of a single well (212, 214, 218). While curli and cellulose are the chief components of pellicle biofilms, deletion of type-1-pili leads to a less-robust pellicle, demonstrating that pili are involved in pellicle development (214). Flagella are also required for pellicle development (212, 214). Finally, when grown under *csgD*-inducing conditions on agar plates, *E. coli* will form wrinkled, rugose colony biofilms (64, 85, 219) (Fig. 1.4D). While flagella are not required for the wrinkled colony morphotype, rugose biofilms contain an interior population of heavily flagellated cells (220).

Rugose Biofilms

E. coli is one of a variety of bacterial species that produce wrinkled colony biofilms on agar plates. The nomenclature for this phenotype varies between species, but common names are rugose biofilms, wrinkled colony biofilms, and red dry and rough (rdar) biofilms. For the purpose of this thesis all colony biofilms on agar plates will be referred to as rugose biofilms. The mechanics of rugose biofilm formation have been studied extensively in *Vibrio cholerae*, *Pseudomonas aeruginosa*, *Bacillus subtilis*, *E. coli*, and *S. enterica* ser. Typhimurium (64, 74, 77, 221-227).

V. cholerae displays two distinct colony variants, smooth and rugose (228). Rugose colony development correlates with increased production of *Vibrio* polysaccharide (VPS) and an increase in cyclic-di-GMP (229, 230). The transcriptional

regulators VpsR and VpsT are responsible for inducing the *vps* biosynthetic genes during rugose colony development (222, 223, 231, 232). *V. cholerae* rugose colony formation is correlated with increased resistance to stresses that could be encountered in the non-host environment, including chlorinated water, flagellate predation, and osmotic and oxidative stress (221, 230, 233).

P. aeruginosa forms polysaccharide-dependent rugose biofilms that are finely tuned to the redox state of the cell. The increased surface area conferred by rugose colony development exposes more *P. aeruginosa* cells to molecular oxygen when terminal electron acceptors are limited (225, 234). The production of phenazines, small redox active electron shuttles, allows respiration to occur deeper within the biofilm and therefore prevents colony wrinkling (225).

B. subtilis produces both amyloid fibers and polysaccharides in rugose biofilms (109), the formation of which is induced by iron and dependent on cellular redox balance (227). Cell death can also trigger wrinkle formation (224). The surface of *B. subtilis* rugose biofilms is very resistant to gas exchange, due to both its composition and shape (226). Enough evaporation happens at the surface, however, to drive liquid flow through individual wrinkles (235).

Rugose Biofilms In *Enterobacteriaceae*

Rugose biofilms in the *Enterobacteriaceae* family have been most extensively described in *E. coli* and *S. enterica* ser. Typhimurium. Curli and cellulose are required for rugose development, and are the major extracellular structures in the rugose biofilm matrix (64, 236). *E. coli* K12 strains, therefore, do not produce rugose biofilms unless the defect in cellulose synthesis is repaired (160). However, recent isolates of commensal *E. coli*, ExPEC, and IPEC form rugose biofilms (85, 86, 237, 238). Likewise, a higher proportion of *Salmonella* spp. clinical isolates form rugose biofilms as compared to domesticated lab strains (87). Indeed, repeated culturing tends to select for genetic suppressors of biofilm formation in a variety of bacteria (239). Curli, cellulose, and rugose biofilm formation has also been demonstrated in *Citrobacter* spp. (84, 85). The environmental signals leading to rugose development coincide with those affecting CsgD expression (77, 161). As such, cyclic-di-GMP networks play a large role in rugose biofilm development. (77, 79).

Rugose biofilms are a simple model to study various aspects of biofilm formation. When I started my thesis project, I was especially interested in determining how environmental conditions affected *E. coli* rugose biofilm development. My rationale was that insight into natural *E. coli* biofilm regulators would provide information about biofilm function. Therefore, I started my project by testing the ability of various chemicals to affect curli production and rugose biofilm formation in a uropathogenic *E. coli* isolate UTI89. Due to its ability to affect the polymerization of disease-associated amyloids, I was particularly interested in iron (240). Plating UTI89 in low iron conditions resulted in a smooth colony phenotype, although the bacteria still bound to Congo red, a diazo dye that binds to both curli and cellulose (85) (Fig. 1.5). Addition of iron resulted in typical rugose biofilm formation (Fig. 1.5). Throughout my thesis work, I have utilized iron and rugose biofilm formation to address three overarching questions.

I.) Iron and Biofilm Architecture

How does iron affect matrix production during rugose biofilm development?

II.) Biofilm Regulation

What regulatory pathways affect rugose biofilm formation?

III.) Biofilm Function

What survival advantages do curli/cellulose-mediated biofilms confer?

Figures:

Figure 1.1 Genetics of *E. coli* biofilm formation
CsgD is a transcriptional regulator that induces expression of *csgBAC* and *adrA*. *csgBAC* encodes the major and minor curli subunits CsgA and CsgB. AdrA is a diguanylate cyclase that produces the small molecule cyclic-di-GMP (c-di-GMP) which activates the cellulose synthase BcsA. Production of curli and cellulose leads to CsgD-dependent rugose colony biofilms on agar plates in the uropathogenic *E. coli* isolate UTI89. CsgD-dependent matrix production can also be probed for by western blotting for the major curli subunit CsgA.

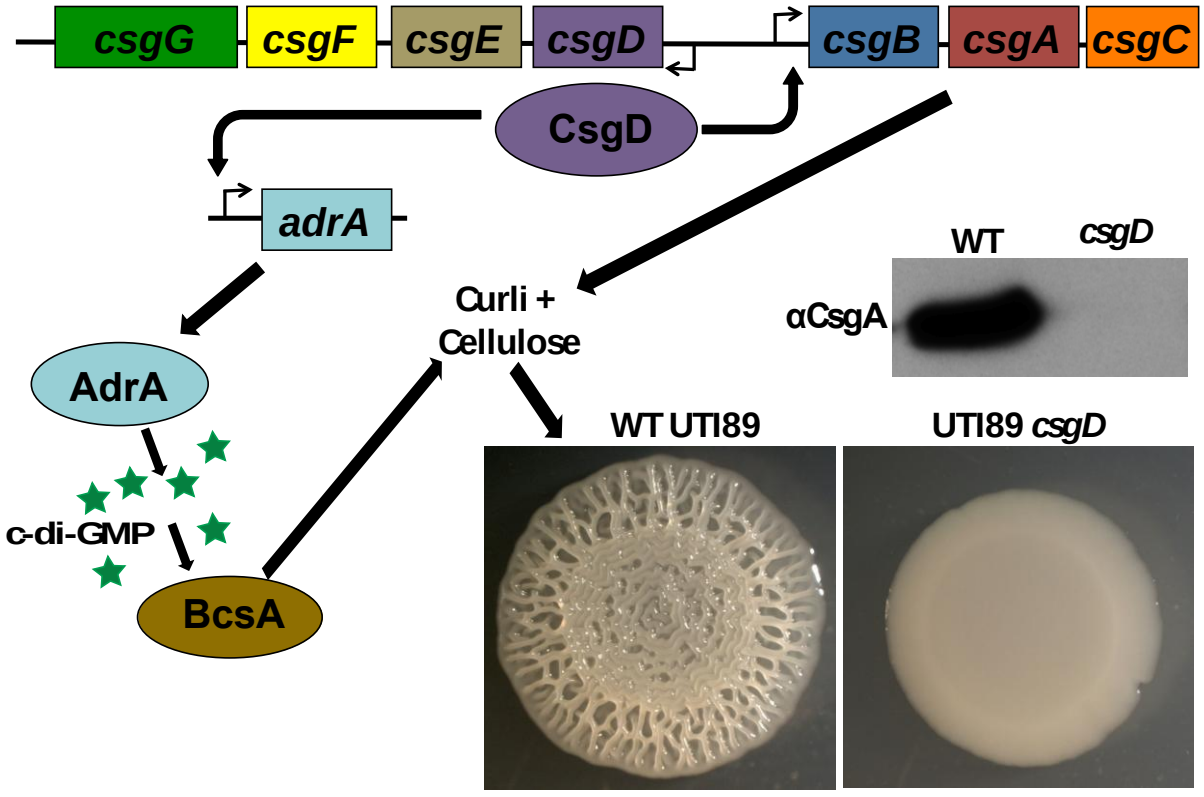

Figure 1.2 Nucleation-precipitation curli fiber assembly
(A) WT *E. coli* secretes soluble CsgA proteins into the extracellular milieu. Once outside the cell, CsgA encounters surface-attached CsgB seeds that nucleate CsgA amyloid formation. **(B)** Inter-bacterial complementation between a CsgA expressing *E. coli csgB* mutant and a CsgB expressing *S. typhimurium csgA* mutant. *E. coli* secretes monomeric CsgA that can interact with CsgB nucleators on the surface of *S. typhimurium.*

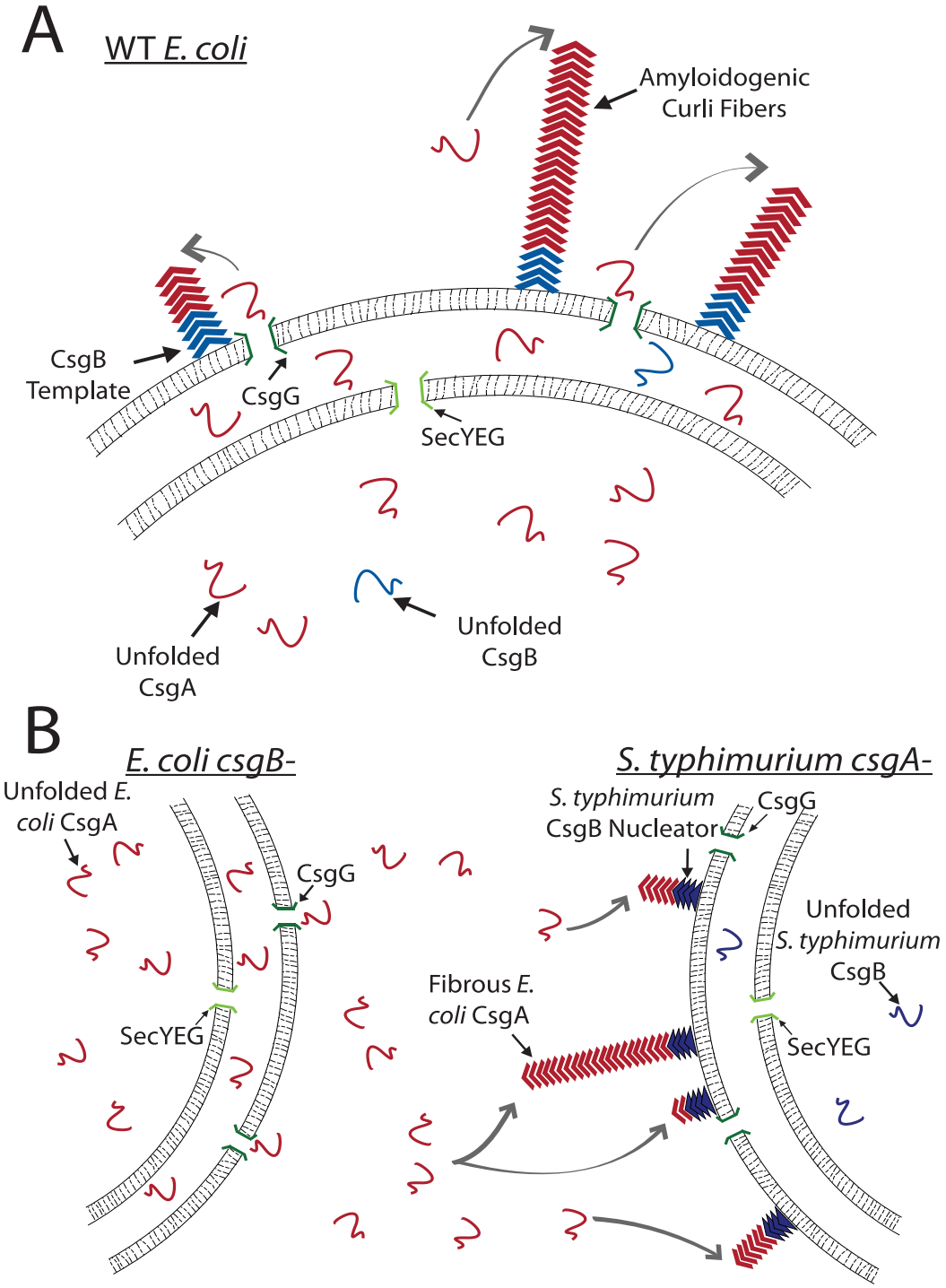

Figure 1.3 General schematic for amyloid polymerization
Unfolded monomers form intermediate oligomers, some of which are toxic, during the lag phase of amyloid assembly. Once the on-pathway oligomers, or seeds, have formed rapid fiber assembly ensues. The lag phase can be bypassed by addition of pre-formed seeds to monomers.

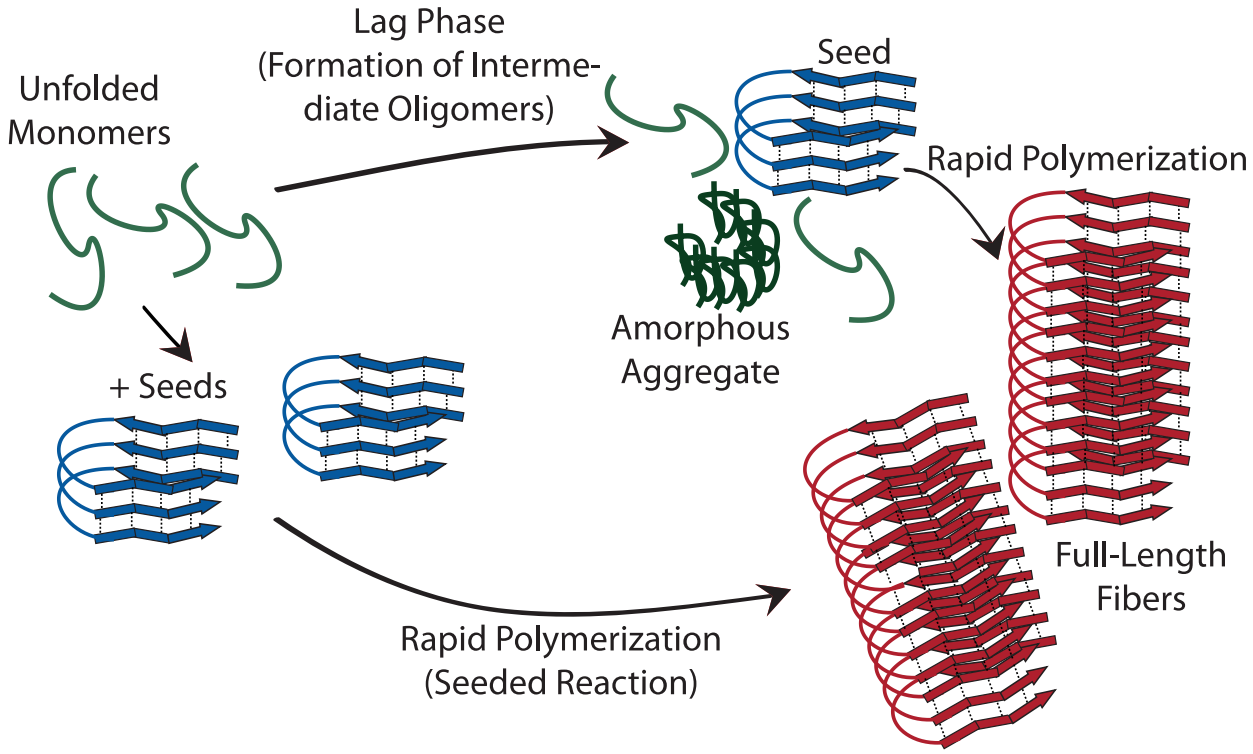

Figure 1.4 UTI89 biofilm models
(A) When grown in LB media, UTI89 can form type 1 pili-dependent biofilms around wells of polystyrene 96-well plates. These biofilms can be stained by crystal violet. **(B)** UTI89 can also form ring biofilms when grown in YESCA media in 96-well plates. However, these biofilms are dependent on curli. **(C)** UTI89 forms curli-dependent pellicle biofilms at the air/culture interface in 24-well plates. These biofilms cover the entire liquid surface. **(D)** When grown on YESCA agar plates, UTI89 forms curli-dependent rugose biofilms.

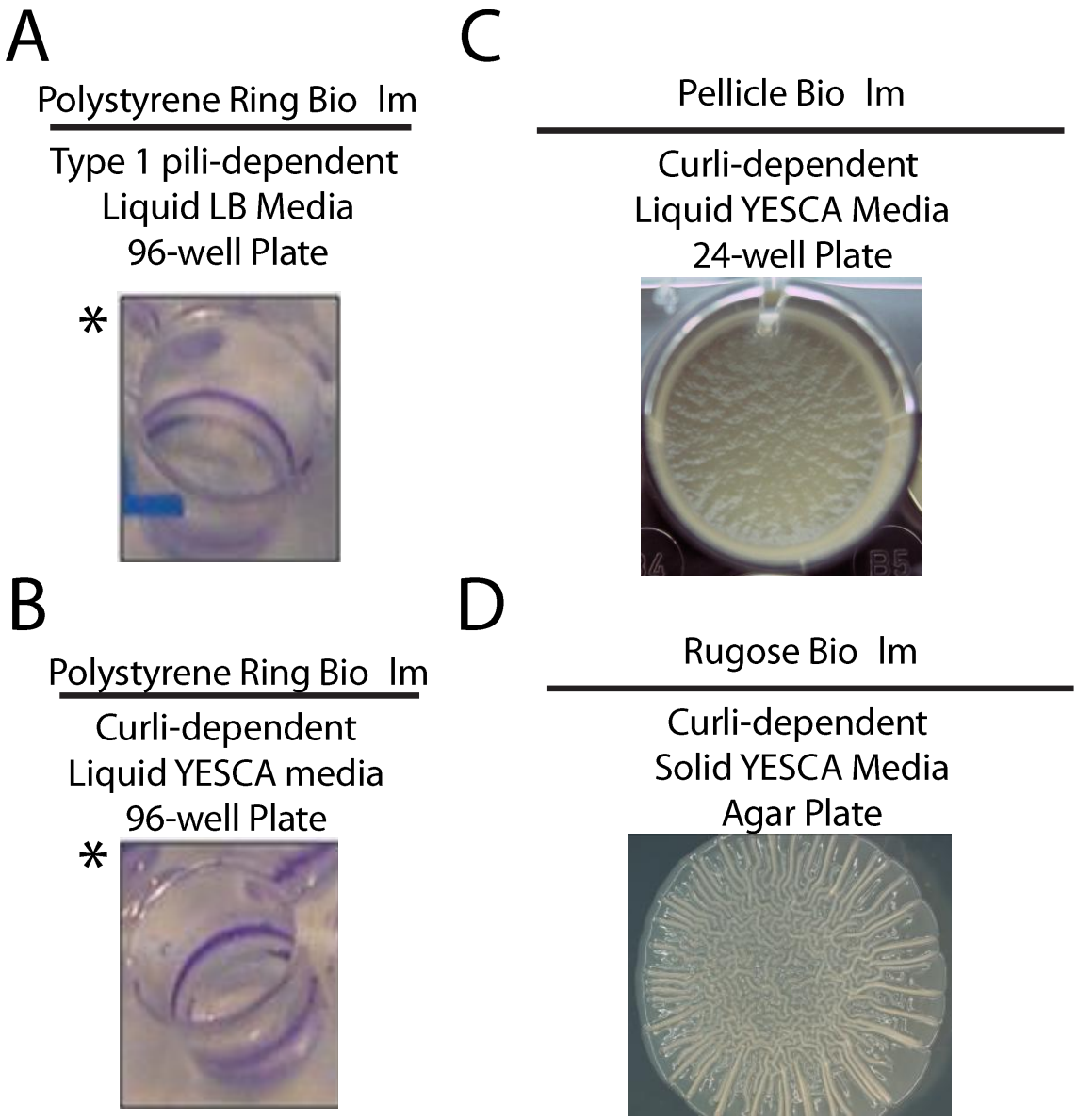

*Adapted from Hadjifrangiskou *et. al.* 2012, *JBac*

Figure 1.5 Iron induces UTI89 rugose biofilm formation
UTI89 was grown ON in LB media, rinsed twice in low iron YESCA media, and plated on low iron YESCA agar plates. On the same plate, a spot of UTI89 mixed with $FeCl_3$ was plated. After two days of growth at 26°C, UTI89 grown in the presence of iron wrinkled. Post-staining with the matrix-binding dye Congo red indicated that matrix was being produced in both conditions.

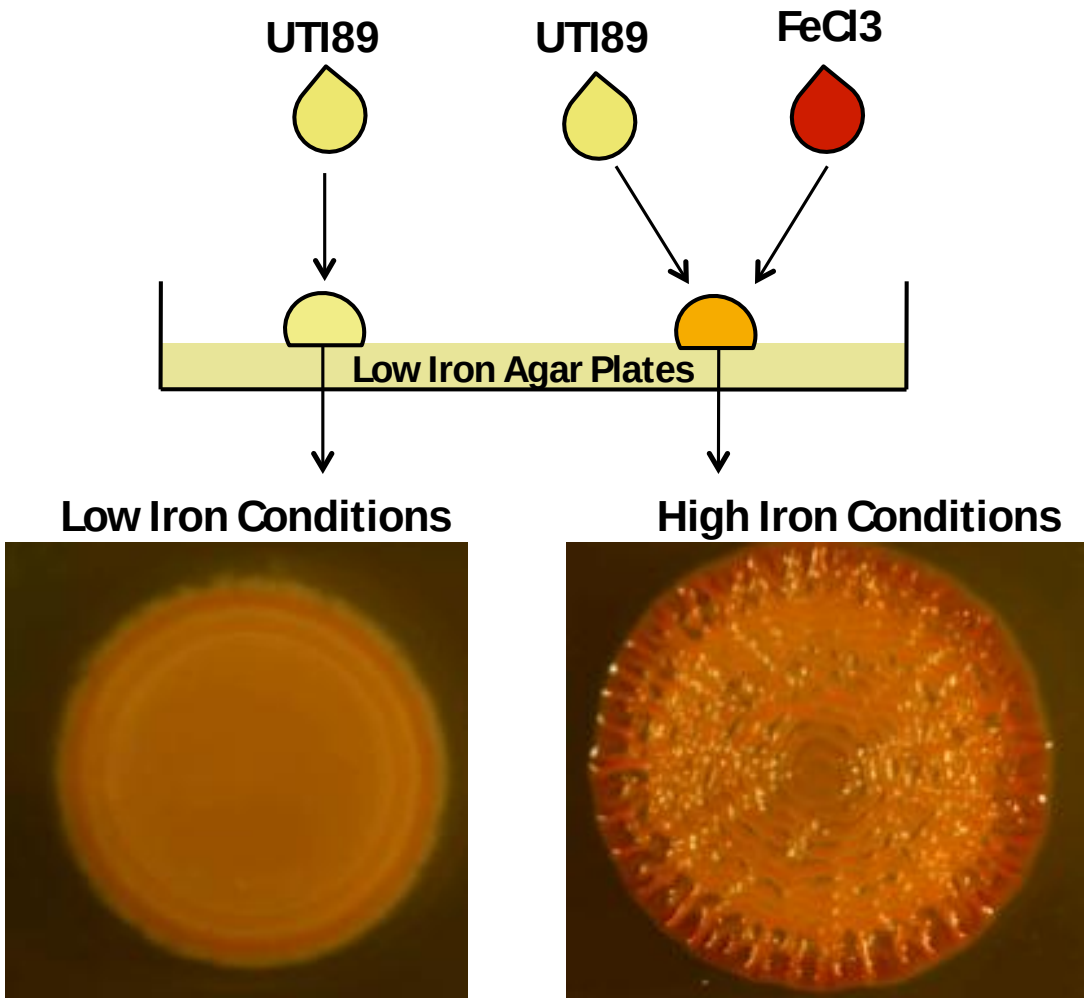

Notes and Acknowledgements:

Portions of this introduction, as well as renditions of Figure 1.2 and Figure 1.3 were published in *Research in Microbiology* (241). Some images for Figure 1.4 were taken from Hadjifrangiskou *et. al*. 2012 *Journal of Bacteriology* (212).

References:

1. **Kaas RS, Friis C, Ussery DW, Aarestrup FM.** 2012. Estimating variation within the genes and inferring the phylogeny of 186 sequenced diverse *Escherichia coli* genomes. *BMC Genomics* **13:**577.
2. **Touchon M, Hoede C, Tenaillon O, Barbe V, Baeriswyl S, Bidet P, Bingen E, Bonacorsi S, Bouchier C, Bouvet O, Calteau A, Chiapello H, Clermont O, Cruveiller S, Danchin A, Diard M, Dossat C, Karoui ME, Frapy E, Garry L, Ghigo JM, Gilles AM, Johnson J, Le Bouguenec C, Lescat M, Mangenot S, Martinez-Jehanne V, Matic I, Nassif X, Oztas S, Petit MA, Pichon C, Rouy Z, Ruf CS, Schneider D, Tourret J, Vacherie B, Vallenet D, Medigue C, Rocha EP, Denamur E.** 2009. Organised genome dynamics in the *Escherichia coli* species results in highly diverse adaptive paths. *PLoS genetics* **5:**e1000344.
3. **Kaper JB, Nataro JP, Mobley HL.** 2004. Pathogenic *Escherichia coli*. *Nature reviews Microbiology* **2:**123-140.
4. **Tenaillon O, Skurnik D, Picard B, Denamur E.** 2010. The population genetics of commensal *Escherichia coli*. *Nature Reviews Microbiology* **8:**207-217.
5. **Mitsuoka T, Hayakawa K, Kimura N.** 1975. [The fecal flora of man. III. Communication: The composition of Lactobacillus flora of different age groups (author's transl)]. *Zentralblatt fur Bakteriologie, Parasitenkunde, Infektionskrankheiten und Hygiene. Erste Abteilung Originale. Reihe A: Medizinische Mikrobiologie und Parasitologie* **232:**499-511.
6. **Savageau MA.** 1983. Escherichia-Coli Habitats, Cell-Types, and Molecular Mechanisms of Gene-Control. *American Naturalist* **122:**732-744.
7. **Unden G, Bongaerts J.** 1997. Alternative respiratory pathways of *Escherichia coli*: energetics and transcriptional regulation in response to electron acceptors. *Biochimica et biophysica acta* **1320:**217-234.
8. **Jones SA, Chowdhury FZ, Fabich AJ, Anderson A, Schreiner DM, House AL, Autieri SM, Leatham MP, Lins JJ, Jorgensen M, Cohen PS, Conway T.** 2007. Respiration of *Escherichia coli* in the mouse intestine. *Infection and Immunity* **75:**4891-4899.
9. **Jones SA, Gibson T, Maltby RC, Chowdhury FZ, Stewart V, Cohen PS, Conway T.** 2011. Anaerobic respiration of *Escherichia coli* in the mouse intestine. *Infection and Immunity* **79:**4218-4226.
10. **Lapointe TK, O'Connor PM, Buret AG.** 2009. The role of epithelial malfunction in the pathogenesis of enteropathogenic *E. coli*-induced diarrhea. *Laboratory investigation; a journal of technical methods and pathology* **89:**964-970.

11. **McDaniel TK, Jarvis KG, Donnenberg MS, Kaper JB.** 1995. A genetic locus of enterocyte effacement conserved among diverse enterobacterial pathogens. *Proceedings of the National Academy of Sciences of the United States of America* **92:**1664-1668.
12. **Jores J, Rumer L, Wieler LH.** 2004. Impact of the locus of enterocyte effacement pathogenicity island on the evolution of pathogenic *Escherichia coli*. *International journal of medical microbiology* **294:**103-113.
13. **Nguyen Y, Sperandio V.** 2012. Enterohemorrhagic *E. coli* (EHEC) pathogenesis. *Frontiers in cellular and infection microbiology* **2:**90.
14. **Bergan J, Dyve Lingelem AB, Simm R, Skotland T, Sandvig K.** 2012. Shiga toxins. *Toxicon : official journal of the International Society on Toxinology* **60:**1085-1107.
15. **Matsushiro A, Sato K, Miyamoto H, Yamamura T, Honda T.** 1999. Induction of prophages of enterohemorrhagic *Escherichia coli* O157:H7 with norfloxacin. *Journal of Bacteriology* **181:**2257-2260.
16. **Wong CS, Jelacic S, Habeeb RL, Watkins SL, Tarr PI.** 2000. The risk of the hemolytic-uremic syndrome after antibiotic treatment of *Escherichia coli* O157:H7 infections. *The New England journal of medicine* **342:**1930-1936.
17. **Pitout JD.** 2012. Extraintestinal pathogenic *Escherichia coli*: an update on antimicrobial resistance, laboratory diagnosis and treatment. *Expert review of anti-infective therapy* **10:**1165-1176.
18. **Foxman B, Brown P.** 2003. Epidemiology of urinary tract infections: transmission and risk factors, incidence, and costs. *Infectious disease clinics of North America* **17:**227-241.
19. **Wiles TJ, Kulesus RR, Mulvey MA.** 2008. Origins and virulence mechanisms of uropathogenic *Escherichia coli*. *Experimental and molecular pathology* **85:**11-19.
20. **Alteri CJ, Mobley HL.** 2007. Quantitative profile of the uropathogenic *Escherichia coli* outer membrane proteome during growth in human urine. *Infection and Immunity* **75:**2679-2688.
21. **Garcia EC, Brumbaugh AR, Mobley HL.** 2011. Redundancy and specificity of *Escherichia coli* iron acquisition systems during urinary tract infection. *Infection and Immunity* **79:**1225-1235.
22. **Alteri CJ, Hagan EC, Sivick KE, Smith SN, Mobley HL.** 2009. Mucosal immunization with iron receptor antigens protects against urinary tract infection. *PLoS Pathogens* **5:**e1000586.
23. **Brumbaugh AR, Smith SN, Mobley HL.** 2013. Immunization with the yersiniabactin receptor, FyuA, protects against pyelonephritis in a murine model of urinary tract infection. *Infection and Immunity* **81:**3309-3316.
24. **Sabri M, Houle S, Dozois CM.** 2009. Roles of the extraintestinal pathogenic *Escherichia coli* ZnuACB and ZupT zinc transporters during urinary tract infection. *Infection and Immunity* **77:**1155-1164.
25. **Hannan TJ, Totsika M, Mansfield KJ, Moore KH, Schembri MA, Hultgren SJ.** 2012. Host-pathogen checkpoints and population bottlenecks in persistent and intracellular uropathogenic *Escherichia coli* bladder infection. *FEMS Microbiology Reviews* **36:**616-648.

26. **Nielubowicz GR, Mobley HL.** 2010. Host-pathogen interactions in urinary tract infection. *Nature reviews. Urology* **7:**430-441.
27. **Martinez JJ, Mulvey MA, Schilling JD, Pinkner JS, Hultgren SJ.** 2000. Type 1 pilus-mediated bacterial invasion of bladder epithelial cells. *The EMBO journal* **19:**2803-2812.
28. **Hung CS, Bouckaert J, Hung D, Pinkner J, Widberg C, DeFusco A, Auguste CG, Strouse R, Langermann S, Waksman G, Hultgren SJ.** 2002. Structural basis of tropism of *Escherichia coli* to the bladder during urinary tract infection. *Molecular Microbiology* **44:**903-915.
29. **Wright KJ, Hultgren SJ.** 2006. Sticky fibers and uropathogenesis: bacterial adhesins in the urinary tract. *Future microbiology* **1:**75-87.
30. **Wang H, Min G, Glockshuber R, Sun TT, Kong XP.** 2009. Uropathogenic *E. coli* adhesin-induced host cell receptor conformational changes: implications in transmembrane signaling transduction. *Journal of Molecular Biology* **392:**352-361.
31. **Eto DS, Jones TA, Sundsbak JL, Mulvey MA.** 2007. Integrin-mediated host cell invasion by type 1-piliated uropathogenic *Escherichia coli*. *PLoS Pathogens* **3:**e100.
32. **Mulvey MA, Lopez-Boado YS, Wilson CL, Roth R, Parks WC, Heuser J, Hultgren SJ.** 1998. Induction and evasion of host defenses by type 1-piliated uropathogenic *Escherichia coli*. *Science* **282:**1494-1497.
33. **Bishop BL, Duncan MJ, Song J, Li G, Zaas D, Abraham SN.** 2007. Cyclic AMP-regulated exocytosis of *Escherichia coli* from infected bladder epithelial cells. *Nature Medicine* **13:**625-630.
34. **Anderson GG, Palermo JJ, Schilling JD, Roth R, Heuser J, Hultgren SJ.** 2003. Intracellular bacterial biofilm-like pods in urinary tract infections. *Science* **301:**105-107.
35. **Anderson GG, Goller CC, Justice S, Hultgren SJ, Seed PC.** 2010. Polysaccharide capsule and sialic acid-mediated regulation promote biofilm-like intracellular bacterial communities during cystitis. *Infection and Immunity* **78:**963-975.
36. **Justice SS, Hung C, Theriot JA, Fletcher DA, Anderson GG, Footer MJ, Hultgren SJ.** 2004. Differentiation and developmental pathways of uropathogenic *Escherichia coli* in urinary tract pathogenesis. *Proceedings of the National Academy of Sciences of the United States of America* **101:**1333-1338.
37. **Ferens WA, Hovde CJ.** 2011. *Escherichia coli* O157:H7: animal reservoir and sources of human infection. *Foodborne pathogens and disease* **8:**465-487.
38. **Gyles CL.** 2007. Shiga toxin-producing *Escherichia coli*: an overview. *Journal of animal science* **85:**E45-62.
39. **Laven RA, Ashmore A, Stewart CS.** 2003. *Escherichia coli* in the rumen and colon of slaughter cattle, with particular reference to *E. coli* O157. *Veterinary journal* **165:**78-83.
40. **Widiasih DA, Ido N, Omoe K, Sugii S, Shinagawa K.** 2004. Duration and magnitude of faecal shedding of Shiga toxin-producing *Escherichia coli* from naturally infected cattle. *Epidemiology and infection* **132:**67-75.

41. **Fegan N, Vanderlinde P, Higgs G, Desmarchelier P.** 2004. The prevalence and concentration of *Escherichia coli* O157 in faeces of cattle from different production systems at slaughter. *Journal of Applied Microbiology* **97:**362-370.
42. **Kudva IT, Blanch K, Hovde CJ.** 1998. Analysis of *Escherichia coli* O157:H7 survival in ovine or bovine manure and manure slurry. *Applied and Environmental Microbiology* **64:**3166-3174.
43. **Locking ME, O'Brien SJ, Reilly WJ, Wright EM, Campbell DM, Coia JE, Browning LM, Ramsay CN.** 2001. Risk factors for sporadic cases of *Escherichia coli* O157 infection: the importance of contact with animal excreta. *Epidemiology and infection* **127:**215-220.
44. **Solomon EB, Yaron S, Matthews KR.** 2002. Transmission of *Escherichia coli* O157:H7 from contaminated manure and irrigation water to lettuce plant tissue and its subsequent internalization. *Applied and Environmental Microbiology* **68:**397-400.
45. **Islam M, Doyle MP, Phatak SC, Millner P, Jiang X.** 2004. Persistence of enterohemorrhagic *Escherichia coli* O157:H7 in soil and on leaf lettuce and parsley grown in fields treated with contaminated manure composts or irrigation water. *Journal of Food Protection* **67:**1365-1370.
46. **Jablasone J, Warriner K, Griffiths M.** 2005. Interactions of *Escherichia coli* O157:H7, *Salmonella typhimurium* and Listeria monocytogenes plants cultivated in a gnotobiotic system. *International journal of food microbiology* **99:**7-18.
47. **Manges AR, Johnson JR.** 2012. Food-borne origins of *Escherichia coli* causing extraintestinal infections. *Clinical infectious diseases : an official publication of the Infectious Diseases Society of America* **55:**712-719.
48. **Johnson JR, Kuskowski MA, Smith K, O'Bryan TT, Tatini S.** 2005. Antimicrobial-resistant and extraintestinal pathogenic *Escherichia coli* in retail foods. *The Journal of Infectious Diseases* **191:**1040-1049.
49. **Phillips I, Eykyn S, King A, Gransden WR, Rowe B, Frost JA, Gross RJ.** 1988. Epidemic multiresistant *Escherichia coli* infection in West Lambeth Health District. *Lancet* **1:**1038-1041.
50. **Yamamoto S, Tsukamoto T, Terai A, Kurazono H, Takeda Y, Yoshida O.** 1997. Genetic evidence supporting the fecal-perineal-urethral hypothesis in cystitis caused by *Escherichia coli*. *The Journal of Urology* **157:**1127-1129.
51. **Chen SL, Wu M, Henderson JP, Hooton TM, Hibbing ME, Hultgren SJ, Gordon JI.** 2013. Genomic diversity and fitness of *E. coli* strains recovered from the intestinal and urinary tracts of women with recurrent urinary tract infection. *Science Translational Medicine* **5:**184ra160.
52. **Winfield MD, Groisman EA.** 2003. Role of nonhost environments in the lifestyles of *Salmonella* and *Escherichia coli*. *Applied and Environmental Microbiology* **69:**3687-3694.
53. **Hall-Stoodley L, Costerton JW, Stoodley P.** 2004. Bacterial biofilms: from the natural environment to infectious diseases. *Nature reviews Microbiology* **2:**95-108.
54. **Stewart PS, Franklin MJ.** 2008. Physiological heterogeneity in biofilms. *Nature reviews Microbiology* **6:**199-210.

55. **Chai Y, Chu F, Kolter R, Losick R.** 2008. Bistability and biofilm formation in *Bacillus subtilis*. *Molecular Microbiology* **67:**254-263.
56. **Boles BR, Thoendel M, Singh PK.** 2004. Self-generated diversity produces "insurance effects" in biofilm communities. *Proceedings of the National Academy of Sciences of the United States of America* **101:**16630-16635.
57. **Boles BR, Singh PK.** 2008. Endogenous oxidative stress produces diversity and adaptability in biofilm communities. *Proceedings of the National Academy of Sciences of the United States of America* **105:**12503-12508.
58. **Xu KD, Stewart PS, Xia F, Huang CT, McFeters GA.** 1998. Spatial physiological heterogeneity in *Pseudomonas aeruginosa* biofilm is determined by oxygen availability. *Applied and Environmental Microbiology* **64:**4035-4039.
59. **Williamson KS, Richards LA, Perez-Osorio AC, Pitts B, McInnerney K, Stewart PS, Franklin MJ.** 2012. Heterogeneity in *Pseudomonas aeruginosa* biofilms includes expression of ribosome hibernation factors in the antibiotic-tolerant subpopulation and hypoxia-induced stress response in the metabolically active population. *Journal of Bacteriology* **194:**2062-2073.
60. **Lewis K.** 2008. Multidrug tolerance of biofilms and persister cells. *Current topics in microbiology and immunology* **322:**107-131.
61. **Beloin C, Roux A, Ghigo JM.** 2008. *Escherichia coli* biofilms. *Current topics in microbiology and immunology* **322:**249-289.
62. **Hammar M, Arnqvist A, Bian Z, Olsen A, Normark S.** 1995. Expression of two csg operons is required for production of fibronectin- and congo red-binding curli polymers in *Escherichia coli* K-12. *Molecular Microbiology* **18:**661-670.
63. **Romling U, Bian Z, Hammar M, Sierralta WD, Normark S.** 1998. Curli fibers are highly conserved between *Salmonella typhimurium* and *Escherichia coli* with respect to operon structure and regulation. *Journal of Bacteriology* **180:**722-731.
64. **Zogaj X, Nimtz M, Rohde M, Bokranz W, Romling U.** 2001. The multicellular morphotypes of *Salmonella typhimurium* and *Escherichia coli* produce cellulose as the second component of the extracellular matrix. *Molecular Microbiology* **39:**1452-1463.
65. **Gao R, Mack TR, Stock AM.** 2007. Bacterial response regulators: versatile regulatory strategies from common domains. *Trends in biochemical sciences* **32:**225-234.
66. **Skerker JM, Perchuk BS, Siryaporn A, Lubin EA, Ashenberg O, Goulian M, Laub MT.** 2008. Rewiring the specificity of two-component signal transduction systems. *Cell* **133:**1043-1054.
67. **Stock AM, Robinson VL, Goudreau PN.** 2000. Two-component signal transduction. *Annual Review of Biochemistry* **69:**183-215.
68. **Sitnikov DM, Schineller JB, Baldwin TO.** 1995. Transcriptional regulation of bioluminesence genes from Vibrio fischeri. *Molecular Microbiology* **17:**801-812.
69. **Zakikhany K, Harrington CR, Nimtz M, Hinton JCD, Romling U.** 2010. Unphosphorylated CsgD controls biofilm formation in *Salmonella enterica* serovar Typhimurium. *Molecular Microbiology* **77:**771-786.
70. **Wang L, Tian X, Wang J, Yang H, Fan K, Xu G, Yang K, Tan H.** 2009. Autoregulation of antibiotic biosynthesis by binding of the end product to an

atypical response regulator. *Proceedings of the National Academy of Sciences of the United States of America* **106:**8617-8622.
71. **Evans ML, Chapman MR.** 2013. Curli biogenesis: Order out of disorder. *Biochimica et biophysica acta*.
72. **Mika F, Hengge R.** 2013. Small Regulatory RNAs in the Control of Motility and Biofilm Formation in *E. coli* and *Salmonella*. *International journal of molecular sciences* **14:**4560-4579.
73. **Olsen A, Jonsson A, Normark S.** 1989. Fibronectin binding mediated by a novel class of surface organelles on *Escherichia coli*. *Nature* **338:**652-655.
74. **Romling U, Sierralta WD, Eriksson K, Normark S.** 1998. Multicellular and aggregative behaviour of *Salmonella typhimurium* strains is controlled by mutations in the agfD promoter. *Molecular Microbiology* **28:**249-264.
75. **Zheng D, Constantinidou C, Hobman JL, Minchin SD.** 2004. Identification of the CRP regulon using *in vitro* and *in vivo* transcriptional profiling. *Nucleic acids research* **32:**5874-5893.
76. **Olsen A, Arnqvist A, Hammar M, Sukupolvi S, Normark S.** 1993. The RpoS sigma factor relieves H-NS-mediated transcriptional repression of *csgA*, the subunit gene of fibronectin-binding curli in *Escherichia coli*. *Molecular Microbiology* **7:**523-536.
77. **Romling U.** 2005. Characterization of the rdar morphotype, a multicellular behaviour in *Enterobacteriaceae*. *Cellular and molecular life sciences* **62:**1234-1246.
78. **Weber H, Pesavento C, Possling A, Tischendorf G, Hengge R.** 2006. Cyclic-di-GMP-mediated signalling within the sigma network of *Escherichia coli*. *Molecular Microbiology* **62:**1014-1034.
79. **Sommerfeldt N, Possling A, Becker G, Pesavento C, Tschowri N, Hengge R.** 2009. Gene expression patterns and differential input into curli fimbriae regulation of all GGDEF/EAL domain proteins in *Escherichia coli*. *Microbiology* **155:**1318-1331.
80. **Brombacher E, Dorel C, Zehnder AJ, Landini P.** 2003. The curli biosynthesis regulator CsgD co-ordinates the expression of both positive and negative determinants for biofilm formation in *Escherichia coli*. *Microbiology* **149:**2847-2857.
81. **Gualdi L, Tagliabue L, Landini P.** 2007. Biofilm formation-gene expression relay system in *Escherichia coli*: modulation of sigmaS-dependent gene expression by the CsgD regulatory protein via sigmaS protein stabilization. *Journal of Bacteriology* **189:**8034-8043.
82. **Ogasawara H, Yamamoto K, Ishihama A.** 2011. Role of the biofilm master regulator CsgD in cross-regulation between biofilm formation and flagellar synthesis. *Journal of Bacteriology* **193:**2587-2597.
83. **Collinson SK, Doig PC, Doran JL, Clouthier S, Trust TJ, Kay WW.** 1993. Thin, aggregative fimbriae mediate binding of *Salmonella enteritidis* to fibronectin. *Journal of Bacteriology* **175:**12-18.
84. **Zogaj X, Bokranz W, Nimtz M, Romling U.** 2003. Production of cellulose and curli fimbriae by members of the family *Enterobacteriaceae* isolated from the human gastrointestinal tract. *Infection and Immunity* **71:**4151-4158.

85. **DePas WH, Hufnagel DA, Lee JS, Blanco LP, Bernstein HC, Fisher ST, James GA, Stewart PS, Chapman MR.** 2013. Iron induces bimodal population development by *Escherichia coli*. *Proceedings of the National Academy of Sciences of the United States of America* **110:**2629-2634.
86. **Bokranz W, Wang X, Tschape H, Romling U.** 2005. Expression of cellulose and curli fimbriae by *Escherichia coli* isolated from the gastrointestinal tract. *Journal of Medical Microbiology* **54:**1171-1182.
87. **White AP, Surette MG.** 2006. Comparative genetics of the rdar morphotype in *Salmonella*. *Journal of Bacteriology* **188:**8395-8406.
88. **Zhou Y, Smith D, Leong BJ, Brannstrom K, Almqvist F, Chapman MR.** 2012. Promiscuous cross-seeding between bacterial amyloids promotes interspecies biofilms. *The Journal of Biological Chemistry* **287:**35092-35103.
89. **Dueholm MS, Albertsen M, Otzen D, Nielsen PH.** 2012. Curli functional amyloid systems are phylogenetically widespread and display large diversity in operon and protein structure. *Plos One* **7:**e51274.
90. **Wang X, Hammer ND, Chapman MR.** 2008. The molecular basis of functional bacterial amyloid polymerization and nucleation. *The Journal of Biological Chemistry* **283:**21530-21539.
91. **Hammar M, Bian Z, Normark S.** 1996. Nucleator-dependent intercellular assembly of adhesive curli organelles in *Escherichia coli*. *Proceedings of the National Academy of Sciences of the United States of America* **93:**6562-6566.
92. **Bian Z, Normark S.** 1997. Nucleator function of CsgB for the assembly of adhesive surface organelles in *Escherichia coli*. *The EMBO journal* **16:**5827-5836.
93. **Hammer ND, Schmidt JC, Chapman MR.** 2007. The curli nucleator protein, CsgB, contains an amyloidogenic domain that directs CsgA polymerization. *Proceedings of the National Academy of Sciences of the United States of America* **104:**12494-12499.
94. **Nenninger AA, Robinson LS, Hultgren SJ.** 2009. Localized and efficient curli nucleation requires the chaperone-like amyloid assembly protein CsgF. *Proceedings of the National Academy of Sciences of the United States of America* **106:**900-905.
95. **Loferer H, Hammar M, Normark S.** 1997. Availability of the fibre subunit CsgA and the nucleator protein CsgB during assembly of fibronectin-binding curli is limited by the intracellular concentration of the novel lipoprotein CsgG. *Molecular Microbiology* **26:**11-23.
96. **Robinson LS, Ashman EM, Hultgren SJ, Chapman MR.** 2006. Secretion of curli fibre subunits is mediated by the outer membrane-localized CsgG protein. *Molecular Microbiology* **59:**870-881.
97. **Epstein EA, Reizian MA, Chapman MR.** 2009. Spatial clustering of the curlin secretion lipoprotein requires curli fiber assembly. *Journal of Bacteriology* **191:**608-615.
98. **Chapman MR, Robinson LS, Pinkner JS, Roth R, Heuser J, Hammar M, Normark S, Hultgren SJ.** 2002. Role of *Escherichia coli* curli operons in directing amyloid fiber formation. *Science* **295:**851-855.

99. **Harper JD, Lansbury PT, Jr.** 1997. Models of amyloid seeding in Alzheimer's disease and scrapie: mechanistic truths and physiological consequences of the time-dependent solubility of amyloid proteins. *Annual Review of Biochemistry* **66:**385-407.
100. **Nelson R, Sawaya MR, Balbirnie M, Madsen AO, Riekel C, Grothe R, Eisenberg D.** 2005. Structure of the cross-beta spine of amyloid-like fibrils. *Nature* **435:**773-778.
101. **O'Nuallain B, Williams AD, Westermark P, Wetzel R.** 2004. Seeding specificity in amyloid growth induced by heterologous fibrils. *The Journal of Biological Chemistry* **279:**17490-17499.
102. **Scheibel T, Kowal AS, Bloom JD, Lindquist SL.** 2001. Bidirectional amyloid fiber growth for a yeast prion determinant. *Current Biology* **11:**366-369.
103. **Serpell LC, Sunde M, Blake CC.** 1997. The molecular basis of amyloidosis. *Cellular and Molecular Life Sciences* **53:**871-887.
104. **Sunde M, Serpell LC, Bartlam M, Fraser PE, Pepys MB, Blake CC.** 1997. Common core structure of amyloid fibrils by synchrotron X-ray diffraction. *Journal of Molecular Biology* **273:**729-739.
105. **Wetzel R.** 2006. Kinetics and thermodynamics of amyloid fibril assembly. *Accounts of Chemical Research* **39:**671-679.
106. **Dueholm MS, Petersen SV, Sonderkaer M, Larsen P, Christiansen G, Hein KL, Enghild JJ, Nielsen JL, Nielsen KL, Nielsen PH, Otzen DE.** 2010. Functional amyloid in *Pseudomonas*. *Molecular Microbiology* **77:**1009-1020.
107. **Jordal PB, Dueholm MS, Larsen P, Petersen SV, Enghild JJ, Christiansen G, Hojrup P, Nielsen PH, Otzen DE.** 2009. Widespread abundance of functional bacterial amyloid in mycolata and other gram-positive bacteria. *Applied and Environmental Microbiology* **75:**4101-4110.
108. **Larsen P, Nielsen JL, Dueholm MS, Wetzel R, Otzen D, Nielsen PH.** 2007. Amyloid adhesins are abundant in natural biofilms. *Environmental Microbiology* **9:**3077-3090.
109. **Romero D, Aguilar C, Losick R, Kolter R.** 2010. Amyloid fibers provide structural integrity to *Bacillus subtilis* biofilms. *Proceedings of the National Academy of Sciences of the United States of America* **107:**2230-2234.
110. **Schwartz K, Syed AK, Stephenson RE, Rickard AH, Boles BR.** 2012. Functional Amyloids Composed of Phenol Soluble Modulins Stabilize *Staphylococcus aureus* Biofilms. *PLOS Pathogens* **8:**e1002744.
111. **Chamberlain AK, MacPhee CE, Zurdo J, Morozova-Roche LA, Hill HA, Dobson CM, Davis JJ.** 2000. Ultrastructural organization of amyloid fibrils by atomic force microscopy. *Biophysical Journal* **79:**3282-3293.
112. **Dobson CM.** 2004. Principles of protein folding, misfolding and aggregation. *Seminars in Cell & Developmental Biology* **15:**3-16.
113. **Gordon DJ, Meredith SC.** 2003. Probing the role of backbone hydrogen bonding in beta-amyloid fibrils with inhibitor peptides containing ester bonds at alternate positions. *Biochemistry* **42:**475-485.
114. **Kheterpal I, Zhou S, Cook KD, Wetzel R.** 2000. Abeta amyloid fibrils possess a core structure highly resistant to hydrogen exchange. *Proceedings of the National Academy of Sciences of the United States of America* **97:**13597-13601.

115. **Kaji R, Goto S, Tamiya G, Ando S, Makino S, Lee LV.** 2005. Molecular dissection and anatomical basis of dystonia: X-linked recessive dystonia-parkinsonism (DYT3). *The journal of medical investigation* **52 Suppl:**280-283.
116. **Carny O, Gazit E.** 2005. A model for the role of short self-assembled peptides in the very early stages of the origin of life. *FASEB journal : official publication of the Federation of American Societies for Experimental Biology* **19:**1051-1055.
117. **Chiti F, Webster P, Taddei N, Clark A, Stefani M, Ramponi G, Dobson CM.** 1999. Designing conditions for *in vitro* formation of amyloid protofilaments and fibrils. *Proceedings of the National Academy of Sciences of the United States of America* **96:**3590-3594.
118. **Chiti F, Taddei N, Bucciantini M, White P, Ramponi G, Dobson CM.** 2000. Mutational analysis of the propensity for amyloid formation by a globular protein. *The EMBO Journal* **19:**1441-1449.
119. **Ramirez-Alvarado M, Merkel JS, Regan L.** 2000. A systematic exploration of the influence of the protein stability on amyloid fibril formation *in vitro*. *Proceedings of the National Academy of Sciences of the United States of America* **97:**8979-8984.
120. **Esteras-Chopo A, Serrano L, Lopez de la Paz M.** 2005. The amyloid stretch hypothesis: recruiting proteins toward the dark side. *Proceedings of the National Academy of Sciences of the United States of America* **102:**16672-16677.
121. **Pastor MT, Esteras-Chopo A, Serrano L.** 2007. Hacking the code of amyloid formation: the amyloid stretch hypothesis. *Prion* **1:**9-14.
122. **Tenidis K, Waldner M, Bernhagen J, Fischle W, Bergmann M, Weber M, Merkle ML, Voelter W, Brunner H, Kapurniotu A.** 2000. Identification of a penta- and hexapeptide of islet amyloid polypeptide (IAPP) with amyloidogenic and cytotoxic properties. *Journal of Molecular Biology* **295:**1055-1071.
123. **Ivanova MI, Sawaya MR, Gingery M, Attinger A, Eisenberg D.** 2004. An amyloid-forming segment of beta2-microglobulin suggests a molecular model for the fibril. *Proceedings of the National Academy of Sciences of the United States of America* **101:**10584-10589.
124. **Ventura S, Zurdo J, Narayanan S, Parreno M, Mangues R, Reif B, Chiti F, Giannoni E, Dobson CM, Aviles FX, Serrano L.** 2004. Short amino acid stretches can mediate amyloid formation in globular proteins: the Src homology 3 (SH3) case. *Proceedings of the National Academy of Sciences of the United States of America* **101:**7258-7263.
125. **Elghetany MT, Saleem A.** 1988. Methods for staining amyloid in tissues: a review. *Stain technology* **63:**201-212.
126. **Hrncic R, Wall J, Wolfenbarger DA, Murphy CL, Schell M, Weiss DT, Solomon A.** 2000. Antibody-mediated resolution of light chain-associated amyloid deposits. *The American Journal of Pathology* **157:**1239-1246.
127. **Kayed R, Head E, Thompson JL, McIntire TM, Milton SC, Cotman CW, Glabe CG.** 2003. Common structure of soluble amyloid oligomers implies common mechanism of pathogenesis. *Science* **300:**486-489.
128. **Kayed R, Head E, Sarsoza F, Saing T, Cotman CW, Necula M, Margol L, Wu J, Breydo L, Thompson JL, Rasool S, Gurlo T, Butler P, Glabe CG.** 2007. Fibril specific, conformation dependent antibodies recognize a generic epitope

common to amyloid fibrils and fibrillar oligomers that is absent in prefibrillar oligomers. *Molecular Neurodegeneration* **2:**18.
129. **O'Nuallain B, Wetzel R.** 2002. Conformational Abs recognizing a generic amyloid fibril epitope. *Proceedings of the National Academy of Sciences of the United States of America* **99:**1485-1490.
130. **Horvath I, Weise CF, Andersson EK, Chorell E, Sellstedt M, Bengtsson C, Olofsson A, Hultgren SJ, Chapman M, Wolf-Watz M, Almqvist F, Wittung-Stafshede P.** 2012. Mechanisms of protein oligomerization: inhibitor of functional amyloids templates alpha-synuclein fibrillation. *Journal of the American Chemical Society* **134:**3439-3444.
131. **Hardy J, Selkoe DJ.** 2002. The amyloid hypothesis of Alzheimer's disease: progress and problems on the road to therapeutics. *Science* **297:**353-356.
132. **Breydo L, Wu JW, Uversky VN.** 2012. Alpha-synuclein misfolding and Parkinson's disease. *Biochimica et Biophysica Acta* **1822:**261-285.
133. **Zuccato C, Valenza M, Cattaneo E.** 2010. Molecular mechanisms and potential therapeutical targets in Huntington's disease. *Physiological Reviews* **90:**905-981.
134. **Westermark P, Andersson A, Westermark GT.** 2011. Islet amyloid polypeptide, islet amyloid, and diabetes mellitus. *Physiological Reviews* **91:**795-826.
135. **Caughey B, Lansbury PT.** 2003. Protofibrils, pores, fibrils, and neurodegeneration: separating the responsible protein aggregates from the innocent bystanders. *Annual Review of Neuroscience* **26:**267-298.
136. **Bucciantini M, Giannoni E, Chiti F, Baroni F, Formigli L, Zurdo J, Taddei N, Ramponi G, Dobson CM, Stefani M.** 2002. Inherent toxicity of aggregates implies a common mechanism for protein misfolding diseases. *Nature* **416:**507-511.
137. **Deshpande A, Mina E, Glabe C, Busciglio J.** 2006. Different conformations of amyloid beta induce neurotoxicity by distinct mechanisms in human cortical neurons. *Journal of Neuroscience* **26:**6011-6018.
138. **Lambert MP, Barlow AK, Chromy BA, Edwards C, Freed R, Liosatos M, Morgan TE, Rozovsky I, Trommer B, Viola KL, Wals P, Zhang C, Finch CE, Krafft GA, Klein WL.** 1998. Diffusible, nonfibrillar ligands derived from Abeta1-42 are potent central nervous system neurotoxins. *Proceedings of the National Academy of Sciences of the United States of America* **95:**6448-6453.
139. **Engel MF.** 2009. Membrane permeabilization by Islet Amyloid Polypeptide. *Chemistry and Physics of Lipids* **160:**1-10.
140. **Haass C, Selkoe DJ.** 2007. Soluble protein oligomers in neurodegeneration: lessons from the Alzheimer's amyloid beta-peptide. *Nature Reviews Molecular Cell Biology* **8:**101-112.
141. **Volles MJ, Lansbury PT, Jr.** 2003. Zeroing in on the pathogenic form of alpha-synuclein and its mechanism of neurotoxicity in Parkinson's disease. *Biochemistry* **42:**7871-7878.
142. **Hammer ND, Wang X, McGuffie BA, Chapman MR.** 2008. Amyloids: friend or foe? *Journal of Alzheimer's Disease* **13:**407-419.
143. **Hammer ND, McGuffie BA, Zhou Y, Badtke MP, Reinke AA, Brannstrom K, Gestwicki JE, Olofsson A, Almqvist F, Chapman MR.** 2012. The C-Terminal

Repeating Units of CsgB Direct Bacterial Functional Amyloid Nucleation. *Journal of Molecular Biology*.
144. **Wang X, Chapman MR.** 2008. Sequence determinants of bacterial amyloid formation. *Journal of Molecular Biology* **380:**570-580.
145. **Dueholm MS, Nielsen SB, Hein KL, Nissen P, Chapman M, Christiansen G, Nielsen PH, Otzen DE.** 2011. Fibrillation of the major curli subunit CsgA under a wide range of conditions implies a robust design of aggregation. *Biochemistry* **50:**8281-8290.
146. **Chiti F, Mangione P, Andreola A, Giorgetti S, Stefani M, Dobson CM, Bellotti V, Taddei N.** 2001. Detection of two partially structured species in the folding process of the amyloidogenic protein beta 2-microglobulin. *Journal of Molecular Biology* **307:**379-391.
147. **Marcon G, Plakoutsi G, Canale C, Relini A, Taddei N, Dobson CM, Ramponi G, Chiti F.** 2005. Amyloid formation from HypF-N under conditions in which the protein is initially in its native state. *Journal of Molecular Biology* **347:**323-335.
148. **Collinson SK, Parker JM, Hodges RS, Kay WW.** 1999. Structural predictions of AgfA, the insoluble fimbrial subunit of *Salmonella* thin aggregative fimbriae. *Journal of Molecular Biology* **290:**741-756.
149. **Wang X, Chapman MR.** 2008. Curli provide the template for understanding controlled amyloid propagation. *Prion* **2:**57-60.
150. **Wang X, Smith DR, Jones JW, Chapman MR.** 2007. *In vitro* polymerization of a functional *Escherichia coli* amyloid protein. *The Journal of Biological Chemistry* **282:**3713-3719.
151. **Wang X, Zhou Y, Ren JJ, Hammer ND, Chapman MR.** 2010. Gatekeeper residues in the major curlin subunit modulate bacterial amyloid fiber biogenesis. *Proceedings of the National Academy of Sciences of the United States of America* **107:**163-168.
152. **Smith DR, Chapman MR.** 2010. Economical evolution: microbes reduce the synthetic cost of extracellular proteins. *MBio* **1**.
153. **Evans ML, Schmidt JC, Ilbert M, Doyle SM, Quan S, Bardwell JC, Jakob U, Wickner S, Chapman MR.** 2011. *E. coli* chaperones DnaK, Hsp33 and Spy inhibit bacterial functional amyloid assembly. *Prion* **5**.
154. **Nenninger AA, Robinson LS, Hammer ND, Epstein EA, Badtke MP, Hultgren SJ, Chapman MR.** 2011. CsgE is a curli secretion specificity factor that prevents amyloid fibre aggregation. *Molecular Microbiology* **81:**486-499.
155. **Andersson EK, Bengtsson C, Evans ML, Chorell E, Sellstedt M, Lindgren AE, Hufnagel DA, Bhattacharya M, Tessier PM, Wittung-Stafshede P, Almqvist F, Chapman MR.** 2013. Modulation of curli assembly and pellicle biofilm formation by chemical and protein chaperones. *Chemistry & Biology* **20:**1245-1254.
156. **Brown AJ.** 1887. Note on the cellulose formed by Bacterium xylinum. *Journal of the Chemical Society* **51:**643.
157. **Romling U.** 2002. Molecular biology of cellulose production in bacteria. *Research in Microbiology* **153:**205-212.
158. **Ross P, Mayer R, Benziman M.** 1991. Cellulose biosynthesis and function in bacteria. *Microbiological reviews* **55:**35-58.

159. **Da Re S, Ghigo JM.** 2006. A CsgD-independent pathway for cellulose production and biofilm formation in *Escherichia coli*. *Journal of Bacteriology* **188:**3073-3087.
160. **Serra DO, Richter AM, Hengge R.** 2013. Cellulose as an Architectural Element in Spatially Structured *Escherichia coli* Biofilms. *Journal of Bacteriology* **195:**5540-5554.
161. **Romling U, Rohde M, Olsen A, Normark S, Reinkoster J.** 2000. AgfD, the checkpoint of multicellular and aggregative behaviour in *Salmonella typhimurium* regulates at least two independent pathways. *Molecular Microbiology* **36:**10-23.
162. **Simm R, Morr M, Kader A, Nimtz M, Romling U.** 2004. GGDEF and EAL domains inversely regulate cyclic di-GMP levels and transition from sessility to motility. *Molecular Microbiology* **53:**1123-1134.
163. **Ryjenkov DA, Simm R, Romling U, Gomelsky M.** 2006. The PilZ domain is a receptor for the second messenger c-di-GMP: the PilZ domain protein YcgR controls motility in enterobacteria. *The Journal of Biological Chemistry* **281:**30310-30314.
164. **Amikam D, Galperin MY.** 2006. PilZ domain is part of the bacterial c-di-GMP binding protein. *Bioinformatics* **22:**3-6.
165. **Gophna U, Barlev M, Seijffers R, Oelschlager TA, Hacker J, Ron EZ.** 2001. Curli fibers mediate internalization of *Escherichia coli* by eukaryotic cells. *Infection and Immunity* **69:**2659-2665.
166. **Johansson C, Nilsson T, Olsen A, Wick MJ.** 2001. The influence of curli, a MHC-I-binding bacterial surface structure, on macrophage-T cell interactions. *FEMS Immunology and Medical Microbiology* **30:**21-29.
167. **Kikuchi T, Mizunoe Y, Takade A, Naito S, Yoshida S.** 2005. Curli fibers are required for development of biofilm architecture in *Escherichia coli* K-12 and enhance bacterial adherence to human uroepithelial cells. *Microbiology and Immunology* **49:**875-884.
168. **Gophna U, Oelschlaeger TA, Hacker J, Ron EZ.** 2002. Role of fibronectin in curli-mediated internalization. *FEMS Microbiology Letters* **212:**55-58.
169. **Olsen A, Wick MJ, Morgelin M, Bjorck L.** 1998. Curli, fibrous surface proteins of *Escherichia coli*, interact with major histocompatibility complex class I molecules. *Infection and Immunity* **66:**944-949.
170. **Pepys MB.** 2001. Pathogenesis, diagnosis and treatment of systemic amyloidosis. *Philosophical Transactions of the Royal Society B: Biological Sciences* **356:**203-210; discussion 210-201.
171. **Ganowiak K, Hultman P, Engstrom U, Gustavsson A, Westermark P.** 1994. Fibrils from synthetic amyloid-related peptides enhance development of experimental AA-amyloidosis in mice. *Biochemical and Biophysical Research Communications* **199:**306-312.
172. **Kisilevsky R, Lemieux L, Boudreau L, Yang DS, Fraser P.** 1999. New clothes for amyloid enhancing factor (AEF): silk as AEF. *Amyloid* **6:**98-106.
173. **Johan K, Westermark G, Engstrom U, Gustavsson A, Hultman P, Westermark P.** 1998. Acceleration of amyloid protein A amyloidosis by amyloid-like synthetic fibrils. *Proceedings of the National Academy of Sciences of the United States of America* **95:**2558-2563.

174. **Niewold TA, Hol PR, van Andel AC, Lutz ET, Gruys E.** 1987. Enhancement of amyloid induction by amyloid fibril fragments in hamster. *Laboratory Investigation* **56:**544-549.
175. **Lundmark K, Westermark GT, Olsen A, Westermark P.** 2005. Protein fibrils in nature can enhance amyloid protein A amyloidosis in mice: Cross-seeding as a disease mechanism. *Proceedings of the National Academy of Sciences of the United States of America* **102:**6098-6102.
176. **Gebbink MF, Claessen D, Bouma B, Dijkhuizen L, Wosten HA.** 2005. Amyloids--a functional coat for microorganisms. *Nature Reviews Microbiology* **3:**333-341.
177. **Kranenburg O, Bouma B, Kroon-Batenburg LMJ, Reijerkerk A, Wu YP, Voest EE, Gebbink MFBG.** 2002. Tissue-type plasminogen activator is a multiligand cross-beta structure receptor. *Current Biology* **12:**1833-1839.
178. **Nieuwenhuizen W.** 2001. Fibrin-mediated plasminogen activation. *Annals of the New York Academy of Sciences* **936:**237-246.
179. **Gebbink MF.** 2011. Tissue-type plasminogen activator-mediated plasminogen activation and contact activation, implications in and beyond haemostasis. *Journal of Thrombosis and Haemostasis* **9 Suppl 1:**174-181.
180. **Sjobring U, Pohl G, Olsen A.** 1994. Plasminogen, absorbed by *Escherichia coli* expressing curli or by *Salmonella enteritidis* expressing thin aggregative fimbriae, can be activated by simultaneously captured tissue-type plasminogen activator (t-PA). *Molecular Microbiology* **14:**443-452.
181. **BenNasr A, Olsen A, Sjobring U, MullerEsterl W, Bjorck L.** 1996. Assembly of human contact phase proteins and release of bradykinin at the surface of curli-expressing *Escherichia coli*. *Molecular Microbiology* **20:**927-935.
182. **Herwald H, Morgelin M, Olsen A, Rhen M, Dahlback B, Muller-Esterl W, Bjorck L.** 1998. Activation of the contact-phase system on bacterial surfaces--a clue to serious complications in infectious diseases. *Nature Medicine* **4:**298-302.
183. **Persson K, Morgelin M, Lindbom L, Alm P, Bjorck L, Herwald H.** 2000. Severe lung lesions caused by *Salmonella* are prevented by inhibition of the contact system. *The Journal of Experimental Medicine* **192:**1415-1424.
184. **Persson K, Russell W, Morgelin M, Herwald H.** 2003. The conversion of fibrinogen to fibrin at the surface of curliated *Escherichia coli* bacteria leads to the generation of proinflammatory fibrinopeptides. *Journal of Biological Chemistry* **278:**31884-31890.
185. **Maas C, Govers-Riemslag JW, Bouma B, Schiks B, Hazenberg BP, Lokhorst HM, Hammarstrom P, ten Cate H, de Groot PG, Bouma BN, Gebbink MF.** 2008. Misfolded proteins activate factor XII in humans, leading to kallikrein formation without initiating coagulation. *Journal of Clinical Investigation* **118:**3208-3218.
186. **Bian Z, Brauner A, Li Y, Normark S.** 2000. Expression of and cytokine activation by *Escherichia coli* curli fibers in human sepsis. *The Journal of Infectious Diseases* **181:**602-612.
187. **Hung C, Marschall J, Burnham CAD, Byun AS, Henderson JP.** 2014. The Bacterial Amyloid Curli Is Associated with Urinary Source Bloodstream Infection. *Plos One* **9**.

188. **Bian Z, Yan ZQ, Hansson GK, Thoren P, Normark S.** 2001. Activation of inducible nitric oxide synthase/nitric oxide by curli fibers leads to a fall in blood pressure during systemic *Escherichia coli* infection in mice. *The Journal of Infectious Diseases* **183:**612-619.
189. **Tukel C, Raffatellu M, Humphries AD, Wilson RP, Andrews-Polymenis HL, Gull T, Figueiredo JF, Wong MH, Michelsen KS, Akcelik M, Adams LG, Baumler AJ.** 2005. CsgA is a pathogen-associated molecular pattern of *Salmonella enterica* serotype Typhimurium that is recognized by Toll-like receptor 2. *Molecular Microbiology* **58:**289-304.
190. **Tukel C, Wilson RP, Nishimori JH, Pezeshki M, Chromy BA, Baumler AJ.** 2009. Responses to amyloids of microbial and host origin are mediated through toll-like receptor 2. *Cell Host & Microbe* **6:**45-53.
191. **Aliprantis AO, Yang RB, Mark MR, Suggett S, Devaux B, Radolf JD, Klimpel GR, Godowski P, Zychlinsky A.** 1999. Cell activation and apoptosis by bacterial lipoproteins through toll-like receptor-2. *Science* **285:**736-739.
192. **Schwandner R, Dziarski R, Wesche H, Rothe M, Kirschning CJ.** 1999. Peptidoglycan- and lipoteichoic acid-induced cell activation is mediated by toll-like receptor 2. *Journal of Biological Chemistry* **274:**17406-17409.
193. **Poltorak A, He XL, Smirnova I, Liu MY, Van Huffel C, Du X, Birdwell D, Alejos E, Silva M, Galanos C, Freudenberg M, Ricciardi-Castagnoli P, Layton B, Beutler B.** 1998. Defective LPS signaling in C3H/HeJ and C57BL/10ScCr mice: Mutations in Tlr4 gene. *Science* **282:**2085-2088.
194. **Hayashi F, Smith KD, Ozinsky A, Hawn TR, Yi EC, Goodlett DR, Eng JK, Akira S, Underhill DM, Aderem A.** 2001. The innate immune response to bacterial flagellin is mediated by Toll-like receptor 5. *Nature* **410:**1099-1103.
195. **Smith KD, Andersen-Nissen E, Hayashi F, Strobe K, Bergman MA, Barrett SLR, Cookson BT, Aderem A.** 2003. Toll-like receptor 5 recognizes a conserved site on flagellin required for protofilament formation and bacterial motility. *Nature Immunology* **4:**1247-1253.
196. **Chen ES, Song Z, Willett MH, Heine S, Yung RC, Liu MC, Groshong SD, Zhang Y, Tuder RM, Moller DR.** 2010. Serum amyloid A regulates granulomatous inflammation in sarcoidosis through Toll-like receptor-2. *American Journal of Respiratory and Critical Care Medicine* **181:**360-373.
197. **Cheng N, He R, Tian J, Ye PP, Ye RD.** 2008. Cutting edge: TLR2 is a functional receptor for acute-phase serum amyloid A. *Journal of Immunology* **181:**22-26.
198. **He RL, Zhou J, Hanson CZ, Chen J, Cheng N, Ye RD.** 2009. Serum amyloid A induces G-CSF expression and neutrophilia via Toll-like receptor 2. *Blood* **113:**429-437.
199. **Jana M, Palencia CA, Pahan K.** 2008. Fibrillar amyloid-beta peptides activate microglia via TLR2: implications for Alzheimer's disease. *The Journal of Immunology* **181:**7254-7262.
200. **Udan ML, Ajit D, Crouse NR, Nichols MR.** 2008. Toll-like receptors 2 and 4 mediate Abeta(1-42) activation of the innate immune response in a human monocytic cell line. *Journal of Neurochemistry* **104:**524-533.
201. **Liu S, Liu Y, Hao W, Wolf L, Kiliaan AJ, Penke B, Rube CE, Walter J, Heneka MT, Hartmann T, Menger MD, Fassbender K.** 2012. TLR2 is a primary receptor

for Alzheimer's amyloid beta peptide to trigger neuroinflammatory activation. *The Journal of Immunology* **188:**1098-1107.

202. **Tukel C, Nishimori JH, Wilson RP, Winter MG, Keestra AM, van Putten JPM, Baumler AJ.** 2010. Toll-like receptors 1 and 2 cooperatively mediate immune responses to curli, a common amyloid from enterobacterial biofilms. *Cellular Microbiology* **12:**1495-1505.
203. **Rapsinski GJ, Newman TN, Oppong GO, van Putten JPM, Tukel C.** 2013. CD14 Protein Acts as an Adaptor Molecule for the Immune Recognition of *Salmonella* Curli Fibers. *Journal of Biological Chemistry* **288:**14178-14188.
204. **Chromek M, Slamova Z, Bergman P, Kovacs L, Podracka L, Ehren I, Hokfelt T, Gudmundsson GH, Gallo RL, Agerberth B, Brauner A.** 2006. The antimicrobial peptide cathelicidin protects the urinary tract against invasive bacterial infection. *Nature Medicine* **12:**636-641.
205. **Kai-Larsen Y, Luthje P, Chromek M, Peters V, Wang X, Holm A, Kadas L, Hedlund KO, Johansson J, Chapman MR, Jacobson SH, Romling U, Agerberth B, Brauner A.** 2010. Uropathogenic *Escherichia coli* modulates immune responses and its curli fimbriae interact with the antimicrobial peptide LL-37. *PLoS Pathogens* **6:**e1001010.
206. **Kai-Larsen Y, Luthje P, Chromek M, Peters V, Wang XD, Holm A, Kadas L, Hedlund KO, Johansson J, Chapman MR, Jacobson SH, Romling U, Agerberth B, Brauner A.** 2010. Uropathogenic *Escherichia coli* Modulates Immune Responses and Its Curli Fimbriae Interact with the Antimicrobial Peptide LL-37. *Plos Pathogens* **6**.
207. **White AP, Gibson DL, Kim W, Kay WW, Surette MG.** 2006. Thin aggregative fimbriae and cellulose enhance long-term survival and persistence of *Salmonella*. *Journal of Bacteriology* **188:**3219-3227.
208. **White AP, Gibson DL, Grassl GA, Kay WW, Finlay BB, Vallance BA, Surette MG.** 2008. Aggregation via the red, dry, and rough morphotype is not a virulence adaptation in *Salmonella enterica* serovar Typhimurium. *Infection and Immunity* **76:**1048-1058.
209. **Ryu JH, Beuchat LR.** 2005. Biofilm formation by *Escherichia coli* O157:H7 on stainless steel: effect of exopolysaccharide and Curli production on its resistance to chlorine. *Applied and Environmental Microbiology* **71:**247-254.
210. **Macarisin D, Patel J, Bauchan G, Giron JA, Sharma VK.** 2012. Role of curli and cellulose expression in adherence of *Escherichia coli* O157:H7 to spinach leaves. *Foodborne pathogens and disease* **9:**160-167.
211. **Pawar DM, Rossman ML, Chen J.** 2005. Role of curli fimbriae in mediating the cells of enterohaemorrhagic *Escherichia coli* to attach to abiotic surfaces. *Journal of Applied Microbiology* **99:**418-425.
212. **Hadjifrangiskou M, Gu AP, Pinkner JS, Kostakioti M, Zhang EW, Greene SE, Hultgren SJ.** 2012. Transposon mutagenesis identifies uropathogenic *Escherichia coli* biofilm factors. *Journal of Bacteriology* **194:**6195-6205.
213. **Pratt LA, Kolter R.** 1998. Genetic analysis of *Escherichia coli* biofilm formation: roles of flagella, motility, chemotaxis and type I pili. *Molecular Microbiology* **30:**285-293.

214. **Hung C, Zhou YZ, Pinkner JS, Dodson KW, Crowley JR, Heuser J, Chapman MR, Hadjifrangiskou M, Henderson JP, Hultgren SJ.** 2013. *Escherichia coli* Biofilms Have an Organized and Complex Extracellular Matrix Structure. *Mbio* **4**.
215. **Wang X, Preston JF, 3rd, Romeo T.** 2004. The *pgaABCD* locus of *Escherichia coli* promotes the synthesis of a polysaccharide adhesin required for biofilm formation. *Journal of Bacteriology* **186:**2724-2734.
216. **Danese PN, Pratt LA, Dove SL, Kolter R.** 2000. The outer membrane protein, antigen 43, mediates cell-to-cell interactions within *Escherichia coli* biofilms. *Molecular Microbiology* **37:**424-432.
217. **Jubelin G, Vianney A, Beloin C, Ghigo JM, Lazzaroni JC, Lejeune P, Dorel C.** 2005. CpxR/OmpR interplay regulates curli gene expression in response to osmolarity in *Escherichia coli*. *Journal of Bacteriology* **187:**2038-2049.
218. **Cegelski L, Pinkner JS, Hammer ND, Cusumano CK, Hung CS, Chorell E, Aberg V, Walker JN, Seed PC, Almqvist F, Chapman MR, Hultgren SJ.** 2009. Small-molecule inhibitors target *Escherichia coli* amyloid biogenesis and biofilm formation. *Nature Chemical Biology* **5:**913-919.
219. **Lim JY, May JM, Cegelski L.** 2012. Dimethyl sulfoxide and ethanol elicit increased amyloid biogenesis and amyloid-integrated biofilm formation in *Escherichia coli*. *Applied and Environmental Microbiology* **78:**3369-3378.
220. **Serra DO, Richter AM, Klauck G, Mika F, Hengge R.** 2013. Microanatomy at cellular resolution and spatial order of physiological differentiation in a bacterial biofilm. *mBio* **4:**e00103-00113.
221. **Wai SN, Mizunoe Y, Takade A, Kawabata SI, Yoshida SI.** 1998. *Vibrio cholerae* O1 strain TSI-4 produces the exopolysaccharide materials that determine colony morphology, stress resistance, and biofilm formation. *Applied and Environmental Microbiology* **64:**3648-3655.
222. **Yildiz FH, Dolganov NA, Schoolnik GK.** 2001. VpsR, a Member of the Response Regulators of the Two-Component Regulatory Systems, Is Required for Expression of vps Biosynthesis Genes and EPS(ETr)-Associated Phenotypes in *Vibrio cholerae* O1 El Tor. *Journal of Bacteriology* **183:**1716-1726.
223. **Yildiz FH, Liu XS, Heydorn A, Schoolnik GK.** 2004. Molecular analysis of rugosity in a *Vibrio cholerae* O1 El Tor phase variant. *Molecular Microbiology* **53:**497-515.
224. **Asally M, Kittisopikul M, Rue P, Du Y, Hu Z, Cagatay T, Robinson AB, Lu H, Garcia-Ojalvo J, Suel GM.** 2012. Localized cell death focuses mechanical forces during 3D patterning in a biofilm. *Proceedings of the National Academy of Sciences of the United States of America* **109:**18891-18896.
225. **Dietrich LE, Okegbe C, Price-Whelan A, Sakhtah H, Hunter RC, Newman DK.** 2013. Bacterial community morphogenesis is intimately linked to the intracellular redox state. *Journal of Bacteriology* **195:**1371-1380.
226. **Epstein AK, Pokroy B, Seminara A, Aizenberg J.** 2011. Bacterial biofilm shows persistent resistance to liquid wetting and gas penetration. *Proceedings of the National Academy of Sciences of the United States of America* **108:**995-1000.
227. **Kolodkin-Gal I, Elsholz AK, Muth C, Girguis PR, Kolter R, Losick R.** 2013. Respiration control of multicellularity in *Bacillus subtilis* by a complex of the

cytochrome chain with a membrane-embedded histidine kinase. *Genes & Development* **27:**887-899.
228. **White PB.** 1938. The rugose variant of vibrios. *Journal of Pathology and Bacteriology* **46:**1-6.
229. **Beyhan S, Yildiz FH.** 2007. Smooth to rugose phase variation in *Vibrio cholerae* can be mediated by a single nucleotide change that targets c-di-GMP signalling pathway. *Molecular Microbiology* **63:**995-1007.
230. **Morris JG, Jr., Sztein MB, Rice EW, Nataro JP, Losonsky GA, Panigrahi P, Tacket CO, Johnson JA.** 1996. *Vibrio cholerae* O1 can assume a chlorine-resistant rugose survival form that is virulent for humans. *The Journal of Infectious Diseases* **174:**1364-1368.
231. **Yildiz FH, Schoolnik GK.** 1999. *Vibrio cholerae* O1 El Tor: identification of a gene cluster required for the rugose colony type, exopolysaccharide production, chlorine resistance, and biofilm formation. *Proceedings of the National Academy of Sciences of the United States of America* **96:**4028-4033.
232. **Casper-Lindley C, Yildiz FH.** 2004. VpsT is a transcriptional regulator required for expression of *vps* biosynthesis genes and the development of rugose colonial morphology in *Vibrio cholerae* O1 El Tor. *Journal of Bacteriology* **186:**1574-1578.
233. **Matz C, McDougald D, Moreno AM, Yung PY, Yildiz FH, Kjelleberg S.** 2005. Biofilm formation and phenotypic variation enhance predation-driven persistence of *Vibrio cholerae*. *Proceedings of the National Academy of Sciences of the United States of America* **102:**16819-16824.
234. **Dietrich LE, Teal TK, Price-Whelan A, Newman DK.** 2008. Redox-active antibiotics control gene expression and community behavior in divergent bacteria. *Science* **321:**1203-1206.
235. **Wilking JN, Zaburdaev V, De Volder M, Losick R, Brenner MP, Weitz DA.** 2013. Liquid transport facilitated by channels in *Bacillus subtilis* biofilms. *Proceedings of the National Academy of Sciences of the United States of America* **110:**848-852.
236. **McCrate OA, Zhou X, Reichhardt C, Cegelski L.** 2013. Sum of the parts: composition and architecture of the bacterial extracellular matrix. *Journal of Molecular Biology* **425:**4286-4294.
237. **Weiss-Muszkat M, Shakh D, Zhou Y, Pinto R, Belausov E, Chapman MR, Sela S.** 2010. Biofilm formation by and multicellular behavior of *Escherichia coli* O55:H7, an atypical enteropathogenic strain. *Applied and Environmental Microbiology* **76:**1545-1554.
238. **Lim JY, Pinkner JS, Cegelski L.** 2014. Community behavior and amyloid-associated phenotypes among a panel of uropathogenic *E. coli*. *Biochemical and biophysical research communications* **443:**345-350.
239. **Fux CA, Shirtliff M, Stoodley P, Costerton JW.** 2005. Can laboratory reference strains mirror 'real-world' pathogenesis? *Trends in Microbiology* **13:**58-63.
240. **Squitti R.** 2012. Metals in Alzheimer's disease: a systemic perspective. *Frontiers in bioscience* **17:**451-472.
241. **DePas WH, Chapman MR.** 2012. Microbial manipulation of the amyloid fold. *Research in Microbiology* **163:**592-606.

Chapter 2

Iron Induces Bimodal Population Development by *Escherichia coli*

Abstract:

Bacterial biofilm formation is a complex developmental process involving cellular differentiation and the formation of complex 3D structures. Here I demonstrate that exposure to ferric chloride triggers rugose biofilm formation by the uropathogenic *Escherichia coli* strain UTI89 and by enteric pathogens *Citrobacter koseri* and *Salmonella enterica* serovar *typhimurium*. Two unique and separable cellular populations emerge in iron-triggered, rugose biofilms. Bacteria at the air-biofilm interface express high levels of the biofilm regulator *csgD*, the cellulose activator *adrA*, and the curli subunit operon *csgBAC*. Bacteria in the interior of rugose biofilms express low levels of *csgD* and undetectable levels of matrix components curli and cellulose. Iron activation of rugose biofilms is linked to oxidative stress. Superoxide generation, either through addition of phenazine methosulfate or by deletion of *sodA* and *sodB*, stimulates rugose biofilm formation in the absence of high iron. Additionally, overexpression of Mn-superoxide dismutase, which can mitigate iron-derived reactive oxygen stress, decreases biofilm formation in a WT strain upon iron exposure. Not only does reactive oxygen stress promote rugose biofilm formation, but bacteria in the rugose biofilms display increased resistance to H_2O_2 toxicity. Altogether, I demonstrate that iron and superoxide stress trigger rugose biofilm formation in UTI89. Rugose biofilm development involves the elaboration of two distinct bacterial populations and increased resistance to oxidative stress.

Introduction:

By adopting a biofilm lifestyle, bacteria gain resistance to antibiotics, the host immune system, and environmental stresses (1, 2). Gene expression and metabolic

processes can vary drastically from cell to cell in a biofilm community (3, 4), and cellular differentiation within a biofilm contributes to antibiotic resistance (1). Therefore, an in-depth understanding of biofilm formation is critical for the development of antibacterial agents.

Iron is an essential nutrient for almost all bacterial species, but it is efficiently sequestered by the host during an infection (5) and it is largely insoluble in aerobic environments (6). Additionally, ferrous iron can react with H_2O_2 in the Fenton reaction to form reactive hydroxyl radicals, which can damage proteins, DNA, and lipids (7, 8). To counter iron scarcity and toxicity, most bacteria express efficient iron acquisition systems and tightly regulate intracellular iron homeostasis (6, 8).

Iron affects biofilm formation in a variety of bacteria (9-13). In *E. coli*, the master biofilm regulator *csgD* appears to have several indirect ties to iron sensing, transport, and availability. Overexpression of *csgD* inhibits transcription of the iron regulator *fecR* and the outer membrane ferric-coprogen receptor *fhuE* (14). Furthermore, CsgD binding sites are present upstream of the *fepDGC* and *entS* operons, which encode components of a ferric enterobactin transporter and an enterobactin exporter, respectively (15). Finally, iron chelators promote *csgD* expression in *Salmonella enterica* serovar *typhimurium* (16, 17).

In this study I investigated the relationship between curli expression, biofilm formation, and environmental iron levels in an *E. coli* cystitis isolate, UTI89. Uropathogenic *E. coli* (UPEC) is the predominant agent of urinary tract infections, and biofilm formation and the production of curli fibers contribute to UPEC pathogenesis (18, 19). Curli fibers are functional amyloids that form an integral component of the extracellular matrix (20). CsgD controls *E. coli* biofilm formation largely through induction of the curli subunit operon *csgBAC* (21) and the cellulose activator *adrA* (22, 23). Along with curli, cellulose aids cell-to-cell attachment and adherence to inorganic surfaces and host cells (24-26). UTI89 and a variety of other bacterial species form rugose biofilms (also known as rdar) on agar plates (4, 23, 27-29). In both *S. typhimurium* and *E. coli*, the CsgD-regulated matrix components curli and cellulose are necessary for development of rugose biofilms (23, 27, 30).

This work revealed several features of *E. coli* biofilms in response to iron. First, I observed that iron induced UTI89 rugose biofilms without increasing total matrix production. Within a rugose biofilm, distinct and separable bacterial populations emerged. Curli-production was limited to bacteria at the air/biofilm interface and non-curli-producing bacteria filled the interior of rugose biofilm wrinkles. Furthermore, superoxide could activate the rugose biofilm developmental pathway in place of high iron, and rugose biofilm formation coincided with increased survival after H_2O_2 treatment. Altogether I describe a novel biofilm pathway involving formation of a bimodal bacterial population and oxidative stress resistance in enteric bacteria.

Results:

Iron Triggers the Formation of *csgD*-dependent Rugose Biofilms

UTI89 forms *csgD*-dependent rugose biofilms on YESCA agar plates (Fig. 2.1). To test the effect of iron levels on rugose biofilm development, I treated YESCA with Chelex-100, a chelating resin. WT UTI89 grown on Chelex-treated YESCA agar plates (referred to as low iron conditions) did not form rugose biofilms. Addition of 2 mM $FeCl_3$ to the cell mixture before plating (referred to as high iron conditions) restored biofilm formation (Fig. 2.2A). As expected, a *csgD* mutant was unable to form rugose biofilms in either low or high iron conditions (Fig. 2.2A). To determine whether iron-induced rugose biofilm formation coincided with increased curli fiber production, whole cell western blot analysis probing for the major curli subunit CsgA was performed on UTI89 grown in low or high iron conditions. Bacteria grown in low iron conditions unexpectedly expressed more CsgA than rugose-forming UTI89 grown in high iron conditions (Fig. 2.2B). However, rugose biofilms coincided with an increase in cell aggregation after treatment with a tissue homogenizer (Fig. 2.2B). Since aggregation was dependent on *csgD* (Fig. 2.2B), I hypothesized that curli and cellulose were components of the aggregate. This could bias western blot analysis, as non-curliated, suspended bacteria would more likely be sampled. To prevent aggregation, I produced a UTI89 mutant that cannot synthesize cellulose. In most, but not all *E. coli* strains, *csgD* activates cellulose production by inducing transcription of *adrA* (23, 31). In turn, the diguanylate cyclase AdrA stimulates the cellulose synthase BcsA, presumably through production of cyclic-di-GMP, as BcsA

contains a cyclic-di-GMP binding domain (31-33). I verified that UTI89 rugose biofilm formation was dependent on *csgD*, *adrA*, and *bcsA* (22, 23, 31) (Fig. 2.1, 2.2C). No aggregates collected when the *bcsA* mutant was tissue homogenized (Fig. 2.2C). I therefore repeated the CsgA western blot described above in the *bcsA* mutant background and found that overall levels of CsgA remained unchanged in low vs. high iron conditions (Fig. 2.2D). Furthermore, β-galactosidase assays of a *bcsA* mutant transformed with plasmids encoding *csgBAC-lacZ* or *adrA-lacZ* transcriptional fusions revealed that expression of neither operon changed in response to iron (Fig. 2.2E). Our results demonstrate that iron drives rugose biofilm development and cell aggregation in UTI89. However, since overall curli production does not change as a result of varying iron concentrations, I inferred that iron exposure may trigger clustering of curli-producing cells within a rugose biofilm.

To test whether ferrous iron could also induce rugose biofilm formation, I loaded sterile paper discs with either $FeCl_2$ or $FeCl_3$ on low iron plates. UTI89 was spotted next to the discs and incubated for 48 hours. Both types of iron were able to induce rugose biofilm formation (Fig. 2.3).

Rugose Biofilms Contain Two Distinct, Separable Bacterial Populations

Our data lead us to hypothesize that two bacterial populations are present in a rugose biofilm – 1) matrix-associated and 2) non-matrix-associated. To mechanically separate these populations, I flooded a rugose biofilm in potassium phosphate buffer pH 7.2 (KPi) with light shaking, reasoning that a non-matrix-encased population would be washed into suspension. Upon shaking, the biofilm floated off the agar surface (Fig. 2.4A). Bacteria that washed freely into suspension (washout fraction) were separated from the aggregated bacteria (matrix fraction), which maintained its general shape after loss of the washout cells (Fig. 2.4A). Aggregates only settled out of suspension after tissue homogenization of the matrix fraction (Fig. 2.4B), and western blot analysis demonstrated that CsgA was solely associated with matrix fraction bacteria (Fig. 2.4C).

To test whether cellulose, the other major rugose biofilm component, was also absent in the washout fraction, I quantified binding of Congo red (CR) – a diazo dye that binds to both curli and cellulose (31, 34). Washout fraction bacteria bound a similar amount of CR as a *csgBA bcsA* double mutant (Fig. 2.5), indicating that they produce

neither curli nor cellulose (34). Consistent with the CR-binding results, β-galactosidase assays showed that transcription of *csgDEFG, csgBAC,* and *adrA* was significantly reduced in the washout fraction as compared to the matrix fraction (Fig. 2.4D). Therefore I were able to identify and mechanically separate matrix-encased and non-matrix encased bacteria in a rugose biofilm.

Curliated Bacteria are Localized to the Air-Biofilm Interface in Rugose Biofilms

Confocal microscopy was used to locate curli-producing cells within a rugose biofilm. A UTI89 strain harboring a *csgBAC-mCherry* transcriptional fusion at the *attB* site was transformed with the IPTG-inducible GFP expressing plasmid pCKR101-*eGFP*. I reasoned that all metabolically active cells would express GFP while curli-expressing cells would produce both mCherry and GFP. Z-stack videos taken from a rugose biofilm grown on a YESCA agar plate revealed that bacteria expressing mCherry were localized to the biofilm surface, while a population of non-curli-producing bacteria was localized to the interior of the each wrinkle (35). Cross-section images of the biofilm midpoint, as well as 3D reconstructions of biofilm sections, further demonstrated that each wrinkle is filled with a population of non-curli-producing cells (Fig. 2.6A, C, D). After the washout assay, cells were absent from the wrinkle interiors, indicating that interior, non-curli-producing cells were removed as the washout fraction (Fig. 2.6B, C, E) (35).

To specifically probe iron-responsive architectural changes, the *csgBAC-mCherry*/pCKR101-*eGFP* reporter strain was grown on Chelex-treated YESCA plates with or without $FeCl_3$ added to the cell mixture. In the low iron colony, GFP and mCherry were evenly distributed throughout, indicating no large-scale spatial separation between curli-expressing cells and non-curli-expressing cells except for a gradual increase in curli/mCherry-producing cells near the biofilm surface (Fig. 2.7A). When iron was added to the cell mixture before plating on Chelex-treated YESCA plates, the distribution of cells throughout the rugose biofilms matched that seen on YESCA plates (Fig. 2.7B, 2.6D).

Oxygen levels can affect folding and activity of fluorophores (36). Since oxygen penetration into biofilms is generally limited (3), I also imaged expression patterns of a UTI89 *attB*::*csgBAC-eGFP*/pCKR101-*mCherry* strain. In this strain, mCherry producing

cells were localized to the interior of the wrinkles. Bacteria expressing both mCherry and GFP lined the air/biofilm interface (Fig. 2.7C). Since this pattern was essentially the inverse of that seen in Fig. 2.6D, I concluded that both fluorophores can fluoresce in the biofilm interior and that the *csgBAC* promoter is repressed in the interior washout cells.

Superoxide Stress Drives Rugose Biofilm Formation

Since iron triggers rugose biofilm formation, I hypothesized that an iron responsive regulatory protein was involved in the rugose biofilm developmental process. To test this, I knocked out known iron-responsive transcriptional factors that have also been shown to affect biofilm formation. Our candidates included the global iron regulator, Fur (11, 12), the iron-sulfur cluster regulator, IscR (9), the ferric iron sensing two-component system, BasSR (37), and the small RNA, RyhB (10). All of the mutants still formed rugose biofilms in response to iron (Fig. 2.8). However, the *fur* mutant wrinkled more than WT in low iron conditions (Fig. 2.8, 2.9A).

A *fur* mutant constitutively expresses various iron acquisition systems and accumulates toxic amounts of cytoplasmic free ferrous iron (38). To investigate the possibility that the increase in rugose biofilm formation in the *fur* mutant is due to iron-induced toxicity, I constructed a UTI89 *sodA sodB* double mutant that cannot produce cytoplasmic superoxide dismutase. In a *sodA sodB* mutant, cytoplasmic superoxide accumulates and breaks down solvent exposed [4Fe-4s] clusters in vulnerable proteins, freeing ferrous iron (39-41). The *sodA sodB* mutant formed a rugose biofilm under low iron conditions in a similar manner as the *fur* mutant (Fig. 2.9A). I also overexpressed *sodA* in a *fur* mutant to see if rugose biofilm formation was dampened, as reactive oxygen stress in a *fur* mutant can be partly negated by *sodA* overexpression (38). Rugose biofilm formation was decreased under low iron conditions in both the *fur* mutant and *sodA sodB* mutant when *sodA* was overexpressed (Fig. 2.9B).

Since accumulation of endogenous superoxide induced rugose biofilm development, I next tested whether superoxide-producing antibiotics can induce rugose biofilm formation in place of high iron levels. *Pseudomonas aeruginosa* along with a variety of other bacteria produce redox-cycling antibiotics called phenazines (29, 42). In susceptible bacteria such as *E. coli*, phenazines enter the cell and produce superoxide by oxidizing cytoplasmic targets and reducing molecular oxygen (43). Intriguingly,

exogenous phenazine methosulfate exposure resulted in rugose biofilm formation in low iron conditions in UTI89, albeit at a slower rate than iron induction (Fig. 2.9C). A *sodA* mutant developed a rugose biofilm more rapidly than WT in response to phenazine exposure (Fig. 2.9D). As both iron and superoxide can independently induce rugose biofilms, our next question was whether reactive oxygen stress was involved in iron-driven rugose biofilm formation. To this end, I overexpressed *sodA* in WT and observed rugose biofilm formation on Chelex-treated YESCA plates supplemented with 10 μM $FeCl_3$ (Fig. 2.9E). Overexpression of *sodA* decreased rugose biofilm formation after 48 hours. Altogether, these results indicate that both iron and superoxide stress trigger rugose biofilm formation. Furthermore, iron-induced rugose biofilm formation is at least partly dependent on reactive oxygen stress.

Lastly, I sought to determine whether induction of rugose formation was specific to iron. I therefore exposed WT UTI89 to various metals on chelex-100-treated YESCA plates. Among the metals tested, gallium and aluminum were the only other metals besides iron able to induce rugose formation to any degree (Fig. 2.10). Gallium and aluminum are both transition metals that demonstrate toxicity towards bacteria. Gallium has a similar ionic radius as iron, but cannot redox cycle. Therefore it can disrupt iron homeostasis by binding to otherwise Fe^{3+} specific siderophores and proteins and preventing proper protein function (44, 45). The mode of aluminum toxicity is less understood, but like gallium, aluminum has a similar ionic radius to iron, and there is evidence that aluminum can also bind to iron-specific siderophores (46, 47). Altogether, these results indicate that iron-induced oxidative stress triggers rugose biofilm formation.

Rugose Biofilm Formation Coincides with H_2O_2 Resistance

Since rugose biofilm development can be triggered by reactive oxygen stress, I hypothesized that a rugose biofilm would demonstrate increased resistance to H_2O_2. Therefore, UTI89 grown in low or high iron conditions was tissue-homogenized, normalized by OD_{600}, and treated with H_2O_2. Strikingly, iron-induced rugose biofilm development corresponded with H_2O_2 resistance (Fig. 2.11A). I next tested H_2O_2 resistance of the washout and the matrix fractions of rugose biofilms grown on a Chelex-treated YESCA plate with addition of iron. Intriguingly, washout fraction bacteria

were more sensitive to H_2O_2 than matrix fraction cells, while both fractions were more resistant than bacteria grown under low iron conditions (Fig. 2.11A).

Reactive oxygen species are generated as a byproduct of aerobic metabolism (48, 49), and oxygen diffusion into biofilms is generally limited due to respiration by periphery cells (3). I hypothesized that within a rugose biofilm, interior, non-matrix encased bacteria would be exposed to less atmospheric oxygen than matrix-encased, exterior cells. Oxygen microsensor measurements of a rugose biofilm demonstrated that oxygen levels decrease with biofilm depth (Fig. 2.11B). Assuming equal oxygen penetration from both the top and the sides of a single wrinkle, I can then map oxygen penetration depth onto a confocal image of curli-expressing cells in a rugose biofilm (Fig. 2.11C). The interior, non-matrix-associated cells of a rugose biofilm are therefore exposed to roughly 25-70% atmospheric oxygen, depending on their proximity to the surface (Fig. 2.11C). Altogether these data indicate that rugose biofilm formation parallels H_2O_2 resistance. Within a rugose biofilm, interior, washout cells are partly shielded from oxygen and are more susceptible to reactive oxygen stress than their matrix-encased neighbors.

Due to the increase in curli expression and hydrogen peroxide resistance in the matrix fraction, I hypothesized that RpoS levels might be increased in the matrix fraction. RpoS is required for *csgD* expression and for expression of the catalase *katE* (50, 51). Furthermore, Serra *el. al.* suggested that elongated, interior bacteria in rugose biofilms likely have decreased RpoS levels (52, 53). I directly tested catalase activity in each biofilm fraction by utilizing an Amplex red/Horseradish peroxidase assay (54). Catalase activity was equivalent in both rugose biofilm fractions in WT UTI89 (Fig. 2.12A). However, *E. coli* encodes another catalase, *katG*, that is induced upon exposure to hydrogen peroxide by OxyR (54, 55), and is most likely induced during the course of the assay. A *katG* mutant revealed that *katE*-dependent catalase activity was increased in the matrix fraction (Fig. 2.12A). Furthermore, a *katG rpoS* mutant demonstrated the same catalase activity as a *katG katE* double mutant, demonstrating that *katE*-dependent catalase activity is increased in the shell fraction in an *rpoS*-dependent manner (Fig. 2.12B). Western blots suggest that RpoS levels may in fact be slightly decreased in the washout fraction (Fig. 2.12C).

Iron Triggers Bimodal Rugose Biofilms in other Enteric Bacteria

Lastly I wanted to determine if iron-induced rugose biofilm formation was widespread among enterics. To this end *S. typhimurium* and a clinical isolate of *Citrobacter koseri,* which form rugose biofilms on LB – salt and YESCA plates respectively (Fig. 2.13A), were plated on Chelex-treated agar plates with or without addition of $FeCl_3$. Both strains formed rugose biofilms only when exposed to iron (Fig. 2.13B). Furthermore, CsgA was largely localized to the matrix fractions after performing the washout assay (Fig. 2.13C). As in UTI89, rugose biofilm formation paralleled H_2O_2 resistance in each strain (Fig. 2.13D). I conclude that iron-induced bimodal rugose biofilm development and the increase in H_2O_2 resistance as a function of rugose biofilm formation are common features of enteric bacteria.

Discussion:

Our results demonstrate that iron induces macroscopic architectural restructuring and H_2O_2 resistance in UTI89 biofilms (Fig. 2.2,2.11). However, total curli levels did not change in response to varying iron concentrations (Fig. 2.2), indicating that matrix production is not sufficient for rugose biofilm formation. Previous work has found that low iron levels can affect curli production under certain conditions, as iron chelators added to *S. typhimurium* results in lower curli expression (16, 17). However, comparing the *Salmonella* results with ours is difficult because of disparities in strains used and growth conditions. Iron-dependent rugose biofilm formation has likely not been reported before because common laboratory media has sufficient iron to induce rugose biofilm formation, as is evidenced by the fact that WT UTI89, *C. koseri* and *S. typhimurium* form rugose biofilms on YESCA or LB - salt agar plates without the addition of iron (Fig. 2.13A).

Both iron availability and biofilm formation affect UPEC pathogenesis. During infection, UPEC ascends the urethra into the bladder. Once in the bladder, UPEC is able to attach to and invade urothelial cells (56). After cell invasion, UPEC forms biofilm-like pods, termed intracellular bacterial communities (IBCs) (18), and IBC formation helps UPEC avoid the host immune system (18, 56, 57). Growth in urine induces

expression of a variety of iron acquisition systems in UPEC, demonstrating that urine is an iron-limiting environment (58). Additionally, IBC formation correlates with induction of genes involved in acquiring iron from heme and siderophores (59). As iron and biofilm formation both play a significant role in UPEC pathogenesis, it is tempting to speculate that the iron-induced biofilm formation I describe here may contribute to UPEC virulence.

Experiments with UTI89 grown in low and high iron conditions revealed that iron induces aggregation and rugose biofilm development. There are at least two spatially distinct cellular populations within rugose biofilms: matrix-encased and non-matrix-encased (Fig. 2, 3). Studies in *S. typhimurium* have previously demonstrated that levels of CsgD and curli can vary from cell to cell in bacterial communities (17, 60). Here I have demonstrated a distinct bimodal restructuring in which matrix-producing bacteria line the air/biofilm interface while non-matrix-producing bacteria fill the wrinkle interiors. Additionally, the two populations are easily separated, as expression of curli and cellulose imbues a rigidity to the matrix-encased cells that prevents them from being suspended during buffer washes. Separation via the washout assay allows for examination of the two distinct populations by biochemical and genetic techniques. The dramatic disappearance of curli and cellulose and the elevated H_2O_2 susceptibility in the washout fraction imply significant physiological differences between washout and matrix fractions.

We have determined that the iron-induced rugose biofilm developmental pathway is triggered, at least in part, by reactive oxygen stress. However, the mechanism by which high extracellular iron would cause intracellular reactive oxygen stress is unclear. *E. coli* is able to maintain a steady intracellular iron pool, regardless of extracellular iron fluctuations, due to the efficacy of iron homeostasis regulators such as Fur and RyhB (6). Fur is a transcriptional regulator that binds to ferrous iron and represses expression of iron acquisition systems. RyhB is a small RNA that limits production of iron-containing proteins in low iron conditions (6, 61). Therefore high extracellular iron should not necessarily lead to cytoplasmic free iron stress. High iron levels could allow for rapid cell growth and aerobic respiration, resulting in superoxide production from the electron transport chain (48, 49). Additionally, it has been proposed that normal fluxes in

intracellular free iron through Fe-Fur cycling can lead to brief periods of iron stress (38). If this is the case, the summation of oxidative stress from multiple free iron cycles may lead to enough reactive oxygen stress to induce rugose biofilm formation. *sodA* overexpression could temper the amount of free iron stress in each cycle. Future work will elucidate the genetic pathways leading from oxidative stress to the development of rugose biofilms.

A wide-variety of bacterial species form rugose biofilms (4, 23, 28, 29). While the triggers of rugose biofilm development no doubt vary between systems, the conserved wrinkled architecture implies a measure of commonality. Rugose biofilm formation in *P. aeruginosa* is inhibited by self-produced phenazines (29). Intriguingly, I found that *E. coli* forms rugose biofilms when exposed to phenazines or when it is unable to neutralize endogenous superoxide (Fig. 2.9A, C). Furthermore, a recent study in *Bacillus subtilis* determined that localized cell death contributes to the mechanical buckling necessary for rugose biofilm wrinkle formation (28). It is tempting to speculate that superoxide stress could accelerate cell death, although I found that both the washout and matrix fraction cells are viable under conditions that promote rugose biofilm formation (Fig. 2.11A). Additionally, I would expect superoxide toxicity to increase with proximity to molecular oxygen, and I have demonstrated that interior bacteria in a rugose biofilm are exposed to less atmospheric oxygen than their surface-exposed neighbors.

Biofilm formation, and in particular cellular differentiation within biofilms, contributes to bacterial antibiotic resistance (1). The sophisticated genetic tools available in *E. coli*, the large body of literature dedicated to *E. coli* metabolism, and the prevalence of *E. coli*-mediated uropathogenic infections make UTI89 an attractive model for biofilm development. Within iron-induced rugose biofilms, two populations, matrix-encased and non-matrix-encased, emerge. These populations are easily separable due to the loose association of interior cells with the biofilm matrix. Rugose biofilm development also parallels tiered H_2O_2 resistance, with surface-exposed bacteria being more resistant than interior cells. Analysis of the mechanisms of dual-population formation and the genetic pathways involved in H_2O_2 resistance will provide further insight into a biofilm developmental pathway.

Materials and Methods:

Reagents:

Catalase from bovine liver, H_2O_2, $FeCl_3$, tryptophan, and $MnCl_2 \cdot 4H_2O$ were obtained from Sigma-Aldrich. Congo red was obtained from Acros Organics. Casamino acids were obtained from Amresco. Chelex-100 was obtained from Bio-Rad. Noble agar was obtained from BD. ProLong Gold Antifade Reagent was obtained from Invitrogen and $CaCl_2$, $MgCl_2$, IPTG, tryptone, yeast extract, and agar were obtained from Fisher.

Strains, Growth Conditions, and Cloning:

Strains and plasmids are listed in Table 2.1 and primers are listed in Table 2.2. Bacteria were routinely grown in LB broth at 37°C under aeration. Rugose biofilms were grown for 48 hours on agar plates at 26°C unless otherwise noted. UTI89 was obtained from Scott Hultgren (62). *Salmonella enterica* serovar *Typhimurium* strain ATCC 14028 was obtained from the American Type Tissue Collection. *Citrobacter koseri* was obtained from the University of Michigan medical school. Strains were routinely grown in LB at 37°C under aeration. The *sodA sodB* and *fur* mutants were grown without shaking to avoid excessive oxygen exposure. Mutations were introduced into UTI89 by the lambda red recombinase method as described (63). The plasmid pCKR101 (39) was used for all overexpression experiments. For construction of overexpression vectors, inserts were amplified from the UTI89 genome and cloned into the pCKR101 vector using KpnI and XbaI restriction sites. The *lacZ* transcriptional fusion plasmids pRJ800 (empty vector), pBA14 (*csgBAC* promoter driving *lacZ*), and pD1 (*csgDEFG* promoter driving *lacZ*) have been described (64). pRJ800-*adrA* (*adrA* promoter driving *lacZ*) was constructed by cloning a UTI89 genomic fragment including the *adrA* promoter into pRJ800 using BamHI and XbaI. Integration of the *csgBAC-mCherry* transcriptional fusion into the UTI89 *attB* site was performed as described (65, 66), except *mCherry* was cloned from pAH6 (67) into pCD13psk using SpeI and SacI restriction sites while the *csgBAC* promoter was cloned into pCD13psk from the UTI89 genome using HindIII and SpeI.

Rugose Formation and Low Iron Media:

For rugose biofilm development, UTI89 was grown overnight in LB, diluted to 1 OD_{600} and rinsed twice with YESCA media (10 g Casamino acids, 1 g yeast extract/L). 4 µl of

a 1 OD_{600} cell mixture was spotted onto YESCA agar plates (10 g Casamino acids, 1 g yeast extract, 20 g agar/L). Congo red YESCA plates included a 50 µg/mL supplement of Congo red. Bacteria were incubated at 26°C for 48 hours unless otherwise noted. Pictures were taken either with a Canon EOS Rebel XSi camera or a Leica MZ FLIII Stereo-Fluorescence Microscope coupled to a Leica DC480 Microscope camera. For low iron media, YESCA media was incubated with Chelex-100 at 5 g/100 mL for 2 hours at room temp with fresh resin or ON at room temp with regenerated resin. Media was then filtered with 0.22 µM PES bottle-top filters to separate the resin. For Chelex-treated agar plates, media was autoclaved with 1.4% Difco Noble Agar and supplemented with 100 µM $MgCl_2$, 10 µM $CaCl_2$, and 100 µM tryptophan. $FeCl_3$, $MnCl_2$, and IPTG were also supplemented where indicated. For typical rugose biofilm formation on Chelex-treated plates, cells were grown ON in LB, rinsed twice with Chelex-treated YESCA media, and resuspended at 1 OD_{600}. 0 µl or 2 µL of 100 mM $FeCl_3$ (low iron vs. high iron conditions) was added to 100 µL of 1 OD_{600} cells. 4 µl dots of these mixes were plated on Chelex-treated plates. For paper disc assays, 5 µL of indicated chemicals was added to sterile paper discs after cell mixes had been plated and had dried. For overexpression assays IPTG was added to plates at a final concentration of 10 µM or 50 µM as noted. Ampicillin and kanamycin were added when appropriate to final concentrations of 100 mg/mL and 50 mg/mL respectively. For rugose biofilm development, *S. typhimurium* was grown on LB – salt agar plates (10 g tryptone, 5 g yeast extract, 17 g agar /L) or Chelex-treated LB – salt agar plates for 72 hours and *C. koseri* was grown on YESCA agar plates or Chelex-treated YESCA agar plates for 48 hours.

Confocal Microscopy:

4 µL of 1 OD_{600} cells were dotted onto Millipore 0.05 µM MF-Membrane Filters that had been placed on YESCA agar plates or Chelex-treated YESCA plates. For induction of the pCKR101-*eGFP* or pCKR101-*mCherry* plasmids, 1 mM IPTG was added to cell mixtures prior to plating. After 48 hours at 26°C, colonies and their underlying filter were cut out with a razorblade and transferred to a microscope slide. 100 µL of Invitrogen ProLongGold antifade reagent was added to the top of each biofilm, and a 24x60-1.5 coverslip was placed on top. Small spacers roughly 0.3 mM in height were placed in

each corner of the slide before addition of the coverslip to prevent direct contact between the biofilm and the coverslip. Samples were analyzed the next day with a Leica SP5 laser scanning confocal microscope (Leica GmbH, Mannheim Germany) on a DM6000B microscope base using a 20x or 40x objective. A double-dichroic 488/561 beam splitter and a 488nm argon laser (eGFP) and a 561nm DPSS laser (mCherry) were utilized for image capture. Images and movies were analyzed with LAS AF v2.6.3 build 8173 software.

H_2O_2 Viability Assays:

For UTI89, mature biofilms or washout/matrix fractions were suspended in 50 mM KPi pH 7.2, tissue homogenized, and 250 µL of cells normalized to 1 OD_{600} were mixed with 250 µL 1% H_2O_2 in 50 mM KPi pH 7.2. This mixture was incubated for 20 minutes. 500 µL of 1 mg/mL catalase was then added to stop H_2O_2-induced killing, and cells were spun down at 12,000 rpm for 1 minute. Cells were then resuspended in 250 µL 50 mM KPi pH 7.2, and 4 µL dots of 10-fold serial dilutions were plated on LB plates and grown ON at 37°C. *S. typhimurium* and *C. koseri* viability assays were performed identically except *S. typhimurium* was mixed with 1% H_2O_2 for 15 minutes and *C. koseri* was mixed with 3% H_2O_2 for 20 minutes.

Western Blot Analysis:

Western blotting was performed as described (68) with modifications. Briefly, samples were treated with HFIP to solubilize CsgA. After HFIP was removed with a Thermo Savant SPD SpeedVac, samples were resuspended in SDS running buffer. Samples were then electrophoresed in 15% polyacrylamide gels and transferred onto a nitrocellulose membrane in a wet transfer apparatus in 25 mM CAPS transfer buffer pH 11.2 with 10% methanol. Blots were blocked with 5% milk in TBST for 1 hour at room temp or ON at 4°C. After TBST washes, blots were incubated for 1 hour with primary (1:5000 Santa Cruz RNA pol σ D antibody, 1:5000 Santa Cruz RNA pol σ S Antibody, and 1:8500 anti-CsgA peptide antibody (64)) and secondary (horseradish peroxidase-linked anti-mouse and anti-rabbit, both at 1:8500) antibodies in 1% BSA, 1% milk in TBST at room temp.

Oxygen Microelectrode Measurements:

UTI89 was grown on YESCA agar plates for rugose biofilm formation. Oxygen

microsensor measurements were performed as described (69, 70). All microprofiles were performed using Clark-type oxygen micro-electrodes with outside tip diameters of 10 µm, response time 1-3 sec and < 2% stirring sensitivity (Unisense, A/S). Amplification and sensor positioning was controlled with a microsensor multi-meter coupled with a motor controlled micromanipulator. Data collection was aided by software packages, SensorTrace Pro ver.3.0.1 (Unisense. A/S). Two point calibrations were performed in air saturated DI water and in a 1 M NaOH, 0.1 M ascorbic acid solution (anoxic standard). Calibrations were repeatedly checked in the anoxic standard and in air saturated DI water throughout the experiments. Triplicate oxygen measurements (both biological and technical-position replicates) were done in one-dimension (depth-wise) from the biofilm-air interface down in. The step size between measurements was 10 µm.

Quantitative Congo Red Binding:

Congo red (CR) binding assays were performed as described (34) with modifications. Mature biofilms were harvested and suspended in 50 mM KPi pH 7.2. A 300 µL suspension of 2 OD_{600} cells and 5 µg/mL CR was incubated with shaking at 37°C for 30 minutes. Cells were then pelleted at 12,000 RPM for 1 minute, and 100 µL of the supernatant was assayed for absorbance at 490 nm in a Tecan infinite M200 platereader. Absorbances were then subtracted from a CR only negative control, and percentage of CR removal was calculated, with the CR only control representing 0% removed and the KPi only control representing 100% removed. Error bars represent the standard deviation of three biological replicates.

Catalase Activity:

Hydrogen peroxide scavenging by whole cells was performed by the amplex red/horseradish peroxidase assay as described (71) with minor modifications. Briefly, cells were diluted to .1 OD600 in 50 mM kPi pH 7.8 in 100 µL and were added to a well of a 96-well plate. Hydrogen peroxide was added to 150 µM for each sample and this mix was incubated for 15 minutes. 25 µL of a 200 µM stock solution of amplex red (AR) dissolved in 50 mM kPi pH 7.8 and 25 µL of 0.02 mg/mL horseradish peroxidase dissolved in 50 mM kPi pH 7.8 were then added to each well and absorbance was read at 568 nM. Samples were diluted when necessary, a mix of cells, AR, and HRP without

hydrogen peroxide was assayed and subtracted as the blank, and concentrations were measured by plotting on a standard curve obtained with samples of 0-50 μM hydrogen peroxide.

β –galactosidase Assays:

β –galactosidase assays were performed as described (64, 72) with modifications. 100 μL of suspended cells were added to the wells of a 96-well plate and multiple dilutions were added to 90 μl reaction buffer. These reactions were incubated at 30^0C for 30 minutes before addition of 20 μl of 4 mg/mL ONPG. Reactions were stopped via addition of 50 μL 1 M Na_2CO_3 at a light yellow color and the time was recorded. Abs. of each cell suspension at 600 nm and abs. of each reaction mixture at 420 nm and 550 nm were measured using a Tecan infinite M200 platereader. β –galactosidase assays were performed in triplicate on a strain carrying an empty vector (pRJ800) under each condition. Average Miller units from the pRJ800-carrying strains were subtracted from each respective strain carrying pBA14, pD1, or pRJ800-*adrA*. After subtracting out the empty vector values, averages, standard deviations, and p-values were calculated from biological triplicates of strains carrying pBA14, pD1, or pRJ800-*adrA* as noted.

Washout Assay:

After 48 hours of growth on agar plates, a sterile metal spatula was used to cut out and transfer a slab of agar containing an intact colony to a well of a Falcon Tissue-treated Polystyrene 24-well plate. 1 mL of sterile 50 mM KPi pH 7.2 was added to the well and the plate was shaken gently until the matrix fraction had completely dissociated from the agar surface (typically 5 minutes). The KPi buffer was removed and the ‘washout’ cells were spun down. Two more 5-minute washes were performed on the colony, and buffer from each rinse was added to the washout tube and spun down. A pipette tip was used to remove the ‘matrix’ fraction from the third rinse and the entire matrix was placed in a separate eppendorf tube with 1 mL KPi. The matrix fraction was then tissue homogenized. Briefly, a Fisher Scientific Tissuemiser tissue homogenizer was inserted into the eppendorf tube, turned to medium speed, and run for 20 seconds. Aggregates were allowed to settle, and suspended cells from each fraction were then assayed.

Figures and Tables:

Figure 2.1 UTI89 forms CsgD-dependent Rugose Biofilms
WT UTI89 and mutants were plated on YESCA agar plates or Chelex-treated YESCA agar plates with or without the addition of CR. Strains producing either curli or cellulose bind CR, but a curli cellulose double mutant does not. A *csgD* mutant does not bind CR, indicating that CsgD is required for curli and cellulose production in UTI89. Both curli and cellulose are required for WT rugose biofilm formation.

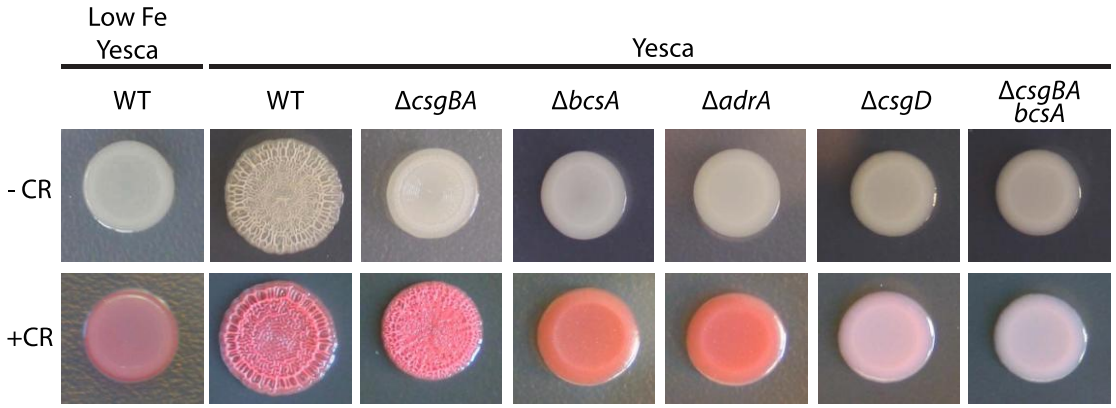

Figure 2.2 Iron induces UTI89 rugose biofilm formation

(A) WT UTI89 or a *csgD* mutant were grown on Chelex-treated YESCA plates with or without 2 mM $FeCl_3$ added to the cell mixture before plating. **(B)** After tissue homogenization, aggregates immediately began falling out of suspension and were fully settled within 10 minutes. Aggregation increased with rugose biofilm formation and was dependent on *csgD* (top of panel). Suspended cells from low iron colonies demonstrate an increase in CsgA protein levels by whole cell western blot compared to suspended cells from high iron conditions, while σ^{70} levels remain constant (bottom of panel). **(C)** A *bcsA* mutant does not form rugose biofilms (left side of panel) and does not form aggregates after tissue homogenization (right side of panel) when grown in either low or high iron conditions. **(D)** A western blot of the *bcsA* mutant shows that total CsgA levels do not change between low and high iron conditions. **(E)** A UTI89 *bcsA* mutant strain carrying *csgBAC* (pBA14) or *adrA* (pRJ800-*adrA*) transcriptional *lacZ* fusion plasmids or an empty vector (pRJ800) were plated on Chelex-treated YESCA plates with or without the addition of $FeCl_3$

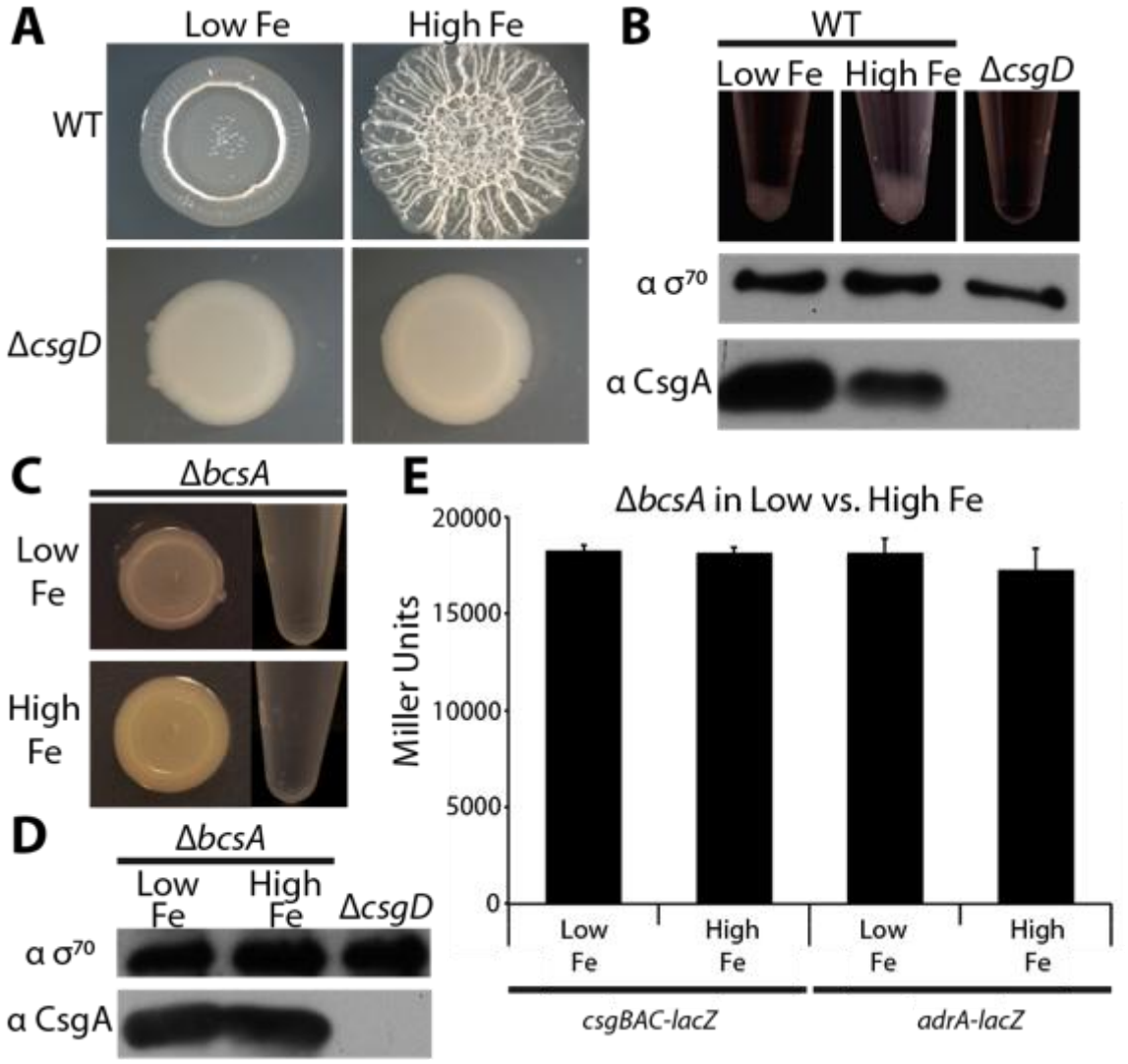

Figure 2.3 Both ferrous and ferric iron can trigger UTI89 rugose biofilms
WT UTI89 was plated on low iron plates next to a disc loaded with 100mM $FeCl_3$ (ferric iron) or $FeCl_2$ (ferrous iron).

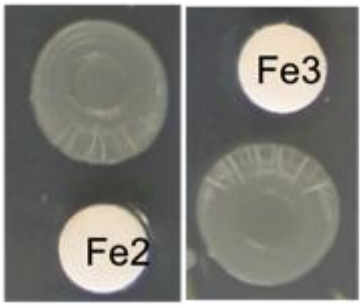

Figure 2.4 Two separable populations, matrix producing and non-matrix-producing, are present in a rugose biofilm (A) Washing a UTI89 rugose biofilm in 50 mM KPi buffer after growth on a YESCA agar plate separates suspended 'washout' from aggregative 'matrix' bacteria. **(B)** Cell aggregates only collect after tissue homogenization of the matrix fraction**. (C)** Western blot analysis demonstrates that CsgA is localized solely to the matrix fraction bacteria. **(D)** WT UTI89 or a *csgD* mutant carrying *csgBAC* (pBA14), *adrA* (pRJ800-*adrA*), or *csgDEFG* (pD1) transcriptional *lacZ* fusion plasmids were grown on YESCA plates. β –galactosidase assays were performed on each strain before (whole) or after the washout assay, and error bars represent the standard deviation of biological triplicates. WT and a *csgD* mutant carrying an empty vector (pRJ800) were also assayed, and average Miller units from these strains were subtracted from the respective samples. Asterisks represent P values (*P < 0.05) evaluated using a Student's t-test.

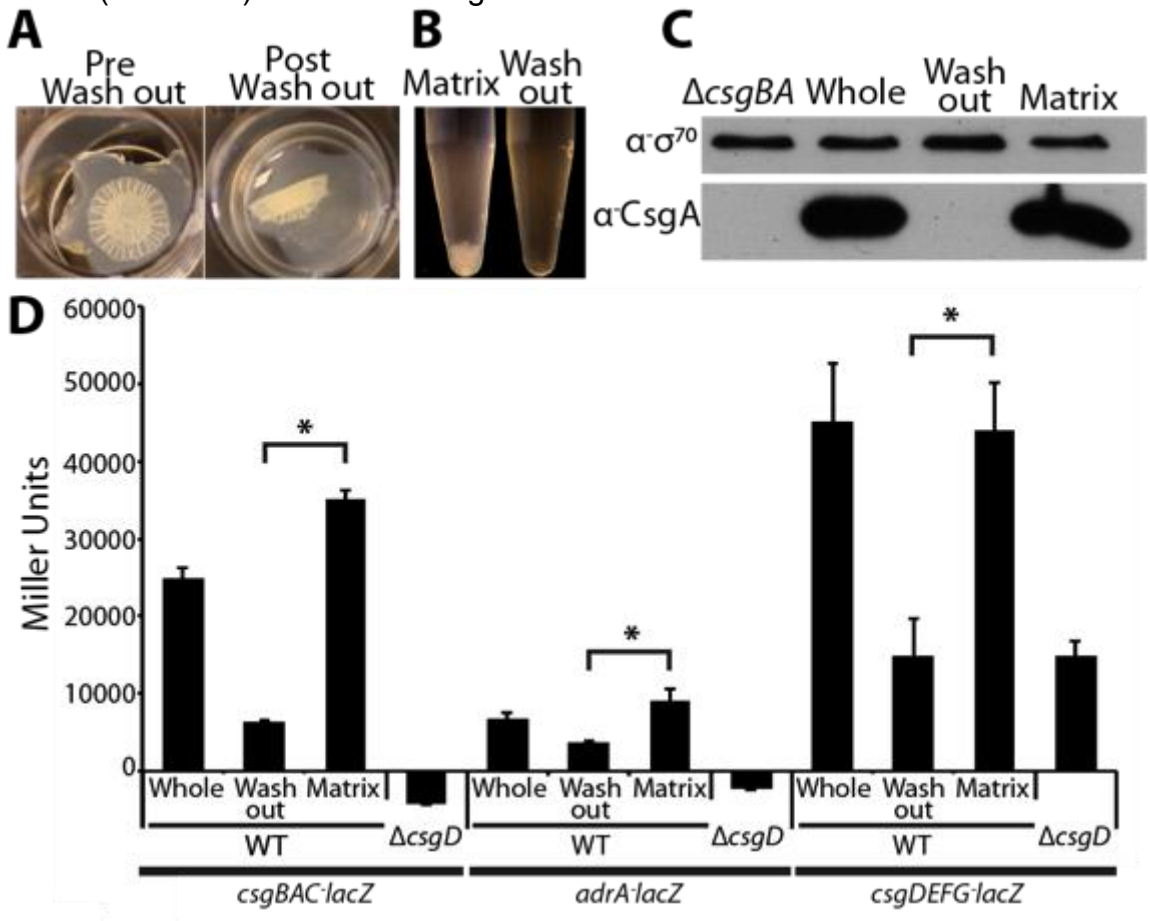

Figure 2.5 Washout bacteria do not produce curli or cellulose
Suspended bacteria were incubated with 5 μg/mL CR in KPi buffer, spun out of suspension, and the percent of CR taken out of solution by the bacteria was assayed by abs. at 490 nm of the supernatant. A CR only control represents 0% CR binding, and a KPi only control represents 100% CR binding. Error bars represent the standard deviation of biological triplicates.

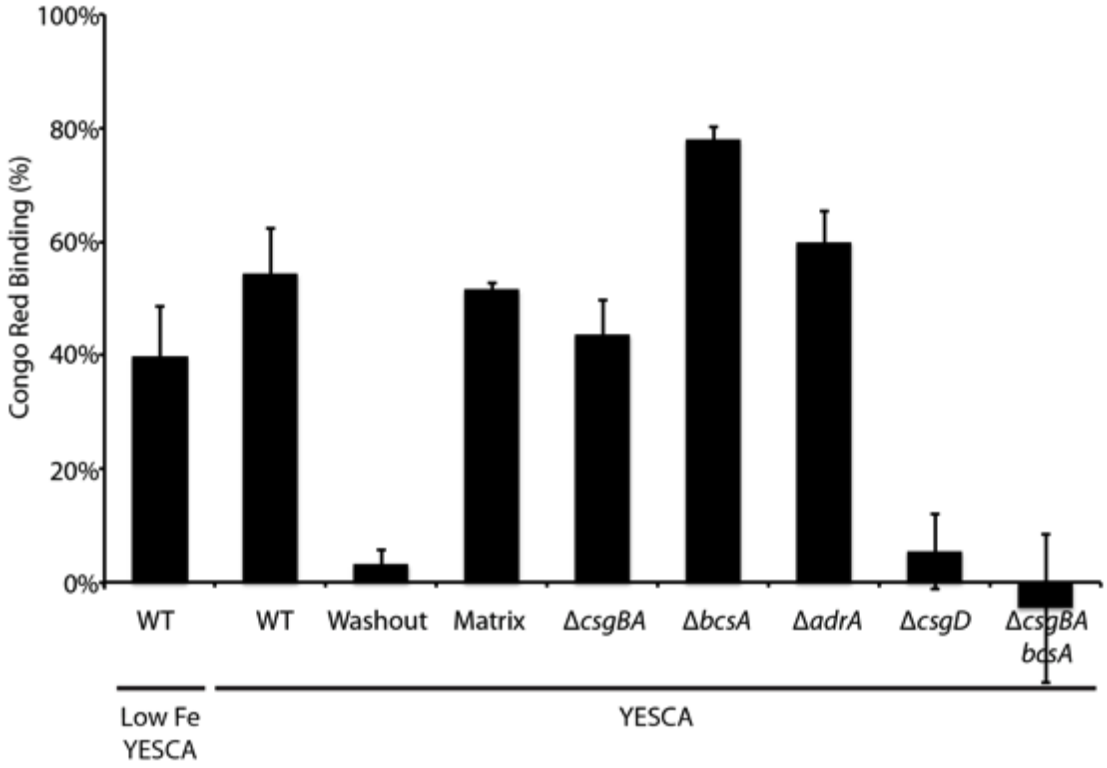

Figure 2.6 Confocal microscopy reveals bimodal rugose biofilm architecture
(A) UTI89 *attB*::*csgBAC-mcherry*/pCKR101-*eGFP* was grown on 0.05 μM cellulose filters on YESCA agar plates with 1 mM IPTG added to the cell mixture before plating. Filter sections containing a biofilm were cut out with a razor blade, placed on a slide, and treated with mounting solution. A 20x confocal microscopy cross-section of a UTI89 *attB*::*csgBAC*-mcherry/pCKR101-*eGFP* rugose biofilm before and **(B)** after the washout assay was imaged. **(C)** Average relative fluorescent intensity of five separate traces across the blue lines in **(A,B)** for each fluorophore was calculated and is graphed against distance along the blue line from each blue circle. **(D)** 3D reconstructions before and **(E)** after washout assay. White arrows indicate wrinkle openings where non-curli-producing bacteria are present before the washout assay but not after.

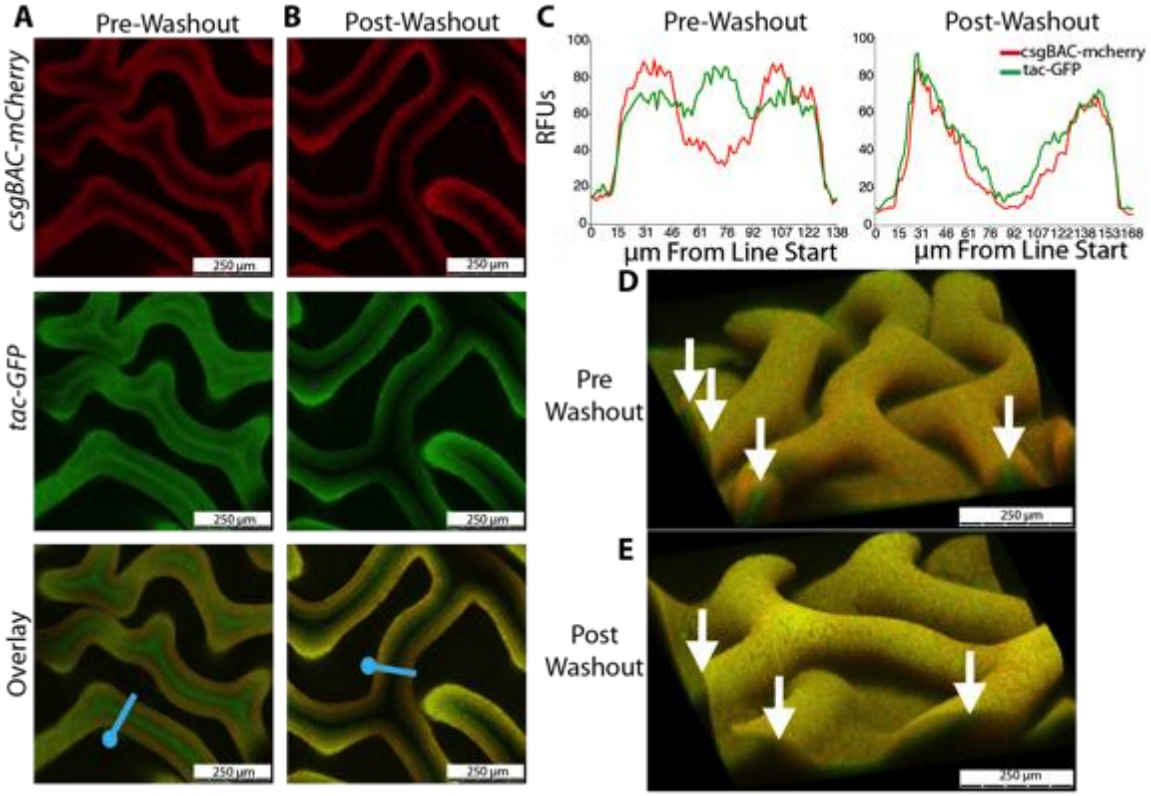

Figure 2.7 Rugose biofilm structure in low and high iron conditions
(A) UTI89 *attB*::*csgBAC-mCherry*/pCKR101-*eGFP* was grown on Chelex-treated YESCA plates on a cellulose filter and visualized by confocal microscopy, revealing little spatial separation of curli-producing and non-curli-producing bacteria. **(B)** UTI89 *attB*::*csgBAC-mCherry*/ pCKR101-*eGFP* with $FeCl_3$ added back to the cell mixture before plating on Chelex-treated YESCA plates demonstrates identical architecture as the same strain grown on YESCA plates. **(C)** A UTI89 *attB*::*csgBAC-eGFP* /pCKR101-*mCherry* strain grown on a YESCA plate demonstrates mCherry-producing cells lining the interior of mCherry/GFP expressing surface bacteria. White arrows indicate sites where non-curli producing bacteria can be seen in wrinkle interiors.

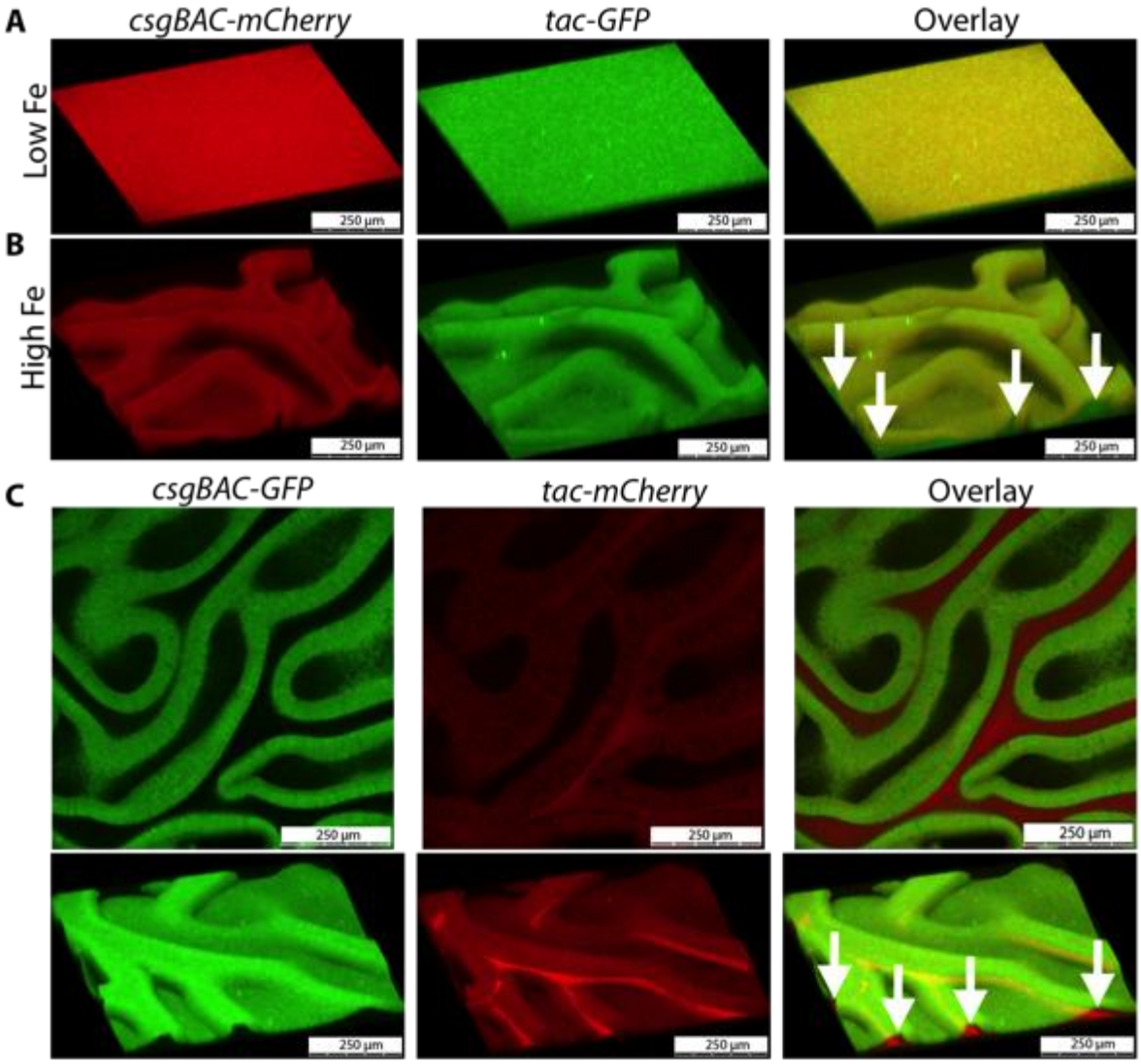

Figure 2.8 A *fur* mutant wrinkles in low iron conditions
WT UTI89 as well as *iscR*, *basSR*, *fur* and *ryhB* mutants were plated on Chelex-treated YESCA agar plates with or without addition of $FeCl_3$ to the cell mixture before plating. Only the *fur* mutant demonstrated an increase in rugose biofilm formation in low iron conditions.

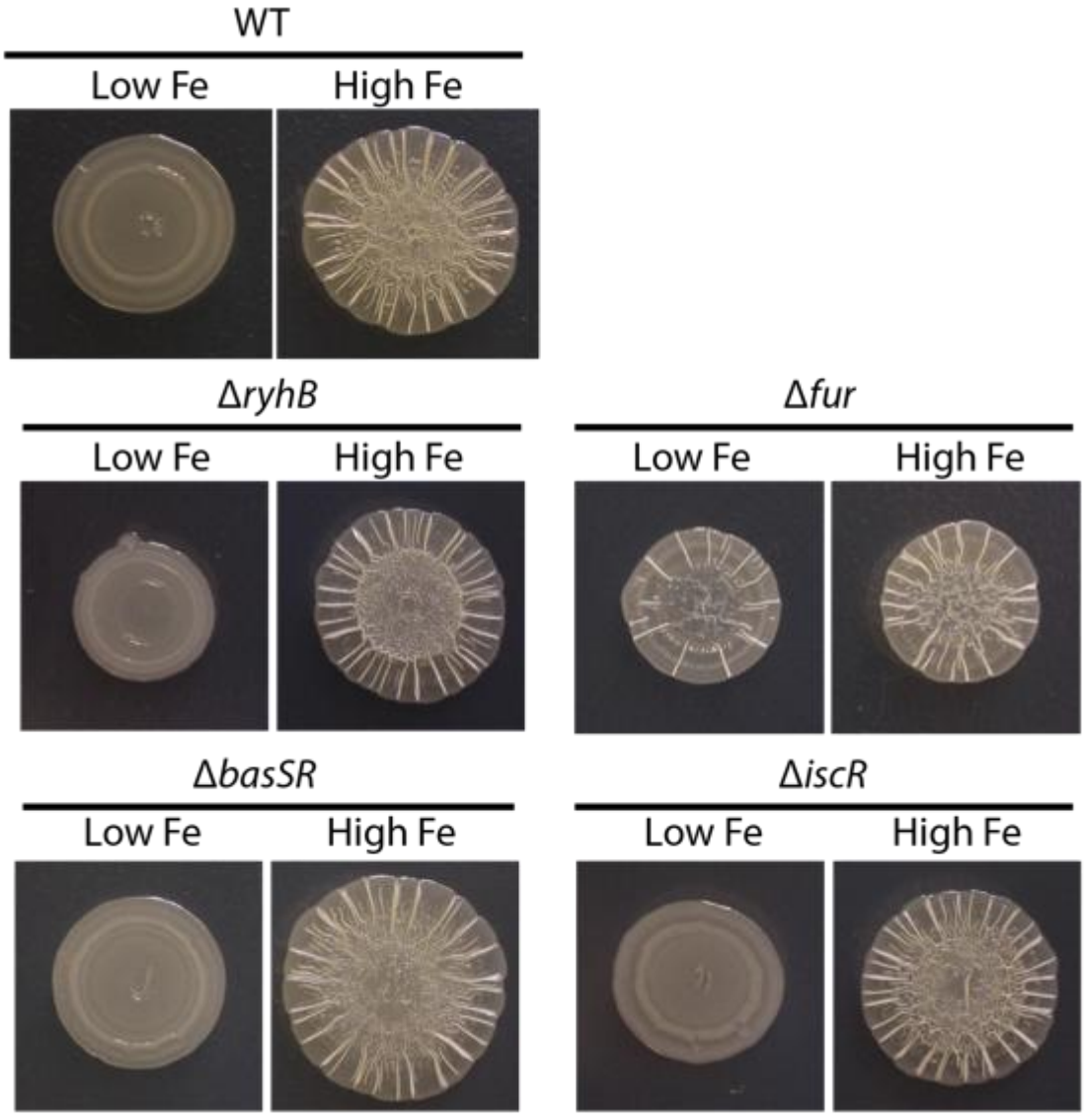

Figure 2.9 Iron and superoxide stress drives rugose biofilm formation
(A) WT UTI89, a *fur* mutant, or a *sodA sodB* double mutant were grown on Chelex-treated YESCA plates with or without the addition of $FeCl_3$ to the cell mixture before plating. **(B)** Over-expression of *sodA* repressed rugose biofilm formation in the *fur* and the *sodA sodB* mutant compared to the empty vector (EV) controls. Strains were grown on chelex-treated YESCA plates supplemented with 100 μM $MnCl_2$ and either 10 μM IPTG (WT and *sodA sodB*) or 50 μM IPTG (*fur*). **(C)** WT UTI89 was exposed to 5 μl H_2O, 100 mM $FeCl_3$, or 10 mM phenazine methosulfate on a sterile paper disc (1 cm to the left of the pictured biofilms). **(D)** Rugose biofilm formation in response to phenazine is more rapid in a *sodA* mutant as compared to WT. **(E)** Rugose biofilm formation in WT UTI89 grown on Chelex-treated YESCA plates supplemented with 100 μM $MnCl_2$, 50 μM IPTG, and 10 μM $FeCl_3$ was repressed by overexpression of *sodA*.

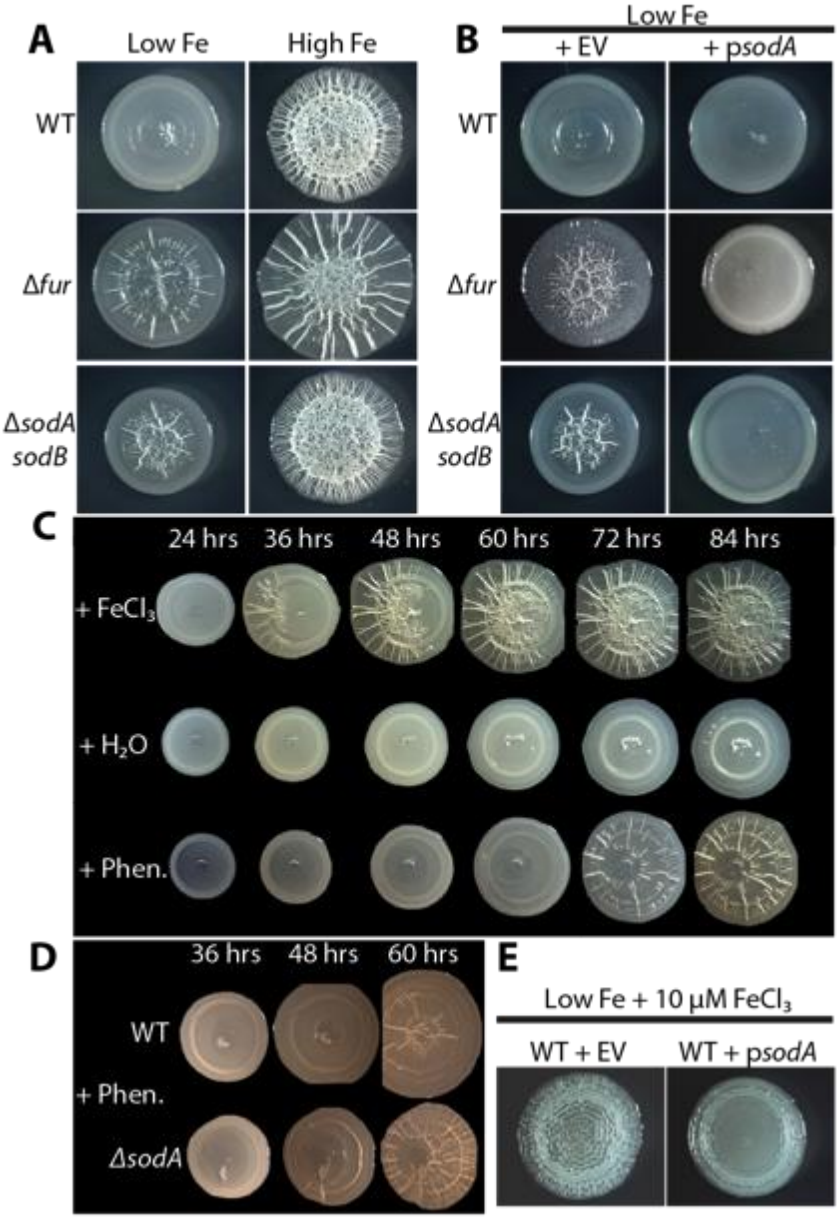

Figure 2.10 Gallium and aluminum can also trigger rugose biofilm formation
WT UTI89 grown on chelex-100 treated YESCA plates and exposed to 10 µL of 100 mM metal salts on paper discs demonstrate that full rugose formation is specific to iron, while gallium and aluminum are also able to induce wrinkling to a degree.

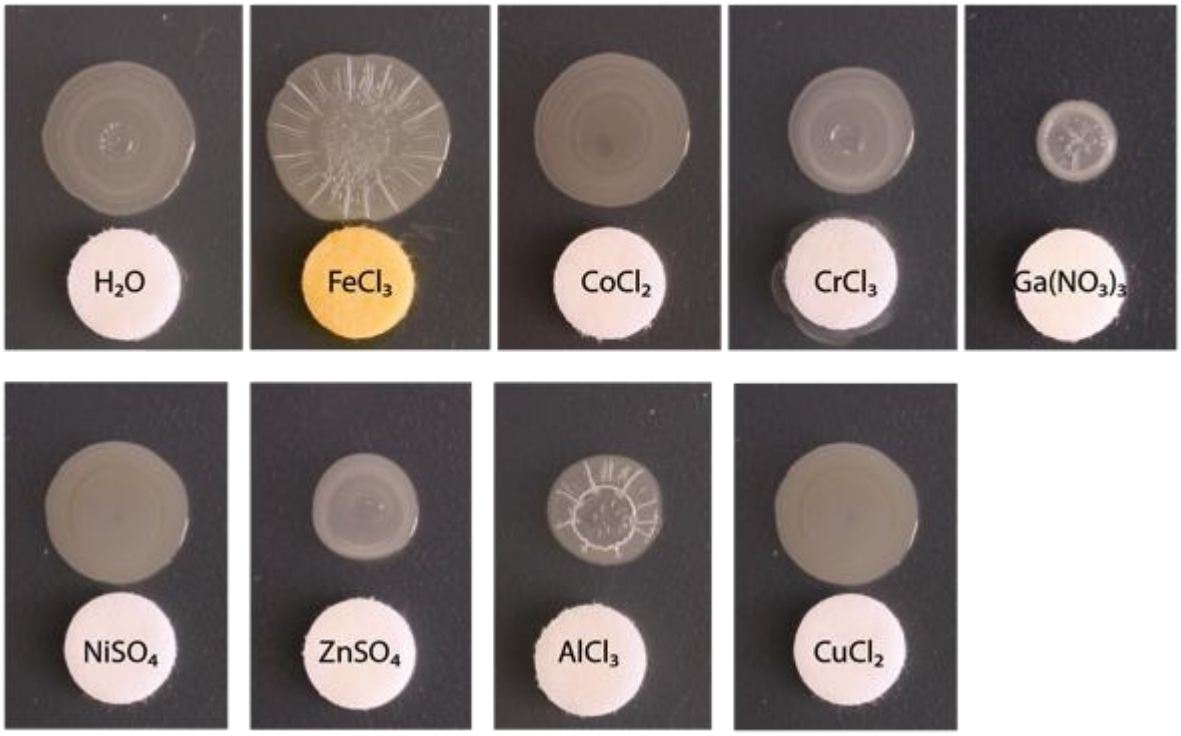

Figure 2.11 Rugose biofilm formation coincides with H_2O_2 resistance
(A) WT UTI89 was grown on Chelex-treated YESCA plates with or without the addition of $FeCl_3$ to the cell mixture before plating. Bacteria from each iron condition, or from washout and matrix fractions from high iron rugose biofilms, were normalized to 1 OD_{600} and exposed to 1% H_2O_2 for 20 minutes. Cells were serially diluted and plated on LB plates. **(B)** A 10 µm oxygen microsensor was used to measure oxygen penetration into WT UTI89 rugose biofilms. Each data point is an average of three technical and three biological replicates. A 6th order polynomial curve was fit to the data points. **(C)** Oxygen penetration depth was mapped onto a 40x confocal cross-section image of the midpoint of a UTI89 *attB*::*csgBAC*-mcherry/pCKR101-*eGFP* rugose biofilm induced with IPTG.

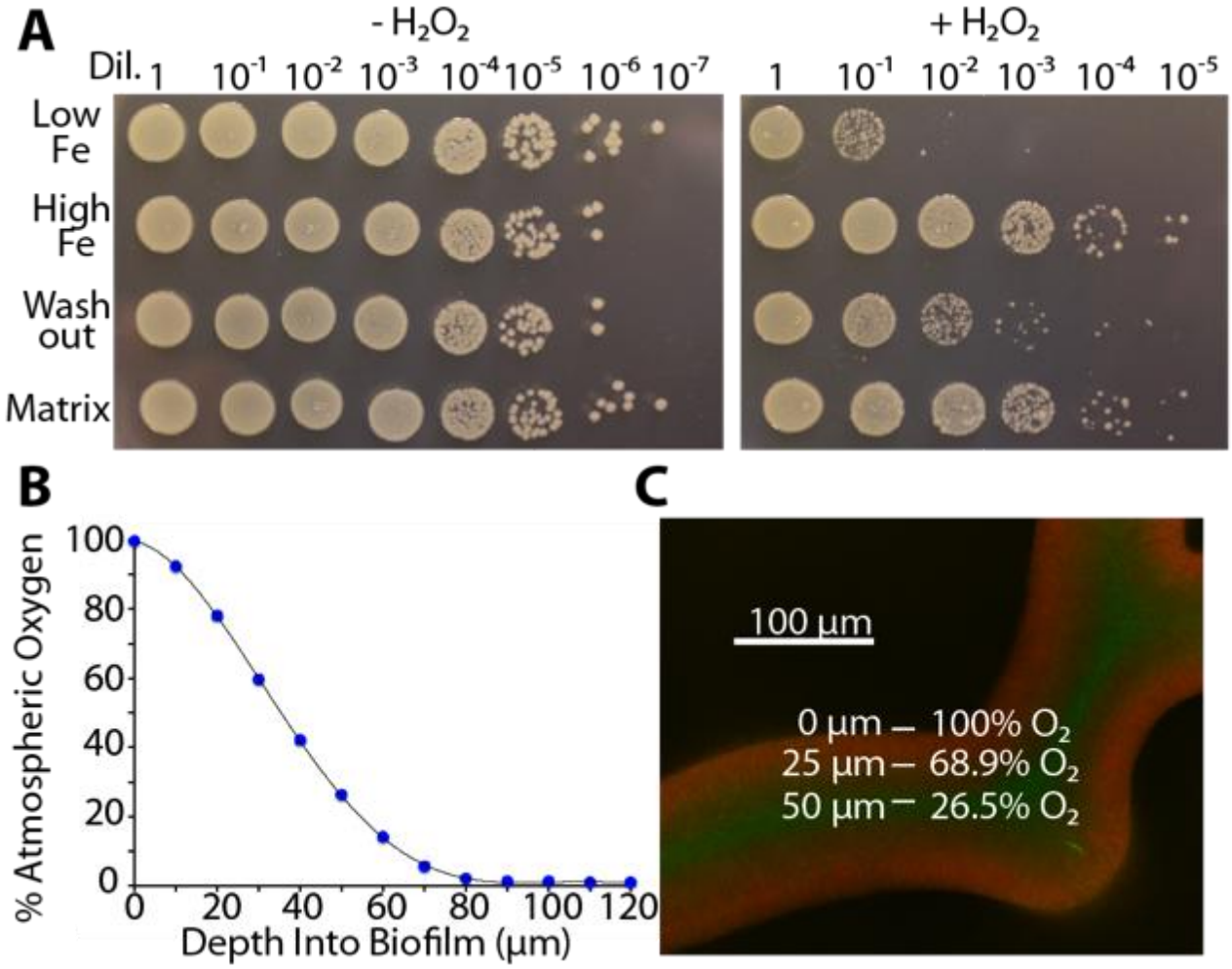

Figure 2.12 RpoS-dependent KatE activity is increased in the matrix fraction
(A,B) The Amplex red/Horseradish peroxidase assay was utilized to determine the catalase activity in the washout and shell fractions of various mutants**. (C)** Western blotting for RpoS and σ70 was performed. All assays were performed after 48 hours of growth on YESCA agar plates at 26°C.

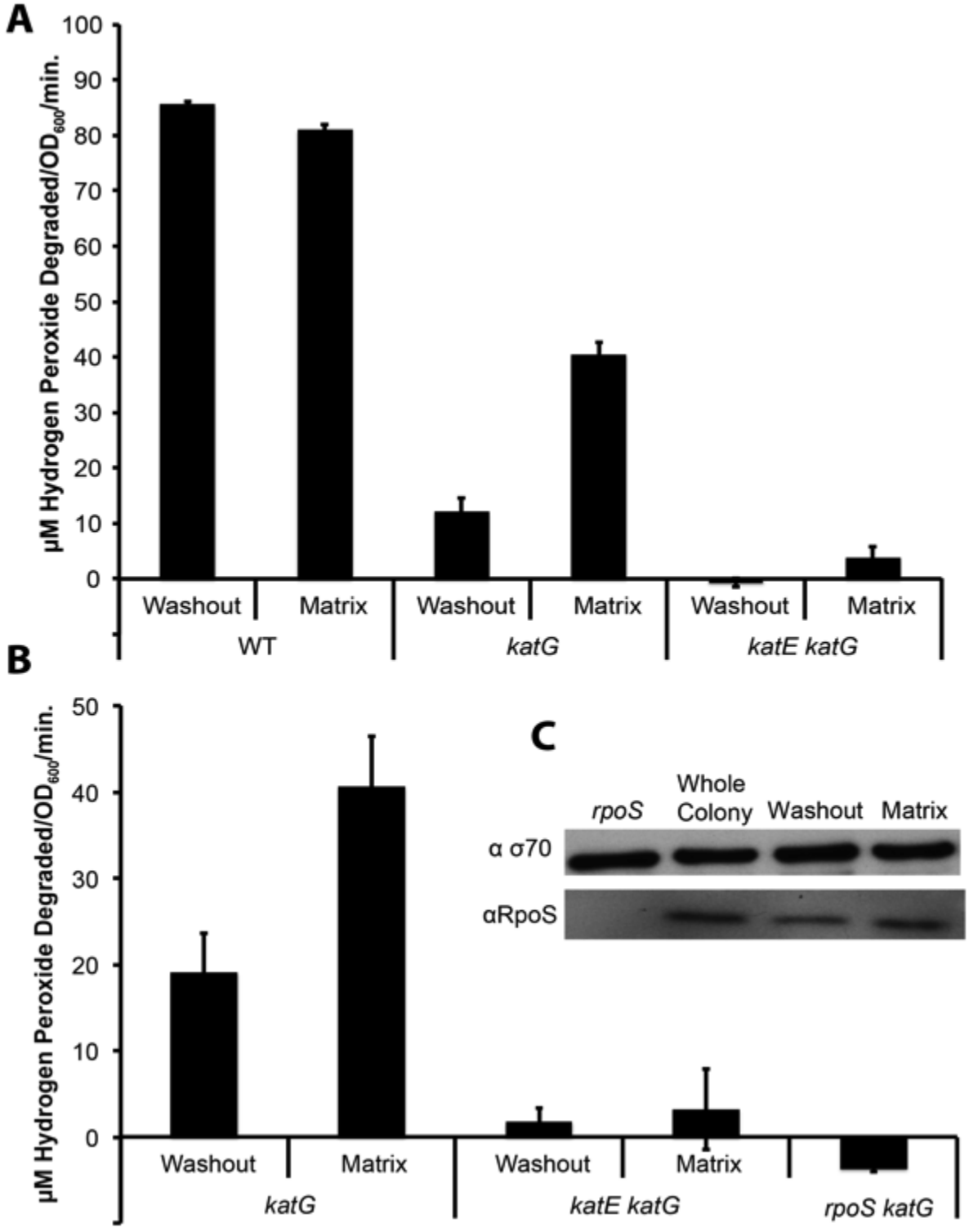

Figure 2.13 Iron-dependent rugose biofilm formation in other enterics
(A) UTI89 and *C. koseri* form rugose biofilms on YESCA plates after 48 hours, and *S. enterica* forms rugose biofilms on LB - salt agar plates after 72 hours. **(B)** Whole cell western blot analysis performed on washout and matrix fractions demonstrates that CsgA is chiefly localized to the matrix fraction in all three strains. **(C)** Iron is required for rugose biofilm formation of UTI89 and *C. koseri* on Chelex-treated YESCA plates and for *S. typhimurium* on Chelex-treated LB – salt plates. **(D)** When grown in low iron conditions, all three strains were more susceptible to H_2O_2 treatment than after growth in high iron conditions. UTI89 was mixed with 1% H_20_2 for 20 minutes as described in materials and methods, *C. koseri* was mixed with 3% H_20_2 for 20 minutes, and *S. typhimurium* was mixed with 1% H_20_2 for 15 minutes.

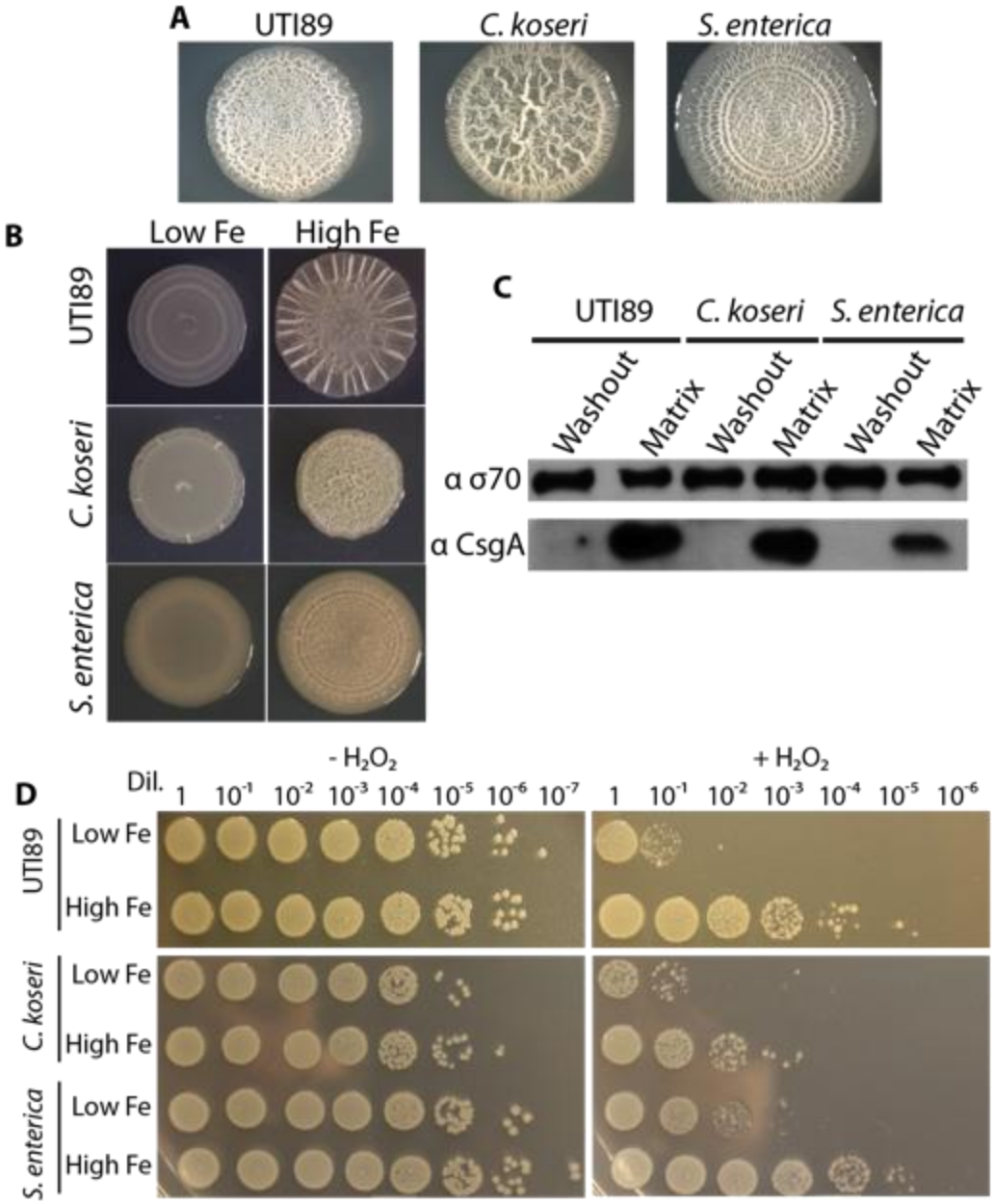

Table 2.1: Strains and Plasmids Used in Chapter 2

Plasmid:	**Reference:**	**Notes:**
pCKR101	(39)	
pCKR101-*sodA*	This Work	*sodA* cloned into KpnI and XbaI sites of pCKR101 with primers WD229 and WD209 from UTI89 genome
pCKR101-*eGFP*	This Work	*eGFP* cloned into KpnI and XbaI sites of pCKR101 with primers WD263 and WD264 from genome of UTI89 attB::*csgBAC-eGFP*
pCKR101-*mCherry*	This Work	*mCherry* cloned into KpnI and XbaI sites of pCKR101 with primers WD244 and WD245 from pAH6
pRJ800	(64)	*lacZ* expressing plasmid with no promoter sequence, used as empty vector for β-galactosidase assays.
pBA14	(64)	*csgBAC* promoter driving *lacZ* in pRJ800 vector.
pD1	(64)	*csgDEFG* promoter driving *lacZ* in pRJ800 vector.
pRJ800-*adrA*	This Work	*adrA* promoter cloned into BamHI and XbaI sites of pRJ800 with primers DH1 and DH2 from the UTI89 genome
pAH6	(67)	
pCD13psk	(65, 66)	
pCD13psk-*mCherry*	This Work	*mCherry* cloned from pAH6 into pCD13psk SpeI and SacI sites using primers WD119 and WD120
pCD13psk-*csgBAC-mcherry*	This Work	UTI89 *csgBAC* promoter from the UTI89 genome cloned into pCD13psk-*mcherry* HindIII and SpeI sites using primers WD214 and WD215
Strain:	**Reference:**	**Notes:**
UTI89	(62)	
Citrobacter Koseri	Isolate from UMich Medical School	
Salmonella enterica serovar *typhimurium* ATCC 14028	Obtained from the ATCC	
UTI89 *csgBA*::kan	This Work	Red swap mutagenesis of WT UTI89 with primers WD6 and WD7
UTI89 *csgD*::kan	This Work	Red swap mutagenesis of WT UTI89 with primers WD36 and WD37
UTI89 *bcsA*::kan	This Work	Red swap mutagenesis of WT UTI89

		with primers WD349 and WD350
UTI89 *adrA*::kan	This Work	Red swap mutagenesis of WT UTI89 with primers WD99 and WD100
UTI89 *csgBA*::flp *bcsA*::kan	This Work	Red swap mutagenesis of UTI89 *csgBA*::flp with primers WD349 and WD350
UTI89 *attB*::*csgBAC-mCherry*	This Work	As described (19), except *mcherry* was cloned from pAH6 into pCD13psk using primers WD119 and WD120
UTI89 *attB*::*csgBAC-mCherry*/pCKR101-*eGFP*	This Work	UTI89 *attB*::*csgBAC-mCherry* electroporated with pCKR101-*eGFP*
UTI89 *attB*::*csgBAC-eGFP*	(19)	
UTI89 *attB*::*csgBAC-eGFP*/pCKR101-*mCherry*	This Work	UTI89 *attB*::*csgBAC-eGFP* electroporated with pCKR101-*mCherry*
UTI89 *sodA*::kan	This Work	Red swap mutagenesis of WT UTI89 with primers WD202 and WD203
UTI89 *sodA*::flp *sodB*::kan	This Work	Red swap mutagenesis of UTI89 *sodA*::flp with primers WD239 and WD240
UTI89 *fur*::kan	This Work	Red swap mutagenesis of WT UTI89 with primers WD15 and WD17
UTI89 *iscR*::kan	This Work	Red swap mutagenesis of WT UTI89 with primers WD18 and WD19
UTI89 *ryhB*::kan	This Work	Red swap mutagenesis of WT UTI89 with primers WD297 and WD79
UTI89 *basSR*::kan	This Work	Red swap mutagenesis of WT UTI89 with primers WD221 and WD252
UTI89/pCKR101	This Work	UTI89 electroporated with pCKR101
UTI89/pCKR101-*sodA*	This Work	UTI89 electroporated with pCKR101-*sodA*
UTI89 *sodA*::flp *sodB*::kan/pCKR101	This Work	UTI89 *sodA*::flp *sodB*::kan electroporated with pCKR101
UTI89 *sodA*::flp *sodB*::flp/pCKR101-*sodA*	This Work	UTI89 *sodA*::flp *sodB*::flp electroporated with pCKR101-*sodA*
UTI89 *fur*::kan/pCKR101	This Work	UTI89 *fur*::kan electroporated with pCKR101
UTI89 *fur*::kan/pCKR101-*sodA*	This Work	UTI89 *fur*::kan electroporated with pCKR101-*sodA*

Table 2.2: Primers Used in Chapter 2

--Non-complementary regions are undercase

Primer Name:	Sequence:
WD6	**5'**AAATACAGGTTGCGTTAACAACCAAGTTGAAATGATTTAATTTCTTAAGT GTGTAGGCTGGAGCTGCTT **3'**
WD7	**5'**CGAAAAAAAACAGGGCTTGCGCCCTGTTTCTTTAATACAGAGGATGTAT ATGAATATCCTCCTTAG **3'**
WD15	**5'**CACTTCTAATGAAGTGAACCGCTTAGTAACAGGACAGATTCCGCATGAT TCCGGGGATCCGTCGACC **3'**
WD17	**5'**GCAGGTTGGCTTTTCTCGTTCAGGCTGGCTTATTTGCCTTCGTGCGCG TGTGTAGGCTGGAGCTGCTTCG **3'**
WD18	**5'**TACAATAAAAAACCCCGGGCAGGGGCGAGTTTGAGGTGAAGTAAGACA TGATTCCGGGGATCCGTCGACC **3'**
WD19	**5'**CACTCCGGCCTGATTCTGAATTCTTTTTATTAAGCGCGTAACTTAACGT CTGTAGGCTGGAGCTGCTTCG **3'**
WD36	**5'**CAATCCAGCGTAAATAACGTTTCATGGCTTTATCGCCTGAGGTTATCGT TCATATGAATATCCTCCTTA **3'**
WD37	**5'**GAGGCAGCTGTCAGGTGTGCGATCAATAAAAAAAGCGGGGTTTCATCA TGGTGTAGGCTGGAGCTGCTTC **3'**
WD79	**5'**TTTGCAAAAAGTGTTGGACAAGTGCGAATGAGAATGATTATTATTGTCT CGCGGTGTAGGCTGGAGCTGCTTC **3'**
WD99	**5'**CTTCTGCCTTTAGCCCCGTCTCTATAATTTGGGAAAATTGTTTCTGAAT GGTGTAGGCTGGAGCTGCTTC **3'**
WD100	**5'**CAGCAAATCCTGATGGCTTTTGCCGGACGTCAGGCCGCCACTTCGGT GCGCATATGAATATCCTCCTTAG **3'**
WD119	**5'** gatcactagtATGGTGAGCAAGGGCGAGGAGGATA **3'**
WD120	**5'** gatcgagctcCTACTTGTACAGCTCGTCCATGCCG **3'**
WD202	**5'**AACGCCTCATTGCAGCAGGCATCAAATGATTATTTTTTCGCTGCGAAAC GGTGTAGGCTGGAGCTGCTTC **3'**
WD203	**5'**CTTACGCGGCATTAACAATCGGCCGCCCGACAACACTGGAGATGAATA TGCATATGAATATCCTCCTTAG **3'**
WD209	**5'** gatctctagaTTATTTTTTCGCTGCGAAACGTGCC **3'**
WD214	**5'** gatcaagcttGTTTTTCCTGCTCAAAGTATCC **3'**
WD215	**5'** gatcactagtTGCGCAACAACCGCCAAAAG **3'**
WD221	**5'**TACCAGGCTGCGGATGATATTCTGCAAACTTGCAGGAGAGTGAGTGAA TGGTGTAGGCTGGAGCTGCTTC **3'**
WD229	**5'** gatcggtaccGCCGCCCGACAACACTGGAGATG **3'**
WD239	**5'**AATAAGGCTATTGTACGTATGCAAATTAATAATAAAGGAGAGTAGCAAT GGTGTAGGCTGGAGCTGCTTC **3'**
WD240	**5'**TCAGATAATGTTGCATTTGCCATCAGTTATTATGCAGCGAGATTTTTCG CCATATGAATATCCTCCTTAG **3'**
WD244	**5'** gatcggtaccTAGGGAGGTTTTAAACATGGTGAGC **3'**
WD245	**5'** gatctctagaTTACTTGTACAGCTCGTCCATGCC **3'**
WD252	**5'**TTCAGCGTGCTGGTGGTCAGCAGCTTTCTTTATATCTGGTTTGCCACGT

	ACATATGAATATCCTCCTTAG **3'**
WD263	**5'** gatcggtaccGGTACCTAGAATTAAAGAGGAGAAA **3'**
WD264	**5'** gatctctagaTTATTTGTATAGTTCATCCATGCCA **3'**
WD297	**5'**AACGAACACAAGCACTTCCCGAGGATAAATTGAGAACGAAAGGTCAAA AAAAAC ATATGAATATCCTCCTTAG **3'**
WD349	**5'**TGCCTGTTAAACTATTCCGGGCTGAAAATGCCAGTCGGGAGTGCATCA TGCATATGAATATCCTCCTTAG **3'**
WD350	**5'**AGAATATTTTTCTTTTCATCGCGTTATCATCATTGTTGAGCCAAAGCCTG GTGTAGGCTGGAGCTGCTTC **3'**
DH1	**5'** gatcggatccCAAAAGATGCGCGAATGTAATAATC **3'**
DH2	**5'** gatctctagaTCAGAAACAATTTTCCCAAATTATA **3'**

Notes and Acknowledgements:

I went to Montana State to perform the oxygen microelectrode measurements with Dr. Philip Stewart. He, along with Hans Bernstein and Steve Fisher were extremely helpful with taking the measurements and analyzing the data from those experiments. Luz Blanco helped me perform the first confocal experiments on UTI89 rugose biofilms that clued us into bimodal population development. Gregg Sobocinski patiently guided me through using the department's Leica confocal microscope. Yizhou Zhou and Neal Hammer trained me on most of the genetic techniques used here and throughout this dissertation. David Hufnagel performed repeat after repeat of many of the β-galactosidase assays included here. John Lee is a former Masters student who helped with various aspects of this chapter. James Imlay and Scott Hultgren generously donated reagents and strains. A majority of this work was published in PNAS (35).

References:

1. **Lewis K.** 2008. Multidrug tolerance of biofilms and persister cells. *Current topics in microbiology and immunology* **322:**107-131.
2. **Hall-Stoodley L, Costerton JW, Stoodley P.** 2004. Bacterial biofilms: from the natural environment to infectious diseases. *Nature reviews Microbiology* **2:**95-108.
3. **Stewart PS, Franklin MJ.** 2008. Physiological heterogeneity in biofilms. *Nature reviews* Microbiology **6:**199-210.
4. **Lopez D, Vlamakis H, Kolter R.** 2010. Biofilms. *Cold Spring Harbor perspectives in biology* **2:**a000398.
5. **Skaar EP.** 2010. The battle for iron between bacterial pathogens and their vertebrate hosts. *PLoS Pathogens* **6:**e1000949.
6. **Cornelis P, Wei Q, Andrews SC, Vinckx T.** 2011. Iron homeostasis and management of oxidative stress response in bacteria. *Metallomics : Integrated Biometal Science* **3:**540-549.
7. **Imlay JA, Chin SM, Linn S.** 1988. Toxic DNA damage by hydrogen peroxide through the Fenton reaction *in vivo* and *in vitro*. *Science* **240:**640-642.
8. **Cabiscol E, Tamarit J, Ros J.** 2000. Oxidative stress in bacteria and protein damage by reactive oxygen species. *International microbiology : the official journal of the Spanish Society for Microbiology* **3:**3-8.
9. **Wu Y, Outten FW.** 2009. IscR controls iron-dependent biofilm formation in *Escherichia coli* by regulating type I fimbria expression. *Journal of Bacteriology* **191:**1248-1257.
10. **Mey AR, Craig SA, Payne SM.** 2005. Characterization of *Vibrio cholerae* RyhB: the RyhB regulon and role of *ryhB* in biofilm formation. *Infection and Immunity* **73:**5706-5719.

11. **Banin E, Vasil ML, Greenberg EP.** 2005. Iron and *Pseudomonas aeruginosa* biofilm formation. *Proceedings of the National Academy of Sciences of the United States of America* **102:**11076-11081.
12. **Johnson M, Cockayne A, Williams PH, Morrissey JA.** 2005. Iron-responsive regulation of biofilm formation in staphylococcus aureus involves fur-dependent and fur-independent mechanisms. *Journal of Bacteriology* **187:**8211-8215.
13. **Banin E, Brady KM, Greenberg EP.** 2006. Chelator-induced dispersal and killing of *Pseudomonas aeruginosa* cells in a biofilm. *Applied and Environmental Microbiology* **72:**2064-2069.
14. **Brombacher E, Baratto A, Dorel C, Landini P.** 2006. Gene expression regulation by the Curli activator CsgD protein: modulation of cellulose biosynthesis and control of negative determinants for microbial adhesion. *Journal of Bacteriology* **188:**2027-2037.
15. **Ogasawara H, Yamamoto K, Ishihama A.** 2011. Role of the biofilm master regulator CsgD in cross-regulation between biofilm formation and flagellar synthesis. *Journal of Bacteriology* **193:**2587-2597.
16. **Romling U, Sierralta WD, Eriksson K, Normark S.** 1998. Multicellular and aggregative behaviour of *Salmonella typhimurium* strains is controlled by mutations in the agfD promoter. *Molecular Microbiology* **28:**249-264.
17. **White AP, Gibson DL, Grassl GA, Kay WW, Finlay BB, Vallance BA, Surette MG.** 2008. Aggregation via the red, dry, and rough morphotype is not a virulence adaptation in *Salmonella enterica* serovar Typhimurium. *Infection and Immunity* **76:**1048-1058.
18. **Anderson GG, Palermo JJ, Schilling JD, Roth R, Heuser J, Hultgren SJ.** 2003. Intracellular bacterial biofilm-like pods in urinary tract infections. *Science* **301:**105-107.
19. **Cegelski L, Pinkner JS, Hammer ND, Cusumano CK, Hung CS, Chorell E, Aberg V, Walker JN, Seed PC, Almqvist F, Chapman MR, Hultgren SJ.** 2009. Small-molecule inhibitors target *Escherichia coli* amyloid biogenesis and biofilm formation. *Nature Chemical Biology* **5:**913-919.
20. **Chapman MR, Robinson LS, Pinkner JS, Roth R, Heuser J, Hammar M, Normark S, Hultgren SJ.** 2002. Role of *Escherichia coli* curli operons in directing amyloid fiber formation. *Science* **295:**851-855.
21. **Hammar M, Arnqvist A, Bian Z, Olsen A, Normark S.** 1995. Expression of two csg operons is required for production of fibronectin- and congo red-binding curli polymers in *Escherichia coli* K-12. *Molecular Microbiology* **18:**661-670.
22. **Romling U, Rohde M, Olsen A, Normark S, Reinkoster J.** 2000. AgfD, the checkpoint of multicellular and aggregative behaviour in *Salmonella typhimurium* regulates at least two independent pathways. *Molecular Microbiology* **36:**10-23.
23. **Zogaj X, Nimtz M, Rohde M, Bokranz W, Romling U.** 2001. The multicellular morphotypes of *Salmonella typhimurium* and *Escherichia coli* produce cellulose as the second component of the extracellular matrix. *Molecular Microbiology* **39:**1452-1463.
24. **Barnhart MM, Chapman MR.** 2006. Curli biogenesis and function. *Annual Review of Microbiology* **60:**131-147.

25. **Saldana Z, Xicohtencatl-Cortes J, Avelino F, Phillips AD, Kaper JB, Puente JL, Giron JA.** 2009. Synergistic role of curli and cellulose in cell adherence and biofilm formation of attaching and effacing *Escherichia coli* and identification of Fis as a negative regulator of curli. *Environmental Microbiology* **11:**992-1006.
26. **Zhou YZ, Smith D, Leong BJ, Brannstrom K, Almqvist F, Chapman MR.** 2012. Promiscuous Cross-seeding between Bacterial Amyloids Promotes Interspecies Biofilms. *The Journal of Biological Chemistry* **287:**35092-35103.
27. **Lim JY, May JM, Cegelski L.** 2012. Dimethyl sulfoxide and ethanol elicit increased amyloid biogenesis and amyloid-integrated biofilm formation in *Escherichia coli*. *Applied and Environmental Microbiology* **78:**3369-3378.
28. **Asally M, Kittisopikul M, Rue P, Du Y, Hu Z, Cagatay T, Robinson AB, Lu H, Garcia-Ojalvo J, Suel GM.** 2012. Localized cell death focuses mechanical forces during 3D patterning in a biofilm. *Proceedings of the National Academy of Sciences of the United States of America* **109:**18891-18896.
29. **Dietrich LE, Teal TK, Price-Whelan A, Newman DK.** 2008. Redox-active antibiotics control gene expression and community behavior in divergent bacteria. *Science* **321:**1203-1206.
30. **Romling U, Bian Z, Hammar M, Sierralta WD, Normark S.** 1998. Curli fibers are highly conserved between *Salmonella typhimurium* and *Escherichia coli* with respect to operon structure and regulation. *Journal of Bacteriology* **180:**722-731.
31. **Da Re S, Ghigo JM.** 2006. A CsgD-independent pathway for cellulose production and biofilm formation in *Escherichia coli*. *Journal of Bacteriology* **188:**3073-3087.
32. **Amikam D, Galperin MY.** 2006. PilZ domain is part of the bacterial c-di-GMP binding protein. *Bioinformatics* **22:**3-6.
33. **Ryjenkov DA, Simm R, Romling U, Gomelsky M.** 2006. The PilZ domain is a receptor for the second messenger c-di-GMP - The PilZ domain protein YcgR controls motility in enterobacteria. *The Journal of Biological Chemistry* **281:**30310-30314.
34. **Kleefeld A, Ackermann B, Bauer J, Kramer J, Unden G.** 2009. The fumarate/succinate antiporter DcuB of *Escherichia coli* is a bifunctional protein with sites for regulation of DcuS-dependent gene expression. *The Journal of Biological Chemistry* **284:**265-275.
35. **DePas WH, Hufnagel DA, Lee JS, Blanco LP, Bernstein HC, Fisher ST, James GA, Stewart PS, Chapman MR.** 2013. Iron induces bimodal population development by *Escherichia coli*. *Proceedings of the National Academy of Sciences of the United States of America* **110:**2629-2634.
36. **Hansen MC, Palmer RJ, Jr., Udsen C, White DC, Molin S.** 2001. Assessment of GFP fluorescence in cells of Streptococcus gordonii under conditions of low pH and low oxygen concentration. *Microbiology* **147:**1383-1391.
37. **Ogasawara H, Shinohara S, Yamamoto K, Ishihama A.** 2012. Novel regulation targets of the metal-response BasS-BasR two-component system of *Escherichia coli*. *Microbiology* **158:**1482-1492.
38. **Touati D, Jacques M, Tardat B, Bouchard L, Despied S.** 1995. Lethal oxidative damage and mutagenesis are generated by iron in delta fur mutants of

Escherichia coli: protective role of superoxide dismutase. *Journal of Bacteriology* **177:**2305-2314.

39. **Keyer K, Imlay JA.** 1996. Superoxide accelerates DNA damage by elevating free-iron levels. *Proceedings of the National Academy of Sciences of the United States of America* **93:**13635-13640.
40. **Liochev SI, Fridovich I.** 1994. The role of O2.- in the production of HO.: *in vitro* and *in vivo*. *Free Radical Biology and Medicine* **16:**29-33.
41. **Liochev SL.** 1996. The role of iron-sulfur clusters in *in vivo* hydroxyl radical production. *Free Radical Research* **25:**369-384.
42. **Mavrodi DV, Peever TL, Mavrodi OV, Parejko JA, Raaijmakers JM, Lemanceau P, Mazurier S, Heide L, Blankenfeldt W, Weller DM, Thomashow LS.** 2010. Diversity and evolution of the phenazine biosynthesis pathway. *Applied and Environmental Microbiology* **76:**866-879.
43. **Hassan HM, Fridovich I.** 1979. Intracellular production of superoxide radical and of hydrogen peroxide by redox active compounds. *Archives of biochemistry and biophysics* **196:**385-395.
44. **Hubbard JA, Lewandowska KB, Hughes MN, Poole RK.** 1986. Effects of iron-limitation of *Escherichia coli* on growth, the respiratory chains and gallium uptake. *Archives of Microbiology* **146:**80-86.
45. **Kaneko Y, Thoendel M, Olakanmi O, Britigan BE, Singh PK.** 2007. The transition metal gallium disrupts *Pseudomonas aeruginosa* iron metabolism and has antimicrobial and antibiofilm activity. *Journal of Clinical Investigation* **117:**877-888.
46. **Carrano CJ, Raymond KN.** 1978. Coordination chemistry of microbial iron transport compounds: rhodotorulic acid and iron uptake in *Rhodotorula pilimanae*. *Journal of Bacteriology* **136:**69-74.
47. **Guida L, Saidi Z, Hughes MN, Poole RK.** 1991. Aluminium toxicity and binding to *Escherichia coli*. *Archives of Microbiology* **156:**507-512.
48. **Messner KR, Imlay JA.** 1999. The identification of primary sites of superoxide and hydrogen peroxide formation in the aerobic respiratory chain and sulfite reductase complex of *Escherichia coli*. *The Journal of Biological Chemistry* **274:**10119-10128.
49. **Imlay JA, Fridovich I.** 1991. Assay of Metabolic Superoxide Production in *Escherichia coli. The Journal of Biological Chemistry* **266:**6957-6965.
50. **Tanaka K, Handel K, Loewen PC, Takahashi H.** 1997. Identification and analysis of the rpoS-dependent promoter of katE, encoding catalase HPII in *Escherichia coli*. *Biochimica et biophysica acta* **1352:**161-166.
51. **Olsen A, Arnqvist A, Hammar M, Sukupolvi S, Normark S.** 1993. The RpoS sigma factor relieves H-NS-mediated transcriptional repression of *csgA*, the subunit gene of fibronectin-binding curli in *Escherichia coli*. *Molecular Microbiology* **7:**523-536.
52. **Serra DO, Richter AM, Hengge R.** 2013. Cellulose as an architectural element in spatially structured *Escherichia coli* biofilms. *Journal of Bacteriology* **195:**5540-5554.

53. **Serra DO, Richter AM, Klauck G, Mika F, Hengge R.** 2013. Microanatomy at cellular resolution and spatial order of physiological differentiation in a bacterial biofilm. *Mbio* **4:**e00103-00113.
54. **Seaver LC, Imlay JA.** 2001. Alkyl hydroperoxide reductase is the primary scavenger of endogenous hydrogen peroxide in *Escherichia coli*. *Journal of Bacteriology* **183:**7173-7181.
55. **Imlay JA.** 2008. Cellular defenses against superoxide and hydrogen peroxide. *Annual Review of Biochemistry* **77:**755-776.
56. **Mulvey MA, Lopez-Boado YS, Wilson CL, Roth R, Parks WC, Heuser J, Hultgren SJ.** 1998. Induction and evasion of host defenses by type 1-piliated uropathogenic *Escherichia coli*. *Science* **282:**1494-1497.
57. **Justice SS, Hung C, Theriot JA, Fletcher DA, Anderson GG, Footer MJ, Hultgren SJ.** 2004. Differentiation and developmental pathways of uropathogenic *Escherichia coli* in urinary tract pathogenesis. *Proceedings of the National Academy of Sciences of the United States of America* **101:**1333-1338.
58. **Snyder JA, Haugen BJ, Buckles EL, Lockatell CV, Johnson DE, Donnenberg MS, Welch RA, Mobley HL.** 2004. Transcriptome of uropathogenic *Escherichia coli* during urinary tract infection. *Infection and Immunity* **72:**6373-6381.
59. **Reigstad CS, Hultgren SJ, Gordon JI.** 2007. Functional genomic studies of uropathogenic *Escherichia coli* and host urothelial cells when intracellular bacterial communities are assembled. *Journal of Biological Chemistry* **282:**21259-21267.
60. **Grantcharova N, Peters V, Monteiro C, Zakikhany K, Romling U.** 2010. Bistable expression of CsgD in biofilm development of *Salmonella enterica* serovar typhimurium. *Journal of Bacteriology* **192:**456-466.
61. **Masse E, Gottesman S.** 2002. A small RNA regulates the expression of genes involved in iron metabolism in *Escherichia coli*. *Proceedings of the National Academy of Sciences of the United States of America* **99:**4620-4625.
62. **Mulvey MA, Schilling JD, Hultgren SJ.** 2001. Establishment of a persistent *Escherichia coli* reservoir during the acute phase of a bladder infection. *Infection and Immunity* **69:**4572-4579.
63. **Datsenko KA, Wanner BL.** 2000. One-step inactivation of chromosomal genes in *Escherichia coli* K-12 using PCR products. *Proceedings of the National Academy of Sciences of the United States of America* **97:**6640-6645.
64. **Barnhart MM, Lynem J, Chapman MR.** 2006. GlcNAc-6P levels modulate the expression of Curli fibers by *Escherichia coli*. *Journal of Bacteriology* **188:**5212-5219.
65. **Platt R, Drescher C, Park SK, Phillips GJ.** 2000. Genetic system for reversible integration of DNA constructs and *lacZ* gene fusions into the *Escherichia coli* chromosome. *Plasmid* **43:**12-23.
66. **Wright KJ, Seed PC, Hultgren SJ.** 2005. Uropathogenic *Escherichia coli* flagella aid in efficient urinary tract colonization. *Infection and Immunity* **73:**7657-7668.

67. **Lauderdale KJ, Boles BR, Cheung AL, Horswill AR.** 2009. Interconnections between Sigma B, agr, and proteolytic activity in *Staphylococcus aureus* biofilm maturation. *Infection and Immunity* **77:**1623-1635.
68. **Zhou Y, Blanco LP, Smith DR, Chapman MR.** 2012. Bacterial amyloids. *Methods in molecular biology* **849:**303-320.
69. **Rani SA, Pitts B, Beyenal H, Veluchamy RA, Lewandowski Z, Davison WM, Buckingham-Meyer K, Stewart PS.** 2007. Spatial patterns of DNA replication, protein synthesis, and oxygen concentration within bacterial biofilms reveal diverse physiological states. *Journal of Bacteriology* **189:**4223-4233.
70. **Revsbech NP.** 1989. An Oxygen Microsensor with a Guard Cathode. *Limnology and Oceanography* **34:**474-478.
71. **Seaver LC, Imlay JA.** 2001. Alkyl hydroperoxide reductase is the primary scavenger of endogenous hydrogen peroxide in *Escherichia coli*. *Journal of Bacteriology* **183:**7173-7181.
72. **Miller JH.** 1972. Experiments in molecular genetics. *Cold Spring Harbor Laboratory, Cold Spring Harbor, NY*.

Chapter 3

ArcAB Modulates *Escherichia coli* Biofilm Formation

Abstract:

Redox-balance drives rugose biofilm formation in multiple bacterial species. *Escherichia coli* rugose biofilms are dependent on the CsgD-induced matrix components curli and cellulose. I have previously found that *E. coli* grown in low iron conditions produces a biofilm matrix, but does not form rugose biofilms unless exposed to either iron or superoxide stress. In this study, I utilized low iron conditions to probe redox-sensitive regulators that affect rugose biofilm formation. I found that the ArcAB two-component system repressed rugose biofilm formation by regulating CsgD expression. *arcA*, *arcB*, and *arcAB* mutants wrinkled in low iron conditions. Overexpresion of a constitutively active $ArcB^{78\text{-}778}$ variant reduced rugose biofilm formation on high iron plates. Furthermore, overexpression of the small RNA ArcZ, which is repressed by ArcAB, stimulated rugose biofilm formation. In *E. coli* rugose biofilms, matrix-encased bacteria are localized specifically to the air/biofilm interface. Non-matrix-encased bacteria line the interior of each wrinkle. ArcAB activity, as determined by ArcAB-dependent promoter expression, was increased in the microaerobic interior of rugose biofilms. Lastly, slightly more curli were produced in the biofilm interior when *arcA* and *arcB* were mutated, suggesting that ArcAB may repress matrix expression in the biofilm interior. Altogether I present data supporting a model where ArcAB modulates both macroscopic and microscopic *E. coli* biofilm architecture in response to cellular redox state.

Introduction:

E. coli is a facultative anaerobe that is capable of fermenting sugars and reducing a variety of alternative electron acceptors in anaerobic conditions (1, 2). To sense the environmental availability of suitable respiratory oxidants, *E. coli* employs an array of regulatory proteins. *E. coli* senses molecular oxygen directly via the proteins FNR and DosCP (3-6). O_2 destroys [4Fe-4S](2+) iron-sulfur clusters bound to FNR, repressing the protein's ability to bind DNA and act as a transcriptional regulator (5-7). The DosCP complex utilizes a heme group to directly bind O_2, and in turn controls production and degradation of the signaling molecule cyclic-di-GMP (3, 4, 8). Environmental concentrations of alternative electron acceptors such as nitrate, fumarate, and trimethylamine-N-oxide are sensed through devoted two-component systems (9-11). The response regulators of these systems activate transcription of the appropriate reductases.

In addition to the direct oxidant sensors, *E. coli* also produces a two-component system, ArcAB, that responds directly to the redox state of the quinone pool (12). When the electron transport chain is oxidized, such as in aerobic conditions, ubiquinone triggers oxidation of cysteine residues in dimeric, membrane-bound ArcB. The resulting intermolecular disulfide bonds prevent ArcB from autophosphorylating (13-16). A reducing quinone pool, specifically the presence of menaquinol, allows for reduction of ArcB cysteine residues and subsequent autophosphorylation (15, 17). ArcB autophosphorylation starts a cascade that results in the phosphorylation of the response regulator ArcA, a process that is enhanced in the presence of fermentation products (18, 19). The relative contribution of the quinone pool and of fermentation byproducts in ArcB autophosphorylation is still a matter of debate (14, 15, 20, 21). ArcA-P is a transcriptional regulator whose regulon mostly consists of genes involved in aerobic/anaerobic metabolism (12, 22).

Several studies have demonstrated that cellular redox state is intricately linked to biofilm formation in *Pseudomonas aeruginosa, Bacillus subtilis,* and *Candida albicans* (23-26). In all three organisms, redox changes drive the formation of wrinkled or rugose colony biofilms. Rugose biofilm formation is correlated with the production of extracellular matrix components. *B. subtilis* controls matrix production in response to

redox balance via two kinases, KinA and KinB (25). KinA binds to NAD+, and KinB associates with the electron transport chain and responds to impaired electron flow (25). In response to iron, KinA and KinB induce expression of polysaccharide synthase and the amyloid protein TasA, leading to rugose biofilm development (25).

In *E. coli*, rugose biofilm formation is dependent on the master biofilm regulator CsgD. Under biofilm-inducing conditions, CsgD induces expression of the *csgBAC* and *adrA* promoters, which result in the production of amyloidogenic curli fibers and the polysaccharide cellulose, respectively (27-29). I have recently reported that iron and superoxide stress drive rugose biofilm formation in *E. coli* (30). Rugose biofilm development involves elaboration of a bimodal population and resistance to hydrogen peroxide stress (30). *E. coli* grown in low iron conditions therefore represents something of a 'ground state' in biofilm formation. Matrix is still expressed on low iron plates, but environmental signals such as reactive oxygen stress are able to drive further biofilm maturation (30).

I utilized low iron conditions to screen for redox-sensitive genetic systems that affected *E. coli* biofilm development. I reasoned that knocking out redox-sensitive regulators that repress biofilm development would lead to rugose biofilm formation under low iron conditions. Conversely, knocking out redox-sensitive regulators that enhance biofilm development would be predicted to repress rugose biofilm formation in high iron conditions. Since I described a role for oxidative stress in rugose biofilm development (30), I included the *soxRS* and *oxyR* mutants in my screen. SoxRS and OxyR respond to superoxide and hydrogen peroxide stress, respectively (31). Additionally I evaluated the effect of two redox-sensitive proteins that modulate intracellular levels of the signaling molecule cyclic-di-GMP, DosCP and YfgF. Cyclic-di-GMP levels affect the expression and activity of CsgD in both *E. coli* and in *S. enterica* ser. Typhimurium (32, 33). DosCP responds to molecular oxygen and YfgF contributes to hydrogen peroxide stress resistance (8, 34). Lastly, I included global regulators FNR and ArcAB in my candidate list. After testing various redox-sensitive systems, I found that the ArcAB two-component system is a chief redox-sensing regulator of rugose biofilm formation. I go on to further describe that ArcAB affects the expression of the major biofilm regulator CsgD, through which it affects matrix production.

Results:

Screen for Redox-sensitive Rugose Biofilm Regulators

To identify redox-responsive regulatory systems that control UTI89 rugose biofilm development, I made mutations of various candidate genes and plated each strain on low iron plates or the same plates that had been supplemented with 10-200 μM $FeCl_3$. The *arcAB* mutant wrinkled in low iron and increased rugose biofilm formation very little if at all in response to iron (Fig. 3.1). All other mutants developed a flat colony morphology in low iron and responded to iron by wrinkling. *oxyR* demonstrated an interesting increase in colony spreading in high iron conditions, but still responded to iron by wrinkling. Addition of 10 μM $FeCl_3$ was sufficient to induce colony wrinkling in all strains (Fig. 3.1). Low iron plates + 10 μM $FeCl_3$ are referred to as "iron replete plates" for the remainder of this chapter.

Genetic Dissection of OxyR's Effect on Rugose Biofilm Formation

OxyR induces expression of reactive oxygen neutralizing proteins in response to hydrogen peroxide (31). An $OxyR^{A233V}$ variant demonstrates constitutively active transcriptional induction activity (35). Whereas an *oxyR* mutant spreads more than WT UTI89, complementation with $oxyR^{A233V}$ results in bundled, unorganized wrinkling (Fig. 3.2). Altogether these results suggest that active OxyR may enhance wrinkling formation in iron replete conditions, whereas inactive OxyR could contribute to colony spreading.

Genetic Dissection of ArcAB's Effect on Rugose Biofilm Formation

Since *arcAB* wrinkled more than WT in low iron conditions (Fig. 3.1), I posited that ArcAB is a repressor of rugose biofilm formation. ArcB is a sensor kinase that autophosphorylates when the quinone pool is in a reduced state, triggering a phosphorelay that results in phosphorylation of the D54 residue of ArcA (12, 18, 36). An *arcB* mutant wrinkled in low iron conditions, and complementation with WT *arcB* restored the smooth colony morphotype (Fig. 3.3A). When the ArcB transmembrane domain is removed, the resulting protein, $ArcB^{78\text{-}778}$, obtains constitutive ArcA kinase activity *in vivo* (37). Overexpression of $arcB^{78\text{-}778}$ complemented a smooth colony morphotype in low iron conditions (Fig. 3.3A). Furthermore $arcB^{78\text{-}778}$ expression decreased rugose biofilm formation on iron replete plates compared to overexpression

of WT *arcB* (Fig. 3.4A), demonstrating that active ArcB can repress rugose development.

To probe the specific role of ArcA in repressing rugose biofilm formation, I made single *arcA* and *arcB* mutants. Both single mutants developed rugose biofilms in low iron conditions. Complementing each single mutant with a WT version of the respective gene restored the smooth colony phenotype in low iron conditions (Fig. 3.3A,B). Since both single mutants wrinkled in low iron conditions, I inferred that both ArcA and ArcB are involved in repression of rugose biofilm formation. *arcB* wrinkling in low iron conditions was not as robust as *arcA* or the *arcAB* double mutant (Fig 3.1, 3.3A,B). Response regulators are often able to accept a phosphate group from phosphodonors such as acetyl-phosphate or from other histidine kinases (38), so in the absence of ArcB, ArcA may still become phosphorylated and repress rugose biofilm formation.

To determine if ArcA phosphorylation is required to inhibit rugose biofilm formation, I engineered an $ArcA^{D54A}$ mutant that renders the protein transcriptionally inactive (39). As expected, $ArcA^{D54A}$ was unable to complement wrinkling in low iron conditions (Fig. 3.3B), indicating that phosphorylation is essential for the ability of ArcA to repress rugose biofilm formation. For some response regulators, a constitutively active phosphomimetic version can be obtained by mutating the aspartate at the phosphorylation site to a glutamate (40). $ArcA^{D54E}$ complemented an *arcA* mutant in terms of repressing rugose development in low iron conditions (Fig. 3.3B). However, overexpressing $ArcA^{D54E}$ in an *arcA* mutant did not repress rugose biofilm formation on iron replete plates (Fig. 3.4B). This result might be explained by a study that demonstrated that WT ArcA-P multimerizes and binds DNA as a tetramer of homodimers (36). $ArcA^{D54E}$ is unable to accept a phosphate group from ArcB, oligomerize, or bind DNA (36). In all, my results suggest that phosphorylation of ArcA is required for its ability to repress biofilm wrinkling in low iron conditions.

ArcB can also affect gene expression independently of ArcA by phosphorylating RssB (41). When phosphorylated, RssB induces RpoS degradation (41, 42). An *rpoS* mutant did not wrinkle in either iron condition, indicating that RpoS is required for rugose biofilm formation in UTI89 (Fig. 3.5A). However, overexpressing *rpoS* in low iron conditions had very little effect on colony wrinkling (Fig. 3.5B). Similarly, an *rssB* mutant

did not wrinkle in low iron conditions (Fig. 3.5A). *rssB* in high iron developed less coordinated wrinkling than WT (Fig. 3.5A). Therefore overexpressing *rpoS* or stabilizing RpoS by overexpression of *rssB* was not sufficient to induce rugose biofilm formation in low iron conditions.

ArcZ is a small RNA whose expression is repressed by active ArcAB (43). To test the effects of ArcZ on UTI89 rugose biofilm formation, I constructed an *arcZ* mutant and tested it for rugose biofilm formation. *arcZ* had a subtle defect in biofilm development compared to WT. After 24 hours of growth on iron replete plates, there was a small but notable lag in wrinkle development in the *arcZ* mutant (Fig. 3.6A). By 48 hours however, *arcZ* was indistinguishable from WT (Fig. 3.6A). Likewise, overexpressing *arcZ* from an IPTG-inducible promoter resulted in a small amount of structure that developed in low iron conditions (Fig. 3.6B). Strains carrying the pBR-*lac* empty vector wrinkled less than typical WT UTI89 in iron replete conditions, but *arcZ* expression restored full rugose development (Fig. 3.6B). These results indicate that ArcZ has a small, but reproducible positive effect on rugose biofilm formation.

ArcAB modulates Rugose Biofilm Formation through CsgD

To determine whether ArcAB exerts its control on biofilm development through CsgD, I constructed an *arcAB csgD* mutant. *arcAB csgD* did not wrinkle in low or high iron conditions (Fig. 3.7), signifying that rugose biofilm formation in an *arcAB* mutant is CsgD-dependent. To directly test the effect of ArcAB on CsgD protein levels, I performed CsgD western blots from WT UTI89 and an *arcAB* mutant grown on low iron plates. After 24 hours of growth, CsgD levels were increased in the UTI89 *arcAB* mutant compared to WT (Fig. 3.8A). Both WT UTI89 and the *arcAB* mutant demonstrated increased CsgD levels in iron replete conditions (Fig. 3.8A). To verify that CsgD protein levels corresponded to CsgD activity, I performed β-galactosidase assays using a UTI89 *lacZ* mutant with a copy of the curli subunit (*csgBAC*) promoter driving *lacZ* at the *attB* site. As expected, *csgBAC* promoter activity was lowest in WT in low iron conditions (Fig. 3.8B). Promoter activity was increased in WT UTI89 grown on iron replete plates and in the *arcAB* mutant in either iron condition (Fig. 3.8B). Altogether these results suggest that in low iron conditions, ArcAB represses CsgD production.

Next, I tested whether *csgD* induction could induce rugose biofilm formation in low iron conditions. Indeed, expression of *csgD* from an IPTG-inducible *tac* promoter resulted in rugose formation in low iron conditions after 72 hours of growth (Fig. 3.8C). WT UTI89 carrying an empty vector did not wrinkle (Fig. 3.8C). In all, I conclude that active ArcAB represses CsgD-mediated rugose biofilm formation in low iron conditions. Overexpression of *csgD* in low iron conditions allows for an increase in rugose biofilm formation.

ArcAB Contributes to Bimodal Population Development

During rugose biofilm development, UTI89 develops two distinct populations. Surface-exposed bacteria express biofilm matrix components, while a non-matrix-expressing population lines the interior of the wrinkles (30). These two populations are easily separable via a washout assay, as the interior population can be suspended in buffer (termed washout fraction), while the matrix-encased population requires tissue homogenization to break apart (termed matrix fraction) (30). Consistent with previous results (30), the washout assay revealed that CsgD levels and *csgBAC* promoter activity were decreased in the washout fraction of both WT UTI89 and an *arcAB* mutant (Fig. 3.8A,B).

Interestingly, while total CsgD levels and *csgBAC* promoter activity were decreased in WT UTI89 compared to an *arcAB* mutant in low iron conditions, no such difference was apparent between washout fractions or between matrix fractions (Fig. 3.8A,B). I hypothesized that this discrepancy was due to a difference in the ratio of washout/matrix cells within each colony. To quantify the washout/matrix ratio, I took the OD_{600} of each fraction after performing the washout assay. After 48 hours of biofilm development, the *arcAB* mutant demonstrated a washout/matrix ratio of ~0.5 in either iron conditions. In contrast, WT UTI89 had a ratio of ~3 in low iron conditions and of ~1 in high iron conditions (Fig. 3.9). Therefore mutating *arcAB* skewed the biofilm architecture towards a more matrix-heavy composition.

One explanation for a decreased washout/matrix ratio in *arcAB* could be an increase in matrix expression in the interior of the biofilm, leading to less diffusible washout cells. I considered that in a WT strain, ArcAB could contribute to matrix repression in the biofilm interior. Indeed, like in most biofilms, oxygen concentrations

decrease within UTI89 rugose biofilms as a function of biofilm depth (30, 44). ArcAB demonstrates peak activity in anaerobic/microaerophilic conditions (20, 45). Therefore, I hypothesized that ArcAB activity would be higher in the biofilm interior in WT UTI89. Indeed, ArcAB-dependent *fadE* promoter activity was increased in the air-exposed shell fraction in both low and high iron conditions (46), signifying that ArcAB is more active in the interior washout fraction (Fig. 3.10A).

Since ArcAB was more active in the biofilm interior, I reasoned that washout cells would have reduced *csgBAC* promoter activity due to repression by ArcAB. To directly assess *csgBAC* promoter activity in a rugose biofilm, I utilized UTI89 attB::*csgBAC-mCherry*/p*eGFP* (30). Bimodal development could be visualized and quantified by tracing fluorescence within a specific area from the bottom of a rugose biofilm to the top (Fig. 3.10B). WT UTI89 grown in low iron conditions or iron replete conditions demonstrated that IPTG-induced GFP was expressed throughout the biofilm, while mCherry was localized specifically to the periphery of the biofilm (Fig. 3.10C,D), which agrees with previous results (30). In keeping with CsgD protein levels and *csgBAC* promoter activity (Fig. 3.8A,B), mCherry expression was significantly decreased in low iron conditions in WT (Fig. 3.10C). In low iron conditions in an *arcAB* mutant, mCherry fluorescence was restored to the high levels observed on iron replete plates (Fig. 3.10C,D).

After two days of growth, confocal microscopy of an *arcAB* mutant revealed that *csgBAC*-driven mCherry fluorescence was still largely localized to the biofilm surface in both low and high iron conditions (Fig. 3.10C,D). However, a small increase in mCherry expression was maintained deeper in the *arcAB* biofilm on iron replete plates (Fig. 3.10C,D). Therefore, although ArcAB affects the levels of *csgBAC* promoter activity, another system apparently assists with matrix repression in the biofilm interior. Preliminary experiments with 5-day old rugose biofilms suggest that ArcAB has a larger impact on matrix production in the interior in older biofilms (data not shown). ArcAB may therefore affect bimodal population development at later states of biofilm development.

Discussion:

Rugose biofilm formation in response to iron provides a unique opportunity to monitor genetic networks that regulate *E. coli* biofilm formation. Typically rugose biofilms are grown on YESCA or LB no salt plates, on which colonies wrinkle fully and rapidly (30). Therefore systems like ArcAB, which repress biofilm formation, would be difficult to identify in mutagenesis screens on YESCA plates, as the fully wrinkled *arcAB* biofilm would not stand out from WT biofilms. In contrast, low iron conditions produce UTI89 biofilms that are not fully developed. Further biofilm maturation can be induced by either iron addition or superoxide stress (30). Therefore my screen on low iron plates revealed that *arcAB* demonstrated a unique wrinkled colony phenotype in low iron conditions, where WT UTI89 does not wrinkle (Fig. 3.1).

While rugose biofilm formation is a useful tool to study biofilm development, it also presents technical problems. Rugose biofilms are characterized by production of a thick extracellular matrix that results in aggregation when biofilms are tissue homogenized (30). Matrix-encased bacteria preferentially aggregate, while washout bacteria tend to stay in suspension, producing sampling biases (30). I have previously utilized a cellulose synthase mutant to bypass aggregation, with which I demonstrated that total curli levels were similar in low and high iron (30). However, polysaccharide production affects matrix expression by influencing osmotic pressure in *B. subtilis*, and matrix production can affect CsgD expression in *S. enterica* ser. Typhimurium (47). Moreover, rugose biofilm formation increases total biofilm surface area (24). Since matrix expression is localized to the air/biofilm interface (30), rugose biofilm formation likely increases total matrix production in part through biofilm wrinkling. Since a UTI89 cellulose mutant does not wrinkle (30), no such increase in total matrix production can take place. Therefore using a cellulose synthase mutant to monitor curli expression is not ideal, so in this manuscript I analyzed only matrix-proficient strains. To minimize the effects of aggregation, I utilized confocal microscopy or I monitored whole colony gene/protein expression after 24 hours of growth, at which time less aggregation developed than after 48 hours of growth (data not shown).

We took a genetic approach to analyze how each arm of the ArcAB pathway affected rugose biofilm formation. An *arcB* mutant wrinkled in low iron conditions (Fig.

3.3A), and overexpression of the constitutively active *arcB*$^{78\text{-}778}$ repressed wrinkling in iron replete conditions (Fig. 3.4A). These results support a model where active ArcB suppresses rugose biofilm formation. An *arcA* mutant still wrinkled in low iron conditions, revealing that ArcA is involved in biofilm suppression (Fig. 3.3B). ArcB may also repress rugose biofilm formation by phosphorylating RssB, leading to RpoS degradation. However, neither deleting *rssB* nor overexpressing *rpoS* resulted in rugose biofilm development in low iron conditions, implying that RpoS on its own is not able to induce wrinkling (Fig. 3.5A,B). However, RpoS may still be involved in rugose biofilm development. In fact, OxyR induces expression of a small RNA, *oxyS*, which regulates *rpoS* translation (48), and OxyR affected rugose biofilm development in high iron conditions (Fig. 3.1, 3.2.). Alternatively, OxyR could affect rugose biofilm formation through regulation of Antigen-43, which affects type 1 pili-dependent *E. coli* biofilms (49, 50).

ArcZ is required for rugose biofilm formation in *S. enterica* ser. Typhimurium (51). In UTI89, an *arcZ* mutant demonstrated a slight delay in rugose biofilm development, and *arcZ* overexpression induced rugose biofilm development (Fig. 3.6A,B). While ArcZ's effect on rugose biofilm formation is subtler in UTI89, it follows the same trend as was described with *S. enterica* ser. Typhimurium (51). Altogether, my genetic data suggests that ArcB controls rugose biofilm development through multiple effectors.

While researching the ArcAB regulon, I was struck by the number of connections between ArcAB and the master biofilm regulator CsgD. First of all, the stationary phase sigma factor RpoS is required for *csgD* transcription (52, 53). ArcA-P inhibits transcription of *rpoS* (52), and ArcB directly phosphorylates and activates RssB, which triggers the degradation of RpoS (41, 42). Futhermore, the *csgD* promoter region contains an ArcA binding site (54), implying that there is direct regulation of *csgD* by ArcA-P. Lastly, Monteiro *et. al.* demonstrated that ArcZ is essential for rugose biofilm formation in *Salmonella enterica* ser. Typhimurium, likely by facilitating *rpoS* and *csgD* translation (43, 51). Collectively these results suggest that active ArcAB could repress CsgD expression through multiple pathways. In most *E. coli* strains, including UTI89, rugose biofilm formation is dependent on CsgD because of its ability to induce expression of curli and cellulose. (28, 30, 55). However, Hufnagel *et. al.* (manuscript in

prep) recently demonstrated that mutations in the periplasmic disulfide bonding system (DSB) induce a CsgD-independent cellulose activation pathway. DSB mutants produce cellulose and form rugose biofilms without *csgD*. An *arcAB csgD* mutant did not wrinkle in low or high iron conditions (Fig. 3.7), suggesting that ArcAB modulates rugose biofilm development through CsgD.

WT UTI89 in low iron conditions demonstrated suppressed CsgD levels and *csgBAC* promoter activity in my assays (Fig.3.8A,B). *csgD* overexpression induced rugose biofilm formation in low iron conditions (Fig. 3.8C). Altogether these data support a model where, in low iron conditions, active ArcAB represses rugose biofilm formation through repression of *csgD*.

ArcAB activity alters as a function of oxygen concentration, with peak activity achieved in anaerobic/microaerophilic conditions (20, 45). I previously demonstrated that oxygen concentrations decrease within rugose biofilms (30), leading us to hypothesize that ArcAB may be more active in interior biofilm cells. Indeed, activity of the Arc-suppressed *fadE* promoter was lower in the washout fraction compared to the matrix fraction (Fig. 3.10A). *csgBAC* promoter activity increased slightly in the biofilm interior in an *arcAB* mutant after two days of biofilm development, but peak activity was still localized to the biofilm surface (Fig. 3.10C,D). Serra *et. al.* showed by SEM that interior cells in *E. coli* W3110 rugose biofilms maintain an elongated shape, typical of *E. coli* cells in the logarithmic phase of growth (56). *E. coli* matrix production is relegated to cells in stationary phase, largely due to the dependence of *csgD* transcription on the stationary phase sigma factor RpoS (52, 53). At earlier time points, it is therefore likely that interior bacteria are still in a logarithmic state, leading to matrix repression via an absence of RpoS. Preliminary experiments with 5 day old biofilms suggest that an *arcAB* mutant displays a more robust increase in curliated bacteria in the biofilm interior (data not shown). Active ArcAB may then assume the role of repressing washout cell matrix production in older biofilms.

It has been convincingly demonstrated that *P. aeruginosa* wrinkles in response to a lack of oxidants, as a way to increase biofilm surface area and expose more biofilm cells to atmospheric oxygen (24, 57). However, as noted by Serra. *et. al., E. coli* is metabolically versatile in terms of its capability to ferment and utilize various alternative

electron acceptors (1, 2), so gaining access to oxygen might not be the chief selective force driving biofilm wrinkling (58). Indeed, my findings that active ArcAB repressed CsgD expression, and therefore rugose biofilm formation, suggests that peak wrinkling occurs in peak oxygenic conditions. Instead, wrinkling in *E. coli* might simply be due to mechanical buckling caused by large-scale matrix production.

Curli and cellulose provide protection against various environmental stresses such as desiccation and bleach stress in *S. enterica* ser. Typhimurium (59). White *et. al.* also demonstrated that the *csgBAC* promoter only activates once *S. enterica* ser. Typhimurium is excreted in feces in a mouse pathogenesis model (60). *E. coli* normally resides in the anaerobic/microaerophilic intestinal tract of mammals and reptiles (61). Excretion in stool likely exposes *E. coli* to atmospheric oxygen and a subsequent increase in cellular oxidation state. I therefore propose that ArcAB generally functions to repress curli expression in the gut environment. Oxygen exposure in the non-host environment could then derepress CsgD and lead to protective biofilm formation.

Interestingly, curli fibers produced from *S. enterica* ser. Typhimurium interact with gut epithelial cells and can decrease epithelial permeability (62, 63). While the gut is generally considered anaerobic, it is clear that oxygen respiration improves *E. coli*'s fitness in the gut environment (64). Oxygen diffuses away from epithelial cells, leading to a small microaerobic zone that can influence bacterial gene expression (65). An intriguing possibility is that close proximity to epithelial cells could inactivate ArcAB and derepress CsgD expression, leading to curli production and subsequent curli-mediated interactions with epithelial cells.

Materials/Methods:

Strains, Media, Cloning, and Growth Conditions:

All plasmids and strains used in this study are listed in Table S1, and primers are listed in Table S2. WT UTI89 and all mutants were routinely cultured in LB media. UTI89 mutants were produced via the lambda red recombinase method as described (66). For complementation and expression studies, genes were cloned from the UTI89 chromosome and inserted into pCKR101 using standard genetic techniques (30). Point mutations were introduced using synthesis by overlapping ends PCR (67).

Chromosomal *lacZ* insertions were produced using pCD13psk as described (68, 69). Briefly, UTI89 *lacZ* was cloned into the XbaI and SacI sites of pCD13psk, and UTI89 promoter regions were introduced using BamHI and XbaI sites. pCD13psk and variants were amplified in DH5α λpir+. Insertion of pCD13psk and variants into the *attB* site of *lacZ* UTI89 or various UTI89 mutants was performed using pINT-ts as described (68, 69).

Rugose Biofilm Assays:

YESCA agar plates were used for all rugose biofilm assays (10 g Casamino Acids/Liter, 1 g Yeast Extract/L). To produce low iron plates, YESCA media was mixed with 5 g/100 mL Chelex-100 resin for 1 hour at room temperature. Media was then filtered to remove the resin. 1.5 g/Liter Noble agar was added and media was autoclaved. Before pouring plates, media was supplemented with 100 µM $MgCl_2$, 10 µM $CaCl_2$, and 10 µM tryptophan. Where indicated 10 or 200 µM $FeCl_3$ was also supplemented. For biofilm assays, overnight cultures were rinsed 2x with low iron YESCA media. 4 µL dots of the indicated strains were then plated and incubated at 26°C to allow for biofilm formation. All pictures were taken using an Olympus DP72® camera mounted on an Olympus SZX16® research stereomicroscope

Washout Assay:

The washout assay has been previously described (30). Briefly, agar chunks including rugose biofilms were removed from agar plates and manually inserted into a well of a 24-well plate. 1 mL of potassium phosphate buffer pH 7.2 (kPi) was added to the well and the biofilm was gently shaken for 5 minutes. When the rugose biofilm lifted off the surface, the cells that washed into the buffer suspension were collected and spun down. *arcAB* mutants stuck to the agar plate, and kPi was pipetted onto the biofilm edges to facilitate colony lift-off. The matrix fraction was washed twice more with kPi, and washout cells were pooled from all three washes. The matrix fraction was then moved into an eppendorf tube filled with 1 mL of kPi and was tissue homogenized at high speed for 15 seconds.

β-galactosidase Assays:

β-galactosidase assays were performed as previously described (30, 70), except that chromosomal *lacZ* transcriptional fusion strains were utilized instead of a plasmid-based

system. All β-galactosidase assays were performed in a UTI89 *lacZ* mutant background. All experiments were performed in biological triplicate, and error bars represent standard deviation.

Western Blot Analysis:

Western blot analysis was performed as previously described (30). Briefly, bacteria grown on agar plates were scraped off and suspended in kPi. After normalizing to 1 OD_{600}, 150 µL was spun down. The pellet was then suspended in 150 µL 2x SDS loading buffer. Samples were electrophoresed in 15% polyacrylamide gels and transferred onto a nitrocellulose membrane in a wet transfer apparatus in 25 mM CAPS transfer buffer pH 11.2 with 10% methanol. After transfer, the blot was blocked in 5% milk in TBST for one hour at room temperature. The blot was then incubated with anti-CsgD primary antibody (1:5000) for 1 hour at room temperature, followed by incubation with 1:15000 IRDye 700CW goat anti-mouse IgG secondary antibody (Licor). Blots were washed with TBST and visualized on a Licor Odyssey CLX imager.

Confocal Microscopy:

Confocal microscopy was performed as described (30). LAS AF v2.6.3 build 8173 software was used to trace fluorescence within a circle drawn onto a Z-stack. Traces represent the high point possible in each rugose biofilm, i.e. if the biofilm contained wrinkles, the circle was drawn so that it traces fluorescence through the center of the wrinkle. Each trace is an average of three separate circles from the same Z-stack.

Figures and Tables:

Figure 3.1 Screening redox-regulators for rugose biofilm formation
WT UTI89 and various mutants were spotted on low iron plates or low iron plates supplemented with 10 or 200 μM $FeCl_3$. Pictures were taken after 48 hours of biofilm development.

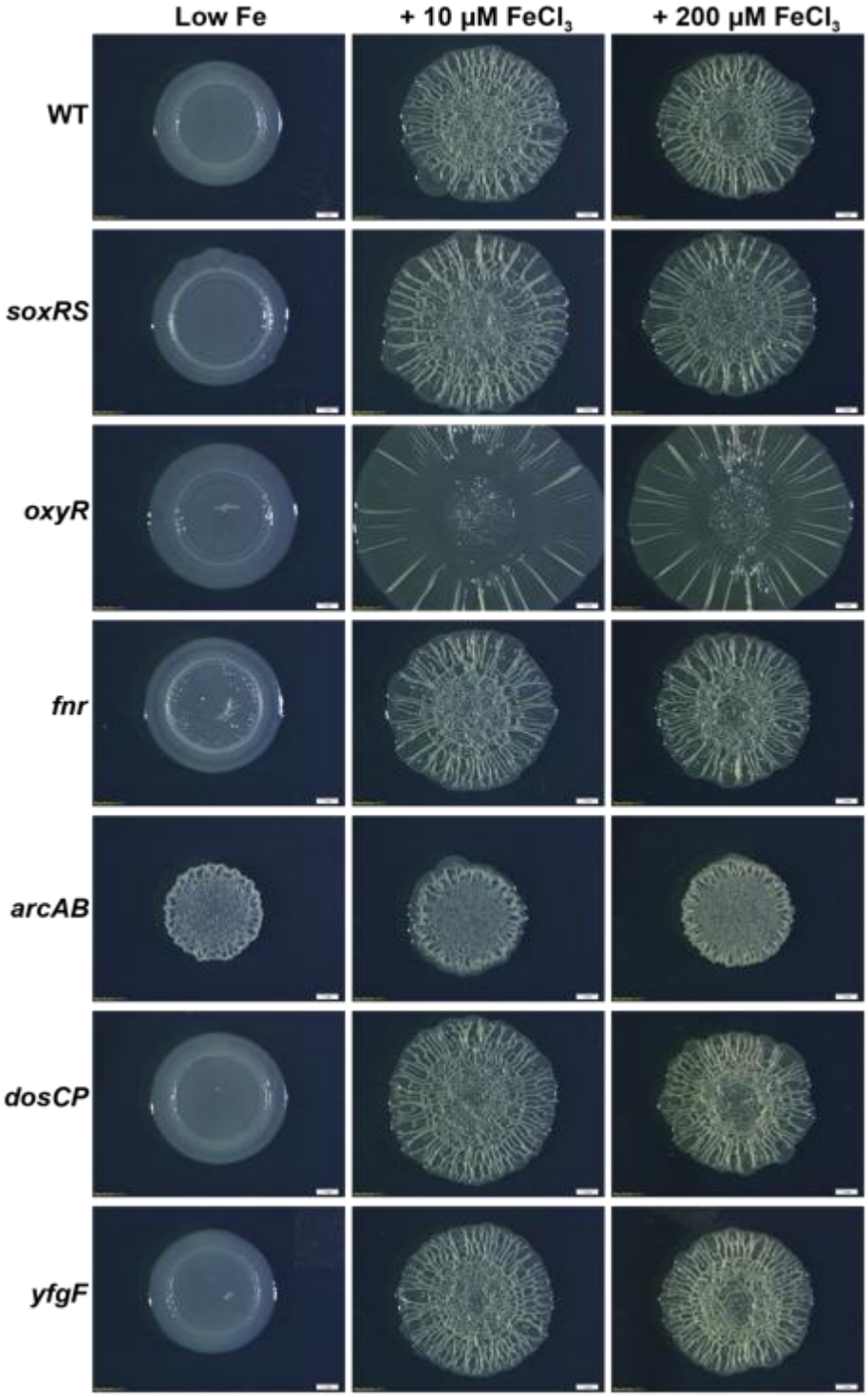

Figure 3.2 OxyR affects colony spreading
WT UTI89 or *oxyR* were transformed with pCKR101 (empty vector (EV)), pCKR101-*oxyR* (p*oxyR*), or pCKR101-*oxyR*^{A233V} (p*oxyR*^{A233V}). Strains were then grown on YESCA plates, and pictures were taken after 48 hours of biofilm development.

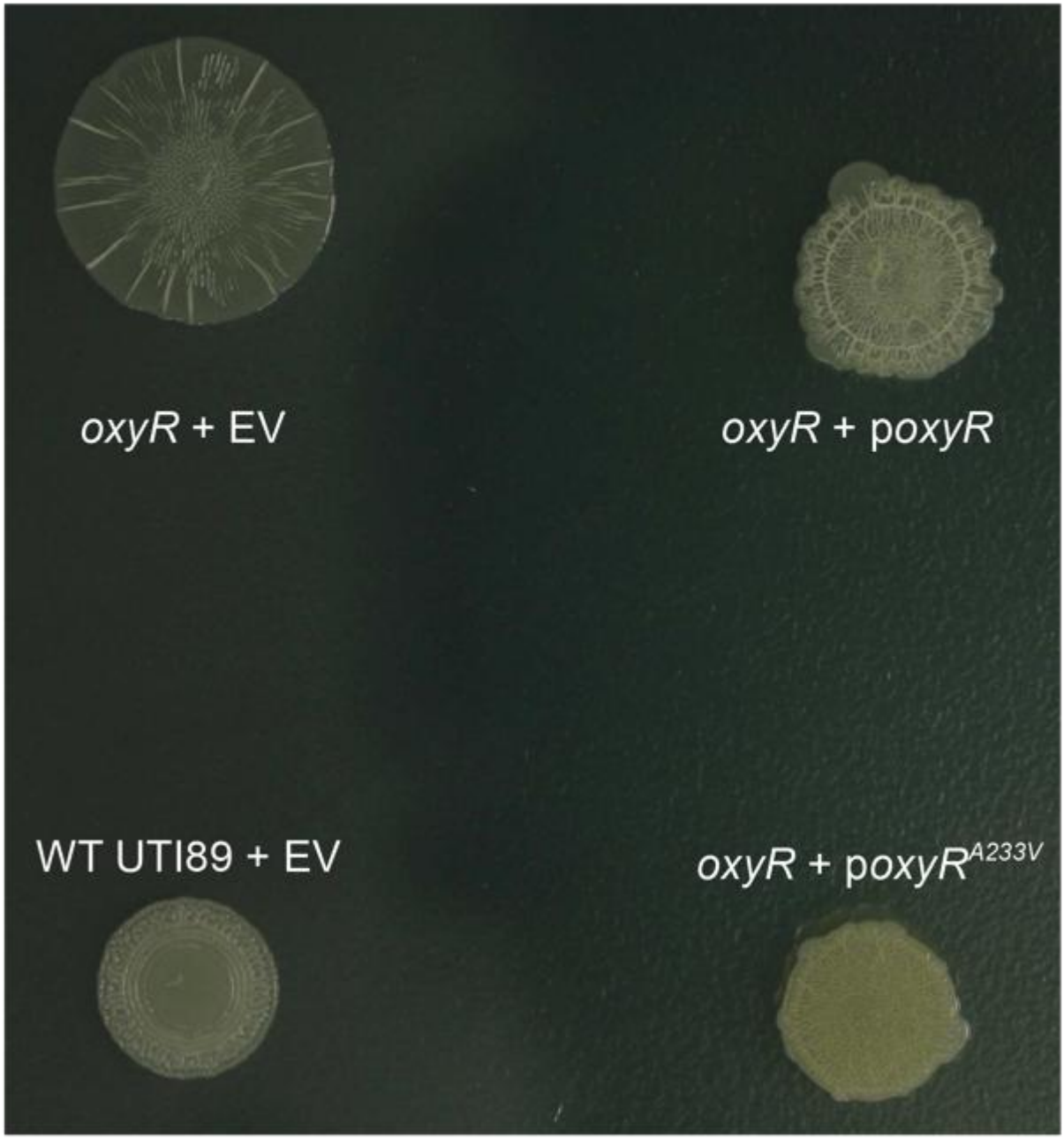

Figure 3.3 Single *arc* mutants and complementation on low iron plates
WT UTI89, *arcB* **(A),** and *arcA* **(B)** were transformed with pCKR101 (EV), pCKR101-*arcA* (p*arcA*), pCKR101-*arcA*^{D54A} (p*arcA*^{D54A}), pCKR101-*arcA*^{D54E} (p*arcA*^{D54E}), pCKR101-*arcB* (p*arcB*) or pCKR101-p*arcB*$^{78\text{-}778}$ (p*arcB*$^{78\text{-}778}$). Strains were then grown on low iron plates supplemented with 25 µM IPTG. Pictures were taken after 48 hours of biofilm development.

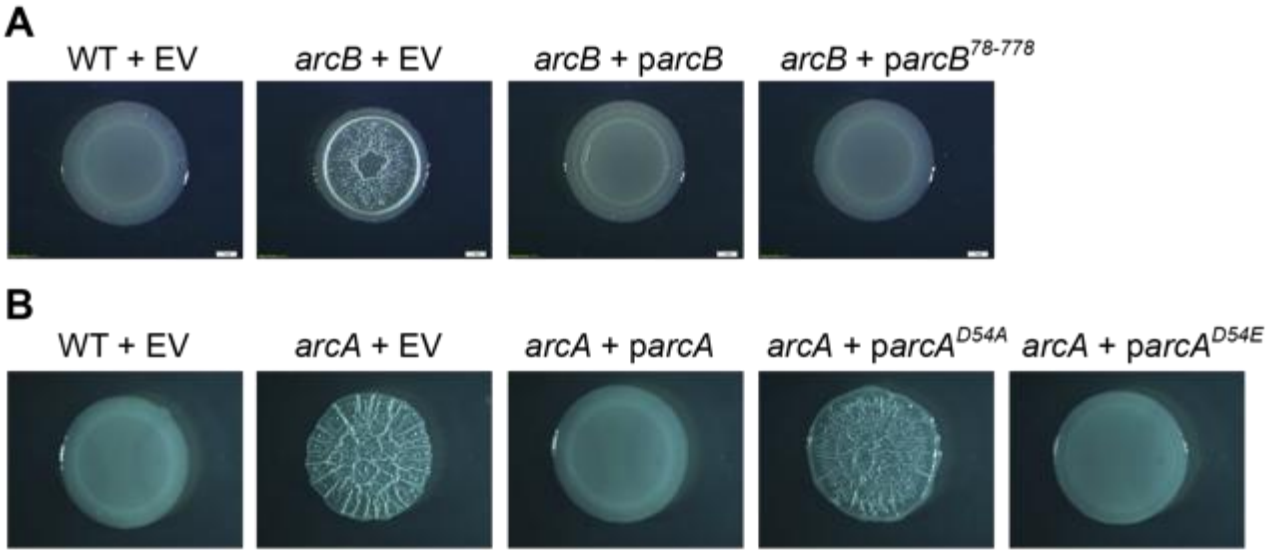

Figure 3.4 ArcB$^{78-778}$ represses rugose biofilm formation on iron replete plates
WT UTI89, *arcB* **(A),** and *arcA* **(B)** were transformed with pCKR101 (EV), pCKR101-*arcA* (p*arcA*), pCKR101-*arcA*^{D54A} (p*arcA*^{D54A}), pCKR101-*arcA*^{D54E} (p*arcA*^{D54E}), pCKR101-*arcB* (p*arcB*) or pCKR101-p*arcB*$^{78-778}$ (p*arcB*$^{78-778}$). Strains were then grown on low iron plates supplemented with 10 µM $FeCl_3$ and 50 µM IPTG. Pictures were taken after 48 hours of biofilm development.

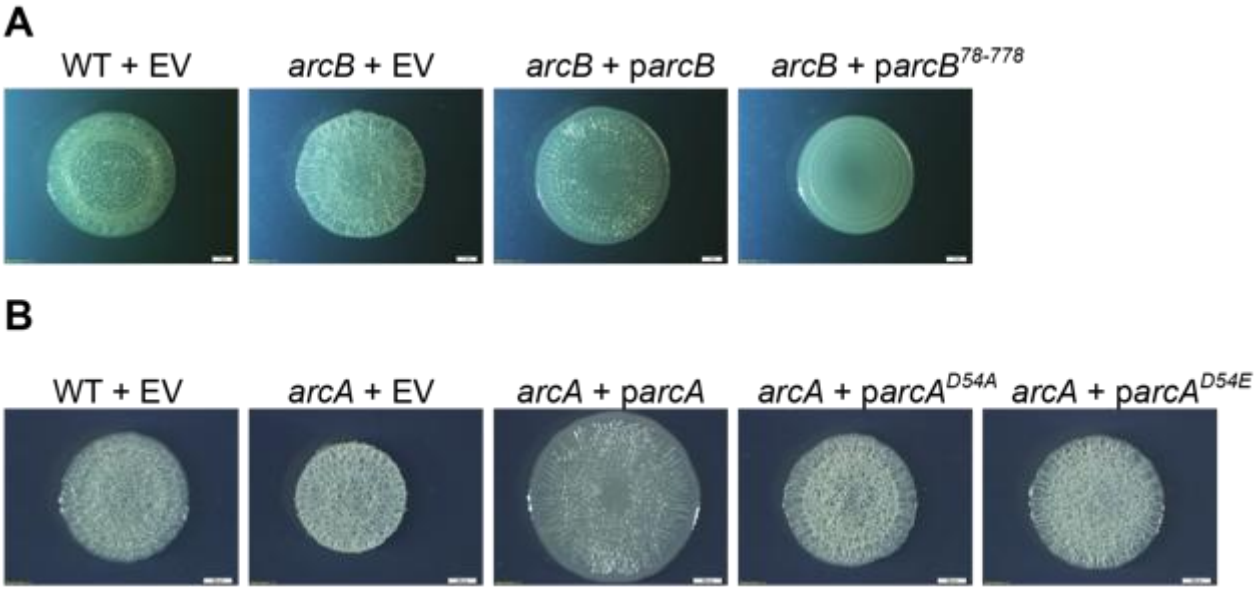

Figure 3.5 *rpoS* expression is required for rugose biofilm formation but is not sufficient to induce rugose biofilm formation
WT UTI89 as well as *rpoS*, *csgBA bcsA*, and *rssB* mutants were grown on low iron plates or low iron plates supplemented with 10 μM $FeCl_3$ **(A)**. Pictures were taken after 48 hours of biofilm development. UTI89/pCKR101 (EV) and UTI89/pCKR101-*rpoS* (p*rpoS*) were grown on low iron plates supplemented with 50 μM IPTG for 72 hours **(B)**.

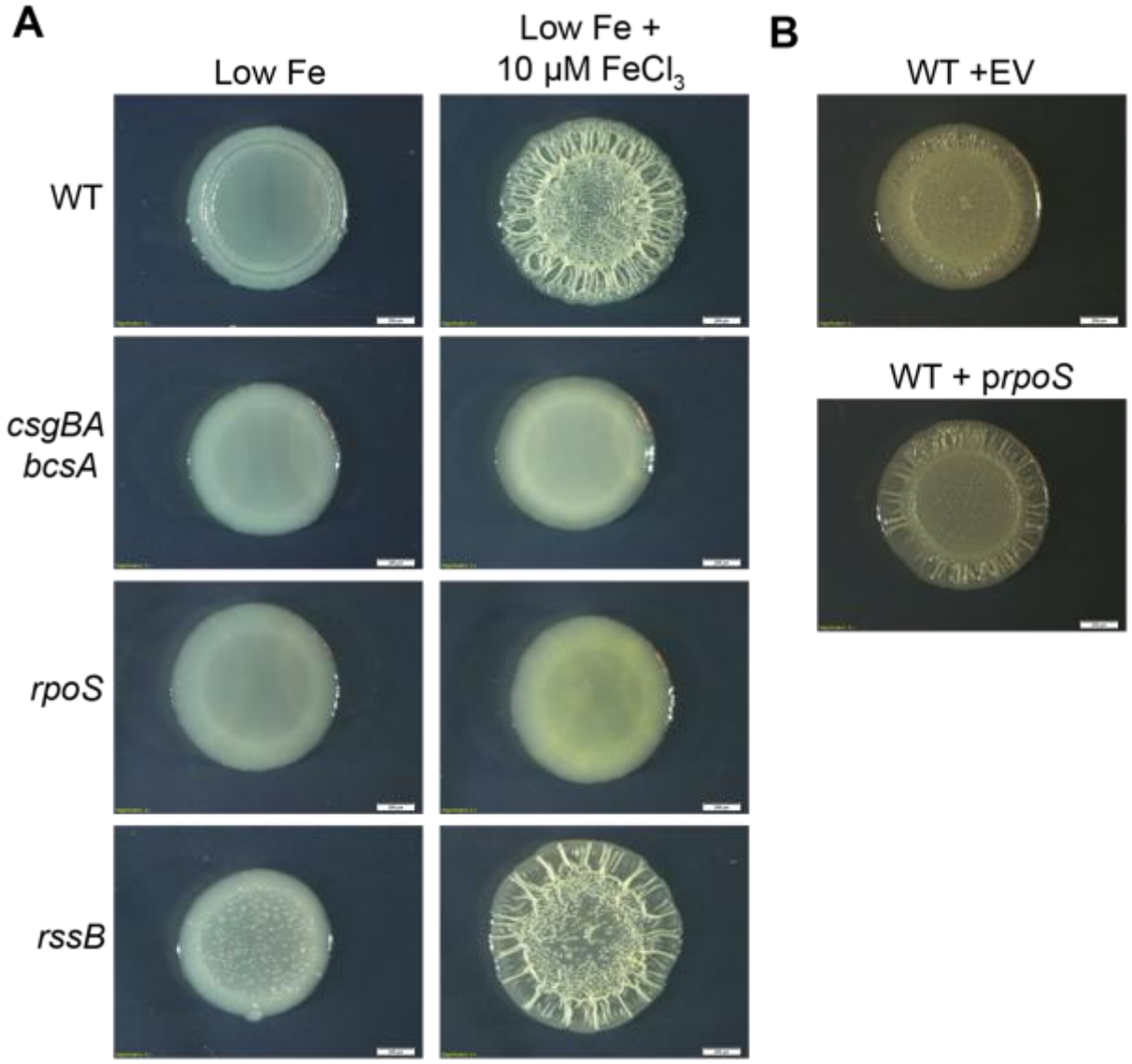

Figure 3.6 ArcZ increases biofilm wrinkling
WT UTI89 and an *arcZ* mutant were grown on low iron plates or low iron plates supplemented with 10 μM $FeCl_3$ **(A)**. Pictures were taken after 24 and 48 hours of biofilm development. UTI89/pBR*lac* (EV) and UTI89/pBR*lac-arcZ* (p*arcZ*) were grown on low iron plates supplemented with 25 μM IPTG or low iron plates supplemented with 25 μM IPTG and 10 μM $FeCl_3$ **(B)**. Pictures were taken after 24 and 48 hours of biofilm development.

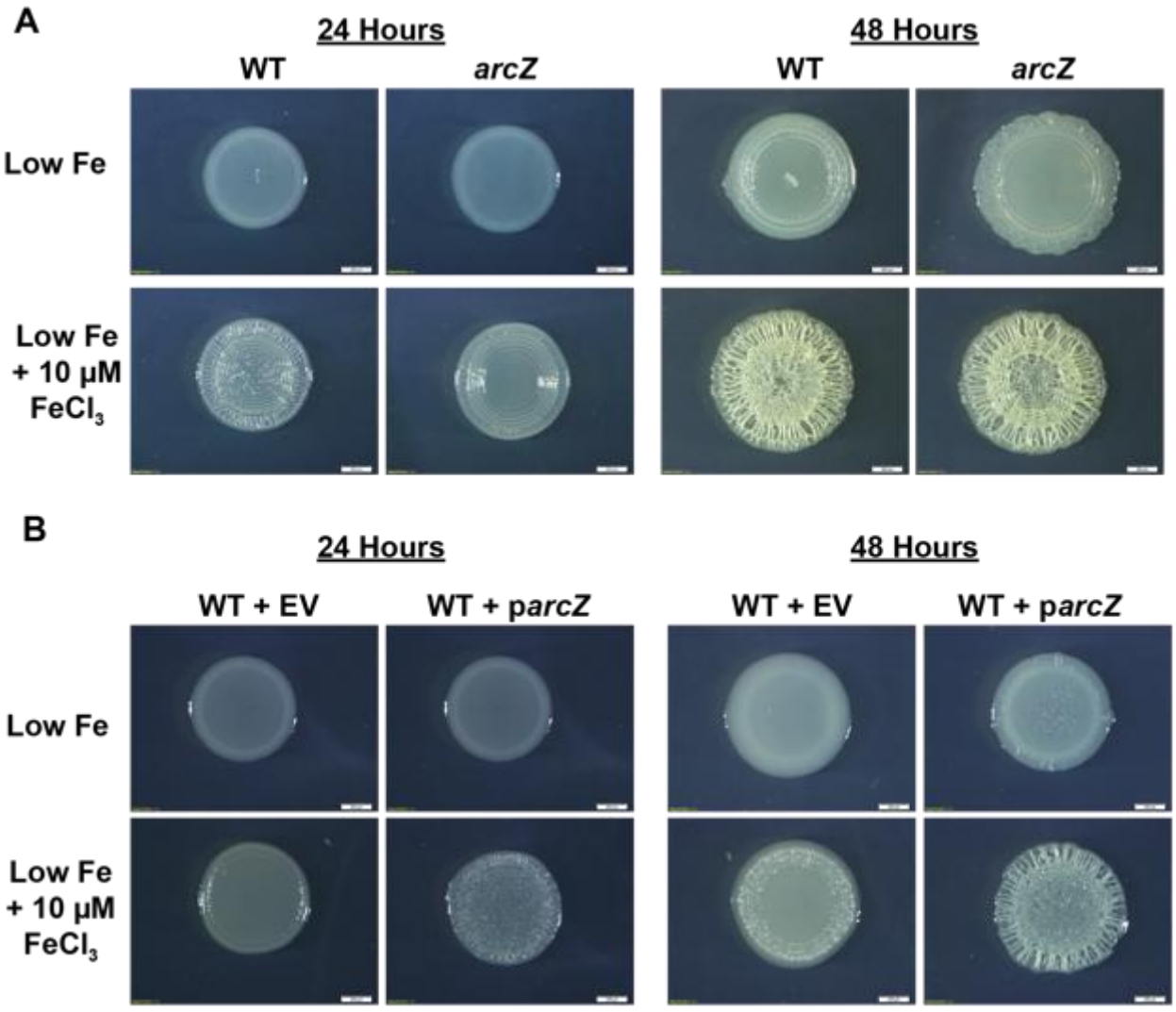

Figure 3.7 Rugose biofilm formation in an *arcAB* mutant is dependent on *csgD*
UTI89, *arcAB*, *csgD*, and *arcAB csgD* were plated on low iron plates or low iron plates supplemented with 10 μM $FeCl_3$. Pictures were taken after 48 hours of biofilm development.

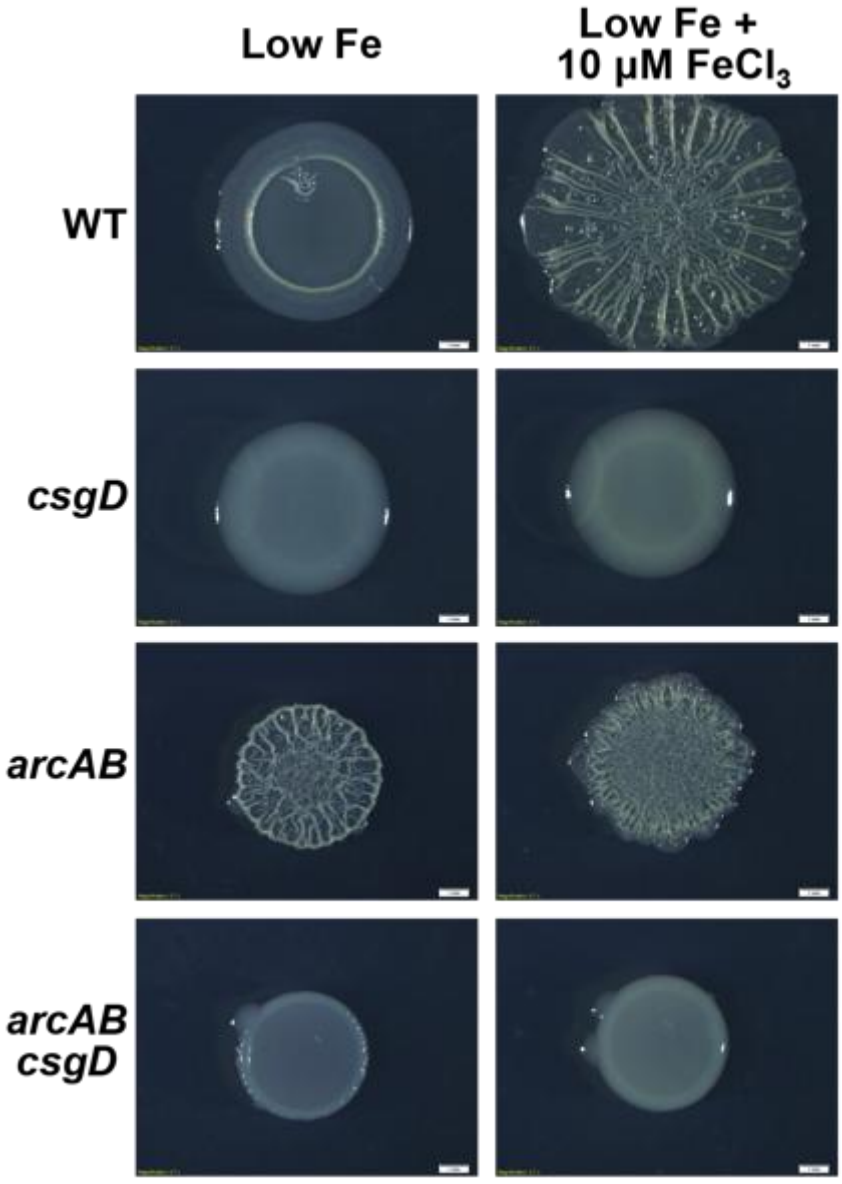

Figure 3.8 ArcAB represses CsgD in low iron conditions
Western blotting for CsgD was performed in WT UTI89 and an *arcAB* mutant after 24 hours of biofilm development on low iron plates or low iron plates supplemented with 10 μM $FeCl_3$. Whole colonies were analyzed, and the washout and matrix fractions were also separated via the washout assay and analyzed separately **(A)**. B-galactosidase assays were performed on UTI89 *lacZ attB::csgBAC-lacZ* and UTI89 *arcAB lacZ attB::csgBAC-lacZ* grown on low iron plates or low iron plates supplemented with 10 μM $FeCl_3$ for 24 hours **(B)**. Whole colonies and washout and matrix fractions were analyzed. WT UTI89/pCKR101 (EV) and WT UTI89/pCKR101-*csgD* (*pcsgD*) were grown on low iron plates supplemented with 25 μM IPTG or low iron plates supplemented with 10 μM $FeCl_3$ and 25 μM IPTG **(C)**. Pictures were taken after 72 hours of biofilm development.

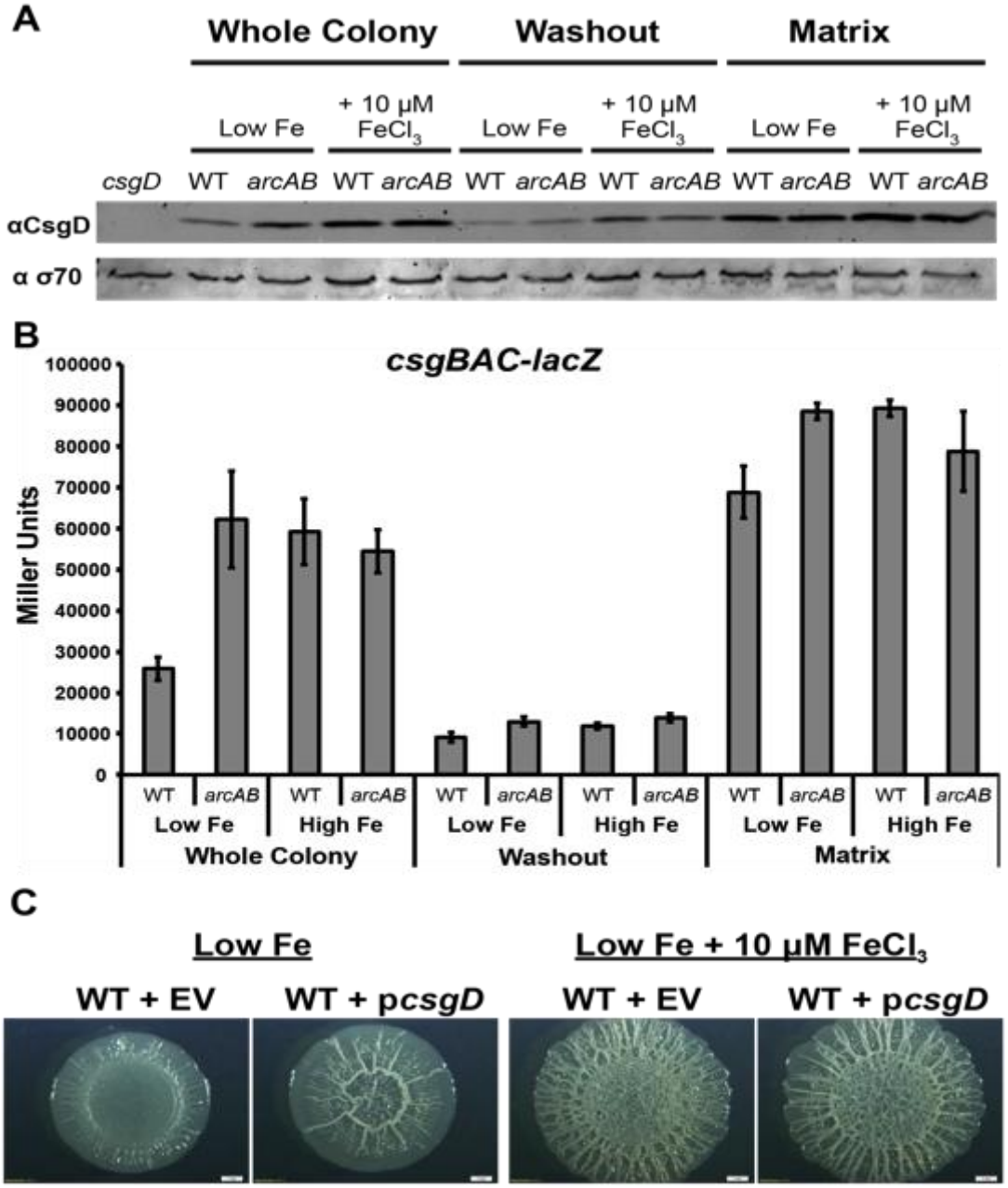

Figure 3.9 *arcAB* mutant has a decreased washout/matrix ratio
The washout assay was performed on WT UTI89 and an arcAB mutant after 24 or 48 hours of growth on low iron plates or low iron plates supplemented with 10 μM $FeCl_3$. The OD_{600} of each fraction was taken, and the ratio of washout OD_{600}/matrix OD_{600} was calculated. Each bar represents biological triplicates, and error bars represent standard deviation.

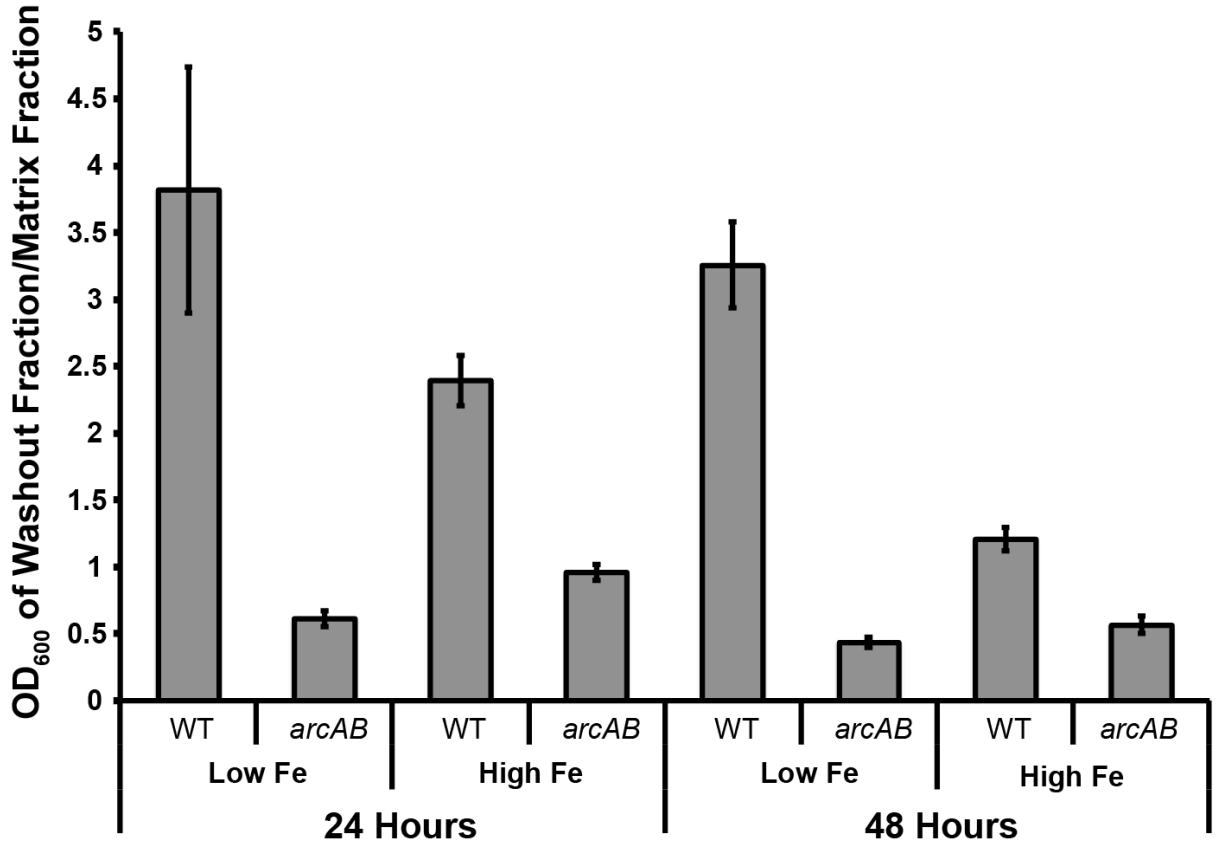

Figure 3.10 Effect of ArcAB on bimodal population development
(A) β-galactosidase assays were performed on UTI89 *lacZ attB::fadE-lacZ* and UTI89 *arcAB lacZ attB::fadE-lacZ* grown on low iron plates or low iron plates supplemented with 10 μM $FeCl_3$ for 48 hours after performing the washout assay. Each bar represents biological triplicates, and error bars represent standard deviation. **(B)** A mid-Z-stack cross section of WT UTI89 *attB::csgBAC-mcherry*/pCKR101-*eGFP* after 48 hours of growth on a low iron plate supplemented with 10 μM $FeCl_3$. Circles represent areas where fluorescence was traced and averaged from the bottom of the Z-stack to the top. Fluorescent traces of WT UTI89 *attB::csgBAC-mcherry*/pCKR101-*eGFP* and UTI89 *arcAB attB::csgBAC*-mcherry/pCKR101-*eGFP* grown on low iron plates **(C)** or low iron plates supplemented with 10 μM $FeCl_3$ **(D)**. Green corresponds to IPTG-induced GFP expression, and red corresponds to *csgBAC*-induced mCherry expression. Each trace is an average of three separate circles drawn on the same Z-stack.

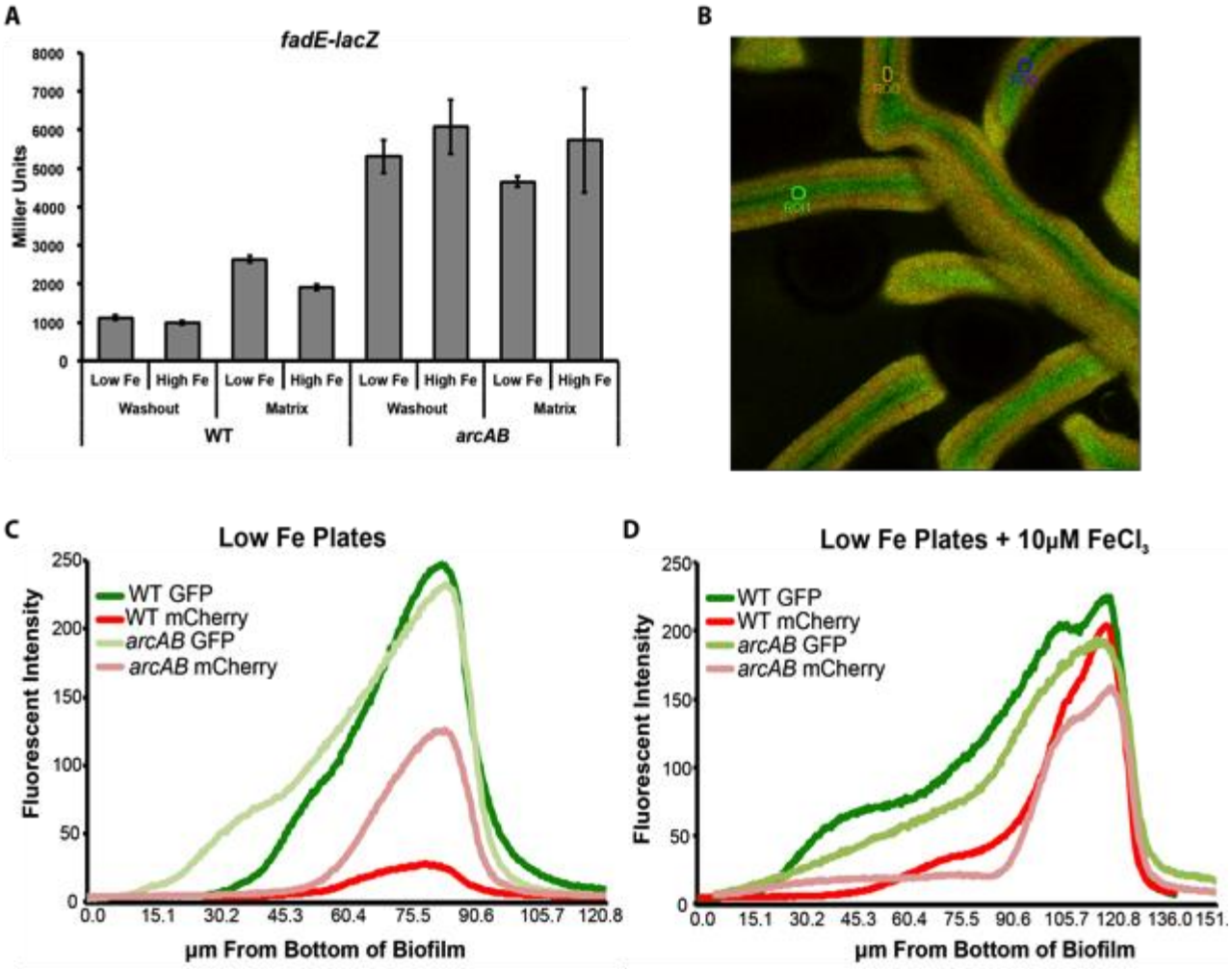

Table 3.1: Strains and Plasmids Used in Chapter 3

Plasmid:	Reference:	Notes:
pCKR101	(1, 2)	
pCKR101-*rpoS*	This Work	*rpoS* cloned into KpnI and XbaI sites of pCKR101 with primers WD419 and WD420 from UTI89 genome
pCKR101-*csgD*	This Work	*csgD* cloned into KpnI and XbaI sites of pCKR101 with primers WD403 and WD404 from UTI89 genome
pCKR101-*eGFP*	(2)	
pCKR101-*arcB*	This Work	*arcB* cloned into KpnI and XbaI sites of pCKR101 with primers WD490 and WD491 from UTI89 genome
pCKR101-$arcB^{78\text{-}778}$	This Work	$arcB^{78\text{-}778}$ cloned into KpnI and XbaI sites of pCKR101 with primers WD492 and WD491 from UTI89 genome
pCKR101-*arcA*	This Work	*arcA* cloned into KpnI and XbaI sites of pCKR101 with primers WD514 and WD515 from UTI89 genome
pCKR101-$arcA^{D54A}$	This Work	$arcA^{D54A}$ amplified in two-step PCR using primer pairs WD518/WD515 and WD519/WD514. End-joined final product was cloned into KpnI and XbaI sites of pCKR101.
pCKR101-$arcA^{D54E}$	This Work	$arcA^{D54E}$ amplified in two-step PCR using primer pairs WD516/WD515 and WD517/WD514. End-joined final product was cloned into KpnI and XbaI sites of pCKR101.
pCKR101-*oxyR*	This Work	*oxyR* cloned into KpnI and XbaI sites of pCKR101 with primers WD255 and WD256 from UTI89 genome
pCKR101-$oxyR^{A233V}$	This Work	$oxyR^{A233V}$ amplified in two-step PCR using primer pairs WD257/WD256 and WD258/WD255. End-joined final product was cloned into KpnI and XbaI sites of pCKR101.
pCD13psk-*lacZ*	This Work	*lacZ* cloned from UTI89 genome into XbaI and SacI site of pCD13psk using primers WD465 and WD466.
pCD13psk-*csgBAC-lacZ*	This Work	UTI89 *csgBAC* promoter from the UTI89 genome cloned into pCD13psk-*lacZ* BamHI and XbaI sites using primers WD459 and WD474
pCD13psk-*fadE-lacZ*	This Work	UTI89 *fadE* promoter from the UTI89 genome cloned into pCD13psk-*lacZ* BamHI and XbaI sites using primers WD540 and WD541

Strain:	**Reference:**	**Notes:**
UTI89	(2, 3)	
UTI89 *csgD*::kan	(2)	
UTI89 *csgBA*::flp *bcsA*::kan	(2)	
UTI89 *arcA*::kan	This Work	Red swap mutagenesis of WT UTI89 with primers WD259 and WD260
UTI89 *arcB*::kan	This Work	Red swap mutagenesis of WT UTI89 with primers WD376 and WD377
UTI89 *fnr::*kan	This Work	Red swap mutagenesis of WT UTI89 with primers WD298 and WD299
UTI89 *dosCP*::kan	This Work	Red swap mutagenesis of WT UTI89 with primers WD361 and WD362
UTI89 *oxyR*::kan	This Work	Red swap mutagenesis of WT UTI89 with primers WD216 and WD217
UTI89 *rpoS*::kan	This Work	Red swap mutagenesis of WT UTI89 with primers WD415 and WD416
UTI89 *rssB*::kan	This Work	Red swap mutagenesis of WT UTI89 with primers WD431 and WD432
UTI89 *soxRS*::kan	This Work	Red swap mutagenesis of WT UTI89 with primers WD131 and WD133
UTI89 *arcA*::flp *arcB*::kan	This Work	Red swap mutagenesis of UTI89 *arcA*::flp with primers WD376 and WD377
UTI89 *arcA*::flp *arcB*::flp *csgD*::kan	This Work	Red swap mutagenesis of UTI89 *arcA*::flp *arcB*::flp with primers WD36 and WD37
UTI89 *lacZ*::kan	This Work	Red swap mutagenesis of WT UTI89 with primers WD534 and WD535
UTI89 *lacZ*::kan *attB::csgBAC-lacZ*	This Work	As described (2, 4), except pCD13psk-*csgBAC-lacZ* was inserted into *attB* site of UTI89 *lacZ*.
UTI89 *lacZ*::kan *attB::fadE-lacZ*	This Work	As described (2, 4), except pCD13psk-*fadE-lacZ* was inserted into *attB* site of UTI89 *lacZ*.
UTI89 *attB*::*csgBAC-mCherry*/pCKR101-*eGFP*	(2)	UTI89 *attB*::*csgBAC-mCherry* electroporated with pCKR101-*eGFP*
UTI89 *arcA*::flp *arcB*::kan *attB*::*csgBAC-mCherry*	This Work	As described (2, 4), except pCD13psk-*csgBAC-mCherry* was inserted into *attB* site of UTI89 *arcA*::flp *arcB*::kan
UTI89 *arcA*::flp *arcB*::kan *attB*::*csgBAC-mCherry*/pCKR101-*eGFP*	This Work	UTI89 *arcA*::flp *arcB*::kan *attB*::*csgBAC-mCherry* electroporated with pCKR101-*eGFP*

Table 3.2: Primers Used in this Study

--Non-complementary regions are undercase

Primer Name:	Sequence:
WD419	**5'** gatcggtaccTGCCGCAGCGATAAATCGGC **3'**
WD420	**5'** gatctctagaTTATTCGCGGAACAGCGCTT **3'**
WD403	**5'** gatcggtacCCTGTCAGGTGTGCGATCAAT **3'**
WD404	**5'** gatctctagaTCTGCCGCCACAATCCAGCG **3'**
WD490	**5'** gatcggtaccTGAAGGAATTCCCTAATGAA **3'**
WD491	**5'** gatctctagaTCATTTTTTAGTGGCTTTTG **3'**
WD492	**5'** gatcggtaccTGAAGGAATTCCCTAATGGAGCAACTGGAGGAGTCACGAC **3'**
WD514	**5'** gatcggtaccTGGCAATTTAGGTAGCAAAC **3'**
WD515	**5'** gatctctagaGACGGTGGTAAAGCCGATTA **3'**
WD516	**5'** AACCTGGTGATCATGGAAATCAATCTGCCGGGT **3'**
WD517	**5'** ACCCGGCAGATTGATTTCCATGATCACCAGTGG **3'**
WD518	**5'** AACCTGGTGATCATGGCTATCAATCTGCCGGGT **3'**
WD519	**5'** ACCCGGCAGATTGATAGCCATGATCACCAGGTT **3'**
WD255	**5'** gatcggtaccCTATCGTGGCAATGGAGGATGGATA **3'**
WD256	**5'** gatctctagaTTAAACCGCCTGTTTTAACACTTTA **3'**
WD257	**5'** CGCAACATGGTGGCGGTAGGTAGCGGGATCACT **3'**
WD258	**5'** AGTGATCCCGCTACCTACCGCCACCATGTTGCG **3'**
WD465	**5'** gatctctagaATTTCACACAGGATACAGCTATGAC **3'**
WD466	**5'** gatcgagctcTTATTTTTGACACCAGACCAACTGG **3'**
WD459	**5'** gatcggatccAACGTTCTTGTTTTTTCTCCATAC **3'**
WD474	**5'** gatctctagaTTAAGAAATTAAATCATTTCAACTT **3'**
WD540	**5'** gatcggatccAAAAGTTAGCCAGCGTTTCC **3'**
WD541	**5'** gatctctagaAACGAAAAGCCCCTTACTTG **3'**
WD259	**5'**GCCGTTTTTATTGACGGTGGTAAAGCCGATTAATCTTCCAGATCACCGCACATATGAATATCCTCCTTAG **3'**
WD260	**5'**CTTTTGTACTTCCTGTTTCGATTTAGTTGGCAATTTAGGTAGCAAACATGGTGTAGGCTGGAGCTGCTTC **3'**
WD376	**5'**AGTATTCGCGCACCCCGGTCTAGCCGGGGTCATTTTTTAGTGGCTTTTGCCATATGAATATCCTCCTTAG **3'**
WD377	**5'**TCAGAATTGGGTATTATTGGGGCAGGTTGTCGTGAAGGAATTCCCTAATGGTGTAGGCTGGAGCTGCTTC **3'**
WD298	**5'**ACAGAAGGATAGTGAGTTATGCGGAAGAATCAGGCAACGTTACGCGTATGCATATGAATATCCTCCTTAG **3'**
WD299	**5'**AAAAGATGTTAAAATTGACAAATATCAATTACGGCTTGAGCAGACCCTATGGTGTAGGCTGGAGCTGCTTC **3'**

WD361	**5'**TCTTCATATTTCAGGAAAATATGGTGCAGTTAGTCGATCTCGCACGTTGGTGTAGGCTGGAGCTGCTTC **3'**
WD362	**5'**AACCCGCGAGTGCGGGCGAGAGGAATTTATCAGATTTTCAGCGGTAACACCATATGAATATCCTCCTTAG **3'**
WD131	**5'**GCGCGGGAGTTAACGCGCGGGCAATAAAACTACAGGCGGTGGCGATAATCCATATGAATATCCTCCTTAG **3'**
WD133	**5'**CTGGAAGATGAACAAAACTAAAGCGCCACAAGGGCGCTTTAGTTTGTTTTGTGTAGGCTGGAGCTGCTTC **3'**
WD216	**5'**CTATGCTACCTATCGCCGCGAACTATCGTGGCAATGGAGGATGGATAATGGTGTAGGCTGGAGCTGCTTC **3'**
WD217	**5'**AAGCCTATCGGGTAGCTGCGCTAAATGGCTTAAACCGCCTGTTTTAAAACCATATGAATATCCTCCTTAG **3'**
WD534	**5'**GGCAGACATGGCCTGCCCGGTTATTATTATTTTTGACACCAGACCAACTGCATATGAATATCCTCCTTAG **3'**
WD535	**5'**GAGCGAATAACAATTTCACACAGGATACAGCTATGACTATGATTACGGATGTGTAGGCTGGAGCTGCTTC **3'**
WD36	**5'**CAATCCAGCGTAAATAACGTTTCATGGCTTTATCGCCTGAGGTTATCGTTCATATGAATATCCTCCTTA **3'**
WD37	**5'**GAGGCAGCTGTCAGGTGTGCGATCAATAAAAAAAGCGGGGTTTCATCATGGTGTAGGCTGGAGCTGCTTC **3'**
415	**5'**TGAGACTGGCCTTTCTGACAGATGCTTACTTATTCGCGGAACAGCGCTTCCATATGAATATCCTCCTTAG **3'**
416	**5'**CTTTTGCTTGAATGTTCCGTCAAGGGATCACGGGTAGGAGCCACCTTATGGTGTAGGCTGGAGCTGCTTC **3'**
WD431	**5'**TGGCAATAGCATGCCACTATTGAGTAAAGCCAGTCAGGGGAGAGAACATGGTGTAGGCTGGAGCTGCTTC **3'**
WD432	**5'**ATGCAAATTTAGCCCGTGTTATCGTTTGCTCATTCTGCAGACAACATCAACATATGAATATCCTCCTTAG **3'**

Notes and Acknowledgements:

A former post-doc, Luz Blanco and a former rotation student, Katie Parzych performed experiments with BW25113 *arcAB* in anaerobic conditions that suggested that ArcAB represses curli when oxygen is limiting. Furthermore, a former student, Dan Smith found that curli was inhibited in BW in an *arcA* mutant. Altogether these results support the phenotypes I have described in this chapter. David Hufnagel is going to submit a manuscript in the near future describing a *csgD*-independent rugose biofilm pathway. His results inspired some experiments for this chapter, particularly the construction of the *arcAB csgD* mutant. Susan Gottesman generously donated pBR*lac* and pBR*lac-arcZ.*

References:

1. **Clark DP.** 1989. The fermentation pathways of *Escherichia coli*. *FEMS Microbiology Reviews* **5:**223-234.
2. **Unden G, Bongaerts J.** 1997. Alternative respiratory pathways of *Escherichia coli*: energetics and transcriptional regulation in response to electron acceptors. *Biochimica et biophysica acta* **1320:**217-234.
3. **Delgado-Nixon VM, Gonzalez G, Gilles-Gonzalez MA.** 2000. Dos, a heme-binding PAS protein from *Escherichia coli*, is a direct oxygen sensor. *Biochemistry* **39:**2685-2691.
4. **Sasakura Y, Hirata S, Sugiyama S, Suzuki S, Taguchi S, Watanabe M, Matsui T, Sagami I, Shimizu T.** 2002. Characterization of a direct oxygen sensor heme protein from *Escherichia coli*. Effects of the heme redox states and mutations at the heme-binding site on catalysis and structure. *The Journal of Biological Chemistry* **277:**23821-23827.
5. **Khoroshilova N, Popescu C, Munck E, Beinert H, Kiley PJ.** 1997. Iron-sulfur cluster disassembly in the FNR protein of *Escherichia coli* by O2: [4Fe-4S] to [2Fe-2S] conversion with loss of biological activity. *Proceedings of the National Academy of Sciences of the United States of America* **94:**6087-6092.
6. **Jervis AJ, Crack JC, White G, Artymiuk PJ, Cheesman MR, Thomson AJ, Le Brun NE, Green J.** 2009. The O2 sensitivity of the transcription factor FNR is controlled by Ser24 modulating the kinetics of [4Fe-4S] to [2Fe-2S] conversion. *Proceedings of the National Academy of Sciences of the United States of America* **106:**4659-4664.
7. **Green J, Bennett B, Jordan P, Ralph ET, Thomson AJ, Guest JR.** 1996. Reconstitution of the [4Fe-4S] cluster in FNR and demonstration of the aerobic-anaerobic transcription switch *in vitro*. *The Biochemical journal* **316 (Pt 3):**887-892.

8. **Tuckerman JR, Gonzalez G, Sousa EH, Wan X, Saito JA, Alam M, Gilles-Gonzalez MA.** 2009. An oxygen-sensing diguanylate cyclase and phosphodiesterase couple for c-di-GMP control. *Biochemistry* **48:**9764-9774.
9. **Rabin RS, Stewart V.** 1993. Dual response regulators (NarL and NarP) interact with dual sensors (NarX and NarQ) to control nitrate- and nitrite-regulated gene expression in *Escherichia coli* K-12. *Journal of Bacteriology* **175:**3259-3268.
10. **Zientz E, Bongaerts J, Unden G.** 1998. Fumarate regulation of gene expression in *Escherichia coli* by the DcuSR (dcuSR genes) two-component regulatory system. *Journal of Bacteriology* **180:**5421-5425.
11. **Jourlin C, Bengrine A, Chippaux M, Mejean V.** 1996. An unorthodox sensor protein (TorS) mediates the induction of the tor structural genes in response to trimethylamine N-oxide in *Escherichia coli*. *Molecular Microbiology* **20:**1297-1306.
12. **Malpica R, Sandoval GR, Rodriguez C, Franco B, Georgellis D.** 2006. Signaling by the arc two-component system provides a link between the redox state of the quinone pool and gene expression. *Antioxidants & Redox Signaling* **8:**781-795.
13. **Georgellis D, Kwon O, Lin ECC.** 2001. Quinones as the redox signal for the Arc two-component system of bacteria. *Science* **292:**2314-2316.
14. **Bekker M, Alexeeva S, Laan W, Sawers G, Teixeira de Mattos J, Hellingwerf K.** 2010. The ArcBA two-component system of *Escherichia coli* is regulated by the redox state of both the ubiquinone and the menaquinone pool. *Journal of Bacteriology* **192:**746-754.
15. **Alvarez AF, Rodriguez C, Georgellis D.** 2013. Ubiquinone and menaquinone electron carriers represent the yin and yang in the redox regulation of the ArcB sensor kinase. *Journal of Bacteriology* **195:**3054-3061.
16. **Malpica R, Franco B, Rodriguez C, Kwon O, Georgellis D.** 2004. Identification of a quinone-sensitive redox switch in the ArcB sensor kinase. *Proceedings of the National Academy of Sciences of the United States of America* **101:**13318-13323.
17. **Pena-Sandoval GR, Georgellis D.** 2010. The ArcB sensor kinase of *Escherichia coli* autophosphorylates by an intramolecular reaction. *Journal of Bacteriology* **192:**1735-1739.
18. **Georgellis D, Lynch AS, Lin EC.** 1997. *In vitro* phosphorylation study of the arc two-component signal transduction system of *Escherichia coli*. *Journal of Bacteriology* **179:**5429-5435.
19. **Georgellis D, Kwon O, Lin EC.** 1999. Amplification of signaling activity of the arc two-component system of *Escherichia coli* by anaerobic metabolites. An *in vitro* study with different protein modules. *The Journal of Biological Chemistry* **274:**35950-35954.
20. **Rolfe MD, Ter Beek A, Graham AI, Trotter EW, Asif HM, Sanguinetti G, de Mattos JT, Poole RK, Green J.** 2011. Transcript profiling and inference of *Escherichia coli* K-12 ArcA activity across the range of physiologically relevant oxygen concentrations. *The Journal of Biological Chemistry* **286:**10147-10154.

21. **Sharma P, Stagge S, Bekker M, Bettenbrock K, Hellingwerf KJ.** 2013. Kinase Activity of ArcB from *Escherichia coli* Is Subject to Regulation by Both Ubiquinone and Demethylmenaquinone. *PloS one* **8**.
22. **Iuchi S, Matsuda Z, Fujiwara T, Lin EC.** 1990. The *arcB* gene of *Escherichia coli* encodes a sensor-regulator protein for anaerobic repression of the *arc* modulon. *Molecular Microbiology* **4:**715-727.
23. **Dietrich LE, Teal TK, Price-Whelan A, Newman DK.** 2008. Redox-active antibiotics control gene expression and community behavior in divergent bacteria. *Science* **321:**1203-1206.
24. **Dietrich LE, Okegbe C, Price-Whelan A, Sakhtah H, Hunter RC, Newman DK.** 2013. Bacterial community morphogenesis is intimately linked to the intracellular redox state. *Journal of Bacteriology* **195:**1371-1380.
25. **Kolodkin-Gal I, Elsholz AK, Muth C, Girguis PR, Kolter R, Losick R.** 2013. Respiration control of multicellularity in *Bacillus subtilis* by a complex of the cytochrome chain with a membrane-embedded histidine kinase. *Genes & Development* **27:**887-899.
26. **Morales DK, Grahl N, Okegbe C, Dietrich LE, Jacobs NJ, Hogan DA.** 2013. Control of Candida albicans metabolism and biofilm formation by *Pseudomonas aeruginosa* phenazines. *Mbio* **4:**e00526-00512.
27. **Romling U, Rohde M, Olsen A, Normark S, Reinkoster J.** 2000. AgfD, the checkpoint of multicellular and aggregative behaviour in *Salmonella typhimurium* regulates at least two independent pathways. *Molecular Microbiology* **36:**10-23.
28. **Zogaj X, Nimtz M, Rohde M, Bokranz W, Romling U.** 2001. The multicellular morphotypes of *Salmonella typhimurium* and *Escherichia coli* produce cellulose as the second component of the extracellular matrix. *Molecular Microbiology* **39:**1452-1463.
29. **Ogasawara H, Yamamoto K, Ishihama A.** 2011. Role of the biofilm master regulator CsgD in cross-regulation between biofilm formation and flagellar synthesis. *Journal of Bacteriology* **193:**2587-2597.
30. **DePas WH, Hufnagel DA, Lee JS, Blanco LP, Bernstein HC, Fisher ST, James GA, Stewart PS, Chapman MR.** 2013. Iron induces bimodal population development by *Escherichia coli*. *Proceedings of the National Academy of Sciences of the United States of America* **110:**2629-2634.
31. **Imlay JA.** 2008. Cellular defenses against superoxide and hydrogen peroxide. *Annual Review of Biochemistry* **77:**755-776.
32. **Povolotsky TL, Hengge R.** 2012. 'Life-style' control networks in *Escherichia coli*: signaling by the second messenger c-di-GMP. *Journal of Biotechnology* **160:**10-16.
33. **Kader A, Simm R, Gerstel U, Morr M, Romling U.** 2006. Hierarchical involvement of various GGDEF domain proteins in rdar morphotype development of *Salmonella enterica* serovar Typhimurium. *Molecular Microbiology* **60:**602-616.
34. **Lacey MM, Partridge JD, Green J.** 2010. *Escherichia coli* K-12 YfgF is an anaerobic cyclic di-GMP phosphodiesterase with roles in cell surface remodelling and the oxidative stress response. *Microbiology* **156:**2873-2886.

35. **Kullik I, Toledano MB, Tartaglia LA, Storz G.** 1995. Mutational analysis of the redox-sensitive transcriptional regulator OxyR: regions important for oxidation and transcriptional activation. *Journal of Bacteriology* **177:**1275-1284.
36. **Jeon Y, Lee YS, Han JS, Kim JB, Hwang DS.** 2001. Multimerization of phosphorylated and non-phosphorylated ArcA is necessary for the response regulator function of the Arc two-component signal transduction system. *The Journal of Biological Chemistry* **276:**40873-40879.
37. **Kwon O, Georgellis D, Lynch AS, Boyd D, Lin EC.** 2000. The ArcB sensor kinase of *Escherichia coli*: genetic exploration of the transmembrane region. *Journal of Bacteriology* **182:**2960-2966.
38. **Laub MT, Goulian M.** 2007. Specificity in two-component signal transduction pathways. *Annual Review of Genetics* **41:**121-145.
39. **Jovanovic G, Engl C, Buck M.** 2009. Physical, functional and conditional interactions between ArcAB and phage shock proteins upon secretin-induced stress in *Escherichia coli*. *Molecular Microbiology* **74:**16-28.
40. **Lan CY, Igo MM.** 1998. Differential expression of the OmpF and OmpC porin proteins in *Escherichia coli* K-12 depends upon the level of active OmpR. *Journal of Bacteriology* **180:**171-174.
41. **Mika F, Hengge R.** 2005. A two-component phosphotransfer network involving ArcB, ArcA, and RssB coordinates synthesis and proteolysis of sigmaS (RpoS) in *E. coli*. *Genes & Development* **19:**2770-2781.
42. **Zhou Y, Gottesman S, Hoskins JR, Maurizi MR, Wickner S.** 2001. The RssB response regulator directly targets sigma(S) for degradation by ClpXP. *Genes & Development* **15:**627-637.
43. **Mandin P, Gottesman S.** 2010. Integrating anaerobic/aerobic sensing and the general stress response through the ArcZ small RNA. *The EMBO journal* **29:**3094-3107.
44. **Stewart PS, Franklin MJ.** 2008. Physiological heterogeneity in biofilms. *Nature reviews Microbiology* **6:**199-210.
45. **Tseng CP, Albrecht J, Gunsalus RP.** 1996. Effect of microaerophilic cell growth conditions on expression of the aerobic (*cyoABCDE and cydAB*) and anaerobic (*narGHJI, frdABCD*, and *dmsABC*) respiratory pathway genes in *Escherichia coli*. *Journal of Bacteriology* **178:**1094-1098.
46. **Cho BK, Knight EM, Palsson BO.** 2006. Transcriptional regulation of the fad regulon genes of *Escherichia coli* by ArcA. *Microbiology* **152:**2207-2219.
47. **Grantcharova N, Peters V, Monteiro C, Zakikhany K, Romling U.** 2010. Bistable expression of CsgD in biofilm development of *Salmonella enterica* serovar typhimurium. *Journal of Bacteriology* **192:**456-466.
48. **Zhang A, Altuvia S, Tiwari A, Argaman L, Hengge-Aronis R, Storz G.** 1998. The OxyS regulatory RNA represses rpoS translation and binds the Hfq (HF-I) protein. *The EMBO journal* **17:**6061-6068.
49. **Henderson IR, Owen P.** 1999. The major phase-variable outer membrane protein of *Escherichia coli* structurally resembles the immunoglobulin A1 protease class of exported protein and is regulated by a novel mechanism involving Dam and oxyR. *Journal of Bacteriology* **181:**2132-2141.

50. **Danese PN, Pratt LA, Dove SL, Kolter R.** 2000. The outer membrane protein, antigen 43, mediates cell-to-cell interactions within *Escherichia coli* biofilms. *Molecular Microbiology* **37:**424-432.
51. **Monteiro C, Papenfort K, Hentrich K, Ahmad I, Le Guyon S, Reimann R, Grantcharova N, Romling U.** 2012. Hfq and Hfq-dependent small RNAs are major contributors to multicellular development in *Salmonella enterica* serovar Typhimurium. *RNA biology* **9:**489-502.
52. **Olsen A, Arnqvist A, Hammar M, Sukupolvi S, Normark S.** 1993. The RpoS sigma factor relieves H-NS-mediated transcriptional repression of *csgA*, the subunit gene of fibronectin-binding curli in *Escherichia coli*. *Molecular Microbiology* **7:**523-536.
53. **Romling U, Sierralta WD, Eriksson K, Normark S.** 1998. Multicellular and aggregative behaviour of *Salmonella typhimurium* strains is controlled by mutations in the *agfD* promoter. *Molecular Microbiology* **28:**249-264.
54. **Liu X, De Wulf P.** 2004. Probing the ArcA-P modulon of *Escherichia coli* by whole genome transcriptional analysis and sequence recognition profiling. *The Journal of Biological Chemistry* **279:**12588-12597.
55. **Hammar M, Arnqvist A, Bian Z, Olsen A, Normark S.** 1995. Expression of two csg operons is required for production of fibronectin- and congo red-binding curli polymers in *Escherichia coli* K-12. *Molecular Microbiology* **18:**661-670.
56. **Serra DO, Richter AM, Klauck G, Mika F, Hengge R.** 2013. Microanatomy at cellular resolution and spatial order of physiological differentiation in a bacterial biofilm. *Mbio* **4:**e00103-00113.
57. **Kempes CP, Okegbe C, Mears-Clarke Z, Follows MJ, Dietrich LE.** 2014. Morphological optimization for access to dual oxidants in biofilms. *Proceedings of the National Academy of Sciences of the United States of America* **111:**208-213.
58. **Serra DO, Richter AM, Hengge R.** 2013. Cellulose as an architectural element in spatially structured *Escherichia coli* biofilms. *Journal of Bacteriology* **195:**5540-5554.
59. **White AP, Gibson DL, Kim W, Kay WW, Surette MG.** 2006. Thin aggregative fimbriae and cellulose enhance long-term survival and persistence of *Salmonella*. *Journal of Bacteriology* **188:**3219-3227.
60. **White AP, Gibson DL, Grassl GA, Kay WW, Finlay BB, Vallance BA, Surette MG.** 2008. Aggregation via the red, dry, and rough morphotype is not a virulence adaptation in *Salmonella enterica* serovar Typhimurium. *Infection and Immunity* **76:**1048-1058.
61. **Tenaillon O, Skurnik D, Picard B, Denamur E.** 2010. The population genetics of commensal *Escherichia coli*. *Nature reviews Microbiology* **8:**207-217.
62. **Oppong GO, Rapsinski GJ, Newman TN, Nishimori JH, Biesecker SG, Tukel C.** 2013. Epithelial cells augment barrier function via activation of the Toll-like receptor 2/phosphatidylinositol 3-kinase pathway upon recognition of *Salmonella enterica* serovar Typhimurium curli fibrils in the gut. *Infection and Immunity* **81:**478-486.
63. **Hufnagel DA, Tukel C, Chapman MR.** 2013. Disease to dirt: the biology of microbial amyloids. *PLoS Pathogens* **9:**e1003740.

64. **Jones SA, Chowdhury FZ, Fabich AJ, Anderson A, Schreiner DM, House AL, Autieri SM, Leatham MP, Lins JJ, Jorgensen M, Cohen PS, Conway T.** 2007. Respiration of *Escherichia coli* in the mouse intestine. *Infection and Immunity* **75:**4891-4899.
65. **Marteyn B, West NP, Browning DF, Cole JA, Shaw JG, Palm F, Mounier J, Prevost MC, Sansonetti P, Tang CM.** 2010. Modulation of Shigella virulence in response to available oxygen *in vivo*. *Nature* **465:**355-358.
66. **Datsenko KA, Wanner BL.** 2000. One-step inactivation of chromosomal genes in *Escherichia coli* K-12 using PCR products. *Proceedings of the National Academy of Sciences of the United States of America* **97:**6640-6645.
67. **Hammer ND, McGuffie BA, Zhou Y, Badtke MP, Reinke AA, Brannstrom K, Gestwicki JE, Olofsson A, Almqvist F, Chapman MR.** 2012. The C-Terminal Repeating Units of CsgB Direct Bacterial Functional Amyloid Nucleation. *Journal of Molecular Biology* **422:**376-389.
68. **Platt R, Drescher C, Park SK, Phillips GJ.** 2000. Genetic system for reversible integration of DNA constructs and *lacZ* gene fusions into the *Escherichia coli* chromosome. *Plasmid* **43:**12-23.
69. **Wright KJ, Seed PC, Hultgren SJ.** 2005. Uropathogenic *Escherichia coli* flagella aid in efficient urinary tract colonization. *Infection and Immunity* **73:**7657-7668.
70. **Miller JH.** 1972. Experiments in molecular genetics. *Cold Spring Harbor Laboratory*, Cold Spring Harbor, NY.

Chapter 4

Biofilm Formation Protects *Escherichia coli* against Predation

Abstract:

Enteric bacteria such as *E. coli* are exposed to a variety of environmental stresses in the non-host environment. A key tactic *E. coli* employs to counter such stresses is CsgD-mediated biofilm formation. CsgD is a transcriptional regulator that induces expression of the biofilm matrix components curli and cellulose. Expression of curli and cellulose confers protection against various stresses such as desiccation, reactive oxygen species, and bleach. I found that production of the biofilm matrix protected *E. coli* against predation from the nematode *Caenorhabditis elegans* and the predatory bacteria *Myxococcus xanthus*. Additionally, matrix-encased bacteria at the air/biofilm interface exhibited roughly 40-fold increased survival after *C. elegans* and *M. xanthus* killing compared to interior, non-matrix-encased cells. CsgD expression is under complex transcriptional control, with a variety of environmental signals that contribute to its regulation. Here I demonstrated that non-host reservoirs of *E. coli*, including pig and cow feces and commonly contaminated foods such as beef, chicken, and spinach provided a nutritional environment that supports biofilm matrix production. Altogether I showed that common non-host reservoirs of *E. coli* and other *Enterobacteriaceae* supported CsgD-mediated matrix production and that biofilm formation protected *E. coli* against predation.

Introduction:

E. coli is a Gram-negative, rod-shaped, facultative anaerobe which commonly lives as a commensal in the mammalian gut. Through acquisition of various virulence factors, particular *E. coli* strains have gained the ability to colonize and cause disease at specific host sites. Enterohemorrhagic *E. coli* (EHEC) and enteropathogenic *E. coli*

(EPEC) are common causative agents of gastroenteritis (1-3). Additionally, extraintestinal pathogenic *E. coli* (ExPEC) occupy host niches other than the intestinal tract. ExPEC cause various diseases such as sepsis, neonatal meningitis, and urinary tract infections (UTIs). Uropathogenic *E. coli* (UPEC) accounts for approximately 80% of the acute UTIs reported in the US (3-5). ExPEC are becoming increasingly problematic due to a recent rise in antibiotic resistance (5, 6).

Intestinal pathogenic *E. coli* (IPEC) is spread through the fecal-oral route. A common mechanism of transmission is shedding of bacteria in the feces of pathogen-bearing farm animals (7-10). Indeed, contact with animal feces is a risk factor for sporadic infection with EHEC (11). Compared to the transmission of IPEC, the transmission of ExPEC strains such as UPEC is poorly understood. Recent studies have demonstrated that UPEC strains, although they are adapted to colonize the bladder, show no fitness defects in the gut (12). The intestine may serve as a reservoir for UPEC in patients with recurrent UTIs, and it is generally accepted that UPEC from the gastrointestinal tract is able to infect and colonize the urethra (13-15). UPEC outbreaks have been reported, with a likely cause being UPEC contamination of food, suggesting that ExPEC can be transmitted via the fecal-oral route (16-19).

Compared to the host or lab setting, the physiology of *E. coli* in non-host environmental reservoirs is poorly understood. A detailed understanding of the mechanisms involved in non-host persistence is paramount in developing effective strategies to prevent contamination of food products by *E. coli* and other pathogenic *Enterobacteriaceae*. One important aspect of non-host persistence and survival for *E. coli* is biofilm formation (20). Biofilms are bacterial communities characterized by the presence of a self-produced extracellular matrix. *E. coli* biofilm formation has been well described. CsgD is the master biofilm regulator in *E. coli* and in other *Enterobacteriaceae* such as *Salmonella enterica* ser. Typhimurium (21-23). CsgD is a transcriptional regulator required for production of the two major extracellular matrix components: amyloidogenic curli fibers and the polysaccharide cellulose. CsgD directly induces the curli subunit operon, while cellulose is activated via CsgD induction of the diguanylate cyclase gene *adrA* (22, 24, 25). AdrA produces the second messenger cyclic-di-GMP (c-di-GMP), which activates the cellulose synthase BcsA (25, 26). Curli

and cellulose production has been correlated with increased resistance to desiccation, reactive oxygen species, and disinfectants (27-30). Furthermore, matrix production has been implicated in EHEC attachment to commonly contaminated foods such as spinach and to abiotic surfaces (31, 32). While curli and cellulose have various roles during enteric pathogenesis (20, 33), an expression study demonstrated that the curli promoter is relatively inactive during *S. enterica* ser. Typhimurium passage through a mouse host. However, curli expression is immediately induced once the bacteria are excreted in stool (29). Altogether these results suggest that biofilm formation is an important aspect of non-host persistence for *Enterobacteriaceae* such as *E. coli*.

In the non-host environment, bacteria are exposed to a variety of predators. In a similar manner to biofilm formation inhibiting immune cell phagocytosis, biofilm matrix can block predator feeding. Biofilm-associated *Vibrio cholerae* and *Pseudomonas aeruginosa* survive protozoan grazing better than planktonic cells (34-36). Biofilm formation by *Yersinia pestis* and *Staphyococcus epidermidis* have been shown to respectively block food intake and prevent efficient digestion by the nematode *C. elegans* (37, 38). Additionally, *C. elegans* is less efficient at feeding on *Myxococcus xanthus* colonies that produce a more robust biofilm matrix (39). In this study I sought to determine whether *E. coli* biofilms confer protection against predators, and I assessed how relevant non-host environmental conditions influence *E. coli* biofilm formation. I first assessed the ability of the nematode *C. elegans* and the soil-dwelling bacteria *M. xanthus* to prey on biofilm-encased UPEC. As both predators require direct bacterial contact to efficiently kill prey cells (40-42), I hypothesized that CsgD-dependent biofilms would protect enteric bacteria such as *E. coli* against both *C. elegans* and *M. xanthus* predation. I also tested the ability of *E. coli* to produce CsgD-mediated biofilms in environments that mimic those encountered outside the host.

Results:

C. elegans Predation Assay

Bacteria encounter many stressors while outside the host, including predation. Free-living nematodes such as the model organism *C. elegans* are ubiquitous bacterial predators that have large-scale affects on soil bacterial communities (43). To determine

whether *E. coli* biofilm formation protects against nematode predation, I developed a feeding assay on YESCA agar plates. Briefly, ~25 L1-L2 *C. elegans* worms were moved to the center of an agar plate on which four UTI89 strains had grown for two days in biofilm-inducing conditions. The four UTI89 strains that I tested were WT (curli+ cellulose+), *bcsA* (curli+ cellulose-), *csgBA* (curli- cellulose+) and *csgBA bcsA* (curli- cellulose-). *C. elegans* was then allowed to feed for 15 days at 20°C. Plates were harvested at three day intervals, and colony forming units (CFUs)/colony were determined. Each plate with *C. elegans* was randomly paired with a control plate with no *C. elegans* added, and percent survival was calculated.

By day nine, *C. elegans* decreased the CFUs/colony of all the strains by roughly 10-fold (Fig. 4.1). However, at day 12, there was a dramatic survival difference between WT UTI89 and mutants that express neither curli nor cellulose. The WT rugose colony was still visible, and CFUs had leveled out after their initial day 9 loss. Conversely, the *csgBA bcsA* mutant had visually disappeared from the plate, and CFU counts decreased precipitously compared to the no-*C. elegans* control (Fig. 4.1A,B). By day 15 the CFUs of a WT UTI89 colony were reduced to 2.5% of a no-*C. elegans* control, while the *csgBA bcsA* mutant was decreased to 0.0082%. The *bcsA* mutant demonstrated a slight but significant survival advantage compared to the *csgBA bcsA* double mutant, indicating that curli alone provides slight predation resistance. In contrast, the *csgBA* mutant phenocopied WT through day 12 in terms of CFUs/colony, and no significant difference in percent survival between WT and *csgBA* was determined at day 15 (Figure 4.1A, B). Cellulose is therefore the more important matrix component in regard to *C. elegans* resistance.

I also tested WT UTI89 and a *csgD* mutant in a “non-competition” assay. That is, I spotted six WT UTI89 dots on an agar plate, added worms, and at three day intervals harvested a single colony from that plate for CFU counts. Separately, I dotted six UTI89 *csgD* colonies on an agar plate and did a parallel assay. Each plate was spotted in triplicate. As with the competition assay, WT displayed a dramatic resistance phenotype compared to the matrix deficient mutant (Fig. 4.2).

C. elegans Tracking Assay

I hypothesized that the biofilm matrix either provides a mechanical barrier to *C. elegans* feeding or that *C. elegans* is preferentially attracted to non-matrix-encased bacteria. Indeed, it has been demonstrated that *P. aeruginosa* polysaccharide production changes the feeding behavior of *C. elegans* (44). To determine whether matrix expression affected colony occupancy, a mixed population of *C. elegans myo-2::rfp ceh22::gfp* was moved onto the center of a plate that contained one WT colony and one *csgBA bcsA* colony (Fig. 4.3A). At intervals, the number of worms on each colony was counted (Fig. 4.3B,C). At 1, 6, or 24 hours post-inoculation, no significant difference between the number of worms on the WT colony compared to the number of worms on the *csgBA bcsA* colony could be determined (Fig. 4.3C), favoring the alternate model that *E. coli* biofilm matrix provides a mechanical barrier to predation by *C. elegans*.

Determining the Susceptibility of Two Biofilm Populations to *C. elegans* Feeding

A key factor contributing to the resistance of biofilms to various stresses is the development of distinct subpopulations within a biofilm (45). Biofilm-mediated antibiotic resistance is mostly attributable to development of a small population of persister cells, which resist antibiotic killing by virtue of a reduced growth rate (46). Matrix production can be monitored by the formation of wrinkled or rugose biofilms on agar plates, which is indicative of curli and cellulose expression in a variety of species from *Enterobacteriaceae* (24, 28, 47). I have previously demonstrated that UTI89, *S. enterica* ser. Typhimurium, and *Citrobacter koseri* develop at least two distinct populations within rugose biofilms (28). A population of matrix-encased bacteria lines the air-biofilm interface (termed the “matrix fraction”), whereas a distinct population of non-matrix-encased cells lines the biofilm interior (termed the “washout fraction”). These two populations can be separated using a washout assay, which involves suspending the washout fraction bacteria in buffer (28). To test whether non-matrix encased washout cells were more susceptible to predation, I allowed *C. elegans* to feed on WT UTI89 rugose colonies for 12 days -- the amount of time required for *C. elegans* to reduce WT CFUs by ~10-fold (Figure 4.1A). At days 6 and 12, the washout assay was performed and CFUs/fraction were determined for WT colonies exposed to *C. elegans* as well as

WT colonies under no predation. At day 12, the washout assay could still be performed on WT rugose colonies (Fig. 4.4), and CFUs from each fraction were similar. The washout fraction contained $4.9 \times 10^9 \pm 4.7 \times 10^8$ CFUs and the matrix fraction contained $2.4 \times 10^9 \pm 4.9 \times 10^8$ CFUs. Nematode predation led to a fragile biofilm that broke into small pieces when washed in buffer (Fig. 4.4). The washout assay was therefore performed by allowing the stable aggregates to settle to the bottom of the well. Bacteria from three buffer washes were collected as the washout fraction. After 12 days of nematode feeding, $3.9 \times 10^6 \pm 1.2 \times 10^6$ CFUs (0.074% survival) were recovered from the washout fraction and $7.0 \times 10^7 \pm 2.4 \times 10^7$ CFUs (3.0% survival) were recovered from the matrix fraction (Fig. 4.5A), indicating that even within a single biofilm, *C. elegans* is able to feed more efficiently on non-matrix-encased bacteria. Western blot analysis for CsgA from 12-day old rugose biofilms without nematode predation revealed that in WT UTI89 a bimodal population is maintained throughout the experiment (Fig. 4.5B).

Biofilm Integrity Analysis After Predation

In *E. coli* biofilms, curli and cellulose form a dense matrix, surrounding cells in what appears to be an “egg in a carton” arrangement (48-50). *C. elegans* preys on bacteria by contracting and relaxing the pharynx, creating a suction that results in the intake of bacterial cells (40). For the biofilm matrix to act as a barrier to feeding, it is reasonable to speculate that the structural integrity of the biofilm would have to be maintained even amid predation. As a measure of biofilm integrity, I assayed the SDS-solubility of the major curli subunit CsgA. CsgA forms amyloidogenic polymers that do not migrate into an SDS-PAGE gel (51). Depolymerizing amyloids such as curli requires pretreatment with a strong denaturant such as HFIP (52). To assay the stability of curli fibers after nematode predation, I tested the SDS-solubility of CsgA polymers. CsgA was completely SDS-insoluble, both with and without nematode predation stress, indicating that *C. elegans* was not able to decompose the amyloid component of the biofilm matrix (Fig 4.5B). Not enough cells could be harvested from the washout fraction of biofilms that had been fed on by *C. elegans* for western blot analysis.

M. xanthus Predation Assay

In addition to predation by nematodes, which rely on mechanical suction to feed on bacteria, a variety of bacterial predators secrete toxins to kill prey cells. *M. xanthus* is a common saprophytic soil bacteria that uses an array of secondary metabolites to kill and lyse target cells (53, 54). *M. xanthus* can commonly be found in feces from herbivorous animals, so non-host interactions with *E. coli* or other *Enterobacteriaceae* are plausible (54). *M. xanthus* needs to contact prey cells to efficiently kill them (41, 42), so I hypothesized that the biofilm matrix would also protect *E. coli* against *M. xanthus* predation. To test killing by *Myxococcus*, YESCA agar plates were buffered to pH 7.4, which falls within the optimum range for *M. xanthus* growth (55), and which still allows UTI89 rugose biofilm development (Fig. 4.6A). WT UTI89 or UTI89 matrix mutants were spotted next to *M. xanthus* DK1622 on agar filled wells of a 24-well plate. After 2 days of biofilm development at 26°C, the plates were moved into humidity chambers within 30°C incubators (day 0), and tracked visually.

M. xanthus completely spread through both WT UTI89 and the matrix mutants after 10 days of co-incubation, with the rate of spreading being approximately equal (Fig. 4.6A). The rugose biofilm maintained some semblance of its original shape even after *M. xanthus* feeding (Fig. 4.6A). As with the nematode assays, percent survival was calculated as CFUs from *M. xanthus* exposed colonies/CFUs from no-*M. xanthus* controls. CFU counts from the WT colony demonstrated that biofilm formation conferred robust protection compared to the *csgBA bcsA* double mutant (Fig. 4.6B), from which no CFUs could be recovered. In contrast to the nematode predation results, the *bcsA* mutant (only producing curli) was the only single mutant that demonstrated *M. xanthus* resistance. No colonies could be recovered from the *csgBA* mutant (only producing cellulose). However, both matrix components conferred greater resistance than curli only, as WT survived to a greater degree than *bcsA* (Fig. 4.6B). Matrix production therefore confers protection against both *C. elegans* and *M. xanthus* predation.

M. xanthus kills prey cells by secreting a variety of proteases and degradative enzymes (53, 56). The protective phenotype conferred by WT UTI89 and the *bcsA* mutant implies that curli fibers must resist protease-mediated degradation. Indeed, a general property of amyloids such as curli is protease resistance (51, 57). I tested the

SDS-solubility of CsgA from WT UTI89 with and without *M. xanthus* predation, and curli remained SDS-insoluble even after *M. xanthus* predation (Fig. 4.7). Interestingly though, multiple species of CsgA were visible after *M. xanthus* of WT UTI89 (Fig. 4.7). No reactive band could be detected in a *M. xanthus* only control or from the UTI89 *csgBA bcsA* mutant (Fig. 4.7). Even though curli remained SDS-insoluble, WT rugose biofilms exposed to *M. xanthus* were fragile and broke into pieces upon buffer washing (Fig. 4.8). Interestingly, after *M. xanthus* killing, the *csgBA* colony remained intact upon washing with buffer (Fig. 4.8). Therefore it is unlikely that *M. xanthus* degrades the cellulose matrix. Tissue homogenization was required to break up both WT UTI89 biofilms and the *csgBA* colony. Both the *bcsA* and the *csgBA bcsA* colony went into suspension freely (data not shown).

Susceptibility of Two Biofilm Populations to *M. xanthus*

Since M. xanthus required prey contact for efficient killing (41, 42, 58), matrix production could prevent killing by *M. xanthus* by blocking efficient prey recognition. Such a mechanism of protection could leave matrix-free, washout bacteria susceptible to *M. xanthus* killing. I therefore performed the washout assay on WT UTI89 after 10 days of coincubation with *M. xanthus*. As with the nematode predation assay, matrix fraction cells demonstrated a robust survival phenotype compared to washout bacteria (Fig. 4.6C).

Growth and Matrix Expression of Enteric Bacteria in Non-Host Environment-Mimicking Conditions

Nematodes and Myxobacteria are both ubiquitous soil predators (43, 54). Enterobacteriacea such as *E. coli* would likely be exposed to such predators after excretion from the host. Common lab media such as LB typically inhibit curli expression (59) (Fig. 4.9). However, if biofilm formation by *E. coli* provides predation resistance in non-host environments, I hypothesized that non-host environmental conditions would induce matrix expression. Pathogenic *E. coli* can be shed in the dung of farm animals, and such fecal contamination can lead to human infection (7-10, 60). To test if animal dung provides the correct nutritional environment for biofilm formation, I collected pig dung from a local farm, filter-sterilized it, and used it as the sole nutrient source in agar plates. I monitored growth and curli production on dung agar plates of UTI89 as well as

two other pathogenic members of the *Enterobacteriaceae* family, *S. enterica* ser. Typhimurium and *Citrobacter koseri*, both of which produce curli and cellulose and form rugose biofilms (28). Both *S. enterica* ser. Typhimurium and UTI89 formed rugose colonies on pig dung agar plates, and no such colony structure was apparent in the UTI89 *csgBA bcsA* mutant (Fig. 4.10A). Western blot analysis of the major curli subunit CsgA demonstrated that UTI89, *S. enterica* ser. Typhimurium, and *C. koseri* produced curli on pig dung agar plates (Fig. 4.10B). As expected no CsgA was detectable in the UTI89 *csgBA bcsA* mutant (Fig. 4.10B). Curli production and rugose formation were enhanced at 26°C compared to 37°C (Fig. 4.10A,B), which agrees with previous findings (61). To further test the ability of dung to support biofilm formation, I isolated two *E. coli* strains from pig dung. When these isolates were plated on pig dung agar plates, they also produced CsgA (Fig. 4.10B). Cow dung was also tested for its ability to support biofilm formation. Although growth was very limited on cow dung agar plates, rugose biofilm formation was apparent in UTI89 and *S. enterica* ser. Typhimurium at 26°C (Fig. 4.11).

CsgD-mediated biofilm formation increases EHEC attachment to spinach and abiotic surfaces (31, 32). I next tested whether extracts from commonly contaminated foods provided the nutritional environment to support matrix production. UTI89, *C. koseri*, and both pig dung *E. coli* isolates produced curli on beef, chicken, and spinach agar plates (Fig. 4.12A,B,C). Curli was detected from *S. enterica* ser. Typhimurium on chicken agar plates (Fig. 4.12B). On all three food plates, incubation at 26°C supported more curli production than growth at 37°C (61) (Fig. 4.12A,B,C). UTI89 and *C. koseri* produced rugose biofilms on beef plates (Fig. 4.13). Intriguingly, both pig dung *E. coli* isolates produced CsgA on all three food plates (Fig. 4.12A,B,C).

The use of untreated manure to fertilize produce can lead to EHEC contamination of food (7, 62, 63). Furthermore, contact with animal feces is a risk factor for spontaneous EHEC infections (11). I therefore tested growth and curli production of two EHEC O157:H7 strains, EDL933 and 86-24, on dung and food agar plates. Intriguingly, EDL933 produced curli on all media tested, while 86-24 produced curli on pig dung and spinach plates (Fig. 4.14). Also of note is that both EHEC strains showed growth defects on spinach plates at 37°C, but grew well at 26°C (Fig. 4.14).

Altogether, my results demonstrated that curli and cellulose production protected *E. coli* against predation and that biofilm formation was induced by *E. coli* and other pathogenic *Enterobacteriaceae* in non-host environments.

Discussion:

Various bacterial species utilize biofilms to survive the non-host environment. Rugose biofilm formation by *V. cholerae* involves synthesis of extracellular polysaccharides and protects the bacteria against flagellate predation, chlorinated water, and osmotic and oxidative stress (64-67). *P. aeruginosa* biofilms formation can likewise protect against amoebae feeding (34, 35). *Y. pestis*, *S. epidermidis*, and *M. xanthus* utilize biofilms to either inhibit feeding or digestion by *C. elegans* (37-39). Finally, CsgD-mediated biofilms protect *S. enterica* ser. Typhimurium against various non-host stresses such as desiccation and disinfectants (27, 29).

While *E. coli* is one of the most studied organisms on Earth, disproportionately little is understood about the physiology of *E. coli*, or indeed any members of the *Enterobacteriaceae*, in non-host environment reservoirs besides the laboratory. Here I present evidence in support of a model where CsgD-mediated biofilm formation is in part an adaptation to the non-host branch of the *E. coli* lifecycle. A variety of organisms, including nematodes and predatory bacteria such as *M. xanthus* consume bacterial prey in the non-host environment. I hypothesized that the extracellular matrix produced during biofilm formation would serve as a physical barrier to predation. As my model *E. coli* strain, I chose the UPEC isolate UTI89. UTI89 provides the benefits of being genetically tractable as well as being a relatively recent clinical isolate. Repeated culturing of bacterial strains introduces selective pressure to genetically suppress biofilm production (68, 69), and indeed *E. coli* K12 strains have lost the ability to produce one of the two major matrix components, cellulose (50). In contrast, WT UTI89 is able to produce both curli and cellulose and form robust rugose biofilms (28). Moreover, a transmission route for ExPEC strains such as UTI89 is likely through contaminated foods (16, 60), making their survival in the non-host environment relevant as a public health concern.

Nematodes such as *C. elegans* graze on bacterial prey, and intake cells by contraction of the pharynx (40). I hypothesized that the dense matrix present in *E. coli* biofilms would inhibit efficient nematode feeding. Indeed, my results demonstrated that biofilm formation provided a robust survival advantage to UTI89 when exposed to *C. elegans*. After 15 days of predation, WT matrix production increased survival by roughly 300 fold compared to a matrix deficient mutant. Interestingly, deletions of the individual matrix genes revealed that cellulose is the more important component, as the cellulose mutant only had a slight increase in fitness over a curli and cellulose double mutant. SEM studies of *E. coli* colony and pellicle biofilms have revealed that cellulose forms sheet-like structures throughout the colony, while curli surrounds individual cells in an "egg-in-a-carton" arrangement (48-50). Curli production on its own imbues colony biofilms with a rigid architecture, while cellulose-only biofilms demonstrate increased elasticity (50). The size and movement of *C. elegans* likely applies substantial mechanical stress to the biofilm matrix. Therefore the cohesive properties of cellulose might provide increased resistance compared to a more brittle biofilms formed by curli. Indeed, the *csgBA* mutant maintained a cohesive biomass even after nematode feeding, while the *bcsA* mutant was more easily dispersed (Fig. 1.1B).

Curli and cellulose provide a dense coating for cells within rugose biofilms (48, 50, 70). I hypothesized that such an arrangement would physically protect the cells within the biofilm from *C. elegans*. However, there is precedence for matrix production altering the feeding behavior of *C. elegans* (44), so I designed a tracking assay to test whether *C. elegans* is preferentially attracted to matrix-free colonies. My results demonstrated that both matrix-encased and non-matrix encased bacteria attracted similar numbers of worms at early time points, indicating that matrix primarily acts as a physical barrier against nematode predation. Given that rugose biofilms contain non-matrix-encased bacteria, my results do not conclusively demonstrate that matrix production has no affect on nematode behavior. The main conclusion I take from the tracking assay is that there is not enough of an attraction difference between WT and the matrix mutant to explain the dramatic survival difference.

While *C. elegans* mechanically swallows prey bacteria, predators such as *M. xanthus* secrete antibacterial and lytic agents to kill their prey extracellularly (53).

However, as *M. xanthus* killing requires direct predator-prey contact (41, 42), I hypothesized that an extracellular matrix would protect *E. coli* in a *Myxococcus* killing assay. I demonstrated that biofilm formation also confers a robust survival phenotype to UTI89 after *M. xanthus* predation. Biofilm-mediated antibiotic protection is largely due to a subpopulation of persister cells (46). Rugose biofilm formation could potentially develop concurrently with the formation of a population of persisters. However, my data would also imply that persister formation was almost completely dependent on the extracellular matrix, as a *csgBA bcsA* mutant demonstrated a dramatically reduced survival phenotype. A more likely scenario is that matrix production impedes prey-recognition by *M. xanthus*. Indeed direct contact is required for optimal *M. xanthus* killing, and prey density affects *M. xanthus* predation efficiency (41, 42, 58). Intriguingly, in contrast to nematode killing, curli was more important than cellulose in preventing *M. xanthus* killing. The comparatively small size of *M. xanthus* may allow them to intercalate into the *E. coli* biofilm matrix. However, individual *M. xanthus* cells need to contact prey bacteria to lyse them (41). Therefore the dense curli matrix that surrounds individual cells could provide greater protection than the more diffuse cellulose filaments (48, 50). It is unlikely that *M. xanthus* is able to degrade the cellulose matrix as the *csgBA* colony still maintains its cohesion even after *M. xanthus* predation (Fig. 4.8).

Bimodal population development within rugose biofilms provides a simple model for analyzing cellular differentiation in biofilm communities. The matrix-associated fraction is easily separable from the interior, washout bacteria. Moreover, I have previously demonstrated that the two populations demonstrate differences in stress resistance, as the washout cells are more vulnerable to hydrogen peroxide killing (28). In light of my results showing that matrix production protected *E. coli* against predation, I hypothesized that washout cells would also be more susceptible to killing by both *C. elegans* and *M. xanthus* than their matrix-encased neighbors. As expected, the interior, loosely attached washout bacteria were more susceptible to feeding. The increased susceptibility of the interior, non-matrix-encased fraction of rugose colonies to oxidative stress as well as predation raises the question of the functional role of this population (28). An intriguing possibility is that washout bacteria serve as an easily disseminated population of the biofilm. Indeed, even gently rocking with liquid releases washout cells

from the biofilm community (28). A pair of elegant SEM studies has recently demonstrated that the interior, non-surface-exposed, bacteria of W3110 *E. coli* rugose biofilms produce flagella as an integral component of the biofilm matrix (49, 50). I have previously demonstrated that curli producing cells are limited to the air-interface of UTI89 rugose colonies (28). Such a structural division of labor, with matrix-encased bacteria lining the air-biofilm interface while covering a non-matrix-encased, flagellated population is also observed in UTI89 pellicle biofilms (48). Intriguingly, *Pseudomonas aeruginosa* mushroom biofilms also produce a similar architecture, with polysaccharide production being limited to the biofilm exterior. Flagellated *P. aeruginosa* that lines the biofilm interior are considered to be the chief agents of biofilm dispersal (71). It seems then that the formation of a protective outer coating, surrounding an interior population of easily dispersed cells, is a common biofilm architecture in a variety of bacterial species.

CsgD is under complex transcriptional control, but in general, environments that present low salts, low temperatures (<30°C), and an air-interface allow for maximal *csgD* transcription (28, 48-50, 72). I hypothesized that habitats such as dung, where *E. coli* could encounter nematode and Myxobacteria predators, would provide the nutritional environment for matrix production. Pathogenic *Enterobacteriaceae* can reside in the gut of cattle and pigs (7-10) and, after being shed in feces, can contaminate food products, particularly if untreated feces is used as manure (7, 11, 62, 63). Indeed, EHEC O157:H7 can survive in dung for months, and survival is generally increased when temperatures are <23°C (73). In this study I directly tested pig dung along with commonly contaminated foods for their ability to induce enteric biofilm formation. Intriguingly, pig dung supported rugose biofilm formation by both UTI89 and *S. enterica* ser. Typhimurium. Moreover, all strains tested produced CsgA when grown on pig dung plates. Beef, chicken, and spinach provided the correct nutritional environment for biofilm production by all tested *E. coli* strains and by *C. koseri*. Curli production was significantly higher at 26°C compared to 37°C, which agrees with previous data (61). Altogether my data support a model where *E. coli* and other *Enterobacteriaceae* produce a CsgD-dependent biofilm in environmental conditions commonly encountered outside the host. Biofilm-development involves formation of a stress-resistant, matrix-

producing population along with an easily dispersed, but stress-susceptible interior population.

Materials and Methods:

Organisms, Media, and Growth Conditions:

All *Enterobacteriaceae* strains used in this study were routinely passaged at 37°C in LB media. All UTI89 strains as well as *S. enterica* ser. Typhimurium and *C. koseri* have been previously described (28). EHEC O157:H7 86-24 and EDL933 were kind gifts from Dr. Kathryn Eaton. *M. xanthus* DK1622 was a kind gift from Lawrence Shimkets, and was routinely grown at 30°C on Casitone Yeast Extract (CYE) media (10 mM morpholinepropanesulfonic acid (MOPS) pH 7.6, 10 g/liter Casitone, 5 g/liter yeast extract, and 8 mM $MgSO_4$) in shaking cultures or on 1.5% agar plates. *C. elegans* wild-type strain Bristol N2 worms were routinely grown on OP50 *E. coli* on Nematode Growth Media (NGM) agar plates (3 g/liter NaCl, 2.5 g/liter peptone, 17 g/liter agar, supplemented with 25 mL of 1 M KPO_4 (pH 6.0) and 1 mL each of 1 M $CaCl_2$, 1 M $MgSO_4$, and 5 mg/mL cholesterol in EtOH) at room temperature. Grass-fed cow dung and pig dung was obtained from a local farm. Ground beef, chicken breasts, and spinach were purchased from a local grocery store. Dung and food products were ground up in a blender, and extracts were centrifuged in 50 mL conical tubes for 10 minutes at 7500 RPM. Supernatants were filter sterilized using a 0.5 µm filter followed by a 0.2 µm filter. Fecal extract was diluted 1:3 into water that had been autoclaved with 1.5% noble agar, while food extracts were diluted 1:10. After brief stirring, plates were poured. All pictures were taken using an Olympus DP72® camera mounted on an Olympus SZX16® research stereomicroscope. Pig dung *E. coli* isolates were selected for by streaking pig dung on MacConkey agar plates. Pink colonies were resetreaked and candidates were verified as *E. coli* by sequencing of the 16s gene. In all, two *E. coli* strains were isolated.

C. elegans predation assay:

WT UTI89 and *csgBA*, *bcsA*, and *csgBA bcsA* mutants were grown in LB broth overnight, diluted to 1 OD_{600} in Yeast Extract Casamino Acids (YESCA) media (10 g/liter casamino acids, 1 g/liter yeast extract), and 2 µL dots were spotted at the cardinal

direction points of 2% agar YESCA plates supplemented with 5 ug/mL cholesterol. The plates were then incubated at 26°C for 48 hours. 20-30 L1-L2 stage *C. elegans* worms grown on OP50 were then transferred into the center of the *C. elegans* plus plates, while no worms were added to the *C. elegans* minus plates (designated day 0). At day 0 and at 3 day intervals thereafter, three plates with worms and three plates without worms were harvested. Briefly, chunks of agar containing each colony were cut out from the agar plate. Agar slabs containing a whole colony were placed in a well of a 24-well polypropylene plate. 1 mL of kPi buffer was then added to each well, and the plate was shaken until all cells had gone into suspension or the biofilm had lifted off the agar surface. For WT and the *csgBA* and *bcsA* mutants, the entire sample, including biofilm chunks and the kPi that had been added to the well was moved into an eppendorf tube. These samples were tissue homogenized for 15 seconds on high speed. The *csgBA bcsA* mutant went into suspension without homogenization. Suspensions were serially diluted in kPi, and then 100 µL of an appropriate dilution was plated on an LB plate and grown ON at 37°C for CFU quantitation. Each plate with *C. elegans* was randomly paired with a plate without *C. elegans*, and percent survival was calculated as CFUs from the plate with *C. elegans*/CFUs from the plate without *C. elegans*. All data points are averages of biological triplicates, and error bars represent standard deviation. A student's T-test was employed to compare between strains, and asterisks represent $P<.05$. For non-competition assays, WT UTI89 and a csgD mutant were spotted on separate plates (six dots per plate). At day 0 and at three day intervals afterwards, one spot per plate was harvested for CFU counts. All data points are averages of biological triplicates, and error bars represent standard deviation.

C. elegans tracking assay:

2 µL of one WT UTI89 dot and one UTI89 *csgBA bcsA* dot were spotted on either end of a YESCA + 5 ug/mL cholesterol 2% agar plate. The plate was then incubated at 26°C for 48 hours to allow biofilm development. *C. elegans myo-2::rfp ceh22::gfp* was grown on OP50 NGM plates at room temp. A small chunk of agar containing worms from all growth stages was moved from the NGM plate to the center of each UTI89 plate. At 1, 6, and 24 hour intervals, images were taken on an Olympus DP72® camera mounted on an Olympus SZX16® research stereomicroscope using brightfield or a texas red

filter. Worms were visible as red lines under the texas red filter. All worms within the image frame of each colony picture were counted for that particular strain. The percent of worms present on each colony was calculated (with the total number being the amount of worms on the WT colony + the number of worms on the *csgBA bcsA* colony for a particular plate). Worm totals for each plate at each time point fell between 200-1200. A student's T-test was employed to compare between strains, and asterisks represent P<.05.

M. xanthus predation assays:

M. xanthus predation assays were performed on YESCA MOPS media. To support UTI89 rugose biofilm development and *M. xanthus* growth, YESCA media was buffered to pH 7.4 with 10 mM MOPS. After autoclaving with 1.5% agar, 1 mL of media was added to each well of a 24-well plate. Plates were allowed to dry for 2-3 days at room temperature. 2 µL dots of UTI89 and *M. xanthus* were spotted roughly .5 cm apart in a single well. UTI89 was grown ON at 37°C in LB and *M. xanthus* was grown for 48 hours at 30°C in CYE in shaking cultures prior to dotting, and each strain was normalized to an OD_{600} of 1. After dotting, plates were incubated for two days at 26°C to allow for biofilm formation by UTI89 and for *M. xanthus* growth. Plates were moved into a humidity chamber at 30°C to allow *M. xanthus* predation (designated day 0). Pictures were taken every 2 days. For CFU counts at day 10, contents of each well were suspended in 1 mL kPi. WT UTI89, as well as *csgBA* and *bcsA* mutants, were tissue homogenized in eppendorf tubes along with the buffer that had been added to each well. The *csgBA bcsA* double mutants went into suspension without homogenization. Suspensions were serially diluted on LB agar plates, which do not support Myxobacterial growth (74), and *E. coli* CFUs were determined. As with *C. elegans* predation assays, each well with *M. xanthus* was randomly paired with a well without *M. xanthus*, and percent survival was calculated as CFUs from the well with *M. xanthus* /CFUs from the well without *M. xanthus*. All data points are averages of biological triplicates, and error bars represent standard deviation. A student's T-test was employed to compare between strains, and asterisks represent P<.05.

Washout Assay:

The washout assay was performed as previously described (28). Briefly, agar chunks including the colony of interest were cut out and moved into the well of a 24-well plate. The colony was flooded with 1 mL of kPi and shaken gently. For older colonies (>48 hours), buffer was pipetted gently onto the edge of the colony to facilitate colony lift-off. The original 1 mL kPi was removed from each well, added to an eppendorf tube, and spun down for 1 min at 12,000 rpm. The supernatant was then aspirated off. An additional 1 mL kPi was added to each well and was shaken gently for 5 minutes to remove any residual washout cells from the matrix fraction. The matrix fraction was removed with a pipette tip into a new eppendorf tube with 1 mL of kPi. The remaining kPi in each well was used to resuspend the original washout pellet. Matrix fractions were tissue homogenized at high speed for 15 seconds. For CFU counts, each fraction was then serially diluted and an appropriate dilution was plated. For *M. xanthus* washout assays, 1 mL of kPi was added to the top of each UTI89 strain that had been preyed upon by *M. xanthus*. The plate was gently shaken and kPi was pipetted around the edges of the WT colonies to facilitate colony liftoff. Biofilms that had been fed on by *C. elegans* or *M. xanthus* broke into chunks when suspended in buffer. These chunks were allowed to settle and buffer was removed from the top of the well. Biofilm chunks were suspended and shaken in two additional 1 mL kPi washes. All three washes were collected as the washout fraction, and biofilm chunks were tissue homogenized after washing to free matrix cells.

Western Blot Analysis:

Western blotting for the major curli subunit CsgA was performed as previously described (28) with minor changes. Briefly 150 µL of a 1 OD_{600} suspension of each respective strain/fraction was spun down at 12,000 rpm for 1 minute. Pellets were resuspended in 150 µL of hexafluoroisopropanol (HFIP), incubated at room temperature for 10 minutes, and then HFIP was removed using a Thermo Savant SPD SpeedVac. Samples were resuspended in 150 µL of 2x SDS running buffer, boiled for 10 minutes, and electrophoresed in 15% polyacrylamide gels. HFIP-minus samples were directly suspended in 150 µL of 2x SDS running buffer. For CsgA blots, samples were then transferred onto polyvinylidene difluoride membranes using standard techniques. Blots

were blocked with 5% milk in TBST ON at 4°C, followed by incubation with 1:8500 anti-CsgA peptide antibody for 1 hour at room temperature. After TBST washes, blots were then incubated with 1:15000 LI-COR IRDYE® 800CW Goat Anti-Rabbit IgG secondary antibody. For blots that also include σ70 probing, samples were transferred onto nitrocellulose membranes in a wet transfer apparatus in 25 mM CAPS transfer buffer pH 11.2 with 10% methanol. After transfer, the blot was blocked in 5% milk in TBST for one hour at room temperature. CsgA probing was performed the same, and blots were also incubated with 1:5000 Santa Cruz RNA pol σ D antibody primary antibody (1:5000) for 1 hour at room temperature, followed by incubation with 1:15000 LI-COR IRDYE® 700CW Goat Anti-Mouse IgG secondary antibody. Blots were washed with TBST and visualized on a Licor Odyssey CLX imager.

Figures:

Figure 4.1 Biofilm formation protects *E. coli* against *C. elegans* predation
WT UTI89 or matrix mutants were grown on the same YESCA agar plates + cholesterol for two days to allow biofilm development. ~25 L1-L2 *C. elegans* worms were then added to the center of each agar plate (Day 0). At three day intervals, plates to which worms had been added and worm-free control plates were harvested for CFU counts. *C. elegans* minus plates were randomly paired with *C. elegans* plus plates, and percent survival was calculated as CFUs on the plus *C. elegans* plate divided by CFUs on the minus *C. elegans* plate for each particular strain **(A)**. An image was taken of each strain at each time point from a representative plus *C. elegans* plate that was harvested at day 15 **(B).**

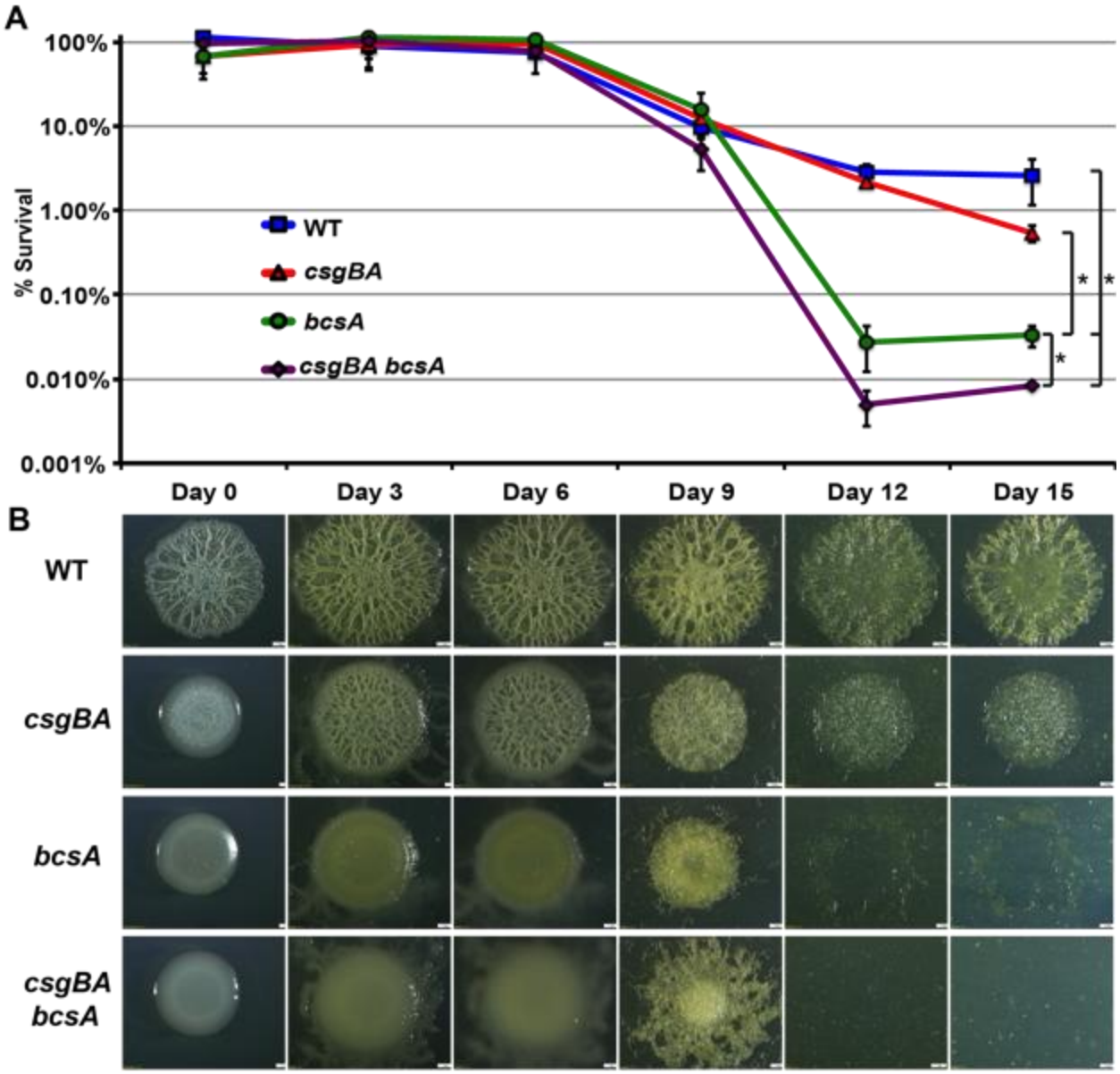

Figure 4.2 Non-competition assay demonstrates that WT UTI89 is more resistant to *C. elegans* predation than a *csgD* mutant
WT UTI89 or a *csgD* mutants were grown on separate YESCA agar plates + cholesterol for two days to allow biofilm development. ~25 L1-L2 *C. elegans* worms were then added to the center of each agar plate (Day 0). At three day intervals, plates to which worms had been added and worm-free control plates were harvested for CFU counts. *C. elegans* minus plates were randomly paired with *C. elegans* plus plates, and percent survival was calculated as CFUs on the plus *C. elegans* plate divided by CFUs on the minus *C. elegans* plate for each particular strain.

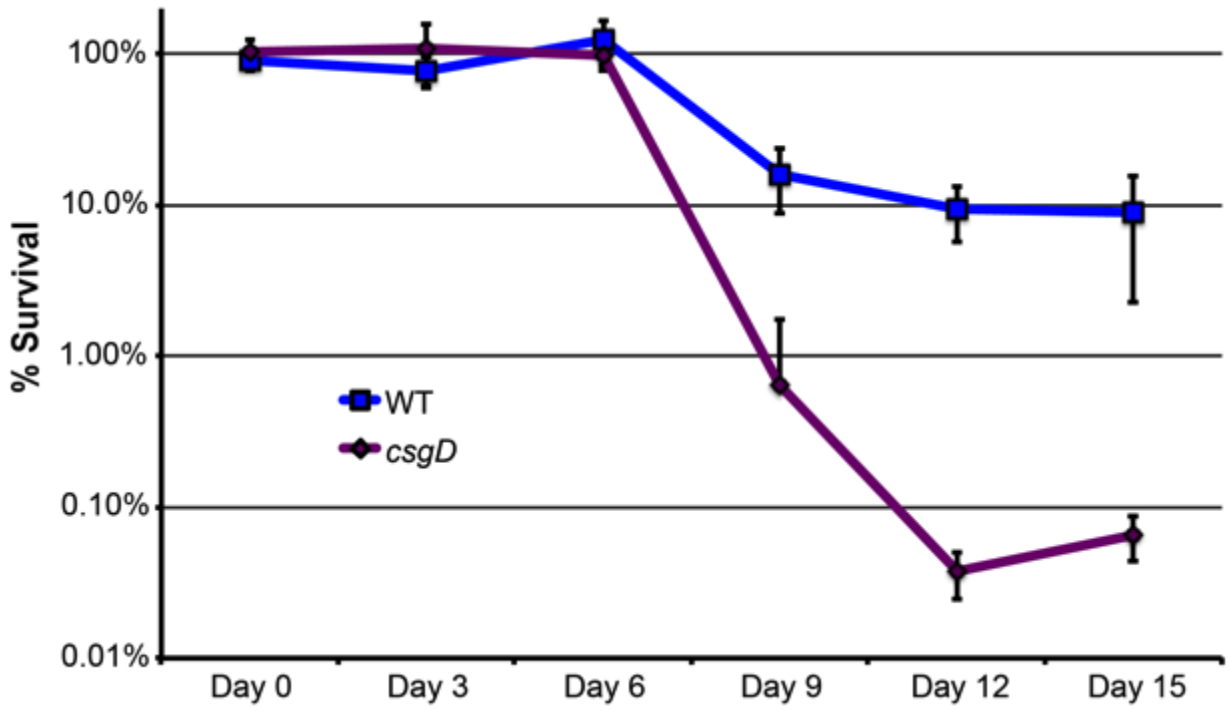

Figure 4.3 *C. elegans* is not preferentially attracted to WT or *csgBA bcsA* UTI89
WT UTI89 or a *csgBA bcsA* mutant were spotted on opposite sides of a YESCA + cholesterol agar plate. After two days of biofilm development at 26°C, *C. elegans myo-2::rfp ceh22::gfp* were moved onto the center of the plate by chunking **(A)**. **(B)** shows a brightfield/texas red overlay of WT or *csgBA bcsA* colonies with fluorescent worms after 6 hours of *C. elegans* exposure. At 1, 6, and 24 hours post-*C. elegans* addition, fluorescent images were taken and worms on each strain were counted **(C)**. Five individual plates were averaged, and bars represent the number of worms on each strain divided by the total number of worms counted on that particular plate. Error bars represent standard deviations.

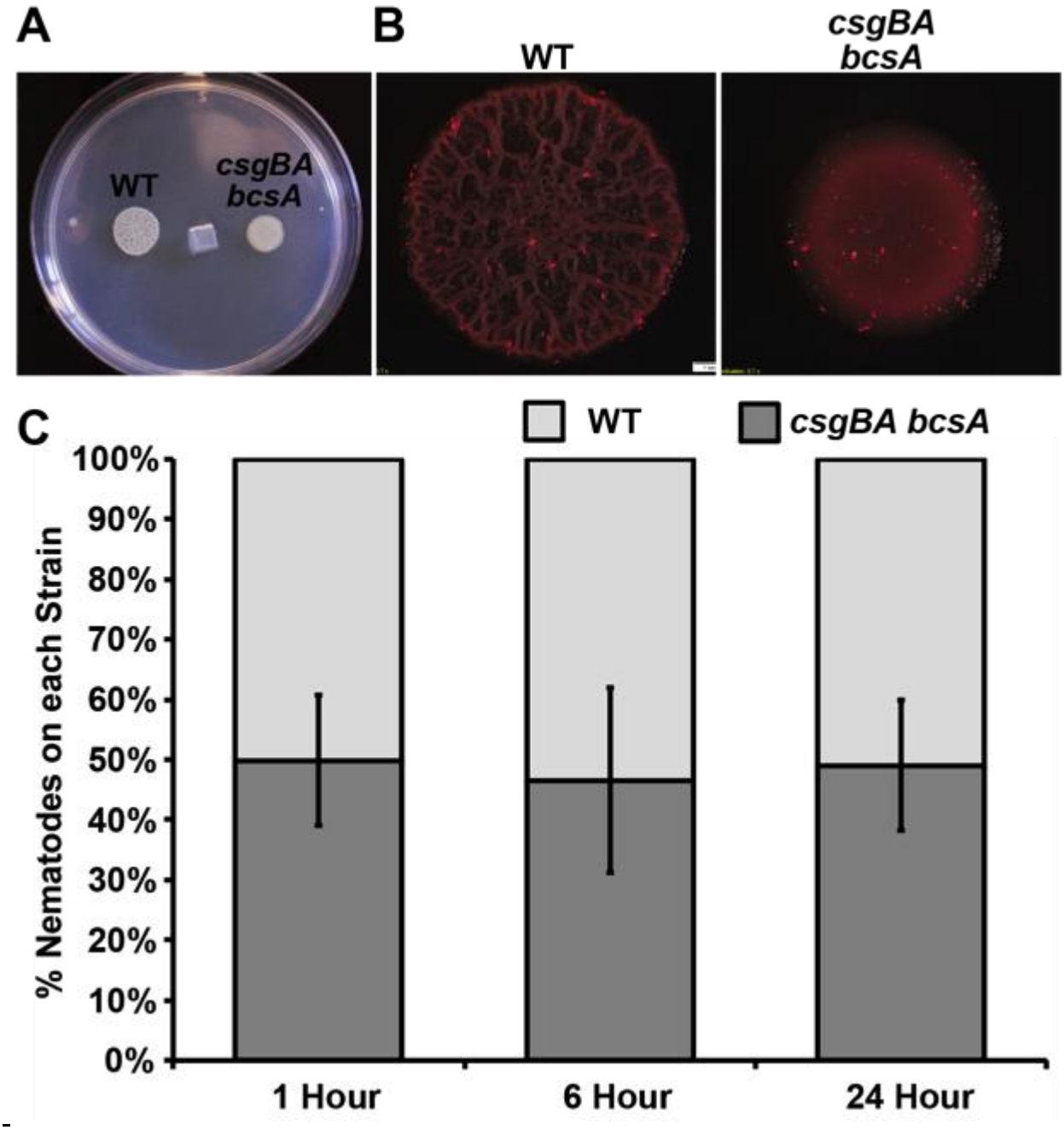

Figure 4.4 *C. elegans* feeding results in a fragile biofilm
After moving an agar chunk to a well of a 24-well plate, 1 mL of kPi buffer was added to a WT UTI89 rugose colony biofilm that had or had not been exposed to *C. elegans* for 12 days. *C. elegans* feeding resulted in a biofilm that was more fragile and that broke apart easily

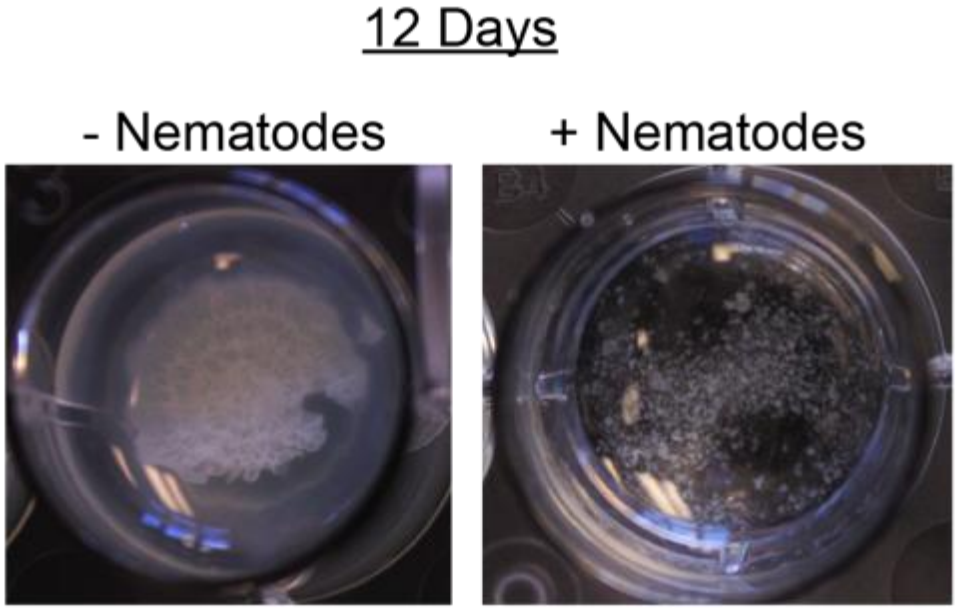

Figure 4.5 Washout cells are more susceptible to *C. elegans* predation than matrix cells

Three WT UTI89 dots were spotted on a YESCA + cholesterol plate. After two days of biofilm development, 20-30 L1-L2 *C. elegans* worms were moved to the center of the plate. Plates were incubated at 20°C, and at days 6 and 12, a dot was harvested and subjected to the washout assay. CFUs were counted for each fraction. The graph represents percent survival compared to a minus-*C. elegans* control plate for each respective fraction at each respective day **(A)**. Each bar represents an average of biological triplicates, and error bars represent standard deviation. Asterisks represent a P-value <0.05 using the Student's T-test. **(B)** shows a western blot probing for the major curli subunit CsgA. A control 2-day old colony demonstrates the prototypical bimodal population present in a rugose biofilm, which is maintained after 12 days of growth. Not enough cells could be harvested from the washout fraction at 12-days with nematode predation to allow for western blot analysis of that fraction. Sigma-70 represents a loading control.

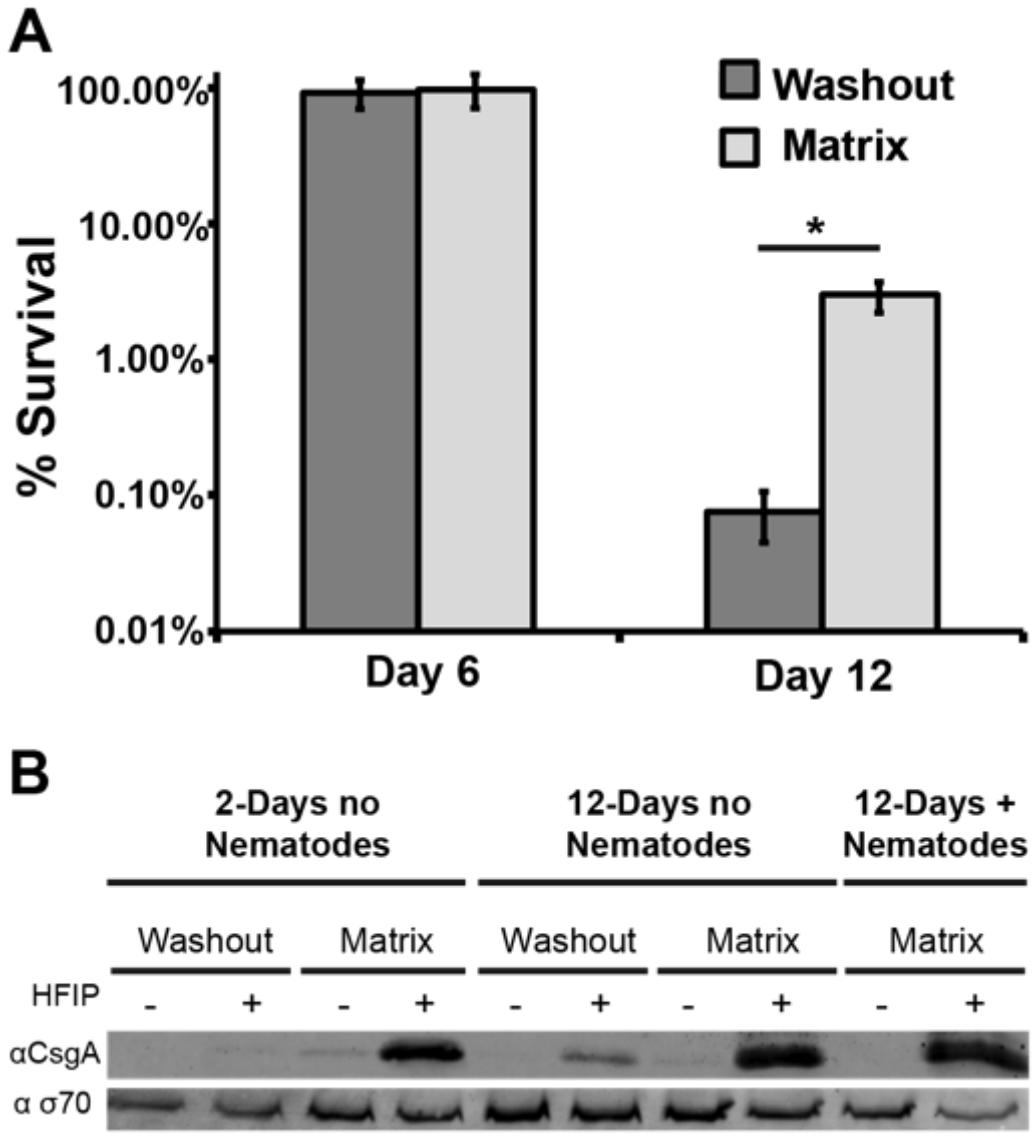

Figure 4.6 UTI89 biofilm formation protects against *M. xanthus* predation
2 µL dots of UTI89 and *M. xanthus* were dotted ~0.5 mm apart in an agar-filled well of a 24-well plate. After 2 days of biofilm development, plates were moved to humidity chambers in a 30°C incubator for *M. xanthus* predation. **(A)** shows pictures taken at 2 day intervals following *M. xanthus* feeding on WT UTI89 and UTI89 matrix mutants. After 10 days, CFUs were harvested from each UTI89 strain. **(B)** represents percent survival compared to *M. xanthus*-free UTI89 colonies. The washout assay was performed on WT UTI89 that had been preyed on by *M. xanthus* for 10 days. CFUs from both the washout and matrix fractions were determined, and percent survival compared to fractions from minus-*M. xanthus* UTI89 colonies subjected to the washout assay was calculated **(C).**

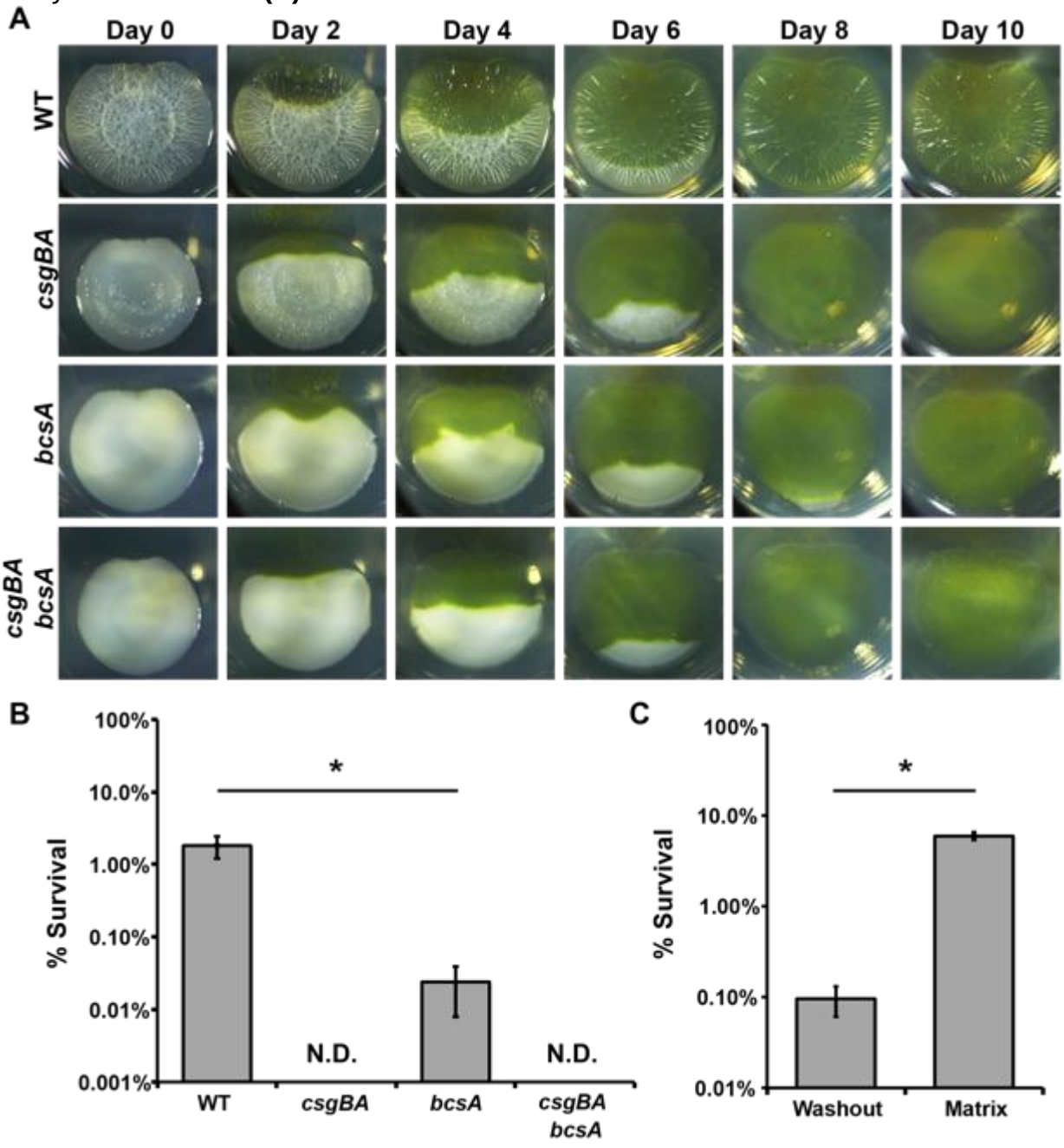

Figure 4.7 SDS-insoluble CsgA still present after *M. xanthus* predation
WT UTI89 was incubated at 30°C for 10 days with or without *M. xanthus* predation. Western blot analysis probing CsgA was performed with or without pre-treatment with HFIP. *M. xanthus* grown on its own and a UTI89 *csgBA bcsA* mutant serve as controls.

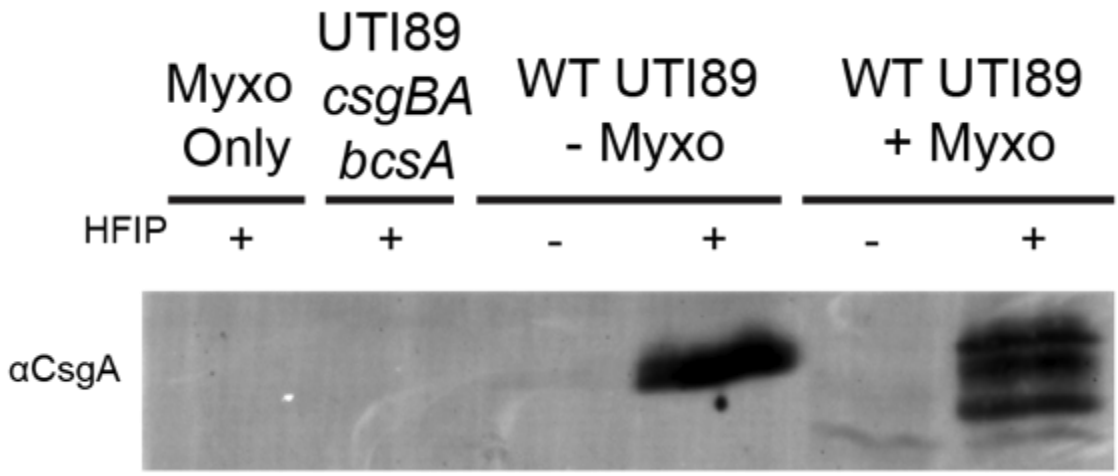

Figure 4.8 Biofilm fragility after *M. xanthus* predation
After *M. xanthus* feeding, 1 mL of kPi was added to WT UTI89 and the *csgBA* mutant. WT broke into large chunks upon agitation, and the *csgBA* colony maintained its shape even after washing off the agar.

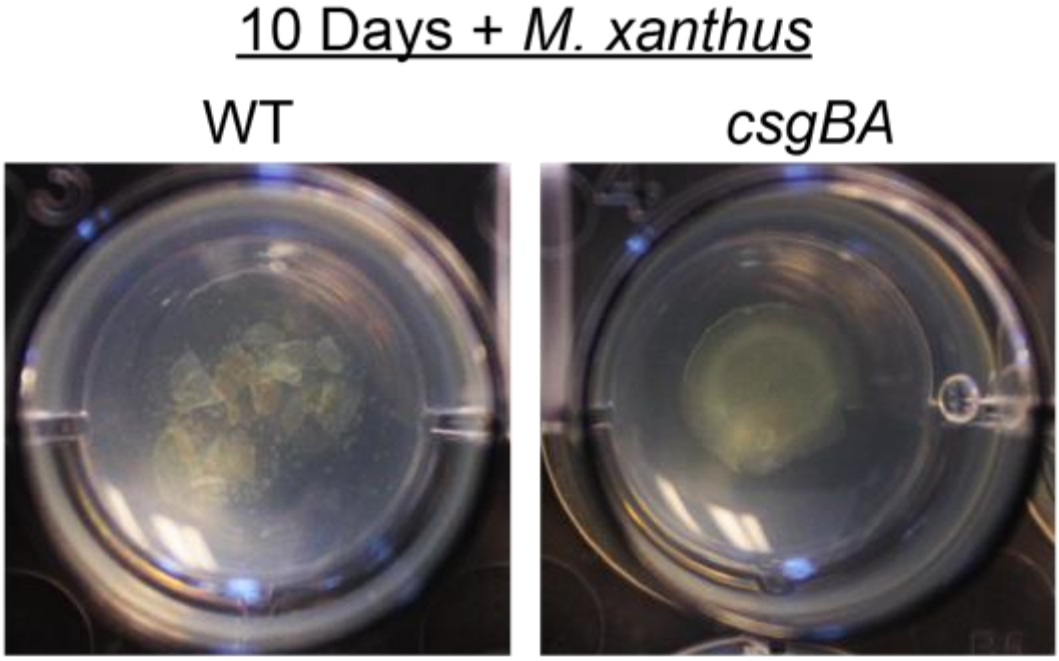

Figure 4.9 *Enterobacteriaceae* curli production on YESCA and LB plates
Western blot for the major curli subunit CsgA was performed on various *Enterobacteriaceae* strains grown on YESCA **(A)** or LB **(B)** agar plates for two days at 26°C or 37°C.

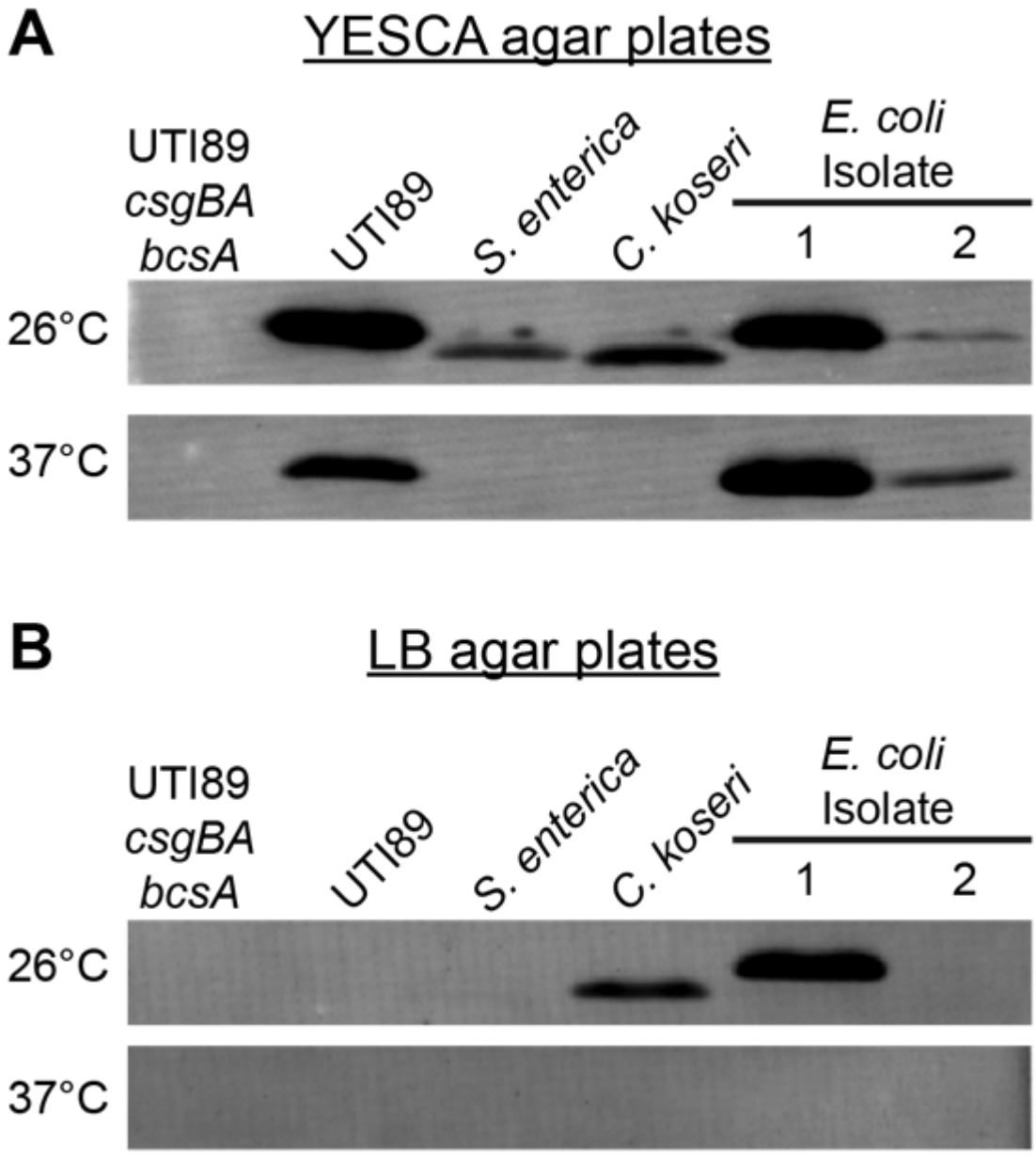

Figure 4.10 Growth and curli expression on pig dung agar plates
UTI89, *S. enterica* ser. Typhimurium, *C. koseri*, and two *E. coli* strains isolated from pig dung were grown on pig dung agar plates for two days at 26°C or 37° C. Rugose biofilm development was apparent by UTI89 and *S. enterica* ser. Typhimurium **(A)**. Western blot analysis for the major curli subunit CsgA revealed that pig dung plates allow robust curli production from all strains **(B)**. All western blot samples were treated with HFIP to depolymerize CsgA.

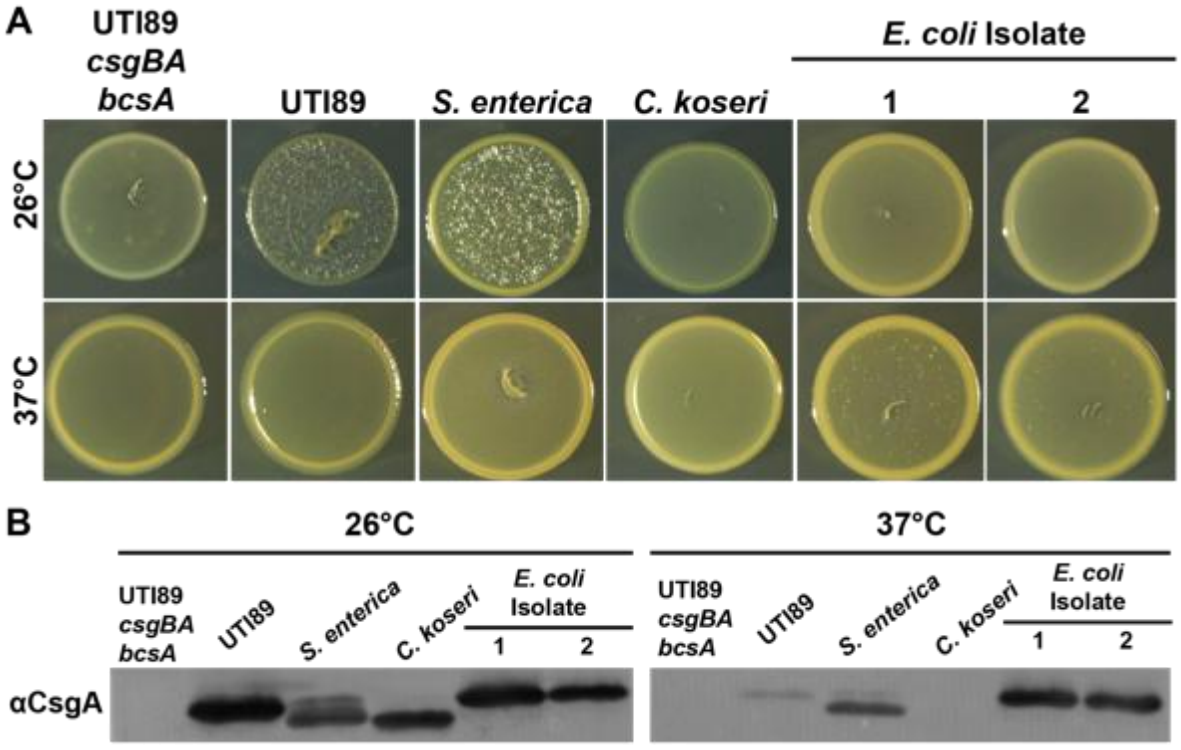

Figure 4.11 Growth on cow dung agar plates
UTI89, *S. enterica* ser. Typhimurium, *C. koseri*, and two *E. coli* strains isolated from pig dung were grown on cow dung agar plates for two days at 26°C or 37° C. Rugose biofilm development was apparent by UTI89 and *S. enterica* ser. Typhimurium.

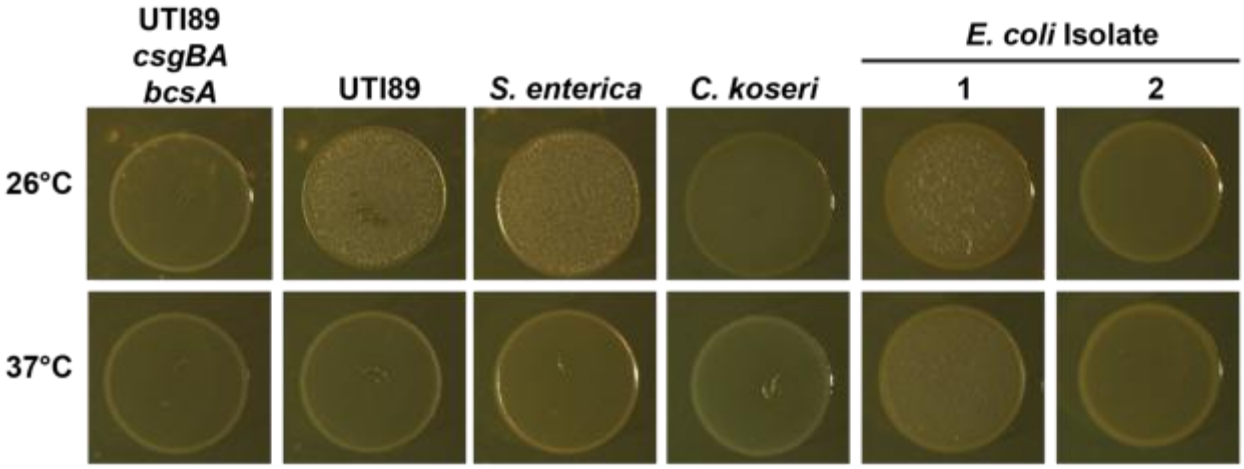

Figure 4.12 Curli production on food agar plates
After 2 days of growth at 26°C or 37°C on beef **(A)**, chicken **(B)**, spinach **(C)** agar plates, western blot analysis to probe for the major curli subunit CsgA was performed. All western blot samples were treated with HFIP to depolymerize CsgA.

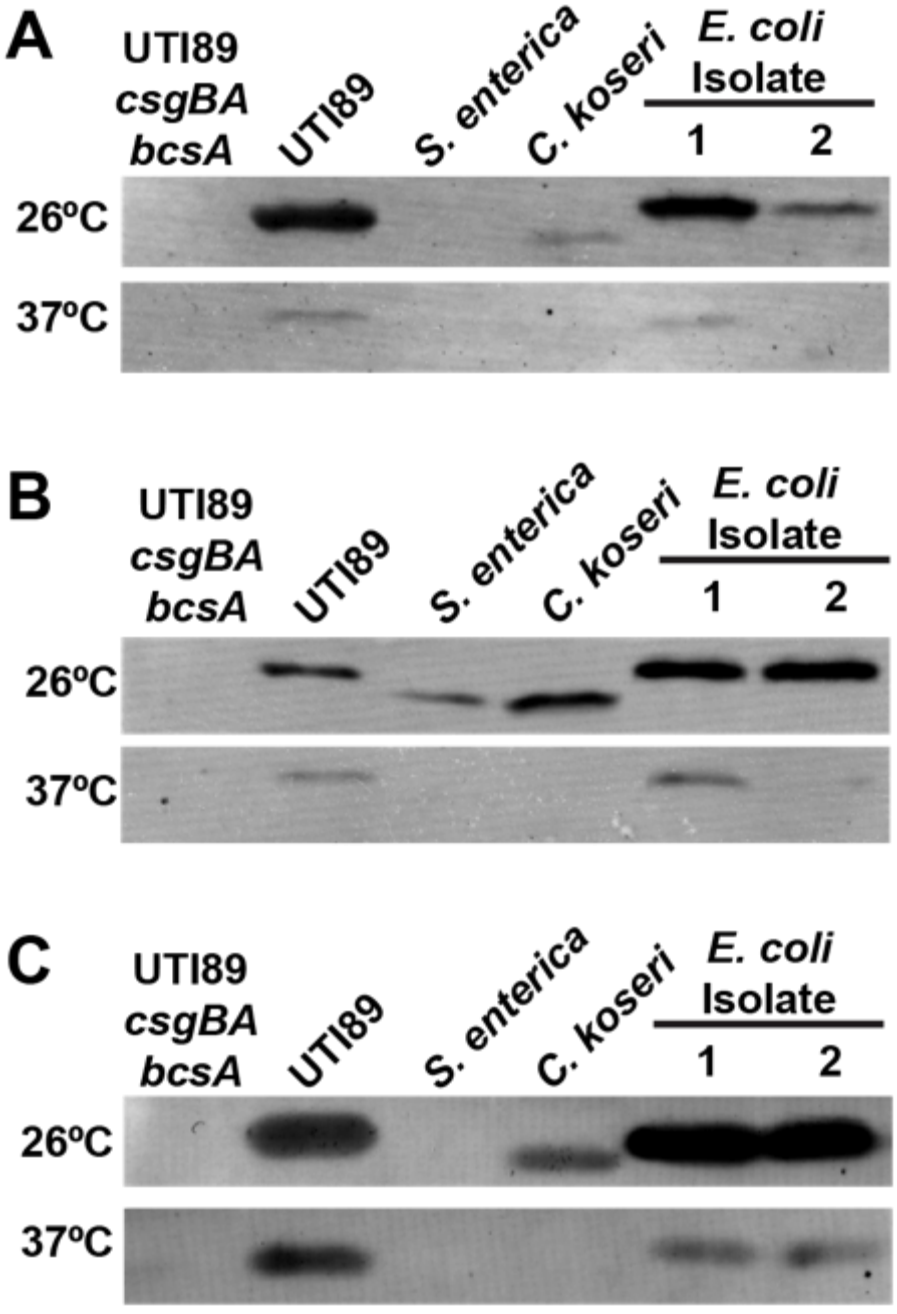

Figure 4.13 Growth and morphology on food agar plates
UTI89, *S. enterica* ser. Typhimurium, *C. koseri*, and two *E. coli* strains isolated from pig dung were grown on beef **(A)**, chicken **(B)**, or spinach **(C)** agar plates for two days at 26°C or 37° C.

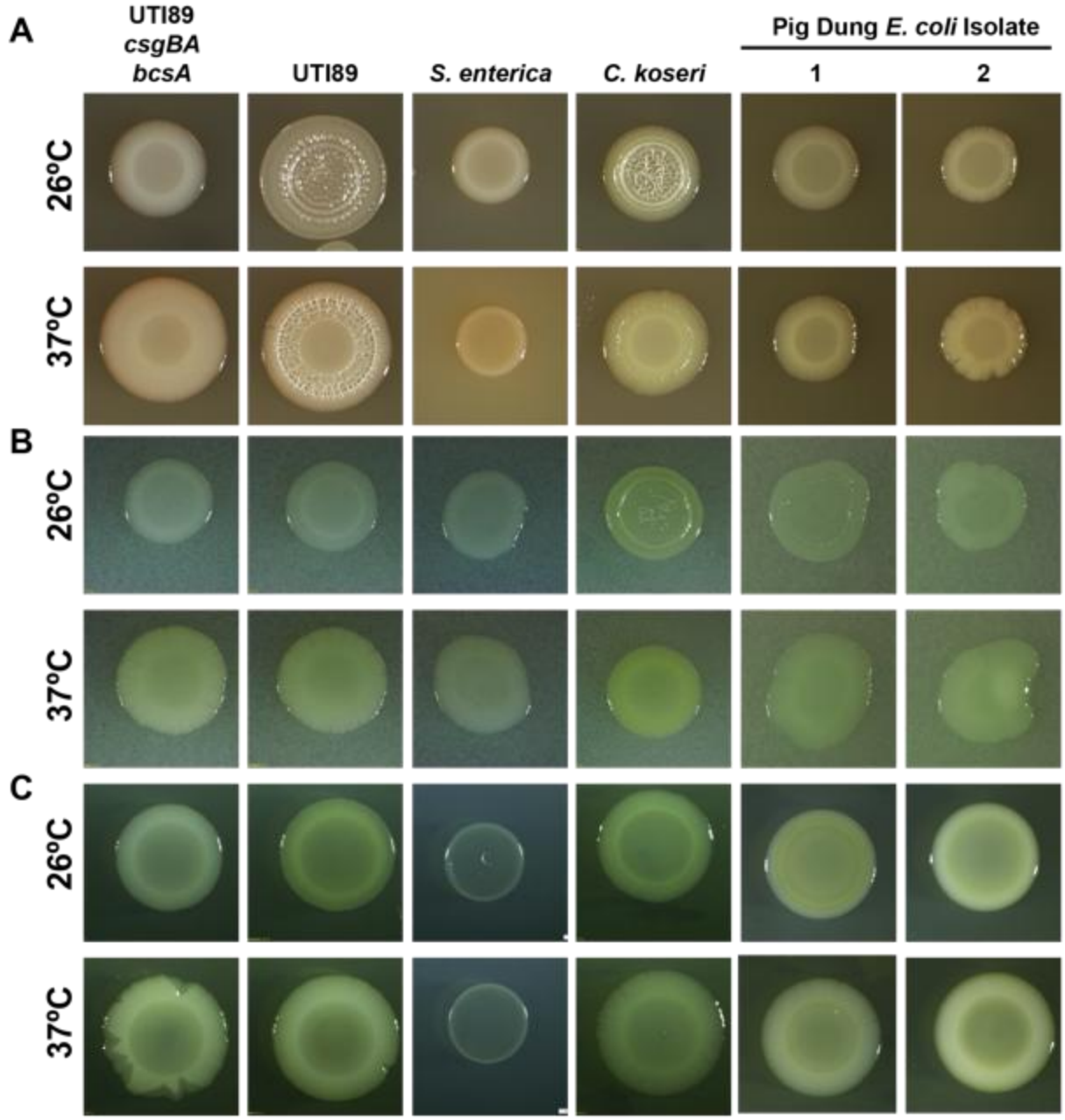

Figure 4.14 EHEC growth and curli production on dung and food plates
EHEC O157:H7 86-24 and EDL933 were grown on various agar plates at 26°C or 37°C. Pictures were taken after 48 hours of growth to monitor colony morphology **(A)**. Western blotting for the major curli subunit CsgA was performed after 48 hours of growth **(B)**.

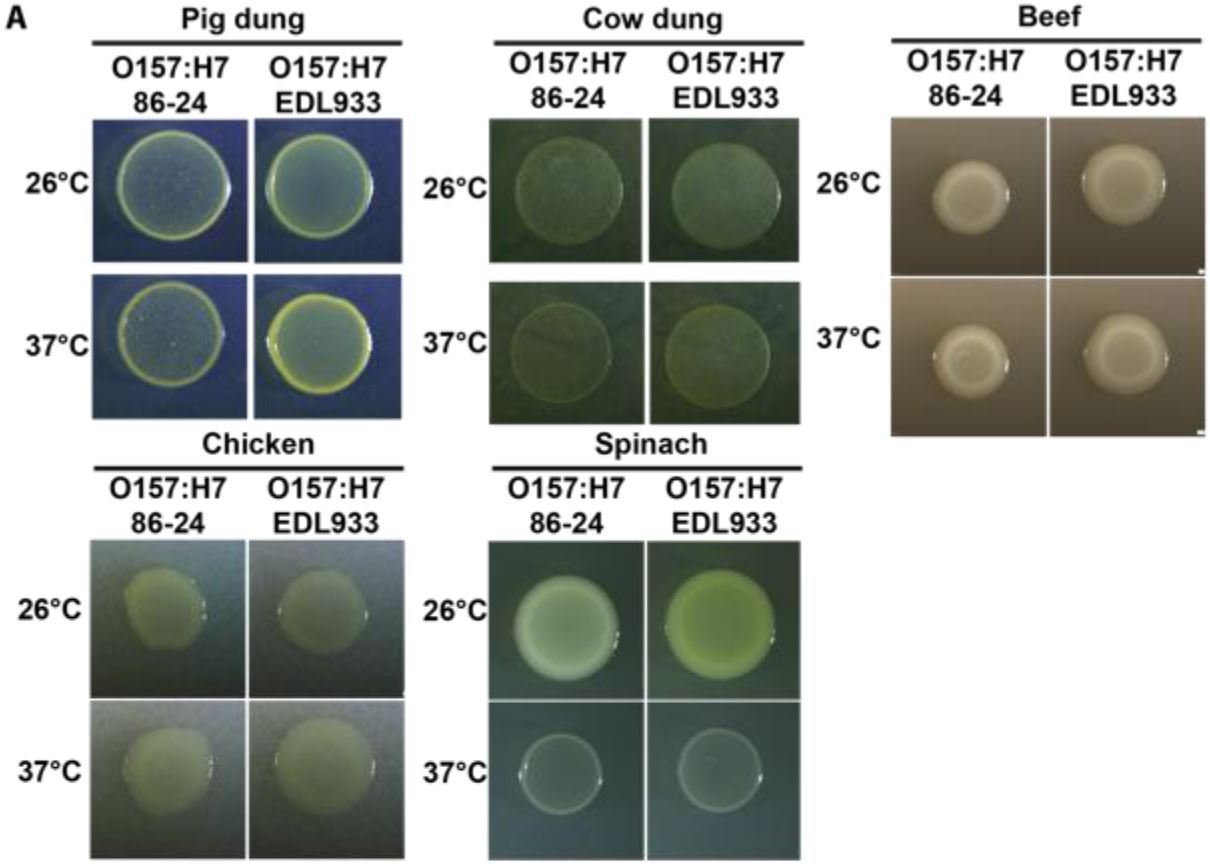

Notes and Acknowledgements:

I started the nematode predation project because I needed something for my undergraduate research assistant, David Warshaw, to do. At one point during lab meeting, Matt had suggested that maybe curli is hard to eat for nematodes, and testing that idea seemed like a good undergrad project. David and John Lee put a lot of time and effort into setting up the initial assays that gave us a great preliminary phenotype. Margarita Sifuentes was extremely helpful in teaching us basic nematode handling procedures and providing strains. After an interesting talk at a meeting, Maggie Evans suggested that I test whether biofilms also protected *E. coli* against *M. xanthus* predation. Another undergraduate research assistant, Vinay Saggar, developed media conditions that supported both UTI89 rugose biofilm development and *M. xanthus* growth and performed the initial *M. xanthus* predation assays. Through a failed attempt at getting *Staphylococcus aureus* to form rugose biofilms, Adnan Syed provided the inspiration for testing curli expression in non-host-mimicking conditions. Adnan put in a lot of work on the ecology side of the project. He was particularly helpful with regards to making food and dung agar plates and isolating bacterial strains from various sources and subsequently genotyping those strains. Adnan also connected me with EMMA Acres farm, from which we acquired cow and pig dung. EMMA Acres was extremely hospitable during our visit there. Dr. Lawrence Shimkets and Dr. Kathryn Eaton graciously donated *M. xanthus* and EHEC strains.

References:

1. **Tauxe RV.** 1997. Emerging foodborne diseases: an evolving public health challenge. *Emerging Infectious Diseases* **3:**425-434.
2. **Mead PS, Slutsker L, Dietz V, McCaig LF, Bresee JS, Shapiro C, Griffin PM, Tauxe RV.** 1999. Food-related illness and death in the United States. *Emerging Infectious Diseases* **5:**607-625.
3. **Kaper JB, Nataro JP, Mobley HL.** 2004. Pathogenic *Escherichia coli. Nature reviews Microbiology* **2:**123-140.
4. **Foxman B, Brown P.** 2003. Epidemiology of urinary tract infections: transmission and risk factors, incidence, and costs. *Infectious disease clinics of North America* **17:**227-241.
5. **Russo TA, Johnson JR.** 2003. Medical and economic impact of extraintestinal infections due to *Escherichia coli:* focus on an increasingly important endemic problem. *Microbes and infection* **5:**449-456.

6. **Pitout JD.** 2012. Extraintestinal pathogenic *Escherichia coli:* an update on antimicrobial resistance, laboratory diagnosis and treatment. *Expert review of anti-infective therapy* **10:**1165-1176.
7. **Ferens WA, Hovde CJ.** 2011. *Escherichia coli* O157:H7: animal reservoir and sources of human infection. *Foodborne pathogens and disease* **8:**465-487.
8. **Fatica MK, Schneider KR.** 2011. *Salmonella* and produce: survival in the plant environment and implications in food safety. *Virulence* **2:**573-579.
9. **Mughini-Gras L, Enserink R, Friesema I, Heck M, van Duynhoven Y, van Pelt W.** 2014. Risk factors for human salmonellosis originating from pigs, cattle, broiler chickens and egg laying hens: a combined case-control and source attribution analysis. *PloS one* **9:**e87933.
10. **Zweifel C, Schumacher S, Beutin L, Blanco J, Stephan R.** 2006. Virulence profiles of Shiga toxin 2e-producing *Escherichia coli* isolated from healthy pig at slaughter. *Veterinary Microbiology* **117:**328-332.
11. **Locking ME, O'Brien SJ, Reilly WJ, Wright EM, Campbell DM, Coia JE, Browning LM, Ramsay CN.** 2001. Risk factors for sporadic cases of *Escherichia coli* O157 infection: the importance of contact with animal excreta. *Epidemiology and infection* **127:**215-220.
12. **Chen SL, Wu M, Henderson JP, Hooton TM, Hibbing ME, Hultgren SJ, Gordon JI.** 2013. Genomic diversity and fitness of *E. coli* strains recovered from the intestinal and urinary tracts of women with recurrent urinary tract infection. *Science Translational Medicine* **5:**184ra160.
13. **Russo TA, Stapleton A, Wenderoth S, Hooton TM, Stamm WE.** 1995. Chromosomal restriction fragment length polymorphism analysis of *Escherichia coli* strains causing recurrent urinary tract infections in young women. *The Journal of Infectious Diseases* **172:**440-445.
14. **Hooton TM.** 2001. Recurrent urinary tract infection in women. *International journal of antimicrobial agents* **17:**259-268.
15. **Yamamoto S, Tsukamoto T, Terai A, Kurazono H, Takeda Y, Yoshida O.** 1997. Genetic evidence supporting the fecal-perineal-urethral hypothesis in cystitis caused by *Escherichia coli. The Journal of Urology* **157:**1127-1129.
16. **Manges AR, Johnson JR.** 2012. Food-borne origins of *Escherichia coli* causing extraintestinal infections. *Clinical infectious diseases : an official publication of the Infectious Diseases Society of America* **55:**712-719.
17. **Johnson JR, Kuskowski MA, Smith K, O'Bryan TT, Tatini S.** 2005. Antimicrobial-resistant and extraintestinal pathogenic *Escherichia coli* in retail foods. *The Journal of Infectious Diseases* **191:**1040-1049.
18. **Phillips I, King A, Rowe B, Gross RJ, Eykyn S, Gransden WR, Frost JA.** 1988. Epidemic Multiresistant *Escherichia coli* Infection in West Lambeth Health District. *Lancet* **1:**1038-1041.
19. **Ramchandani M, Manges AR, DebRoy C, Smith SP, Johnson JR, Riley LW.** 2005. Possible animal origin of human-associated, multidrug-resistant, uropathogenic *Escherichia coli. Clinical infectious diseases : an official publication of the Infectious Diseases Society of America* **40:**251-257.
20. **Hufnagel DA, Tukel C, Chapman MR.** 2013. Disease to dirt: the biology of microbial amyloids. *PLoS Pathogens* **9:**e1003740.

21. **Hammar M, Arnqvist A, Bian Z, Olsen A, Normark S.** 1995. Expression of two csg operons is required for production of fibronectin- and congo red-binding curli polymers in *Escherichia coli* K-12. *Molecular Microbiology* **18:**661-670.
22. **Romling U, Bian Z, Hammar M, Sierralta WD, Normark S.** 1998. Curli fibers are highly conserved between *Salmonella typhimurium* and *Escherichia coli* with respect to operon structure and regulation. *Journal of Bacteriology* **180:**722-731.
23. **Dueholm MS, Albertsen M, Otzen D, Nielsen PH.** 2012. Curli functional amyloid systems are phylogenetically widespread and display large diversity in operon and protein structure. *PloS one* **7:**e51274.
24. **Romling U, Rohde M, Olsen A, Normark S, Reinkoster J.** 2000. AgfD, the checkpoint of multicellular and aggregative behaviour in *Salmonella typhimurium* regulates at least two independent pathways. *Molecular Microbiology* **36:**10-23.
25. **Zogaj X, Nimtz M, Rohde M, Bokranz W, Romling U.** 2001. The multicellular morphotypes of *Salmonella typhimurium* and *Escherichia coli* produce cellulose as the second component of the extracellular matrix. *Molecular Microbiology* **39:**1452-1463.
26. **Ryjenkov DA, Simm R, Romling U, Gomelsky M.** 2006. The PilZ domain is a receptor for the second messenger c-di-GMP: the PilZ domain protein YcgR controls motility in enterobacteria. *The Journal of Biological Chemistry* **281:**30310-30314.
27. **White AP, Gibson DL, Kim W, Kay WW, Surette MG.** 2006. Thin aggregative fimbriae and cellulose enhance long-term survival and persistence of *Salmonella. Journal of Bacteriology* **188:**3219-3227.
28. **DePas WH, Hufnagel DA, Lee JS, Blanco LP, Bernstein HC, Fisher ST, James GA, Stewart PS, Chapman MR.** 2013. Iron induces bimodal population development by *Escherichia coli. Proceedings of the National Academy of Sciences of the United States of America* **110:**2629-2634.
29. **White AP, Gibson DL, Grassl GA, Kay WW, Finlay BB, Vallance BA, Surette MG.** 2008. Aggregation via the red, dry, and rough morphotype is not a virulence adaptation in *Salmonella enterica* serovar Typhimurium. *Infection and Immunity* **76:**1048-1058.
30. **Wang R, Bono JL, Kalchayanand N, Shackelford S, Harhay DM.** 2012. Biofilm formation by Shiga toxin-producing *Escherichia coli* O157:H7 and Non-O157 strains and their tolerance to sanitizers commonly used in the food processing environment. *Journal of Food Protection* **75:**1418-1428.
31. **Macarisin D, Patel J, Bauchan G, Giron JA, Sharma VK.** 2012. Role of curli and cellulose expression in adherence of *Escherichia coli* O157:H7 to spinach leaves. *Foodborne pathogens and disease* **9:**160-167.
32. **Pawar DM, Rossman ML, Chen J.** 2005. Role of curli fimbriae in mediating the cells of enterohaemorrhagic *Escherichia coli* to attach to abiotic surfaces. *Journal of Applied Microbiology* **99:**418-425.
33. **Cegelski L, Pinkner JS, Hammer ND, Cusumano CK, Hung CS, Chorell E, Aberg V, Walker JN, Seed PC, Almqvist F, Chapman MR, Hultgren SJ.** 2009. Small-molecule inhibitors target *Escherichia coli* amyloid biogenesis and biofilm formation. *Nature Chemical Biology* **5:**913-919.

34. **Matz C, Bergfeld T, Rice SA, Kjelleberg S.** 2004. Microcolonies, quorum sensing and cytotoxicity determine the survival of *Pseudomonas aeruginosa* biofilms exposed to protozoan grazing. *Environmental Microbiology* **6:**218-226.
35. **Weitere M, Bergfeld T, Rice SA, Matz C, Kjelleberg S.** 2005. Grazing resistance of *Pseudomonas aeruginosa* biofilms depends on type of protective mechanism, developmental stage and protozoan feeding mode. *Environmental Microbiology* **7:**1593-1601.
36. **Matz C, McDougald D, Moreno AM, Yung PY, Yildiz FH, Kjelleberg S.** 2005. Biofilm formation and phenotypic variation enhance predation-driven persistence of *Vibrio cholerae*. *Proceedings of the National Academy of Sciences of the United States of America* **102:**16819-16824.
37. **Darby C, Hsu JW, Ghori N, Falkow S.** 2002. *Caenorhabditis elegans:* plague bacteria biofilm blocks food intake. *Nature* **417:**243-244.
38. **Begun J, Gaiani JM, Rohde H, Mack D, Calderwood SB, Ausubel FM, Sifri CD.** 2007. *Staphylococcal* biofilm exopolysaccharide protects against *Caenorhabditis elegans* immune defenses. *PLoS Pathogens* **3:**e57.
39. **Dahl JL, Ulrich CH, Kroft TL.** 2011. Role of phase variation in the resistance of *Myxococcus xanthus* fruiting bodies to *Caenorhabditis elegans* predation*. Journal of Bacteriology* **193:**5081-5089.
40. **Avery L, You YJ.** 2012. *C. elegans* feeding. WormBook : the online review of *C. elegans* biology**:**1-23.
41. **McBride MJ, Zusman DR.** 1996. Behavioral analysis of single cells of *Myxococcus xanthus* in response to prey cells of *Escherichia coli*. *FEMS microbiology letters* **137:**227-231.
42. **Pan H, He X, Lux R, Luan J, Shi W.** 2013. Killing of *Escherichia coli* by *Myxococcus xanthus* in aqueous environments requires exopolysaccharide-dependent physical contact. *Microbial Ecology* **66:**630-638.
43. **De Mesel I, Derycke S, Moens T, Van der Gucht K, Vincx M, Swings J.** 2004. Top-down impact of bacterivorous nematodes on the bacterial community structure: a microcosm study. *Environmental Microbiology* **6:**733-744.
44. **Reddy KC, Hunter RC, Bhatla N, Newman DK, Kim DH.** 2011. *Caenorhabditis elegans* NPR-1-mediated behaviors are suppressed in the presence of mucoid bacteria. *Proceedings of the National Academy of Sciences of the United States of America* **108:**12887-12892.
45. **Stewart PS, Franklin MJ.** 2008. Physiological heterogeneity in biofilms. *Nature reviews Microbiology* **6:**199-210.
46. **Lewis K.** 2008. Multidrug tolerance of biofilms and persister cells. *Current topics in microbiology and immunology* **322:**107-131.
47. **Zogaj X, Bokranz W, Nimtz M, Romling U.** 2003. Production of cellulose and curli fimbriae by members of the family *Enterobacteriaceae* isolated from the human gastrointestinal tract. *Infection and Immunity* **71:**4151-4158.
48. **Hung C, Zhou YZ, Pinkner JS, Dodson KW, Crowley JR, Heuser J, Chapman MR, Hadjifrangiskou M, Henderson JP, Hultgren SJ.** 2013. *Escherichia coli* Biofilms Have an Organized and Complex Extracellular Matrix Structure. *Mbio* **4**.

49. **Serra DO, Richter AM, Klauck G, Mika F, Hengge R.** 2013. Microanatomy at Cellular Resolution and Spatial Order of Physiological Differentiation in a Bacterial Biofilm. *Mbio* **4**.
50. **Serra DO, Richter AM, Hengge R.** 2013. Cellulose as an Architectural Element in Spatially Structured *Escherichia coli* Biofilms. *Journal of Bacteriology* **195:**5540-5554.
51. **Chapman MR, Robinson LS, Pinkner JS, Roth R, Heuser J, Hammar M, Normark S, Hultgren SJ.** 2002. Role of *Escherichia coli* curli operons in directing amyloid fiber formation. *Science* **295:**851-855.
52. **Zhou Y, Smith DR, Hufnagel DA, Chapman MR.** 2013. Experimental manipulation of the microbial functional amyloid called curli. *Methods in molecular biology* (Clifton, N J) **966:**53-75.
53. **Berleman JE, Kirby JR.** 2009. Deciphering the hunting strategy of a bacterial wolfpack. *FEMS Microbiology Reviews* **33:**942-957.
54. **Reichenbach H.** 1999. The ecology of the *myxobacteria. Environmental Microbiology* **1:**15-21.
55. **Ramsey WS, Dworkin M.** 1968. Microcyst germination in *Myxococcus xanthus. Journal of Bacteriology* **95:**2249-2257.
56. **Hart BA, Zahler SA.** 1966. Lytic enzyme produced by *Myxococcus xanthus. Journal of Bacteriology* **92:**1632-1637.
57. **DePas WH, Chapman MR.** 2012. Microbial manipulation of the amyloid fold. *Research in microbiology* **163:**592-606.
58. **Hillesland KL, Lenski RE, Velicer GJ.** 2007. Ecological variables affecting predatory success in *Myxococcus xanthus. Microbial Ecology* **53:**571-578.
59. **Romling U, Sierralta WD, Eriksson K, Normark S.** 1998. Multicellular and aggregative behaviour of *Salmonella typhimurium* strains is controlled by mutations in the agfD promoter. *Molecular Microbiology* **28:**249-264.
60. **Belanger L, Garenaux A, Harel J, Boulianne M, Nadeau E, Dozois CM.** 2011. *Escherichia coli* from animal reservoirs as a potential source of human extraintestinal pathogenic *E. coli. FEMS immunology and medical microbiology* **62:**1-10.
61. **Olsen A, Jonsson A, Normark S.** 1989. Fibronectin binding mediated by a novel class of surface organelles on *Escherichia coli. Nature* **338:**652-655.
62. **Solomon EB, Yaron S, Matthews KR.** 2002. Transmission of *Escherichia coli* O157:H7 from contaminated manure and irrigation water to lettuce plant tissue and its subsequent internalization. *Applied and Environmental Microbiology* **68:**397-400.
63. **Mootian G, Wu WH, Matthews KR.** 2009. Transfer of *Escherichia coli* O157:H7 from soil, water, and manure contaminated with low numbers of the pathogen to lettuce plants. *Journal of Food Protection* **72:**2308-2312.
64. **Wai SN, Mizunoe Y, Takade A, Kawabata SI, Yoshida SI.** 1998. *Vibrio cholerae* O1 strain TSI-4 produces the exopolysaccharide materials that determine colony morphology, stress resistance, and biofilm formation. *Applied and Environmental Microbiology* **64:**3648-3655.
65. **Morris JG, Jr., Sztein MB, Rice EW, Nataro JP, Losonsky GA, Panigrahi P, Tacket CO, Johnson JA.** 1996. *Vibrio cholerae* O1 can assume a chlorine-

resistant rugose survival form that is virulent for humans. *The Journal of Infectious Diseases* **174:**1364-1368.
66. **Yildiz FH, Schoolnik GK.** 1999. *Vibrio cholerae* O1 El Tor: identification of a gene cluster required for the rugose colony type, exopolysaccharide production, chlorine resistance, and biofilm formation. *Proceedings of the National Academy of Sciences of the United States of America* **96:**4028-4033.
67. **Yildiz FH, Liu XS, Heydorn A, Schoolnik GK.** 2004. Molecular analysis of rugosity in a *Vibrio cholerae* O1 El Tor phase variant. *Molecular Microbiology* **53:**497-515.
68. **Fux CA, Shirtliff M, Stoodley P, Costerton JW.** 2005. Can laboratory reference strains mirror 'real-world' pathogenesis? *Trends in Microbiology* **13:**58-63.
69. **Davidson CJ, White AP, Surette MG.** 2008. Evolutionary loss of the rdar morphotype in *Salmonella* as a result of high mutation rates during laboratory passage. *The ISME journal* **2:**293-307.
70. **Serra DO, Richter AM, Klauck G, Mika F, Hengge R.** 2013. Microanatomy at cellular resolution and spatial order of physiological differentiation in a bacterial biofilm. *mBio* **4:**e00103-00113.
71. **Ma L, Conover M, Lu H, Parsek MR, Bayles K, Wozniak DJ.** 2009. Assembly and development of the *Pseudomonas aeruginosa* biofilm matrix. *PLoS Pathogens* **5:**e1000354.
72. **Evans ML, Chapman MR.** 2013. Curli biogenesis: Order out of disorder. *Biochimica et biophysica acta.*
73. **Kudva IT, Blanch K, Hovde CJ.** 1998. Analysis of *Escherichia coli* O157:H7 survival in ovine or bovine manure and manure slurry. *Applied and Environmental Microbiology* **64:**3166-3174.
74. **Xiao Y, Wei X, Ebright R, Wall D.** 2011. Antibiotic production by *myxobacteria* plays a role in predation. *Journal of Bacteriology* **193:**4626-4633.

Chapter 5
Discussion, Perspectives, and Future Directions

Dynamics of Bimodal Population Development

Phenotypic variation in isogenic biofilm communities can arise through multiple mechanisms (1). One mechanism is stochastic gene expression, which can trigger biofilm-related differentiation pathways independently of environmental stimuli (1, 2). Stochastic fluctuations are essentially noise, resulting from the cell-to-cell variation in the biochemical process of gene expression (2-4). Therefore, one would expect that if a biofilm population were to develop subpopulations based on stochastic gene expression, those subpopulations would develop in random positions and at random times.

Secondly, mutations can trigger subpopulation development within biofilms. In *Pseudomonas aeruginosa*, RecA-mediated genetic mutations lead to phenotypic differences among members of the same biofilm (5). Intriguingly, these mutations are dependent on endogenous oxidative stress causing double strand DNA breaks (6). Such genetic diversity creates subpopulations that are able to resist different stresses, granting the biofilm community as a whole a broader stress-resistance profile. Since mutations drive these phenotypic changes, they are heritable (5, 6).

Lastly, chemical gradients within biofilms develop because bacteria on the periphery consume nutrients, which prevents those nutrients from diffusing and being available to the cells on the interior of the biofilm (1). For example, oxygen consumption occurs so robustly at the air-exposed periphery of biofilm communities that the underlying bacteria are often oxygen starved (7, 8). Therefore, chemical-induced physiological heterogeneity in a biofilm community is initially triggered by chemical gradients that lead to gene expression changes and subsequent metabolic gradients. As such, this type of biofilm differentiation is reversible and non-inheritable (1).

In this dissertation, I have described two discrete bacterial populations that form in *Escherichia coli* strain UTI89 rugose biofilms. Development of these two populations could feasibly be triggered by mutations, stochastic gene expression, or chemical-induced physiological heterogeneity. I consider each of these possibilities with regards to bimodal population development below.

The clustering of curli producing cells to the air-biofilm interface indicates that an environmental signal affects bimodal population development. Stochastic gene expression is characterized by its independence from external stimuli (1, 3). The precise and large-scale localization of matrix-producing cells to the air interface suggests that, instead of stochastic gene changes, a signal from the environment initiates subpopulation development.

Mutations can be triggered by external stimuli (9), but the repeatable restructuring of rugose biofilms suggests that spontaneous mutations must not be the trigger. Alternatively, reversible genetic alterations such as phase variation might lead to bimodal population development. Phase variation accounts for the transition between rugose and smooth colony phenotypes in *V. cholerae* (10-13). Furthermore, in *S. enterica* ser. Typhimurium, a CsgD-GFP translational fusion demonstrated that individual bacteria either produced high amounts of CsgD or very little, implying that the expression of CsgD might be phase variable (14). However, this work was done before my manuscript on bimodal population development was published, so the authors may have been mixing “washout” bacteria with “matrix” bacteria prior to visualization (15). Furthermore, a former graduate student in the Chapman lab, Dan Smith, failed to find evidence of recombination in the *csgDEFG-csgBAC* intergenic region using a PCR screen (Dan Smith’s thesis). Therefore, although environmentally-induced phase variation can trigger bimodal population development in some cases, it does not seem to be involved in *E. coli* rugose colony development.

Thus, gene expression changes due to alterations in environmental stimuli are the most likely driver of bimodal population development. Such a model predicts that curli is induced in periphery cells because they are exposed to a different chemical environment than interior cells. These types of phenotypic differences are purely due to gene regulation, and are therefore non-heritable. Therefore, one would predict that if

you replated washout and matrix fraction bacteria, new rugose biofilms would develop at the same rate. Indeed, this is the case (Fig. 5.1).

If an environmental signal drives bimodal population development, two obvious questions emerge. 1) What is the environmental signal that drives bimodal population development, and 2) how is this signal interpreted so that the appropriate gene expression changes are manifested? The localization of curli-production to the biofilm exterior suggests that oxygen may affect bimodal population development. Indeed, anaerobic conditions suppress curli production in *S. enterica* ser. Typhimurium (16), and preliminary experiments in the lab have shown that the same is true for *E. coli* (Fig. 5.2). If oxygen is the signal, we can therefore infer that the presence of oxygen induces curli expression, a presumption supported by the fact that higher oxygen levels correlate with matrix production within a UTI89 rugose biofilm (Fig. 2.11)(15). Oxygen sensing systems in *E. coli* have been well-described (17-19), and, in Chapter 3, I created deletion mutants for six candidate regulators and screened for changes in rugose biofilm formation. An *arcAB* mutant wrinkled in low iron conditions (Fig. 3.1). I found that ArcAB suppressed CsgD production. However, an *arcAB* mutant demonstrated only a small increase in *csgBAC* expression in the biofilm interior in two-day-old biofilms (Fig.3.7, 3.9).

Therefore, in addition to ArcAB, another system must contribute to the maintainance of bimodal population development at earlier stages of biofilm development. Due to the elongated shape of cells in the biofilm interior, Sera *et. al.* suggested that cells closer to the agar surface were younger, exposed to more nutrients from the agar, and therefore in logarithmic growth phase, in which curli is not expressed (20, 21). However, the authors also noted that tall wrinkles, where all biofilm cells are far removed from the agar surface, still develop a bimodal population (20, 21). Furthermore, I have shown that bimodal population development is maintained at least as long as 14 days following initial plating (Fig. 4.5), by which time underlying cells should presumably have gone into stationary phase. So, although growth phase does not appear to be the principle driving agent of bimodal population development, I think that it warrants more investigation. An interesting experiment would be to track bimodal population development in WT UTI89 vs. an *arcAB* mutant over an extended period of

time. Without ArcAB suppression of matrix in the interior, once washout cells reach stationary phase they may begin to produce matrix components.

It is possible that multiple oxygen-sensing systems coordinate to suppress matrix production in the biofilm interior. Fnr is a global transcriptional regulator that directly senses and responds to molecular oxygen (18). DosCP binds molecular oxygen and in response regulates intracellular concentrations of cyclid-di-GMP (17, 22, 23). Lastly, YfgF breaks down cyclic-di-GMP in anaerobic conditions (24). Given the roles of cyclic-di-GMP and oxygen in CsgD expression and rugose biofilm formation (16, 25-27), it is tempting to speculate that one of these regulators controls curli production in biofilm interiors. However, preliminary confocal experiments using a *csgBAC-gfp* reporter in *fnr, dosCP,* and *yfgF* mutants suggest that they are not principle regulators of bimodal population development (Fig. 5.3). It is possible that multiple, redundant systems overlap to suppress matrix production in the interior, and the only way to see a phenotype would be to mutate multiple regulators.

Iron and Rugose Biofilm Formation

Iron is an essential nutrient for almost all bacterial species, and it affects *E. coli* gene expression, growth, and metabolism in a variety of ways (28, 29). To determine how iron was causing rugose biofilm formation, I first screened known iron-responsive regulators (Fig. 2.8). A mutant lacking *fur*, which encodes a global iron-responsive regulator, wrinkled slightly in low iron. Therefore, Fur may repress rugose biofilm formation. However, after finding that oxidative stress could drive rugose formation in place of iron, and that overexpression of *sodA* could repress iron-induced rugose biofilm formation, it became apparent that iron may not directly induce rugose biofilm formation. Iron likely induces rugose biofilm formation through oxidative stress. Indeed, free ferrous iron in the cell can participate in the Fenton reaction, resulting in DNA, lipid, and protein damage (29-31). However, the interpretation that, in high iron conditions, *E. coli* is exposed to substantially more oxidative stress presents logical inconsistencies. Iron acquisition is tightly regulated by bacteria, so high levels of exogenous iron may not correlate with an increase in oxidative stress (29). Furthermore, there is not a described regulatory system that responds directly to iron-induced reactive oxygen stress. The hydroxyl radical, which is the direct product of the Fenton reaction, reacts too quickly

with organic compounds to be adequately “sensed” (30, 32). Although superoxide can simulate iron-induced reactive oxygen stress, neither it nor hydrogen peroxide are byproducts of Fenton chemistry (30). Moreover, SoxRS and OxyR, which respond to superoxide and hydrogen peroxide stress, respectively (33), do not affect iron-induced rugose biofilm development to a large degree (Fig.3.1).

Instead, iron might cause an increase in overall cellular oxidation state. Iron influences rugose biofilm formation in *B. subtilis*, and iron exposure in that system results in an increase in the NAD+/NADH ratio (34). Furthermore, Kolodkin-Gal *et. al*. demonstrated that two kinases, KinB and KinA, respond to oxidation by binding to components of the electron transport chain and directly to NAD+, respectively (34). The authors hypothesized that, since iron is required for proper cytochrome function, the presence of iron might affect the efficiency of the electron transport chain and subsequently the overall cellular redox state (34). If iron induces rugose biofilm formation in *E. coli* through an increase in cellular oxidation, the next question becomes what is the regulator? Screening redox-responsive systems supplied me with a good candidate in ArcAB (Fig. 3.1).

It is tempting to propose that in low iron conditions, ArcAB is active due to a reduced cellular state, leading to repression of *csgD* and rugose biofilm formation. The presence of iron could then lead to cellular oxidation and subsequent ArcAB inactivation coupled to *csgD* derepression. Superoxide could also potentially oxidize and inactivate ArcB. Although I could not find a direct connection between superoxide and ArcAB activity in the literature, a principle source of reactive oxygen species in *E. coli* is NADH dehydrogenase II (35). Superoxide is therefore produced in close proximity to the membrane and the electron transport chain, so oxidation of membrane-bound ArcB by superoxide is not a far-fetched hypothesis. To assay ArcAB activity in low vs. high iron, I utilized β-galactosidase assays using two ArcAB-dependent promoters, with mixed results (Fig. 5.4). Both *fadE* and *llpD* are repressed by ArcA-P (36-38). *llpD* expression increased in high iron, while *fadE* did not (Fig. 5.4). A possible reason for this discrepancy is that both *llpD* and *fadE* rely on other regulators besides ArcA to control transcription. One of these regulators might itself be subject to iron regulation. A third ArcAB-dependent promoter should be analyzed to clarify this result.

Given the recent interest in the interplay between redox balance and biofilm development in a variety of organisms (34,39-41), and the major role that ArcAB appears to play in UTI89 rugose biofilm development, the ArcAB narrative seems to me to be urgent and compelling. If ArcAB is responsible for iron-driven rugose formation, it would agree well with the iron-driven oxidation observed in *B. subtilis* (34). It would also be novel in that the same regulator could affect biofilm architecture on the micro (curli expression repressed in the biofilm interior) and macro (wrinkled colony development) scale.

If, however, ArcAB is not responsible for iron-induced rugose biofilm formation, there are multiple other explanations for what could be. A *fur* mutant wrinkles slightly in low iron conditions (Fig. 2.8), so Fur may be involved in iron-dependent rugose biofilm formation. When iron is plentiful, Fur binds to ferrous iron and generally acts as a repressor of gene expression (29). Therefore, if Fur affects biofilm development, it would likely repress a biofilm suppressor in high iron conditions. So far, I have not been able to find any data in the literature that links Fur activity to expression of biofilm genes. An interesting experiment would be to monitor CsgD levels in a *fur* mutant. Part of iron-induced rugose biofilm formation could also be an increased growth rate. Because *sodAB* and *arcAB* both wrinkle in low iron conditions, and both have growth defects, it is evident that increased growth is not necessary for wrinkling in low iron conditions. A difficult question is whether or not increased growth alone is able to cause wrinkling in low iron conditions. A possible experiment to test whether a particular growth rate or growth threshold is necessary for rugose biofilm development would be to subtract other nutrients besides iron from growth media and monitor rugose biofilm formation. However, we currently do not have a defined medium with which we can induce rugose biofilm formation, so these experiments might prove to be technically challenging.

Iron and CsgA Polymerization

Part of the reason we were originally interested in iron's affect on curli was that iron affects the aggregation of multiple disease-associated amyloids (42-45). Iron induces disordered aggregation of the Alzheimer's disease amyloid Aβ, thereby decreasing Aβ ordered amyloid fiber formation (44). Our initial hypotheses were that

iron may also bind to CsgA and influence curli amyloid formation. Furthermore, if there was an iron-curli complex, *E. coli* might use curli fibers as an extracellular iron storage system. I attempted to test these hypotheses in a variety of ways. Thioflavin T (ThT) fluoresces when it binds to amyloid fibers such as CsgA or CsgB, and therefore it can be used as a surrogate for assessing CsgA amyloid polymerization (46, 47). I used ThT assays to test whether iron affected CsgA polymerization into amyloid. Interestingly, preliminary ThT experiments with both CsgA and CsgB demonstrated that addition of .5-5mM $FeCl_3$ decreased the typical lag phase associated with fiber polymerization (Fig. 5.5A,B). Moreover, transmission electron microscopy (TEM) revealed that when CsgA polymerized in the presence of 5mM $FeCl_3$, dark aggregates were present among the fibers. These aggregates were largely absent when CsgA polymerized without added iron (Fig. 5.6). Similarly, iron addition to Aβ polymerization assays results in shorter, more curved fibers (44). Together, these results suggest that environmental iron levels could alter biofilm morphogenesis by modulating amyloid fiber polymerization. However, there are multiple technical caveats that should be considered with these experiments. I was never successful at removing iron from buffer prior to adding CsgA or CsgB. Therefore, if either of those proteins binds iron, they might already be “iron-loaded” prior to ThT assays. Additionally, we use His6x-tagged CsgA and CsgB, and the histidine tag could potentially affect iron binding.

I also attempted to measure iron binding by using the R1, R3, and R5 subunits of CsgA, each of which polymerizes into amyloid fibers *in vitro* (48). Using these subunits bypasses the need to purify CsgA every time you need to do experiments, and they are not his-tagged. However, using subunits instead of the full-length protein is not ideal, as any potential metal-binding motifs in CsgA might not be present in individual subunits. To measure metal binding to subunits, I incubated Fe-NTA complexes, which produce an absorbance shoulder around 250 nm (49), with polymerized subunits. I then took absorbance spectra before and after ultracentrifugation to remove fibers. Fig. 5.7 shows the raw data from one such experiment, using the R1 subunit. No decrease in Fe-NTA specific absorbance after incubation with subunits could be detected, indicating that R1 does not bind Fe-NTA. Neither R3 nor R5 demonstrated a clear phenotype either (data not shown), indicating that CsgA subunits likely do not bind iron.

If curli fibers bound to iron, one might expect a curliated bacterial colony to absorb more iron than a non-curliated colony. To test this idea, I utilized chrome azurol S (CAS) agar plates. CAS agar plates appear blue/greenish, due to the absorbance of Fe-CAS complexes. When bacteria remove iron from the media, Fe-CAS complexes are depleted and a yellow halo evolves around the bacteria colonies (50). No difference in halo size or rate of halo evolution could be determined between WT and a curli mutant (Fig. 5.8), indicating that curli most likely does not help UTI89 colonies to acquire iron.

Rugose Biofilm Function

When considering the function of rugose biofilms, it is important to differentiate between production of biofilm matrix components and the resultant wrinkled colony shape. The resistance to predation I have observed between WT UTI89 and matrix mutants is likely dependent on the presence of the matrix itself, and not colony shape. It is hard to imagine a possibility where a wrinkled shape would provide protection against predators, unless the increased height conferred to wrinkled colonies put some cells out of the reach of *M. xanthus*. However, a *csgBA* mutant wrinkles to some degree and is completely susceptible to *M. xanthus* killing (Fig. 4.6). It is more likely that the dense curli-mediated matrix protects against recognition by *M. xanthus*, as was discussed in Chapter 4.

What advantage then, does the rugose biofilm shape confer? It has been recently demonstrated that *Pseudomonas aeruginosa* rugose biofilm formation increases biofilm surface area as a means to expose more biofilm bacteria to oxygen (39, 40). Within their system, the authors demonstrate that a reduced cellular state triggers wrinkling, leading to more oxygen exposure (39). Those studies were ground-breaking in that they introduced redox balance as a driver of rugose biofilm development. Work in *B. subtilis*, *Candida albicans*, and my work with ArcAB and superoxide stress have since demonstrated that redox balance also controls rugose biofilm formation in other microbial species (15, 34, 41). However, applying the same principle of wrinkling to increase oxygen exposure to *E. coli* presents some problems. First of all, I have shown that oxidative stress can drive rugose biofilm development. Oxidative stress is generated through normal oxygen respiration (33, 35), so *E. coli*

exposing itself to more oxygen in response to oxidative stress seems counterproductive. ArcAB-inhibition of CsgD also demonstrates that cells in an oxidized state develop into rugose biofilm colonies. As noted by Serra *et. al.,* the diverse respiratory/fermentative metabolism of *E. coli* may alleviate selective pressure to develop morphologies that optimize oxygen exposure (20, 51, 52). In line with that idea, it is difficult to imagine an environmental niche where substantial air-exposure would be an adaptive advantage for *E. coli*. Indeed, the only possible niche would be the non-host environment, which is the only place *E. coli* would typically encounter an air interface. One would expect desiccation stress to provide counter selection against development of an increased surface area in the non-host environment (53). An intriguing possibility is that the rugose biofilm shape is optimized for a balance between an oxidant exposing surface area and development of a desiccation-resistant interior population. One would expect a desiccation-resistant structure to resist evaporation, and *B. subtilis* rugose colony biofilms have been shown to resist both wetting and gas exchange (54).

Although it is tempting to speculate about the function of such a striking visual phenotype, in reality it is difficult to form testable hypotheses about the “function” of such a structure. It is easy enough to test if matrix components contribute to protection against predation or if iron-induced rugose formation correlates with oxidative stress resistance, but how do you test if colony wrinkling confers any fitness advantage? The main problem is that production of the biofilm matrix almost always coincides with colony wrinkling. Low iron conditions, where matrix is still produced but no rugose biofilms develop, could potentially be used to differentiate matrix production from rugose biofilm formation. For instance, if a colony grown in high iron conditions resists a particular stress better than a colony grown in low iron conditions, one could potentially attribute that stress resistance to wrinkling. However, iron undoubtedly changes many aspects of cellular physiology, so it would be difficult to attribute a phenotype to either the absence of iron or the absence of a wrinkled colony morphotype. The next best thing would be to model wrinkled colony structure with respect to what you would expect if the shape were optimized for a given purpose. Indeed, these types of models have been successfully employed with *P. aeruginosa* biofilms (39, 55). However, without an

increase in fitness that can be attributable to colony wrinkling, it is difficult to make solid conclusions about what environmental pressures shaped this morphological phenotype. In addition to the wrinkled colony shape, we can also conjecture about where and why bimodal population development has been selected for. Again, I propose that the "where" in this case must be the non-host environment, which presents an air-interface. As with the rugose biofilm shape, determining the survival advantage that a bimodal population confers is difficult. An interesting study in *B. subtilis* demonstrated that liquid flows freely through the "channels" formed under each wrinkle (56). These results agree well with what I and others have observed as far as matrix production being limited to the biofilm exterior (15, 21). The authors concluded that the hollow areas under wrinkles develop to allow nutrient diffusion within the biofilm to occur more efficiently. Perhaps *E. coli* suppresses interior matrix production to allow for similar nutrient channels to develop. Additionally, as discussed in chapter 4, the flagellated interior cells or *E. coli* rugose biofilms may allow for the generation of an easily dispersed population within a biofilm.

In total, this thesis provides a framework for understanding the dynamics of rugose biofilm formation in *E. coli*. The techniques I developed, including analysis of biofilm formation under low iron conditions, the washout assay, confocal microscopy of rugose biofilms, and predation assays, will hopefully be of use to researchers interested in further probing *E. coli* biofilms and *E. coli*/predator relationships. In a broader sense, the ubiquity of rugose biofilm formation implies that my results may be applied to other bacterial systems, adding to what is becoming a dynamic and unifying field in bacterial biofilm research.

Figures:

Figure 5.1 Each rugose biofilm fraction is able to form new rugose biofilms
UTI89 was grown on a YESCA agar plate for 48 hours. The washout assay was then performed, and 4 µL dots of a 1 OD_{600} suspension of each fraction were plated on a new YESCA agar plate. Concurrently, a new UTI89 culture was dotted. Rugose biofilm development was tracked at 24 and 48 hours post-dotting.

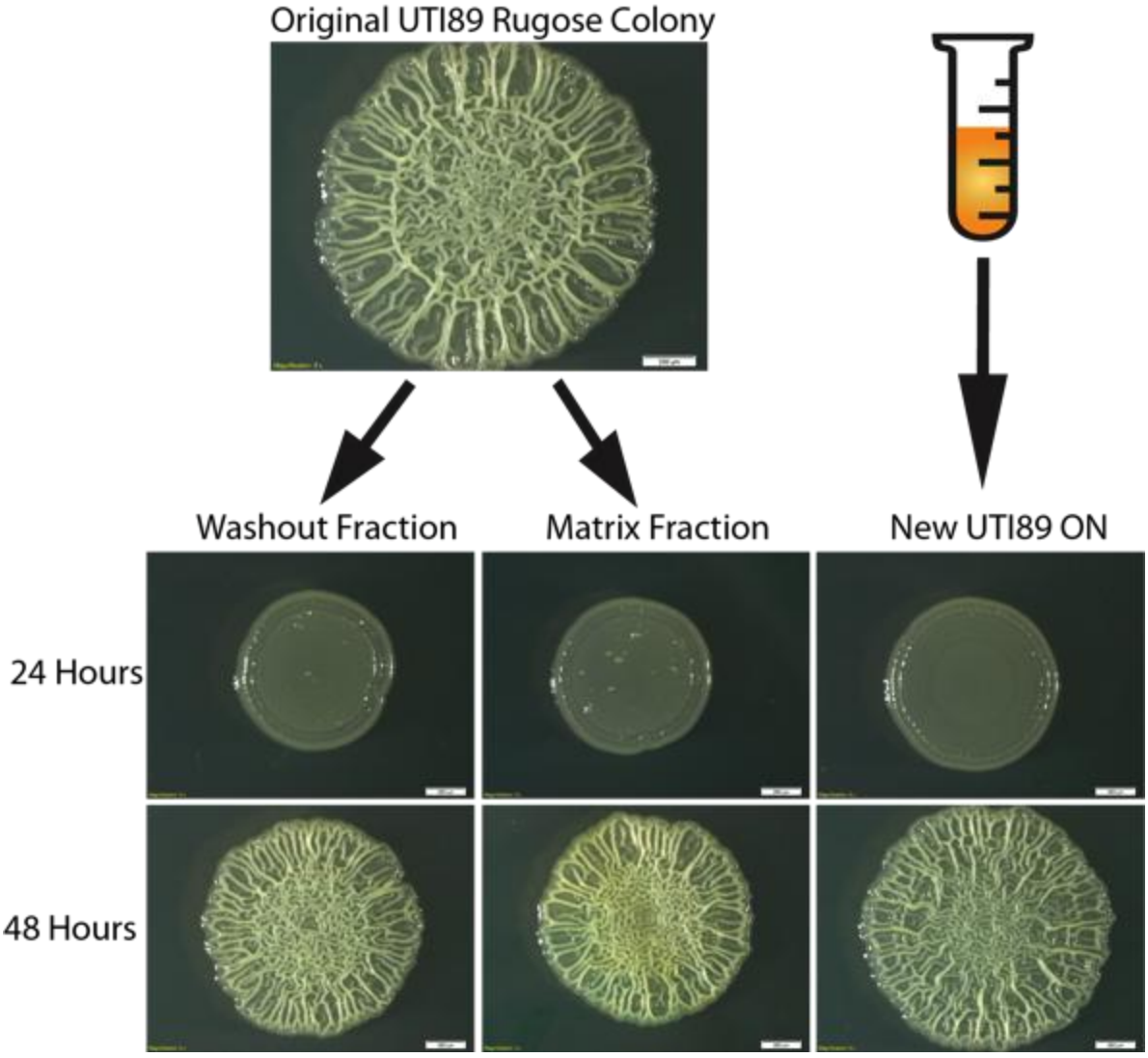

Figure 5.2 UTI89 curli expression is repressed in anaerobic conditions
UTI89 or a *csgBA* mutant were grown on YESCA plates aerobically for 2 days or anaerobically for 20 days. Western blot analysis revealed that CsgG and CsgA are only expressed aerobically.

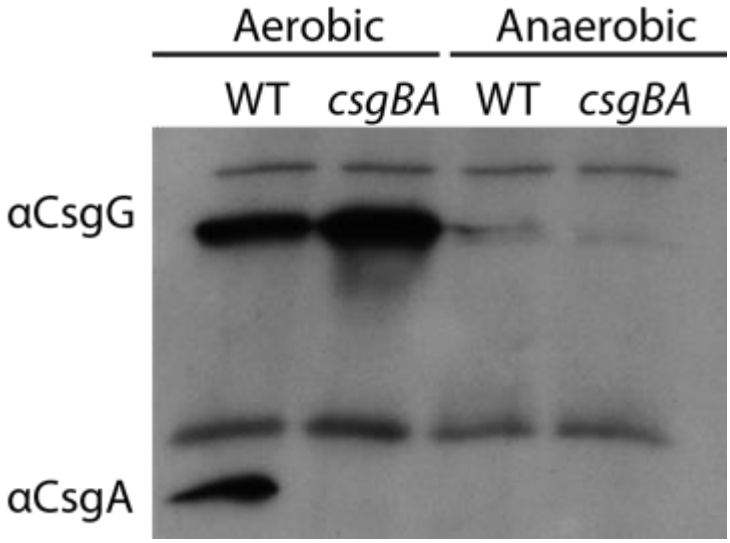

Figure 5.3 Bimodal population development in *fnr*, *dosCP*, and *yfgF* mutants
csgBAC-gfp promoter fusions were inserted into the *attB* site of WT UTI89 and *fnr*, *dosCP*, and *yfgF* mutants. After growth for 2 days at 26°C on YESCA agar plates, colonies were visualized by confocal microscopy. A single cross-section image from the center of each biofilm suggests that in each strain, curli production is limited to the biofilm periphery.

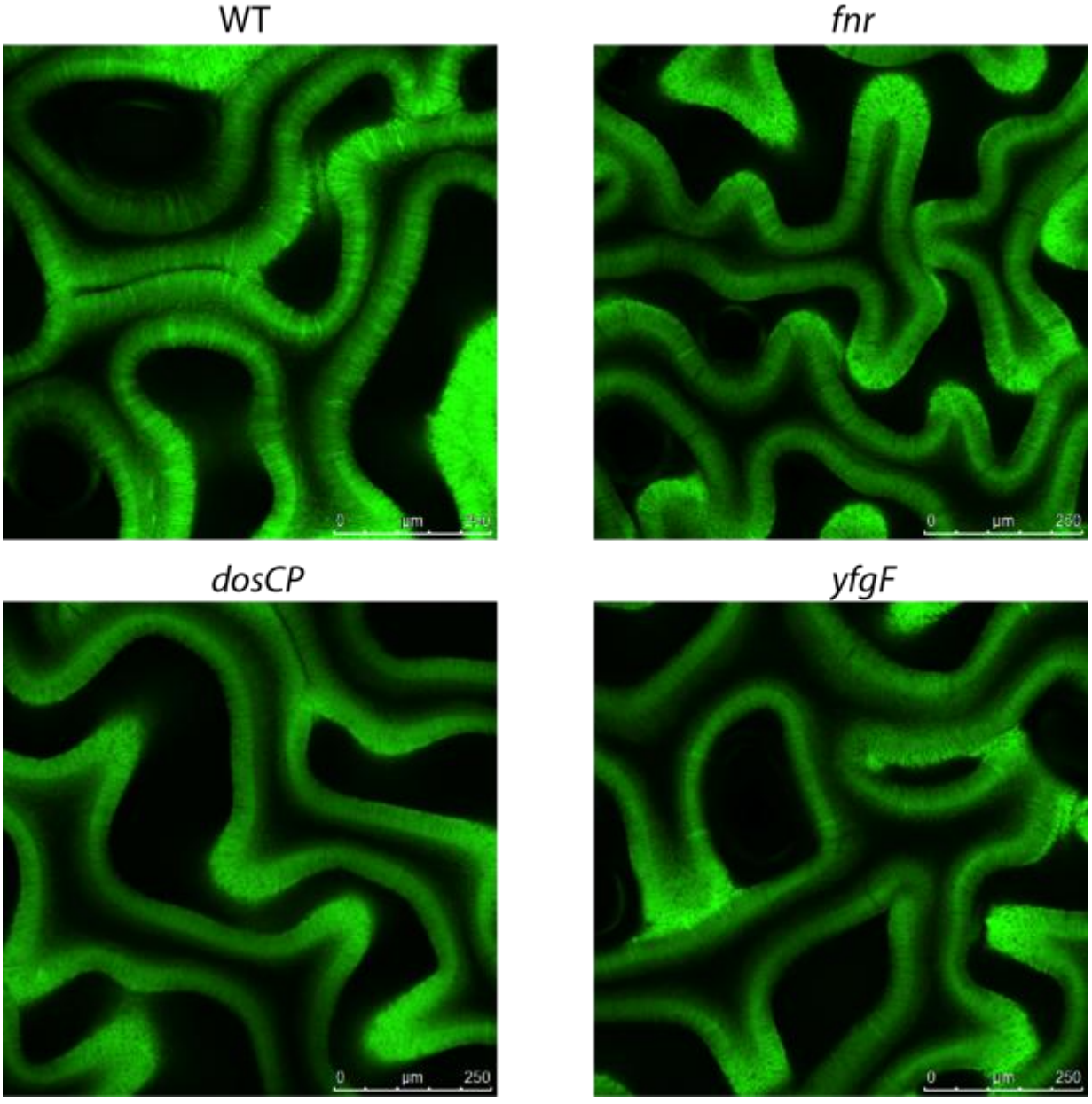

Figure 5.4 ArcAB-dependent promoter expression in low and high iron
UTI89 *lacZ attB::fadE-lacZ* and UTI89 *lacZ attB::llpD-lacZ* were grown on low iron plates or low iron plates supplemented with 10 μM $FeCl_3$. After 24 hours of growth, β-galactosidase assays were performed. Bars represent biological triplicates and error bars represent standard deviation.

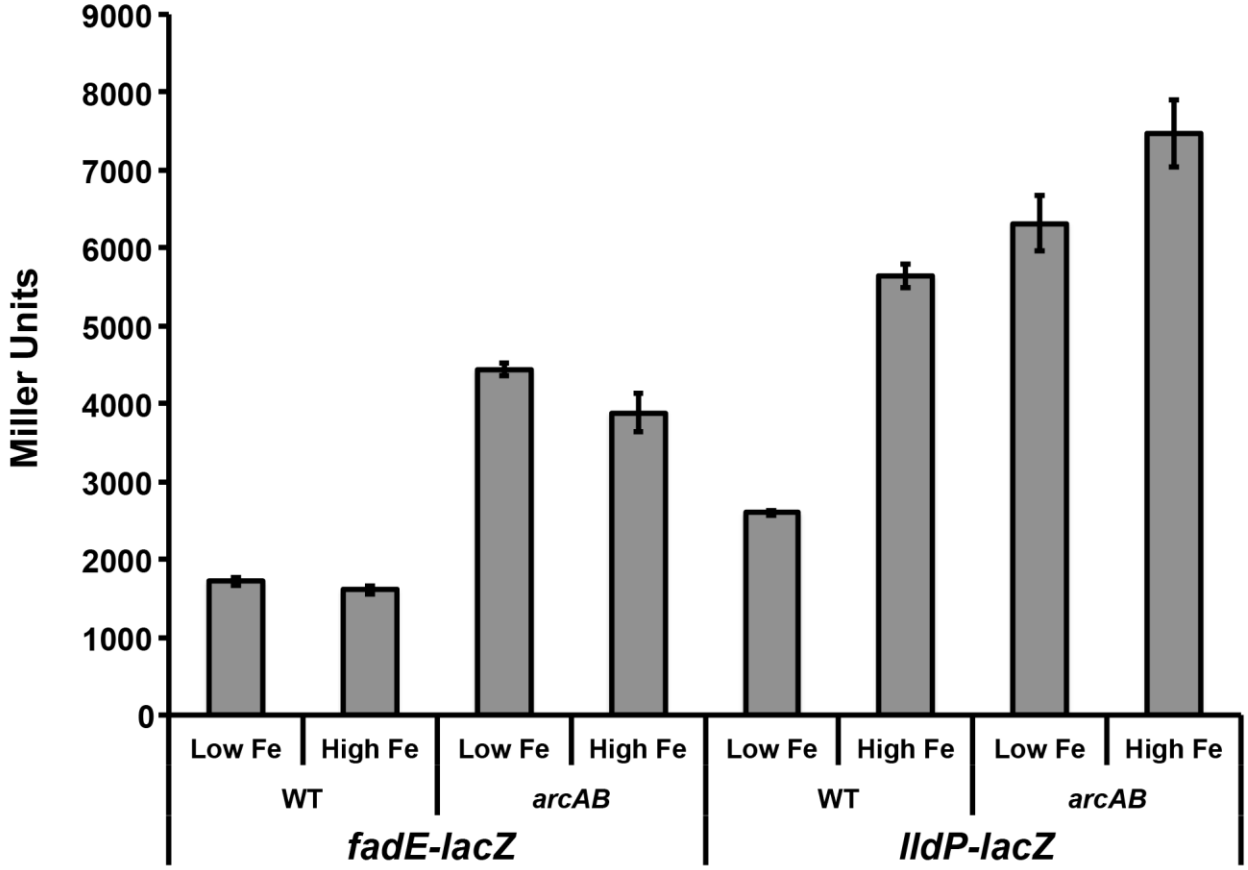

Figure 5.5 CsgA and CsgB polymerization with addition of iron
20.8 μM CsgA **(A)** and CsgB **(B)** were incubated with thioflavin T. Various concentrations of $FeCl_3$ were added to the reaction mixtures to monitor how iron affects polymerization.

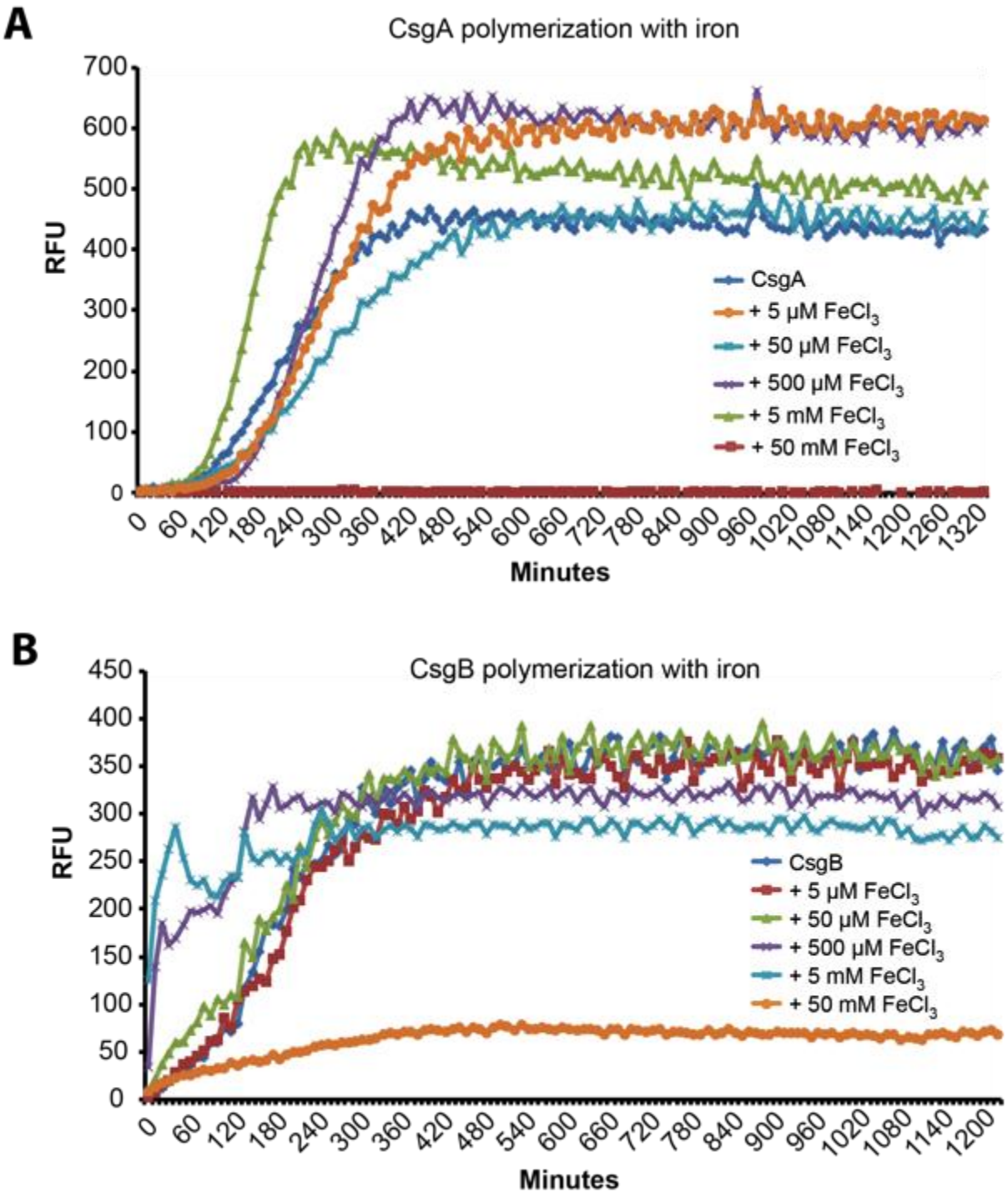

Figure 5.6 Effect of iron on CsgA fiber morphology
CsgA from Fig. 5.5 that polymerized with no additional iron **(A)** or with 5 mM $FeCl_3$ **(B)** was visualized under transmission electron microscopy (TEM).

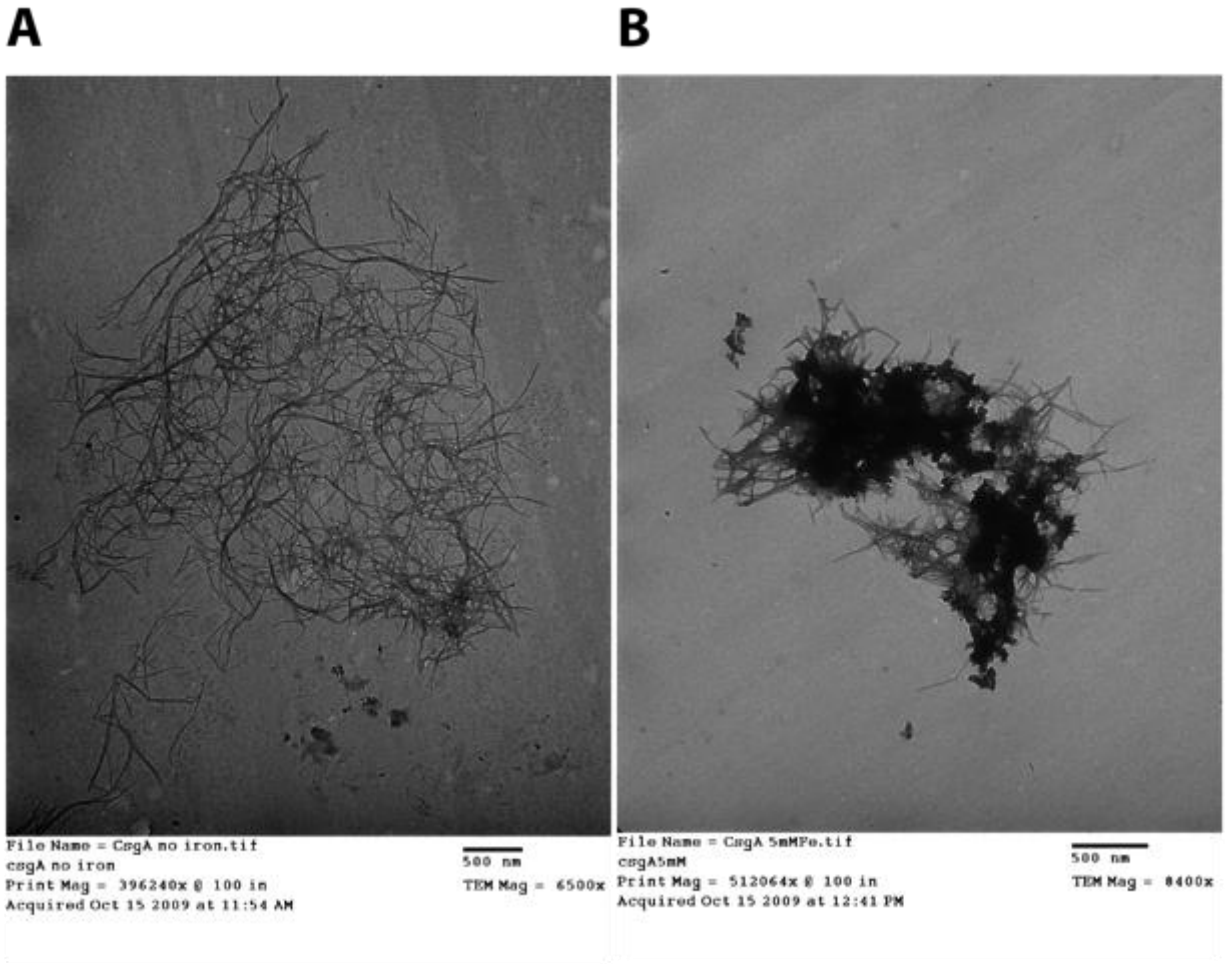

Figure 5.7 CsgA subunit iron-binding assays
CsgA R1 fibers were incubated with Fe3+-NTA complexes and then subjected to ultracentrifugation. Fe3+-NTA demonstrates an absorbance peak around 250 nm, which was used to determine whether spinning down fibers could also remove Fe3+-NTA from solution.

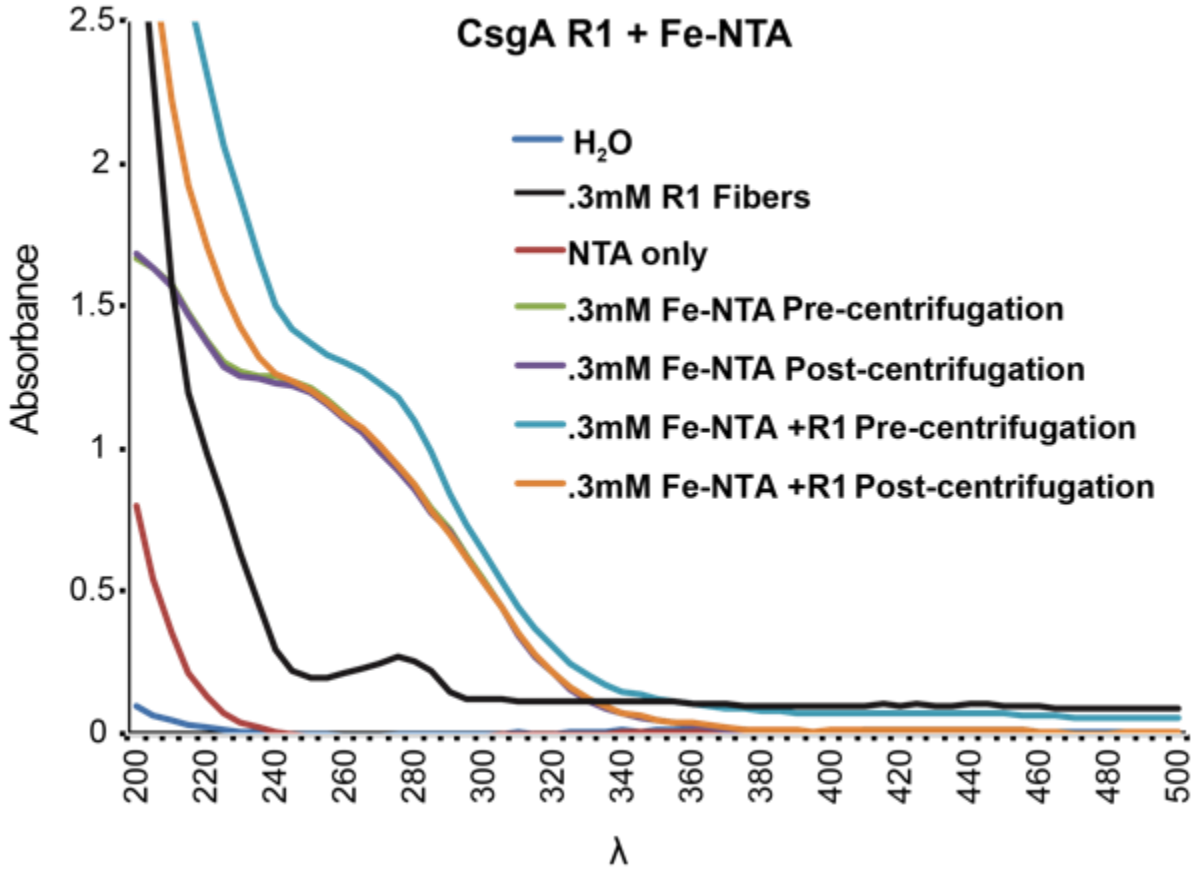

Figure 5.8 Iron uptake visualization with chrome azurol S
WT UTI89 + pLR2 (EV), UTI89 *csgA* + pLR2 (EV), or UTI89 *csgA* + pLR5 (WT *csgA* under the *csgBA* promoter) were plated on YESCA chrome azurol S agar plates and incubated for 2 days at 26°C. Iron uptake can be visualized by a yellow halo that evolves around the dots.

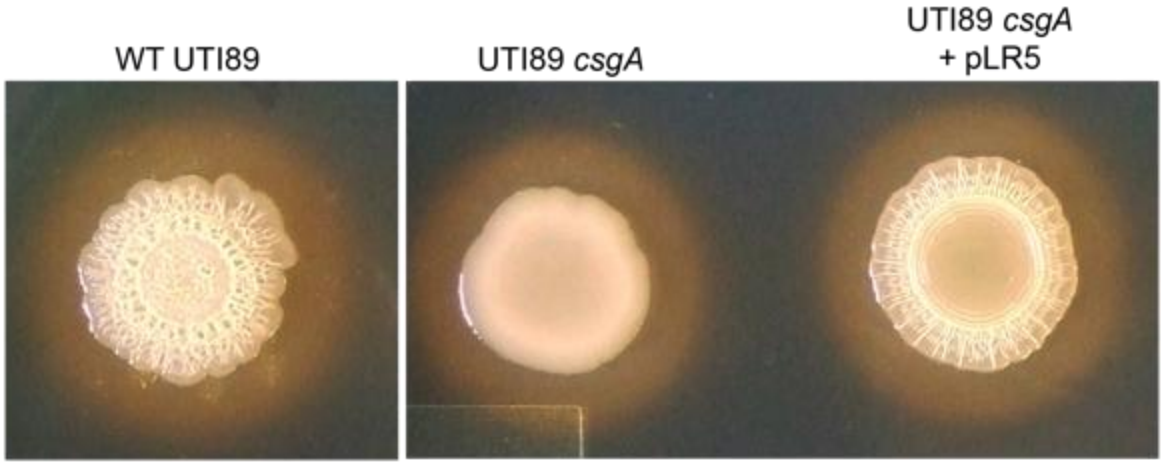

Materials and Methods:

Anaerobic Growth:

For anaerobic growth assays, UTI89 was spotted on YESCA agar plates that had been supplemented with 20 mM $NaNO_3$ and 100 µM $MgCl_2$ 10 µM $CaCl_2$, 10 µM tryptophan. Plates were then placed in anaerobic chambers with 1 GasPak™ EZ anaerobe container system with indicator sachet and incubated at 26°C for 20 days. Aerobic cells were grown for 2 days at 26°C.

β-galactosidase Assays:

β-galactosidase Assays were performed as described (15). Agar plates for UTI89 lacZ *attB::lldP-lacZ* was supplemented with 1mM calcium lactate. Each bar represents an average of biological triplicates, and error bars represent standard deviation.

Confocal Microscopy:

Engineering of GFP-reporter strains and confocal microscopy was performed as described (15).

Protein Purification, ThT Assays, and TEM:

Purification of CsgA and CsgB, as well as ThT polymerization assays and TEM were performed as described (57).

CsgA subunit binding to Fe+3-NTA:

.3mM Fe+3-NTA was mixed with .3mM R1 subunit that had polymerized in water in 1 mL total volume. The sample was incubated for 2 hours on a benchtop rotator, followed by ultracentrifugation at 40,000 rpm for 1 hour at 4°C. Along with controls, 150 µL of sample from the top of the centrifuge tube was then analyzed on a spectrophotometer.

Chrome azurol S plates:

Chrome azurol S agar plates were essentially created as described (58), with minor modifications. Briefly, 60.5mg of chrome azurol S powder was dissolved in 50 mL water. 10 mL of a 1 mM $FeCl_3$, 10 mM HCl solution was mixed in. While stirring, this solution was slowly added to 72.9 mg HDTMA dissolved in 40 mL water. This solution was then autoclaved. Separately, a solution of 900 mL water, 30.24 g pipes, 10 g Casamino acids, and 1 g yeast extract was pH'd to 6.8, mixed with 15 g agar, and autoclaved. After both solutions were autoclaved, the chrome azurol S solution was slowly added to the nutrient mixture under stirring, and agar plates were poured.

Notes and Acknowledgements:

I would like to thank various members of the Chapman and Boles labs for proposing the experiment in Fig. 5.1 multiple times in multiple lab meetings. I finally performed it in time for my thesis and it worked very well. For anyone attempting to recapitulate or expand on the anaerobic experiment in Fig. 5.2, an important note is that UTI89 grows very slowly in anaerobic chambers. It is important to choose a timepoint for aerobically grown UTI89 where the cell density is equal to or lower than that reached in anaerobic chambers before performing any kind of assay to compare the two. I would also like to thank Yizhou Zhou for patiently teaching and reteaching me TEM everytime I needed to use it.

References:

1. **Stewart PS, Franklin MJ.** 2008. Physiological heterogeneity in biofilms. *Nature reviews Microbiology* **6:**199-210.
2. **Chai Y, Chu F, Kolter R, Losick R.** 2008. Bistability and biofilm formation in *Bacillus subtilis*. *Molecular Microbiology* **67:**254-263.
3. **Norman TM, Lord ND, Paulsson J, Losick R.** 2013. Memory and modularity in cell-fate decision making. *Nature* **503:**481-486.
4. **Elowitz MB, Levine AJ, Siggia ED, Swain PS.** 2002. Stochastic gene expression in a single cell. *Science* **297:**1183-1186.
5. **Boles BR, Thoendel M, Singh PK.** 2004. Self-generated diversity produces "insurance effects" in biofilm communities. *Proceedings of the National Academy of Sciences of the United States of America* **101:**16630-16635.
6. **Boles BR, Singh PK.** 2008. Endogenous oxidative stress produces diversity and adaptability in biofilm communities. *Proceedings of the National Academy of Sciences of the United States of America* **105:**12503-12508.
7. **Xu KD, Stewart PS, Xia F, Huang CT, McFeters GA.** 1998. Spatial physiological heterogeneity in *Pseudomonas aeruginosa* biofilm is determined by oxygen availability. *Applied and Environmental Microbiology* **64:**4035-4039.
8. **Williamson KS, Richards LA, Perez-Osorio AC, Pitts B, McInnerney K, Stewart PS, Franklin MJ.** 2012. Heterogeneity in *Pseudomonas aeruginosa* biofilms includes expression of ribosome hibernation factors in the antibiotic-tolerant subpopulation and hypoxia-induced stress response in the metabolically active population. *Journal of Bacteriology* **194:**2062-2073.
9. **Foster PL.** 2007. Stress-induced mutagenesis in bacteria. *Critical reviews in biochemistry and molecular biology* **42:**373-397.
10. **Morris JG, Jr., Sztein MB, Rice EW, Nataro JP, Losonsky GA, Panigrahi P, Tacket CO, Johnson JA.** 1996. *Vibrio cholerae* O1 can assume a chlorine-resistant rugose survival form that is virulent for humans. *The Journal of Infectious Diseases* **174:**1364-1368.

11. **Beyhan S, Bilecen K, Salama SR, Casper-Lindley C, Yildiz FH.** 2007. Regulation of rugosity and biofilm formation in *Vibrio cholerae*: comparison of VpsT and VpsR regulons and epistasis analysis of *vpsT, vpsR*, and *hapR*. *Journal of Bacteriology* **189:**388-402.
12. **Beyhan S, Yildiz FH.** 2007. Smooth to rugose phase variation in *Vibrio cholerae* can be mediated by a single nucleotide change that targets c-di-GMP signalling pathway. *Molecular Microbiology* **63:**995-1007.
13. **Wai SN, Mizunoe Y, Takade A, Kawabata SI, Yoshida SI.** 1998. *Vibrio cholerae* O1 strain TSI-4 produces the exopolysaccharide materials that determine colony morphology, stress resistance, and biofilm formation. *Applied and Environmental Microbiology* **64:**3648-3655.
14. **Grantcharova N, Peters V, Monteiro C, Zakikhany K, Romling U.** 2010. Bistable expression of CsgD in biofilm development of *Salmonella enterica* serovar typhimurium. *Journal of Bacteriology* **192:**456-466.
15. **DePas WH, Hufnagel DA, Lee JS, Blanco LP, Bernstein HC, Fisher ST, James GA, Stewart PS, Chapman MR.** 2013. Iron induces bimodal population development by *Escherichia coli*. *Proceedings of the National Academy of Sciences of the United States of America* **110:**2629-2634.
16. **Romling U, Sierralta WD, Eriksson K, Normark S.** 1998. Multicellular and aggregative behaviour of *Salmonella typhimurium* strains is controlled by mutations in the agfD promoter. *Molecular Microbiology* **28:**249-264.
17. **Delgado-Nixon VM, Gonzalez G, Gilles-Gonzalez MA.** 2000. Dos, a heme-binding PAS protein from *Escherichia coli*, is a direct oxygen sensor. *Biochemistry* **39:**2685-2691.
18. **Green J, Bennett B, Jordan P, Ralph ET, Thomson AJ, Guest JR.** 1996. Reconstitution of the [4Fe-4S] cluster in FNR and demonstration of the aerobic-anaerobic transcription switch *in vitro*. *The Biochemical journal* **316 (Pt 3):**887-892.
19. **Malpica R, Sandoval GR, Rodriguez C, Franco B, Georgellis D.** 2006. Signaling by the *arc* two-component system provides a link between the redox state of the quinone pool and gene expression. *Antioxidants & Redox Signaling* **8:**781-795.
20. **Serra DO, Richter AM, Hengge R.** 2013. Cellulose as an Architectural Element in Spatially Structured *Escherichia coli* Biofilms. *Journal of Bacteriology* **195:**5540-5554.
21. **Serra DO, Richter AM, Klauck G, Mika F, Hengge R.** 2013. Microanatomy at cellular resolution and spatial order of physiological differentiation in a bacterial biofilm. *Mbio* **4:**e00103-00113.
22. **Sasakura Y, Hirata S, Sugiyama S, Suzuki S, Taguchi S, Watanabe M, Matsui T, Sagami I, Shimizu T.** 2002. Characterization of a direct oxygen sensor heme protein from *Escherichia coli*. Effects of the heme redox states and mutations at the heme-binding site on catalysis and structure. *The Journal of Biological Chemistry* **277:**23821-23827.
23. **Tuckerman JR, Gonzalez G, Sousa EH, Wan X, Saito JA, Alam M, Gilles-Gonzalez MA.** 2009. An oxygen-sensing diguanylate cyclase and phosphodiesterase couple for c-di-GMP control. *Biochemistry* **48:**9764-9774.

24. **Lacey MM, Partridge JD, Green J.** 2010. *Escherichia coli* K-12 YfgF is an anaerobic cyclic di-GMP phosphodiesterase with roles in cell surface remodelling and the oxidative stress response. *Microbiology* **156:**2873-2886.
25. **Romling U.** 2005. Characterization of the rdar morphotype, a multicellular behaviour in *Enterobacteriaceae*. *Cellular and molecular life sciences* **62:**1234-1246.
26. **Sommerfeldt N, Possling A, Becker G, Pesavento C, Tschowri N, Hengge R.** 2009. Gene expression patterns and differential input into curli fimbriae regulation of all GGDEF/EAL domain proteins in *Escherichia coli*. *Microbiology* **155:**1318-1331.
27. **Weber H, Pesavento C, Possling A, Tischendorf G, Hengge R.** 2006. Cyclic-di-GMP-mediated signalling within the sigma network of *Escherichia coli*. *Molecular Microbiology* **62:**1014-1034.
28. **Andrews SC, Robinson AK, Rodriguez-Quinones F.** 2003. Bacterial iron homeostasis. *FEMS Microbiology Reviews* **27:**215-237.
29. **Cornelis P, Wei Q, Andrews SC, Vinckx T.** 2011. Iron homeostasis and management of oxidative stress response in bacteria. *Metallomics : Integrated Biometal Science* **3:**540-549.
30. **Imlay JA, Chin SM, Linn S.** 1988. Toxic DNA Damage by Hydrogen-Peroxide through the Fenton Reaction Invivo and Invitro. *Science* **240:**640-642.
31. **Cabiscol E, Tamarit J, Ros J.** 2000. Oxidative stress in bacteria and protein damage by reactive oxygen species. *International microbiology : the official journal of the Spanish Society for Microbiology* **3:**3-8.
32. **Fridovich I.** 1998. Oxygen toxicity: a radical explanation. *The Journal of Experimental Biology* **201:**1203-1209.
33. **Imlay JA.** 2008. Cellular defenses against superoxide and hydrogen peroxide. *Annual Review of Biochemistry* **77:**755-776.
34. **Kolodkin-Gal I, Elsholz AK, Muth C, Girguis PR, Kolter R, Losick R.** 2013. Respiration control of multicellularity in *Bacillus subtilis* by a complex of the cytochrome chain with a membrane-embedded histidine kinase. *Genes & Development* **27:**887-899.
35. **Messner KR, Imlay JA.** 1999. The identification of primary sites of superoxide and hydrogen peroxide formation in the aerobic respiratory chain and sulfite reductase complex of *Escherichia coli*. *The Journal of Biological Chemistry* **274:**10119-10128.
36. **Cho BK, Knight EM, Palsson BO.** 2006. Transcriptional regulation of the fad regulon genes of *Escherichia coli* by ArcA. *Microbiology* **152:**2207-2219.
37. **Lynch AS, Lin EC.** 1996. Transcriptional control mediated by the ArcA two-component response regulator protein of *Escherichia coli*: characterization of DNA binding at target promoters. *Journal of Bacteriology* **178:**6238-6249.
38. **Pena-Sandoval GR, Georgellis D.** 2010. The ArcB sensor kinase of *Escherichia coli* autophosphorylates by an intramolecular reaction. *Journal of Bacteriology* **192:**1735-1739.
39. **Dietrich LE, Okegbe C, Price-Whelan A, Sakhtah H, Hunter RC, Newman DK.** 2013. Bacterial community morphogenesis is intimately linked to the intracellular redox state. *Journal of Bacteriology* **195:**1371-1380.

40. **Dietrich LE, Teal TK, Price-Whelan A, Newman DK.** 2008. Redox-active antibiotics control gene expression and community behavior in divergent bacteria. *Science* **321:**1203-1206.
41. **Morales DK, Grahl N, Okegbe C, Dietrich LE, Jacobs NJ, Hogan DA.** 2013. Control of Candida albicans metabolism and biofilm formation by *Pseudomonas aeruginosa* phenazines. *Mbio* **4:**e00526-00512.
42. **Roberts BR, Ryan TM, Bush AI, Masters CL, Duce JA.** 2012. The role of metallobiology and amyloid-beta peptides in Alzheimer's disease. *Journal of Neurochemistry* **120 Suppl 1:**149-166.
43. **Weinreb O, Mandel S, Youdim MB, Amit T.** 2013. Targeting dysregulation of brain iron homeostasis in Parkinson's disease by iron chelators. *Free Radical Biology & Medicine* **62:**52-64.
44. **Liu B, Moloney A, Meehan S, Morris K, Thomas SE, Serpell LC, Hider R, Marciniak SJ, Lomas DA, Crowther DC.** 2011. Iron promotes the toxicity of amyloid beta peptide by impeding its ordered aggregation. *The Journal of Biological Chemistry* **286:**4248-4256.
45. **Rivera-Mancia S, Perez-Neri I, Rios C, Tristan-Lopez L, Rivera-Espinosa L, Montes S.** 2010. The transition metals copper and iron in neurodegenerative diseases. *Chemico-biological interactions* **186:**184-199.
46. **Wang X, Smith DR, Jones JW, Chapman MR.** 2007. *In vitro* polymerization of a functional *Escherichia coli* amyloid protein. *The Journal of Biological Chemistry* **282:**3713-3719.
47. **Hammer ND, Schmidt JC, Chapman MR.** 2007. The curli nucleator protein, CsgB, contains an amyloidogenic domain that directs CsgA polymerization. *Proceedings of the National Academy of Sciences of the United States of America* **104:**12494-12499.
48. **Wang X, Hammer ND, Chapman MR.** 2008. The molecular basis of functional bacterial amyloid polymerization and nucleation. *The Journal of Biological Chemistry* **283:**21530-21539.
49. **Andrianirinaharivelo SL, Pilichowski JF, Bolte M.** 1993. Nitrilotriacetic Acid Transformation Photoinduced by Complexation with Iron(iii) in Aqueous-Solution. *Transition Metal Chemistry* **18:**37-41.
50. **Martin P, Marcq I, Magistro G, Penary M, Garcie C, Payros D, Boury M, Olier M, Nougayrede JP, Audebert M, Chalut C, Schubert S, Oswald E.** 2013. Interplay between Siderophores and Colibactin Genotoxin Biosynthetic Pathways in *Escherichia coli*. *PLoS Pathogens* **9**.
51. **Unden G, Bongaerts J.** 1997. Alternative respiratory pathways of *Escherichia coli*: energetics and transcriptional regulation in response to electron acceptors. *Biochimica et biophysica acta* **1320:**217-234.
52. **Clark DP.** 1989. The fermentation pathways of *Escherichia coli*. *FEMS Microbiology Reviews* **5:**223-234.
53. **White AP, Gibson DL, Kim W, Kay WW, Surette MG.** 2006. Thin aggregative fimbriae and cellulose enhance long-term survival and persistence of *Salmonella*. *Journal of Bacteriology* **188:**3219-3227.
54. **Epstein AK, Pokroy B, Seminara A, Aizenberg J.** 2011. Bacterial biofilm shows persistent resistance to liquid wetting and gas penetration. *Proceedings of*

the National Academy of Sciences of the United States of America **108:**995-1000.

55. **Kempes CP, Okegbe C, Mears-Clarke Z, Follows MJ, Dietrich LE.** 2014. Morphological optimization for access to dual oxidants in biofilms. *Proceedings of the National Academy of Sciences of the United States of America* **111:**208-213.
56. **Wilking JN, Zaburdaev V, De Volder M, Losick R, Brenner MP, Weitz DA.** 2013. Liquid transport facilitated by channels in *Bacillus subtilis* biofilms. *Proceedings of the National Academy of Sciences of the United States of America* **110:**848-852.
57. **Zhou Y, Smith D, Leong BJ, Brannstrom K, Almqvist F, Chapman MR.** 2012. Promiscuous cross-seeding between bacterial amyloids promotes interspecies biofilms. *The Journal of Biological Chemistry* **287:**35092-35103.
58. **Schwyn B, Neilands JB.** 1987. Universal chemical assay for the detection and determination of siderophores. *Analytical Biochemistry* **160:**47-56.